ABSTRACT

PREDICTION OF SERVICE LOAD OF CONCRETE STRUCTURES AFTER CRACKING USING ULTRASONIC TECHNIQUE

by
Xuezeng Wu

The objective of this study is to investigate the cracking behavior of fractured concrete structures and to introduce a new approach to assess their remaining service lives. A novel ultrasonic technique is utilized to detect crack propagation in notched beams of mortar, plain concrete and reinforced concrete. The study showed that crack growth and microcrack zone in cementitious composites can be quantitatively detected by the ultrasound technique.

To predict crack propagation during the fracture process in plain concrete, an effective compliance fracture model is proposed. A large fracture process zone is incorporated in the analytical model by means of an equivalent elastic beam concept, which makes it possible to determine fracture toughness of the concrete member in terms of critical stress intensity factor, K_{IC}^{e}. The model was evaluated for size dependency using several sizes of notched beams with different notch lengths. The results showed fracture toughness in terms of K_{IC}^{e}, to be size-independent up to a crack over depth ratio of 0.4, making it a material property which may be used for design purpose.

By combining the effects of pure bending and an applied axial force on a cracked flexural member, a new fracture model was proposed to predict crack propagations in RC beams. The model assumes elastic-plastic behavior of the reinforcement and a constant fracture angle of the cracked plane, allowing the model to predict crack growth at any instant during the fracture processes. The predicted values of crack growth were validated

by comparing with those measured using the ultrasonic technique and found to be in good agreement.

Through loading and unloading cycles during testing, the ultrasonic technique was able to detect the size and variation of the fracture process zone during the fracture processes. This is a unique finding that has never been experimentally observed in the past.

Finally, a design diagram showing the energy loss ratio versus the crack growth of any fractured concrete beam was developed. The relationship of normalized crack growth and energy loss ratio for non-reinforced concrete, (mortar and plain concrete) and reinforced concrete beams with different reinforcement ratios (under-reinforced, balanced and over-reinforced) were formulated. By using the existing crack growth over uncracked ligament ratio and the reinforcement of the member, the diagram can easily be applied in practice to predict the remaining service life of any cracked concrete beams.

PREDICTION OF SERVICE LOAD OF CONCRETE STRUCTURES AFTER CRACKING USING ULTRASONIC TECHNIQUE

by
Xuezeng Wu

A Dissertation
Submitted to the Faculty of
New Jersey Institute of Technology
in Partial Fulfillment of the Requirements for the Degree of
Doctor of Philosophy in Civil Engineering

Department of Civil and Environmental Engineering

January 2006

APPROVAL PAGE

PREDICTION OF SERVICE LOAD OF CONCRETE STRUCTURES AFTER CRACKING USING ULTRASONIC TECHNIQUE

Xuezeng Wu

Professor Methi Wecharatana, Dissertation Advisor — Date
Professor of Civil and Environmental Engineering, NJIT

Professor C. T. Thomas Hsu, Committee Member — Date
Professor of Civil and Environmental Engineering, NJIT

Professor Walter Konon, Committee Member — Date
Professor of Civil and Environmental Engineering, NJIT

Professor Dorairaja Raghu, Committee Member — Date
Professor of Civil and Environmental Engineering, NJIT

Dr. John Carlyle, Committee Member — Date
Chief Scientist, Carlyle Consulting

BIOGRAPHICAL SKETCH

Author: Xuezeng Wu

Degree: Doctor of Philosophy

Date: January 2006

Undergraduate and Graduate Education:

- Doctor of Philosophy in Civil and Environmental Engineering,
  New Jersey Institute of Technology, Newark, NJ, 2005

- Master of Science in Hydraulic Structural Engineering,
  Tsinghua University, Beijing, P. R. China, 2000

- Bachelor of Science in Civil Engineering,
  Beijing Institute of Civil and Architecture Engineering, Beijing, P. R. China, 1996

Major: Civil Engineering

Presentations and Publications:

Xuezeng Wu
"Crack Propagations in Cementitious Concrete Structural Members ", Seminar of CE Department, April, 2004.

Xuezeng Wu
"Application of Fracture Mechanics on Concrete and Effective Compliance Model", Seminar of CE Department, March, 2005.

To my beloved family, especially to my parents for their love and unselfish support for any choice I made, to my wife for her every minute with me and to my lovely newborn daughter, Katherine.

ACKNOWLEDGMENT

I would like to express my deepest appreciation to Dr. Methi Wecharatana, who not only served as my research supervisor, providing valuable and countless resources, insight, and intuition, but also constantly gave me support, encouragement, and reassurance.

Special thanks are given to Professor C.T.Thomas, Professor Walter Konon, Professor Dorairaja Raghu and Dr. John Carlyle for actively participating in my dissertation committee. Here the author wants to express his sincere appreciation to Dr. John Carlyle who provided the ultrasonic device for the tests and devoted his time to performing the tests. This study would not have been possible without his contribution.

The author wishes to thank Mr. Allyn Luke and Mr. Frank Johansson for all their efforts and expertise in helping me to perform the tests in the Concrete Laboratory. The help provided by Mr. Sun Punurai in developing testing setups and casting concrete is greatly appreciated.

TABLE OF CONTENTS

TABLE OF CONTENTS
(Continued)

TABLE OF CONTENTS
(Continued)

TABLE OF CONTENTS
(Continued)

LIST OF TABLES

LIST OF FIGURES

LIST OF FIGURES
(Continued)

LIST OF FIGURES
(Continued)

LIST OF FIGURES
(Continued)

LIST OF FIGURES
(Continued)

CHAPTER 1

INTRODUCTION

1.1 General

At present, the national infrastructure system, which includes highways, bridges, dams and levees, is decaying rapidly. Many structural concrete members in those structural systems, in which cracking is frequently found under the service condition are overstressed. There is an urgent need to assess the remaining service lives of these fractured concrete members.

Fracture mechanics is devoted to the analysis of cracked bodies based on Griffith's (1920; 1924) energy balance theory that determined the fracture strength of brittle solids. Since Portland cement concrete is a relatively brittle material, mechanical behaviors of conventionally reinforced concrete, prestressed concrete and fiber reinforced concrete are critically influenced by crack propagation. Thus, many attempts have been made to apply the concept of *Linear Elastic Fracture Mechanics* (LEFM) to quantify the resistance to cracking of cementious composites, which began in 1961 by kaplan.

In this study, the application of fracture mechanics to concrete structural members is investigated by employing the ultrasonic technique for crack growth detection. Emphasis is given to the following objectives:

1. To determine size-independent fracture toughness using an effective compliance approach;
2. To predict crack growth in RC beam based on extension of LEFM concept for Mode I crack propagation;
3. To predict remaining service life of fractured concrete beams.

1.2 Fracture Mechanics on Plain Concrete

During the initial attempts of applying LEFM to concrete, various investigators have carried out tests to determine fracture toughness of cementitious concrete. The most common test is the three-point or four-point bending tests on notched beams. Fracture toughness is usually computed from the length of the pre-cast notch and the maximum load. Unfortunately, the results reported in the literature vary widely, even for essentially similar materials depending on the length of the premolded notch, the depth of the beam, and other testing parameters. One of the primary reasons for the discrepancy is the effect of slow crack growth, partly due to aggregate-interlock behind the crack tip and partly as a result of microcracking ahead of the crack tip. A nonlinear process zone or Fracture Process Zone (FPZ) is generally formed around the crack tip and is responsible for the observed slow crack growth.

In the last few decades, theoretical study on the fracture of concrete has emphasized modeling the fracture process zone, in which Mode I tension failure behavior was assumed. Since many difficulties were encountered in measuring the size of the process zone and the post-cracking and post-peak tensile behavior of brittle materials like concrete, many proposed models assumed these properties and carried out detailed finite element analysis. Based on different experimental studies and assumptions about the fracture propagation process in concrete, many non-linear fracture models were proposed during the past three decades. Among them, fictitious crack model (Hillorberg , 1976), Two Parameter Fracture Model (Jenq and Shah, 1985), Effective Crack Model (Karihaloo,1986), Size-effective Crack Model (Bazant, 1990), and Double K Model (Reinhard and Shilang Xu, 1998) are mostly used and referenced. Unfortunately, these

attempts have not led to a reasonable, unique and widely-accepted set of material parameters which are size-independent and can quantify the resistance of cementitious composites to fracture as similar to metallic materials. Consequently, it is difficult to extrapolate the value of these fracture parameters from small size specimens to practical large-scale concrete members.

In this investigation, a non-linear fracture model, namely *Effective Compliance Fracture Model*, is proposed. A large fracture process zone is incorporated in the analysis using the assumption of an equivalent elastic beam to determine fracture toughness in terms of critical stress intensity factor, K_{IC}^{e}. The model was evaluated for size dependency using several sizes of notched beams with different notch lengths. Different types of cementitious materials were also investigated to confirm the validity of the proposed model. The results showed fracture toughness (in terms of K_{IC}^{e}) to be size-independent, which could possibly be used for practical application.

1.3 Application of Fracture Mechanics to Reinforced Concrete

As commonly known that cracking is present in all existing reinforced concrete structural members, special interest is thus given to reinforced concrete in this study. Even though the proposed effective compliance model is applicable to RC beams, unstable crack propagation generally does not occur in ductile reinforced concrete members due to the presence of reinforcement and therefore is not critical factor here. Before yielding and debonding of reinforcement, crack propagates gradually in RC members and is eventually arrested by the compression zone.

In order to predict crack growth in RC beam, a new method using the relationship between external load and the relative rotation of the crack front, known as "constant fracture angle" and derived by Okamura (1975), was proposed. Carpinteri (1984) and later with Bosco (1992) utilized the same relationship to investigate the fracture behavior of RC beams. Due to difficulties in quantifying the stress in reinforcement, it was therefore assumed to have a rigid-plastic behavior, thus not affecting the overall performance of the member prior to yielding of the reinforcement. This assumption neglects the contribution of reinforcement to fracture resistance of the member during the initial fracturing process of cementitious matrix.

In this proposed model, an elastic-plastic behavior of reinforcement was assumed, which makes it possible predict crack growth prior to the yielding and debonding of the reinforcement. The predicted values of crack growth are in good agreement with those measured using ultrasonic technique.

1.4 Remaining Service Life of Fractured Concrete Structure

Under service condition, most reinforced concrete members experience some degree of cracking. This is due primarily to the low tensile strength of concrete, which then requires reinforcement to compensate for this deficiency. Prior to concrete cracking, steel reinforcement contributes little or no effect to this overall load carrying capacity of the members. It is after the concrete cracks that steel reinforcement playing a primary role in carrying the tensile resistance of the composites.

As concrete members age and are overstressed from repeated or excessive service loads, the existing cracks tend to extend or propagate, further weakening the members.

As the nation's infrastructural continues to decay, the problem proliferates, leading to questioning on the integrity and reliability of our infrastructural system. Also in the post 911 era, damaged concrete structures from terrorists' bombing may be inevitable. In both crises, there is an urgent need to have a fast and reliable non-destructive testing method, together with a proven theoretical concept, to assess the remaining service life of the damaged structures.

In this study, a novel ultrasonic technique is employed to non-destructively monitor the crack growth in non-reinforced and reinforced concrete beams under bending. Through loading and unloading cycles during testing, the technique was able to detect quantitatively the crack growth and, more importantly, the size of the fracture process zone or microcracks, thus allowing the proposed fracture mechanics model to predict the fracture resistance of the concrete members. The approach yields a normalized energy loss versus crack growth relationship, which enables the prediction of the remaining service life of a damaged concrete member.

1.5 Scope and Objectives of Present Study

The current research primarily includes: theoretical analysis, experimental program and practical application, as have been illustrated in Figure 1.1.

A new nonlinear fracture model, namely Effective Compliance Fracture Model, is proposed to investigate fracture toughness of concrete structural members. By assuming constant fracture angle of cracked plane and an elastic-plastic behavior of reinforcement, another fracture model was proposed to predict crack growth prior to the yielding and debonding of the reinforcement. As the most important contribution of this

study, remaining service lives of fractured concrete structural members were investigated theoretically and a prediction diagram was generated based on test results and predicted crack length.

Within experimental program, three series of experimental programs were designed and carried out. And a novel ultrasound technique was utilized in those experiments to detect crack propagation.

As preliminary work of this study, the series I of experiments were performed in order to verify bilinear relationship between load line deflection and CMOD, the sensitivity of ultrasound technique and to generate remaining service life diagram.
The series II of experiments were designed specially for proven the validity of proposed effective compliance fracture model. Variation of specimen size and notch length is to evaluate size-independence of fracture parameter, fracture toughness or critical stress intensity factor.

The emphasis of the series III experiments is on studying fracture behavior of RC beams, especially influences of the amount of reinforcement on crack extension in RC beams.

All the work mentioned above contributes to a remaining service life prediction diagram which can easily be applied in practice to evaluate service condition of fractured concrete elements.

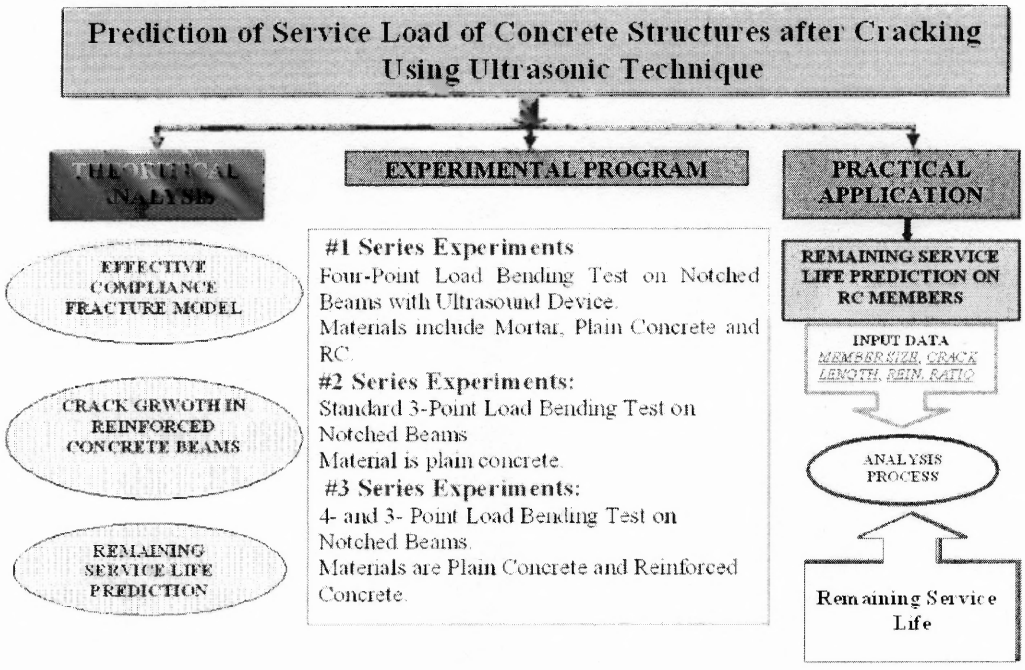

Figure 1.1 Scope of Present Research.

The objectives of the present study are summarized as follows:

1. To propose a non-linear fracture model on concrete which takes into accounts the softening effect of the fracture process zone and calculate its fracture toughness;
2. To proposed an approach to predict the remaining service life of fractured concrete structures using the concept of fracture energy;
3. To proposed a new approach to predict crack growth in RC beam;
4. Experiments with an ultrasonic device to detect crack propagation will be used to produce the "remaining service life design" chart of fractured concrete structural member.

1.6 Research Significance and its Originality

This study deals with how to incorporate the nonlinear fracture process zone into a fracture model to product size-independent fracture parameters and the remaining service life prediction of fractured concrete members based on the concept of fracture mechanics. Size-independent fracture parameters are achieved from the proposed nonlinear fracture

model and a normalized remaining service life prediction chart is created for mortar, plain concrete and reinforced concrete with the variation of reinforcement ratio. This work would significantly enhance the application of fracture mechanics in concrete structures practically.

The originalities of the present study include:

1. A novel ultrasonic technique is first applied to monitor crack propagation during the whole test process and in addition, the size of fracture process zone is first experimentally and quantitatively observed through the use of ultrasonic technique;
2. A model, incorporating the fracture process zone, to analysis the fracturing condition of concrete members is proposed;
3. Fracture processes of reinforced concrete with different reinforcement ratios are investigated;
4. The normalized remaining service life of fractured concrete members is expressed in term of fracture energy and crack growth relationship.

CHAPTER 2

LITERATURE REVIEW

2.1 Linear Elastic Fracture Mechanics (LEFM)

Fracture mechanics, originated in 1921 by A. Griffith, deals with the mechanical responses of a flawed or a cracked body subjected to the application of forces or stresses. Considering a plate subjected to a constant stress σ, which contains a crack of $2a$ long (Figure 2.1), it is possible to derive closed-form expressions for the stresses in the body, assuming an isotropic linear elastic material behavior.

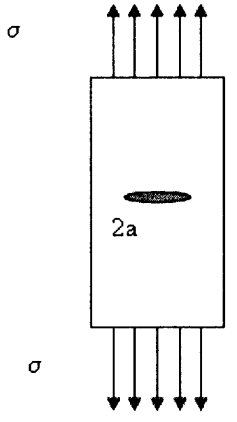

Figure 2.1 A Plate with a Crack 2a Subjected to a Constant Stress.

Westergaard (1939) and Irwin (1957) were among the first to publish such solutions. If we define a polar coordinate axis with the origin at the crack tip, which is assumed as a sharp point (Figure 2.2), the stress field in any linear elastic cracked body can be shown as

$$\sigma_{ij} = \left(\frac{k}{\sqrt{r}}\right) f_{ij}(\theta) + \sum_{m=0}^{\infty} A_m r^{\frac{m}{2}} g_{ij}^{(m)}(\theta) \tag{2.1}$$

where σ_{ij} is the stress tensor, r and θ are defined in Figure 2.2, k is a constant, and f_{ij} is a dimensionless function of θ. The solution for any given configuration contains a leading term that is proportional to $1/\sqrt{r}$. As r approaches zero, the leading term approaches infinity, but the other terms remain finite or approach zero. Equation 2.1 describes a stress *singularity* at the crack tip as r approaches 0.

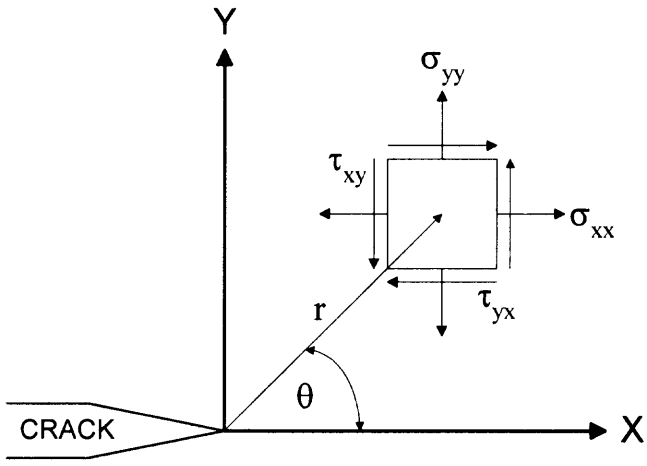

Figure 2.2 The Coordinate Axis Ahead of a Crack Tip and Stress Expression.

In reality, fracture stresses at the crack tip are finite because the crack tip radius is finite; not a sharp point as assumed in the closed-form solution. Also, materials go through inelastic and/or plastic deformation due to a high stress concentration region near the crack tip, which is commonly called *Fracture Process Zone* in concrete or *Plastic Zone* in metal.

2.1.1 Stress Intensity Factor

It is convenient at this point to replace k in Equation 2.1 by the *stress intensity factor*, K, where $K = k\sqrt{2\pi}$. The stress intensity factor is usually given with a subscript to denote

the mode of fracture; i.e., K_I, K_{II} or K_{III} (opening, sliding and tearing mode). Generally, Mode I is the most critical as cracking is directly associated with principal tensile stress. Thus, the stress field (σ_{ij}^{I}) in the vicinity of a crack tip in an isotropic linear elastic material for Mode I can be written as

$$\lim_{r \to o} \sigma_{ij}^{I} = \frac{K_I}{\sqrt{2\pi r}} f_{ij}^{I}(\theta) \tag{2.2}$$

where K_I is the stress intensity factor for Mode I and $f_{ij}(\theta)$ is a polynomial accounting for specimen configuration and crack growth. Since the applied loading in Mode I is perpendicular to the crack plane, all stress components at any point of a linear elastic body must be proportional to the remotely applied stress (σ) and crack length (a).

2.1.2 Critical Stress Intensity Factor

Crack propagation will occur when the combined effect of stress and crack growth (stress intensity) reaches a critical value commonly referred to as the *critical stress intensity factor*, K_{IC}. This value is also called *Fracture Toughness*, which describes the characteristics of material to deform with crack growth and the energy absorption before and during rupture.

"The strength of the fracture mechanics approach to the analysis of brittle fracture is the assertion that a material's fracture resistance can be characterized by a single parameter, ***Fracture Toughness***, regardless of the geometry in a manner analogous to the characterization of yield behavior by the materials' yield strength". (Irwin, 1957)

The critical stress intensity factor is usually determined from the measured peak load, the initial notch depth (a_o) and the related specimen geometry. The relationship between K_I and these related parameters can be expressed as follows:

$$K_I = \sigma\sqrt{\pi a}\, f(a/w) \tag{2.3}$$

where a is the crack length, σ is the applied external stress and $f(a/w)$ is a function of the crack length (a) over thickness ratio (w), along the crack plane accounting for the effect of specimen configuration on the fracture process. $f(a/w)$ for a number of practical specimen configurations were reported by Tada, Paris and Irwin (1985).

The K_I factor is generally a LEFM (linear elastic fracture mechanics) parameter because it is assumed that the material is linearly elastic, isotropic, and homogeneous. However, due to the presence of microcracks in cementitious products, most concrete materials are non-linear and inelastic, making the application of LEFM inaccurate unless the size of the process zone or microcracked zone is incorporated into the analysis.

2.1.3 Energy Release Rate

Due to the inaccurate estimation of fracture stress by the stress concentration approach in the LEFM theory (i.e., infinite stresses at the crack tips), Griffith established an energy-based criterion for crack initiation. Griffith stated that a crack can form (or an existing crack can grow) only if such a process causes the total energy to decrease or remain constant. Thus, the critical conditions for fracture can be defined as the point where crack growth occurs under equilibrium conditions, with no net change in total energy. The Griffith energy balance for an increment of crack length, da, under equilibrium conditions can be expressed as:

$$\frac{dF}{da} = \frac{dW}{da} + \frac{dU}{da} = 0 \tag{2.4a}$$

or

$$-\frac{dU}{da} = \frac{dW}{da} \tag{2.4b}$$

where F is the work done by the external force, W is the energy required to create new crack surface (or for crack growth) and U is the internal strain energy.

In 1956, Irwin proposed the *Energy Release Rate G*, or sometimes referred to as the *Crack Driving Force*, which is a measure of the energy available for an increment of crack extension. The strain energy release rate has the dimension of energy per unit crack surface. The crack surface is the product of the unit thickness and unit crack extension. And strain energy release rate can be expressed as:

$$G = \frac{dU}{Bda} \tag{2.5}$$

where B is the thickness of crack surface.

2.1.4 Critical Strain Energy Release Rate

The critical strain energy release rate, G_C, which is directly related to the measured peak load, generally implies the critical energy absorption of the specimen at the onset of instability of crack growth. At the peak load, G_C can be expressed as

$$G_C = G_{\text{(at peak load)}} \tag{2.6}$$

Based on LEFM, the critical strain energy release rate, G_C, can be expressed in terms of the critical stress intensity factor, K_{IC} as

$$G_C = \frac{K_{IC}^2}{E'} \tag{2.7}$$

And thus, G_C is closely related to K_{IC}.

2.2 Fracture Mechanics on Concrete

After decades of investigation, LEFM has advanced to the stage where it can be employed in engineering design to prevent against the brittle fracture of high-strength materials and highly constrained structures. It can also used to establish material specifications, design rules, quality control and inspection standards, code requirements

and regulations for safe operation. It has been successfully been used on metallic material.

The application of fracture mechanics on concrete is important for various reasons (ACI 446.1 R-91, 1991). Important and compelling reasons can be summarized as follows:

1. Portland cement concrete is a relatively brittle material, (quasi-brittle); as a result, mechanical behavior of concrete, conventionally reinforced, prestressed and fiber reinforced concrete is critically influenced by crack propagation;
2. The reduction in load bearing capacity due to size-dependence of concrete structural component, especially for large structural concrete member and high-strength concrete was not reflected by current ACI design code. Thus the current code leads to an unconservative estimate of shear strength;
3. The need to rationally predict ductility and energy absorption capability;
4. Furthermore, some concrete structural capacitise such as the pull-out capacity of a short anchor bolt, has been demonstrated to be controlled by the fracture resistance instead of the strength of the concrete material.

Various investigators have carried out tests, initiated in 1961 by Kaplan, to determine the fracture toughness of Portland cement, mortar, concrete, and fiber reinforced concrete from LEFM's concepts directly without any modification. The most common test specimens have been beams containing a preformed notch at their centers. Those initial attempts were not successful since the values for these fracture toughness parameter, K_{Ic} or G_{Ic} , vary widely, even in essentially similar materials, depending on the length of the pre-molded notch, the depth of the beam, and other testing parameters. Thus, they are difficult to extrapolate to large construction. One of the primary reasons for the discrepancy is contributed to the existence of the large scale fracture process zone partly resulting from aggregate-interlock behind the crack tip and partly from micro-cracking ahead of the crack tip (sees Figure 2.3).

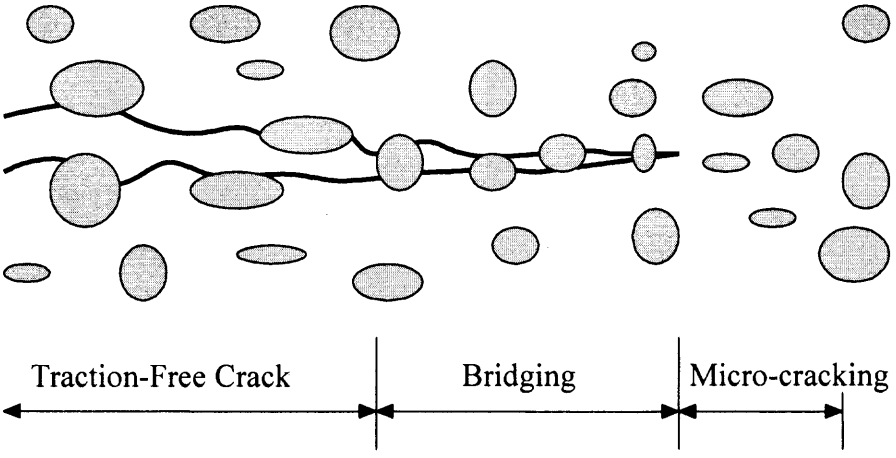

Figure 2.3 Schematic Illustration of Fracture Process Zone in Concrete.

Failure of structures involve the stable crack growth in this large scale fracture process zone and formation of this fracture process zone even before the maximum load is reached. But these attempts led to some important realizations such as the large-scale heterogeneity inherent in the microstructure of concrete, strain softening, micro cracking and large scale process zone, all of which indicate that the classical linear elastic concepts must be significantly modified to predict crack propagation in concrete.

Lack of information on the fracture process zone, the crack opening displacement-crack growth relationship and so on have forced the investigators to make great efforts to identify the slow crack growth, inelastic behavior of concrete, size of process zone and closing pressure in the process zone by non-destructive technique. Finite element analysis also played an important role in increased understanding of unusual aspects of fracture properties of concrete. A.Hillerborg, S.P. Shah, M. Wecharatana and B.L.Karihaloo are of the pioneers in the research of the fracture process zone in concrete.

Table 2.1 Summary of nonlinear fracture model of concrete

Model Category	Fracture Model	Proposed By	Time and Reference	RILEM Proposed Parameters
Fictitious Crack Approach	Fictitious Crack Model	A. Hillerborg and Peterson	1976,1980,1985	G_F
	Crack Band Model	Bazant	1984	
Equivalent Elastic Crack Approach	Two Parameter Fracture Model	Jenq and Shah	1985	K_{ic}^s and $CTOD_c$
	Size-Effective Model	Bazant , Pfeiffer and Kazemi	1987,1990	G_f and c_f
	Effective Crack Model	Karihaloo and Nallathambi	1989a,1989b, 1990	
	Double K model	Reinhardt and Shilang xu	1998,1999	

As a result, several fracture models have been proposed based on different understanding of the experimental observation and theoretical analysis. These models may be categorized as the fictitious crack approach based on the Dugdale-Barenblatt strip yield fracture model, and equivalent elastic (or effective) crack approach based on the Griffith-Irwin energy dissipation concept (see Table 2.1). Each of these nonlinear fracture models introduced some material fracture parameters, which are expected to depend only on material fracture properties regardless of the structure geometry and size. Correspondingly, the test methods to determine the corresponding fracture parameter which are G_F defined by FCM and K_{ic}^s and $CTOD_c$ in TPFM and G_f and c_f in SEM respectively have been recommended by RILEM (1985,1990a,1990b).

2.3 Recent Nonlinear-Fracture Models On Plain Concrete

2.3.1 Fictitious Crack Model (FCM)

Hillerborg, et al. (1976) proposed the fictitious crack model (FCM), also called a cohesive zone model, which was further refined by Peterson (1980) to incorporate the strain-softening behavior of concrete. The model has been shown to correctly predict the experimentally observed fracture behavior and size effect of the notched and un-notched beam specimens.

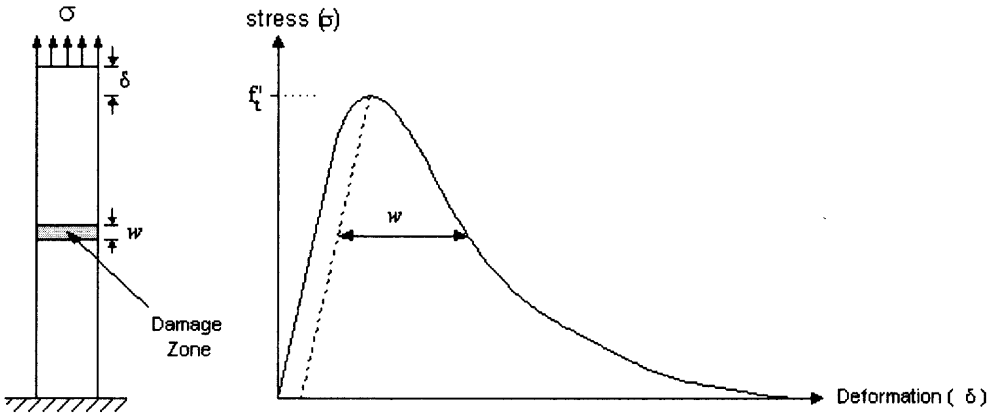

Figure 2.4 Typical Tensile Response of Concrete From a Uniaxial Tension Test.

The model assumes that the crack is to propagate when the stress at the crack tip reaches the tensile strength f_t. When the crack opens, the stress is not assumed to fall to zero, but to decrease with increasing crack width w. At the crack width w_c, which is called *critical crack opening displacement*, the stress has fallen to zero. The stress versus crack opening displacement (σ-w) behavior in the damage zone can be illustrated in Figure 2.4 in uniaxial tensile test. This behavior is assumed to be a material property. The area under this stress versus crack opening displacement curve corresponds to the amount

of energy absorbed per unit crack area in widening the crack from zero to or beyond w_c and was termed as is its Fracture Energy (Figure 2.5):

$$G_F = \int_0^{w_c} \sigma dw \tag{2.8}$$

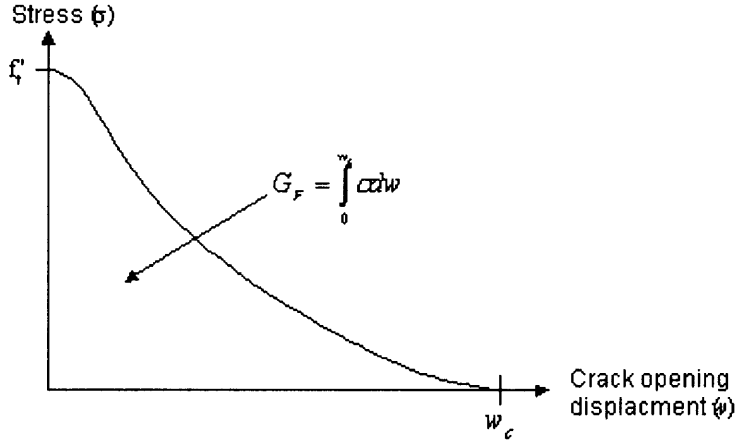

Figure 2.5 Typical Stresses versus Crack Opening Displacement Plot.

The fracture energy, G_F, has a physical meaning similar to the critical strain energy release rate, G_C. However, unlike the determination of G_C which is directly related to the peak load, the fracture energy is determined from the work needed to completely separate the specimen into two halves. The value of G_F should be theoretically calculated using uniaxial direct tension test. However, Peterson [1980; 1981] has described how G_F can be determined from a three-point bend test on notched beams, citing the difficulties in performing a uniaxial direct tensile test. The simple three-point-bend test on notched beams was later proposed by RILEM [1985] to determine the fracture energy of mortar and concrete. From a complete load-deflection curve obtained under a stable fracture condition, the fracture energy is calculated from the following equation:

$$G_F = \frac{W_0 + mg\delta_0}{A_{lig}} \tag{2.9}$$

where W_0 is the energy represented by the area under the load-deflection curve, m is the mass of the specimen, g is the gravity acceleration, δ_0 is the maximum deflection of the beam at failure, A_{lig} is area of the uncracked ligament, and $mg\delta_0$ represents the energy supplied by the weight of the beam.

Although the actual G_F should be determined from a direct uniaxial tensile test, due to the difficulty of conducting the direct tensile test most researchers accept the indirect method using the three-point-bend test on notched beams proposed by Petersson (1980). However, it has been pointed out that experimentally observed values of G_F in the three comparative test series carried out around world (1985) were dependent on specimen sizes and strength of structure, were not sensitive to the G_F but quite sensitive to the f_t, which is not easily and accurately obtained. And it was concluded that the interaction between the process zone and the free boundary of the specimen configuration has some influences on the fracture behavior of the notched beam.

Then special emphasis was placed on several sources of energy dissipation during tests to explain the size-dependence of G_F. M.Elices G.V.Guinea and J.Planas (1992) concluded that neglecting the trail of P-δ curve, the dissipated bulk energy can introduce 20%, even 50% errors for small specimens when fracture energy calculations are based on the Load-δ curve.

Kim (1996) developed a method to improve the measurement of the fracture energy by employing the Load-CMOD relationship rather than the conventional Load-Deflection response to eliminate the energy dissipation, and found that only the beam

specimens, which have the notch depth to beam depth ratio equal to or less than 0.4, (*according to RILEM requirement on 3P Bending Test on G_F, notch depth to beam depth ratio would not less than 0.5*) yield more reliable fracture parameters. He explained that this was because the crack has propagated into the compression zone for beam with large *a/d* ratio, thus restricting the formation of micro-cracks.

Therefore, the dimension of the test specimen must strictly adhere to the recommended requirements. Additionally, the finite element analysis is also required to implement this model.

2.3.2 Two Parameter Fracture Model (TPFM)

The two parameter fracture model was developed by Jenq and Shah (1985) based on the pre-peak nonlinear behavior of concrete in standard three-point bending test on notched beams (Figure 2.6).

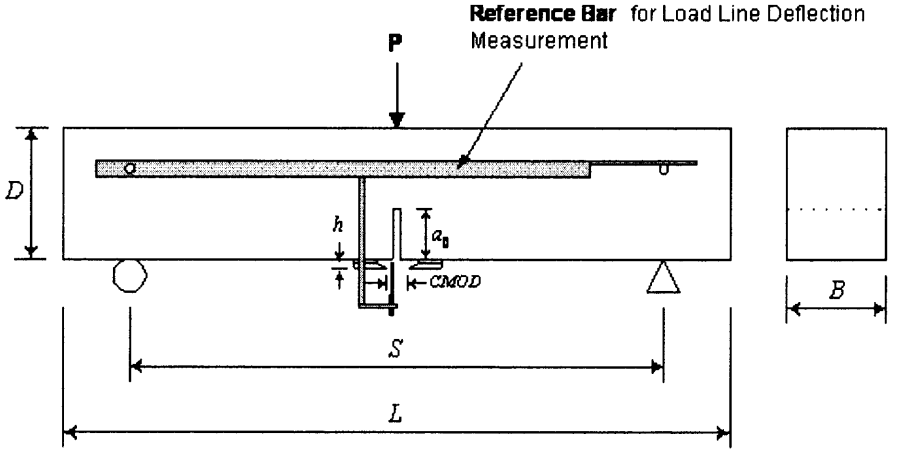

Figure 2.6 Testing Configuration and Geometry of Specimen for Three-Point Bend Tests on Notched Beams.
P = load, L = specimen length, S = specimen loading span
D = beam depth, B = beam thickness, a_0 = initial notch depth
h = thickness of holder of clip gauge
$CMOD$ = crack mouth opening displacement

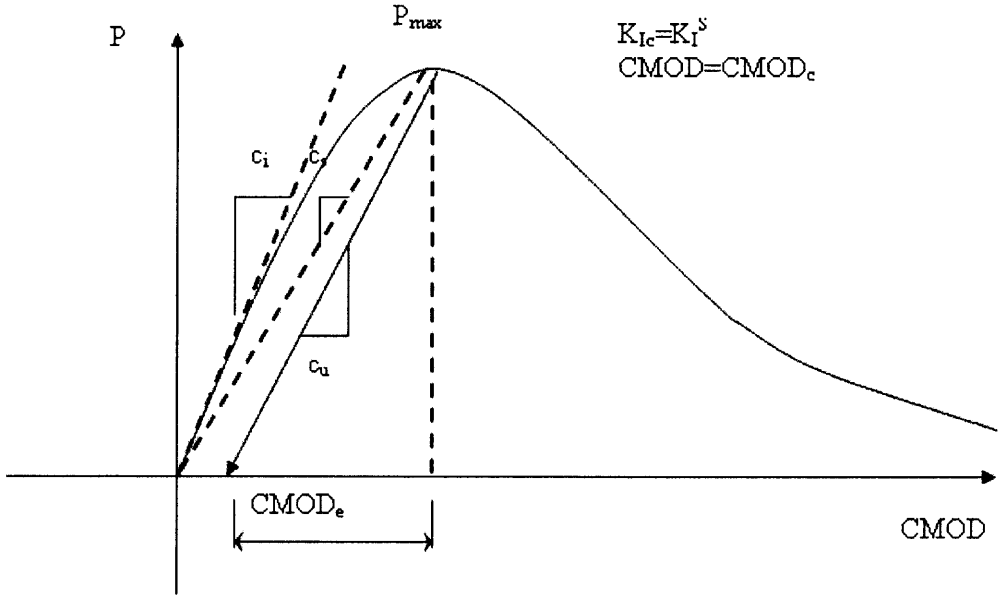

Figure 2.7 Typical Load-CMOD Curve with Unloading and Compliance .

The concept behind the TPFM can be explained from Load-CMOD relationship shown in Fig.2.7. Initially, the load-CMOD is linear up to about half the maximum load. After that, significant inelastic displacement and slow crack growth occur during the nonlinear range. At critical point, the crack tip opening displacement (CTOD) reaches a critical value and $K_I = K_I^s$. Depending upon the geometry of the specimen, the rate of loading, and the method of loading, future crack growth may occur at a steady state value of K_I^s . K_I^s is determined from the maximum load and *Effective Crack Length*, (See Fig 2.8) defined as the length over which all the pre-peak nonlinear behavior of concrete takes place, the results were said to be essentially independent of size and geometry effects. The whole nonlinear behavior of concrete fracture was reflected by the evaluation of the effective crack length.

In general, the measurement of crack path in concrete is tedious and often inaccurate. Furthermore, cracks in concrete may not be traction free due to the effect of aggregate interlocking.

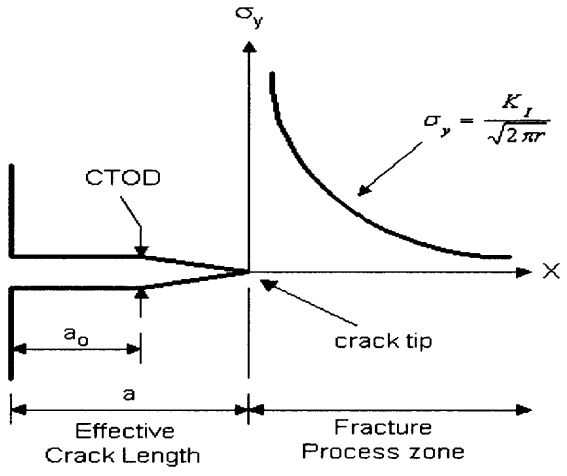

Figure 2.8 Effective Griffith Traction-Free Crack.

As a result, the experimental determination of critical effective crack length, a_c, on a specimen surface is not useful for determining the critical stress intensity factor, K_I^s. An alternate method called the *compliance technique* is used to determine the critical effective crack length (a_c). Compliance is defined as the value of crack mouth opening displacement (*CMOD*) per unit load (see Figure 2.7). For the three point bending test on a notched beam, C_i is the initial compliance at the beginning of loading, and C_u is the unloading compliance just after the peak load by performing unloading and reloading (See Figure 2.7).

Using LEFM readily available relationship (Tada et al. 2000) between compliance and specimen geometry, one can determine the critical effective crack length. However, it was found that the value of a_c depends both on the material properties and on the

specimen's geometry. To overcome this problem, Jenq and Shah (RILEM, 1990) proposed to use the critical crack tip opening displacement at the peak load, $CTOD_C$, as a fracture parameter. Their measurements showed that $CTOD_C$ was essentially independent of the size and geometry of specimens. The available LEFM equations are used to calculate $CTOD_C$ from the compliance measurements. Since the parameters in TPFM are directly determined from LEFM formula, crack tip singularity is automatically incorporated in the model. Therefore K_I^s and $CTOD_C$ become the two parameters that characterize the fracture toughness of concrete.

Based on the load-CMOD curve, the brief procedure involved in the calculation of the two parameters K_{IC} and $CTOD_C$ for three-point-bend specimens proposed by the RILEM Technical Committee 89-FMT (1990a).

In TPFM, only the elastic part *CMODe* or the unloading compliance is taken into account to calculate the effective crack length. This may lead to an underestimate of effective crack length because the interlock of the aggregate can prevent the recovery of the nonlinear displacement. It has been found that the inelastic part or the permanent deformation part of CMOD has an important influence on crack propagation (Bazant, 1996 and 2002). So S.xu and Reinhardt (1999a) suggested using secant compliance instead of unloading compliance to evaluate the effective crack length to incorporate all the nonlinear part during the fracture propagation (see Figure 2.7).

2.3.3 Double K Fracture Models

Recently, Shilang xu and Reihardt (1999,2000,2004) proposed double *K* model to predict both crack initiation and crack propagation. Based on the experimental observation, they divided the whole process of fracture propagation in concrete structures

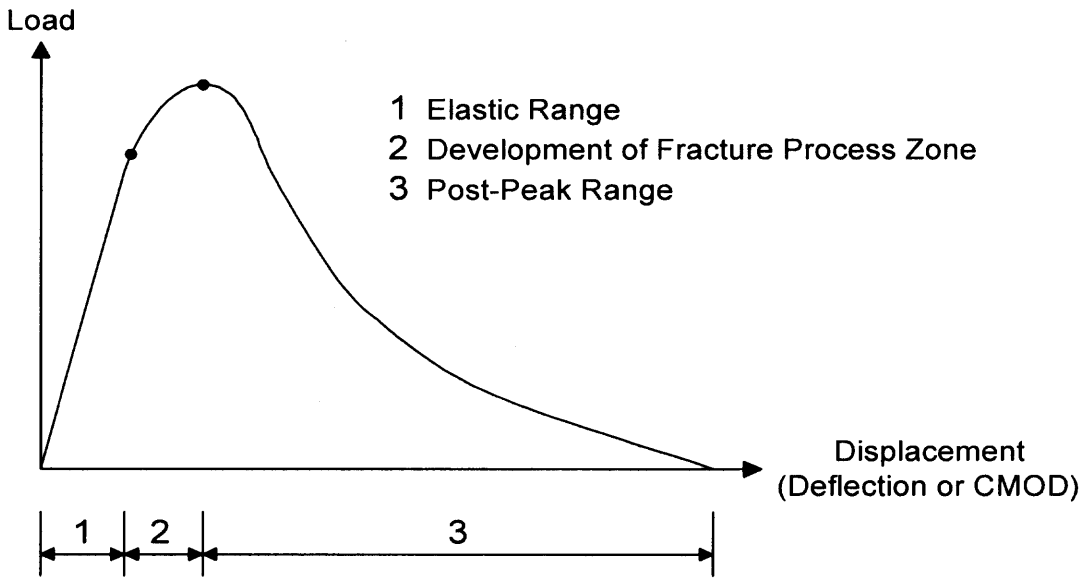

Figure 2.9 Three-Stage Fracture Propagation in Concrete.

into three stages (Figure 2.9): crack initiation, stable crack propagation and unstable propagation (or strain softening). In order to reflect the different stages in concrete fracture, double-K fracture criterion, the two fracture parameters (K_{ini} and K_{un}) are introduced and both of them are given in terms of stress intensity factor. K_{ini} is called initial toughness and its value is determined by inserting the initial cracking load P_{ini} and initial crack length a_0 into a formula of LEFM. K_{un} is termed as the unstable fracture toughness or the critical stress intensity factor and its value is determined by inserting the measured maximum load P_{max} and the measured critical effective crack length a_c into the same formula of LEFM. It is found K_{ini} and K_{un} are size-independent for the tested specimens. Also for determing the double-K parameters, different from TPFM, there is no need to unloading and reloading procedure.

K_{un} in double K model is similar to K_{IC} in TPFM. But double K model use secant compliance instead of unloading compliance in TPFM. The relationship between K_{ini} and K_{un} can be expressed as follow:

$$K_{ini} = K_{un} - K_c \tag{2.10}$$

In which K_c is the stress intensity factor due the cohesion force.

Since it is not easy to determine the initial cracking load P_{ini} , initial toughness can be determined using equation (2.10). Of course, the analytical solution for K_c is not easy to obtain, either. Even Shilang xu adopted bilinear softening-traction separation law for simplication to determine cohesion force, there are still some empirical parameters which are important for determining the breakpoint in bilinear softening-traction separation law but not able to be decided accurately.

2.4 Application of Fracture Mechanics to Reinforced Concrete

As all structural concrete members are reinforced in practice and many reinforced concrete structures in operation are with cracks, cracking in reinforced concrete attracts a lot of attentions in the past.

In engineering practice, crack width and crack space are controlled for obtaining acceptable appearance and for long-term durability of concrete structures, especially those subjected to saltwater spray and deicing chemicals. In the current AASHTO LRFD Specifications and in the ACI 318 Code editions from 1971, flexural crack control requirement were based on the so-called Z-factor method developed by Gergely and Lutz in 1968. Their work was based on extensive statistical evaluation of laboratory experiments. ACI 318 decided in the 1999 edition to greatly simplify crack control requirement based on the work done by Frosch 's crack control research performed in the 1980's and 1990's that failed to demonstrate a credible link between crack width and

problems with long-term durability, for instants of reinforcement corrosion, of reinforced concrete members.

Recently it was becoming realized that "well grounded and accurate methods fro the prediction and evaluation of strength and reliability of contemporary engineering structures and buildings can not be developed without taking into account the fundamental principles of fracture mechanics" (I.I.Luchko and V.F.Lazar, 2002). But comparing many theoretical and experimental investigations performed in formation and propagation of cracks in cement concrete using criteria of the fracture mechanics during the last 20-30 years, there are quite few investigations of propagation of cracks in reinforced concrete (especially with clarification of the role of tensile reinforcement for intensity of crack propagation), in which fracture mechanics of solids is used.

Among those little research work in reinforced concrete, emphasis was made only on under-reinforced concrete, seldom on reinforced concrete with balanced and over reinforcement.

From 1971, the ACI building code has required control of flexural cracking in reinforced concrete structures through the use of the z-factor method. The z-factor approach is a modified form of the Gergely-Lutz crack width equation that was developed from a statistical evaluation of experimental crack width data. Note that crack width here has same physical meaning of CMOD in fracture mechanics.

In order to increase the durability of the concrete, the use of thicker concrete cover is rapidly increasing as well as high-performance concrete. Robert J.Frosh (1999) developed new equation fro calculation crack width that is based on physical phenomenon.

Recently more and more researcher found out that without consideration fracture mechanics it is impossible to achieve a good fracture model of reinforced concrete. But comparing a lot of efforts made to study the formation and propagation of cracks in plain concrete using fracture mechanics during the last 20-30 years, there are comparatively quite few investigations of propagation of cracks in reinforced concrete. Among those little research work in reinforced concrete, emphasis was made only on under-reinforced concrete, seldom on reinforced concrete with balanced and over reinforcement.

Most of theoretical analysis of reinforced concrete using fracture mechanics can be categorized into two branches. One is applying strain-softening behavior of concrete into the structural analysis to find out maximum load capacity of the member. (Hillerborg) Another one is following Hiroyuki Okamura (1975) 's research work on deformation and strength of cracked member under bending moment and axial force. In this branch , Capinteri (1984) and later Bosco & Capinteri (1992) proposed an approximate analytical approach to predicting the flexural failure of reinforced concrete beams in which the concrete and steel actions are coupled. This approach marries simple concepts of fracture mechanics with theorems from structural mechanics familiar to all structural engineers. This approach assumes that the rebar is rigid-elastic-plastic material. We will describe this approach later.

Recently applying fracture mechanics to investigate fracture behavior of reinforced concrete attract much more interesting than before. Vidmantas Jokubaitis (2005), I.I.Luchko and V.F.Lazar (2001.2002) proposed different approach to investigate normal crack in reinforced concrete beams and B.L.Karihaloo (1995) develop a simple

formula from failure stability considerations for calculating the minimum reinforcement requirement for reinforced concrete flexural members.

CHAPTER 3

EXPERIMENTAL PROGRAM AND RESULTS

3.1 Experimental Setup and Materials

3.1.1 Bending Test on Notched Concrete Beams

Bending tests on notched concrete beams are the most common test setup used for studying fracture behavior of concrete. Usually there are two kinds of loading configuration: Three-point load and Four-point load. The three-point loading (3PB) tests illustrated by Figure 2.6, are recommended as standard by RILEM (1985). The four-point loading (4PB) tests are used in order to achieve pure bending, which remains constant throughout the middle portion of the beam.

Analytically, the 3PB test setup yield the maximum moment only at midspan, at which the largest shear force is also present. For 4PB test, the whole middle portion of the beam is subjected to the same maximum moment. There is no shear effect in this region as the shear force is zero. Hence , the main difference between two setups is the shear effect on crack propagation. According to ASTM E-399, the standard fracture tests, both test setups can be used to measure the stress intensity factor provided that the correct shape function polynomial is used.

In this work, due to setup of ultrasound device in the test, four-point load configuration is required to leave some room for the relocation of ultrasound transmitter and receiver during the tests. Both testing setups, i.e. either 3PB or 4PB, are typically designed in order to monitor the load-CMOD response, the load-displacement behavior, the initial compliance (C_i), the maximum load (P_{max}), and the critical crack mouth

opening displacement (CMOD). The tests wee conducted using closed-loop CMOD control at the deformation rate of 1×10^{-4} inches/second on the ascending part and 3×10^{-3} inch/second on the descending portion. The load-line displacement was measured at the center of the beam with reference to a horizontal beam placed at the neutral axis. The test data, consisting of load, CMOD and load line deflection, were recorded using data acquisition and the Labtech Notebook program, whereas crack growth was monitored and recorded by the ultrasonic device.

To ensure that crack propagation will take place at a specified location on the concrete beam so they can be closely monitored by the ultrasonic signal, a notch has to be pre-fabricated typically at the middle of the beam. For plain concrete, saw-cut notches are the simplest choice. As for reinforced concrete members, preparing a saw-cut notch was not possible due to the presence of reinforcement. Thus , a precast notch was made during casting by placing a steel plate at the selected location. Theoretically, the shape of the crack tip, regardless of whether it is saw-cut notch or a precast notch, has some influence on the stress intensity factor. In this study, attempts were made to use the same thickness for the saw blade and the steel plate so that both the saw-cut notch and the precast notch have the same shape of crack tip, thus minimizing its effect on the measured stress intensity factor.

3.1.2 Ultrasonic Technique to Detect Crack Propagation

Measurement of crack growth is commonly one of the most difficult tasks encountered in most fracture tests of concrete and reinforced concrete. The presence of microcracks in the process zone further complicates the measurement process as the exact crack tip is not easily defined since concrete is opaque material, in which exact tortuous crack front is

invisible from outside. The use of ultrasonic technique has overcome this limitation, thus allowing us the closely monitor crack growth during testing.

In this work, a novel ultrasonic technique is applied in four-point loading beam tests to detect crack propagation. Photograph of the real test setup for four-point loading is shown in Figure 3.1.

Ultrasonic transmitter and receiver are placed at the top and bottom of the beam, and at the different sides of pre-molded notch. Crack propagation can be calculated by the decrease of ultrasonic energy received by the ultrasonic receiver. The schematic illustration of this process can be seen in Figure 3.2. Initially the ultrasonic transmitter and receiver are adjusted so that the ultrasonic signal beam is just above the notch tip. At this initial instance with crack propagation, the entire signal from the transmitter can be detected by the receiver, indicated by a very strong signal on the monitor. Once crack propagates, the ultrasonic beam will be shadowed by the crack extension and consequently weakening the signal received. Through some calculations, the observed signal can be converted into crack length.

3.1.3 Compression Test

Information from the compressive stress-strain response is critical to the design of reinforced concrete structures. The primary objective of conducting compression tests on plain concrete was to determine the following properties:

1. Uniaxial compressive strength (fc') ;
2. Modulus of Elasticity (E);
3. The peak strain (ε_c).

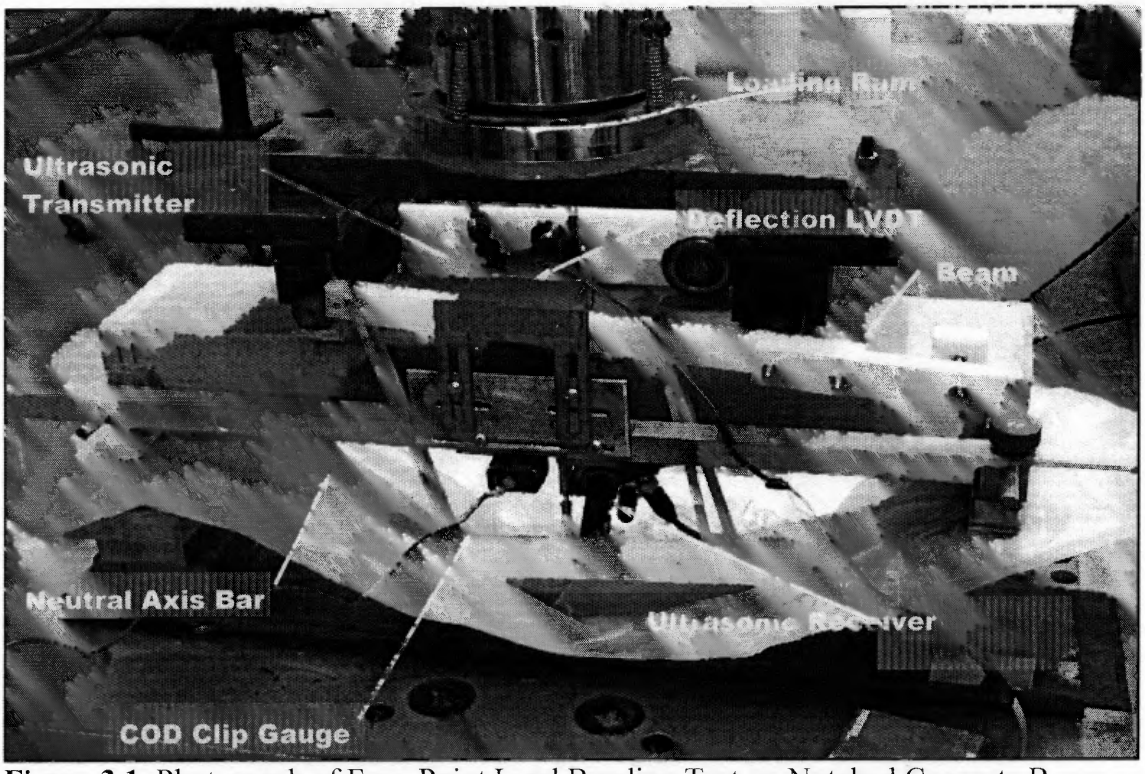

Figure 3.1 Photograph of Four-Point Load Bending Test on Notched Concrete Beam with Ultrasonic Device.

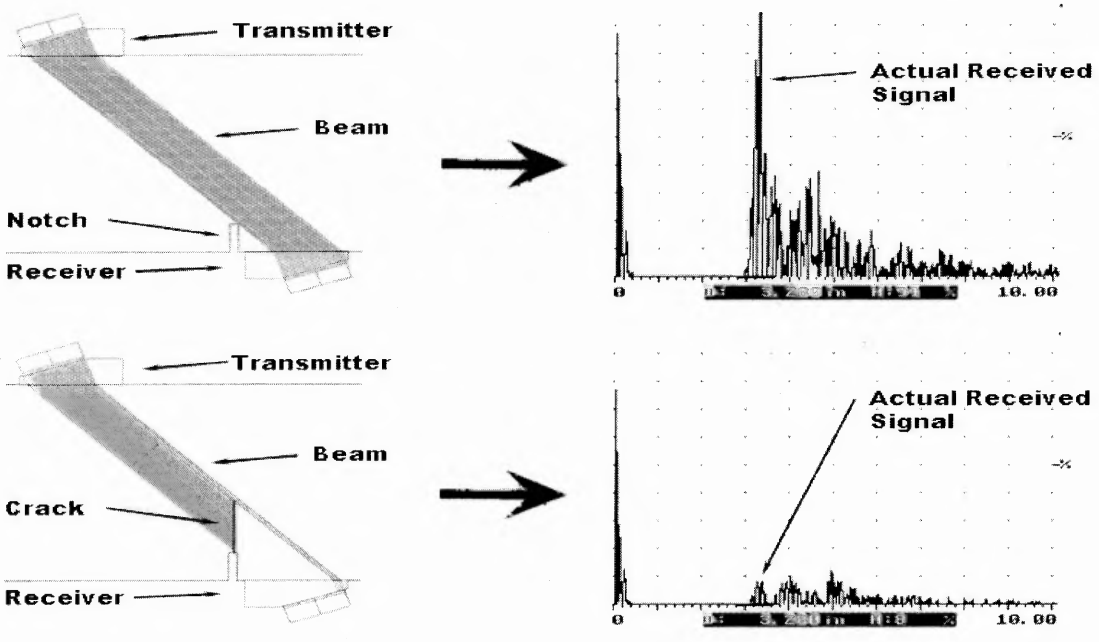

Figure 3.2 Crack Detection Process ---Crack Propagation Shadows Ultrasonic Beam.

All tests are performed in a 100-Kip capacity MTS closed-loop testing system under deformation control. The average rate of axial deformation was measured by the two clip gages. The signal was then electronically averaged and used as the feedback control. The uniaxial deformations were converted to strains by dividing the deformation with the gage length. In this setup, a 2.0-inch gage was used.

Strains were employed to calculate the modulus of Elasticity of concrete in compression. In the pre-peak region, specimens were loaded under deformation (axial strain) control at the rate of 2.0×10^{-7} in./in. per second. For the past peak region, the deformation rate was gradually increased at intervals depending on the load level. The test took approximately 10 minutes to reach the peak load and around 30 minutes to complete the entire test if the specimen did not exhibit abrupt failure at the peak load. Even though there is some technique available to avoid this sudden failure, post-peak response is not important to the parameters we are seeking from this test. The typical stress-strain curve can be seen in Figure 3.3.

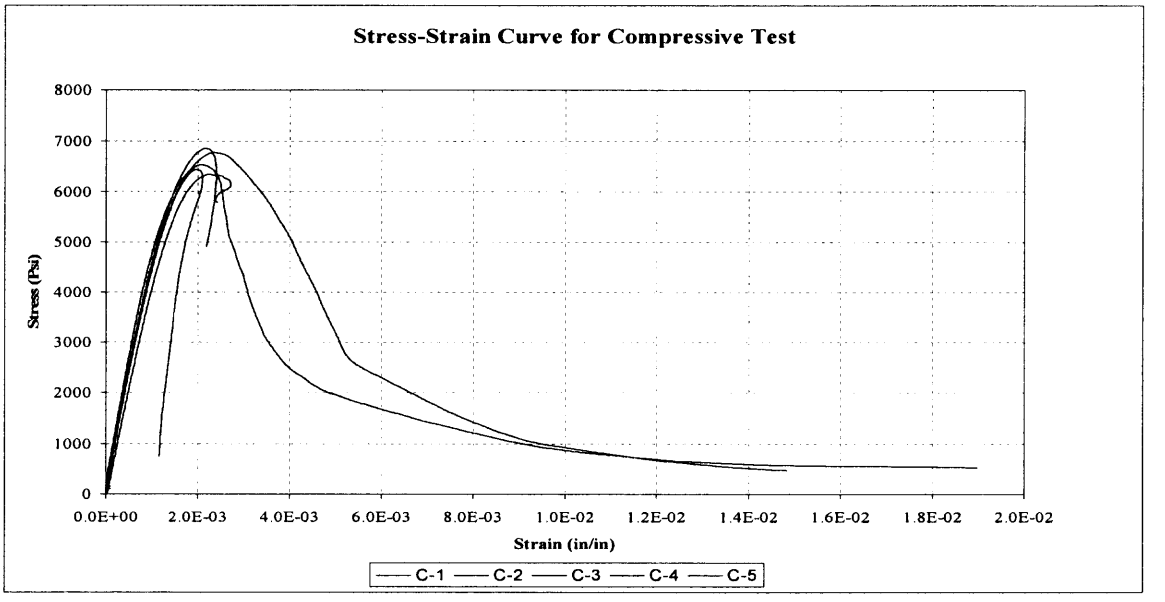

Figure 3.3 Stress-Strain Curves from Compressive Tests.

3.1.4 Concrete Mix

The mix design used for the concrete mixtures is cement: sand: aggregate= 1:2:3 and water-cement ratio varies as 0.4 and 0.5. Coarse aggregates chosen for this study were 3/8 inch basalt. Fine aggregates were river sand conforming to ASTM C33. Type III and Type I Portland cement and conforming to ASTM C 150 were used. The expected compressive strength is 6000 psi.

All samples were left in the mold for 24 hours after casting before demolding. They were then cured in lime-saturated water. Prior to testing the plain concrete beams were notched using a circular diamond blade saw. And notches in RC beams were pro-molded.

3.2 Series I Experimental Design and Results

3.2.1 Design of Series I Experiment

In this series tests, total 14 pieces of beam specimens were tested on mortar, plain concrete and reinforced concrete with ultrasonic device to detect crack growth. The detail testing setup and specimen configuration are presented in Table 3.1.

Table 3.1 Series I Experiment Design

Material	Mortar	Plain Concrete	Reinforced Concrete
Beam Test	Four-Point-load Bending Test		
Mix	C: S: W=1:2:0.5	C: S:A:W=1:2:3:0.5/0.4	C:S:A:W=1:2:3:0.5
t × b× S (in)	4.5×3×20		
a_0 (in)	3/8	3/8	3/8

Note: C: cement; S: sand; W: water; A: aggregate; ρ: reinforcement ratio;
t: thickness of specimen; b: width of specimen; S: span; a_0: notch length.

3.3.2. Results of Series I Experiment

The reliable test results are summarized and are presented in Table 3.2 and typical load-deflection & crack growth curve and load-CMOD & crack growth curve for Mortar, Non-reinforced concrete and reinforced concrete can be seen from Figure 3.4 to Figure 3.9. In order to prove Bi-linear relationship between load line deflection and CMOD to calculate fracture energy, load line deflection and CMOD curves are also plotted and typical one is shown in Figure 3.10.

Table 3.2 Summary of Series I Experiments Results

Test No.	Material	W/C	Pmax (lb)	Delta $_{max}$ (in)	CMOD$_{max}$ (in)	U to peak (Ib-in)	U$_{total}$ (Lb-in)	Gf (Ib-in)
Test 7	RC	0.5	1285.7	0.047	0.0262	3.609	40.87	3.28
Test 5	NRC	0.5	1373.9	0.0297	0.0159	2.75	12.08	0.969
Test 8	Mortar	0.5	934.1	0.0142	0.007	2.04	4.72	0.361
Test 15	RC	0.4	1629.3	0.0319	0.0119	3.2	35.76	2.868
Test 16	NRC	0.4	1298.2	0.0226	0.0123	3.623	13.375	1.073
Test 17	Mortar	0.4	957.3	0.0119	0.006	1.294	4.503	0.361

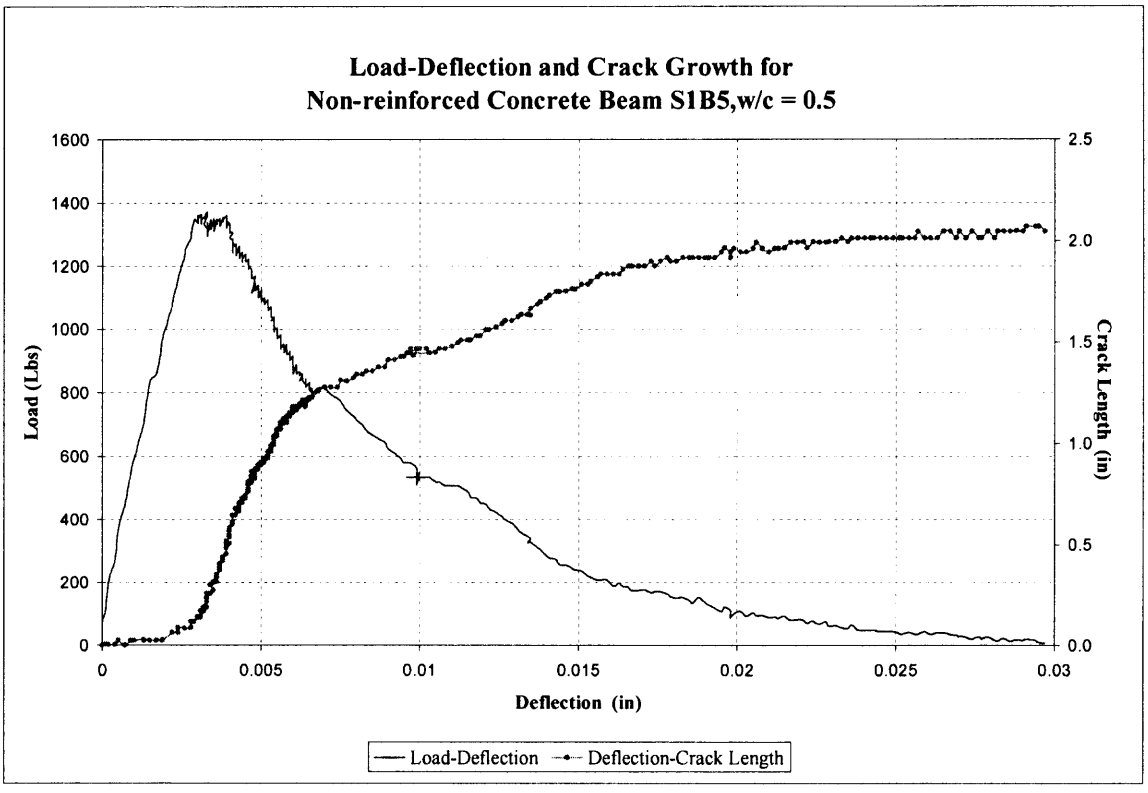

Figure 3.4 Load-Deflections and Crack Growth of Concrete Beam S1B5.

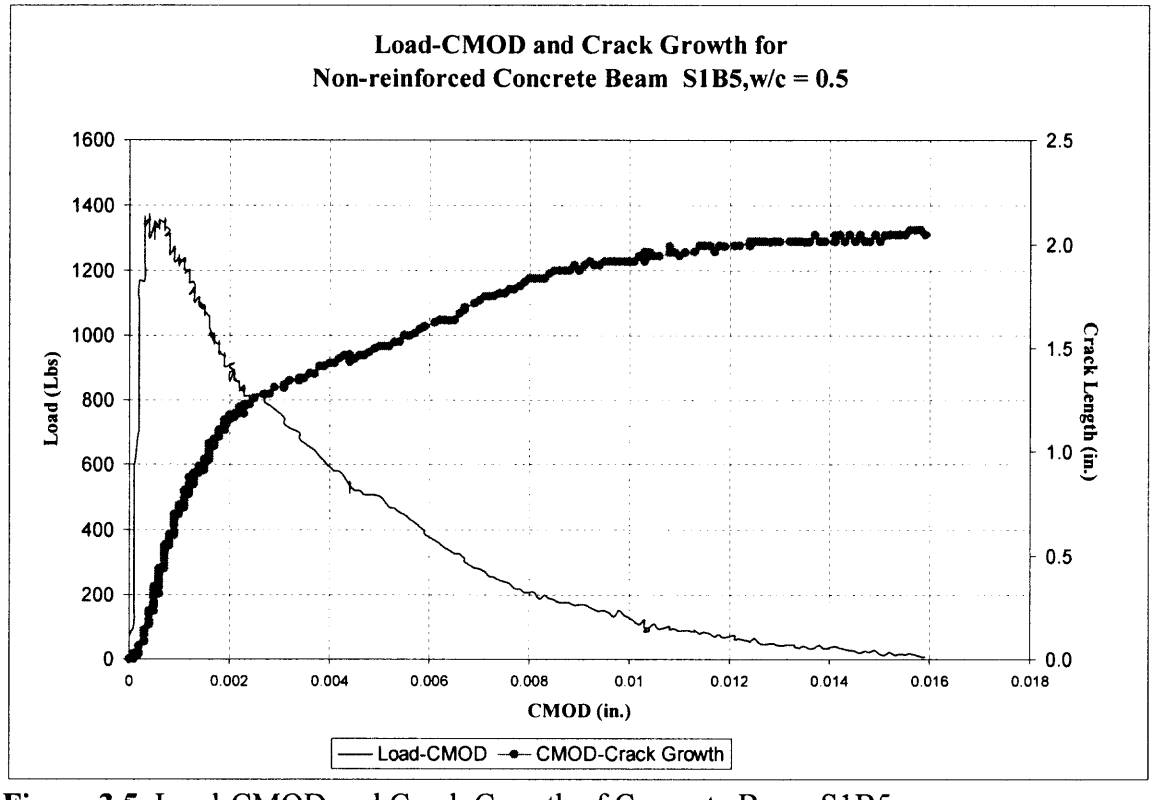

Figure 3.5 Load-CMOD and Crack Growth of Concrete Beam S1B5.

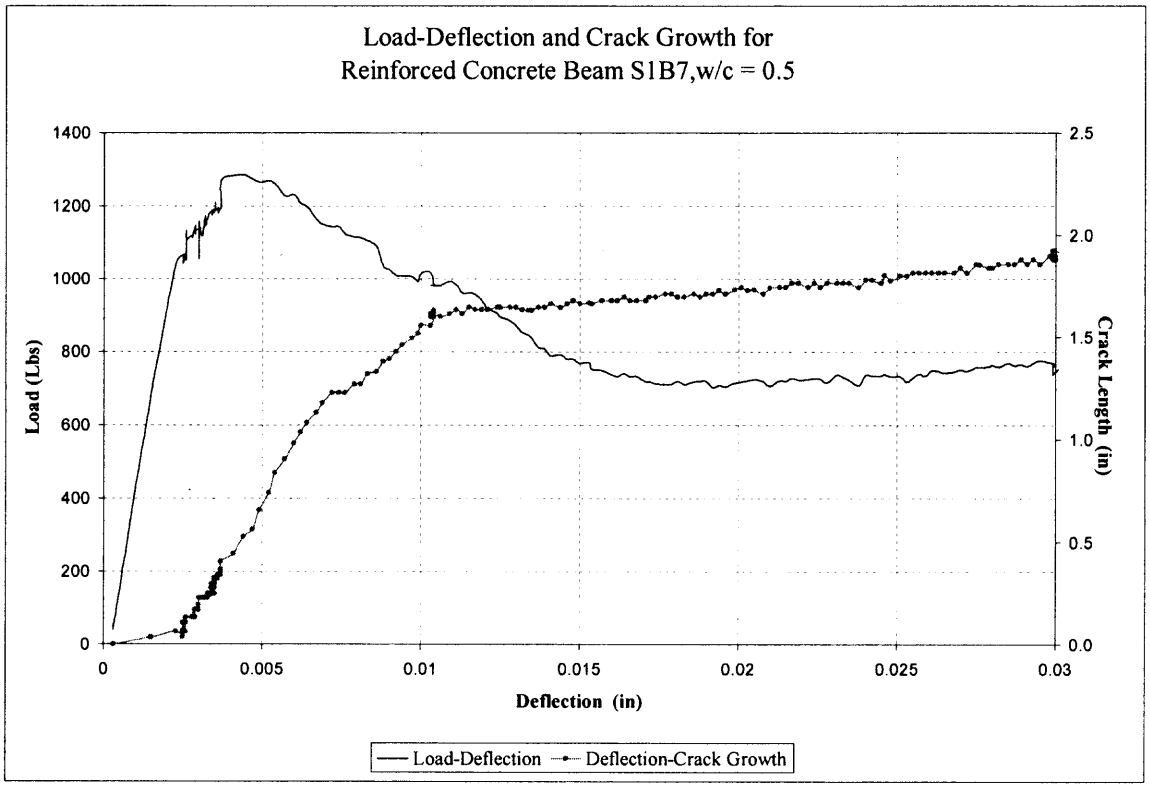

Figure 3.6 Load-CMOD and Crack Growth of Reinforced Concrete Beam S1B7.

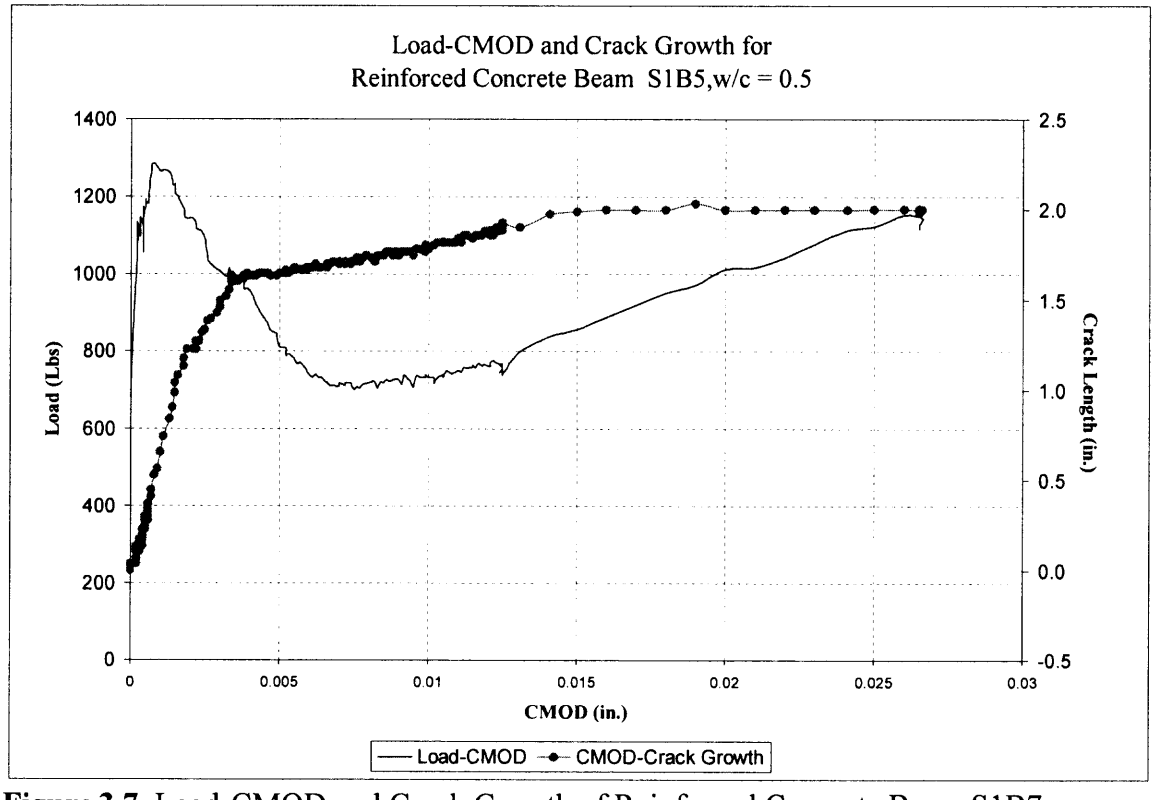

Figure 3.7 Load-CMOD and Crack Growth of Reinforced Concrete Beam S1B7.

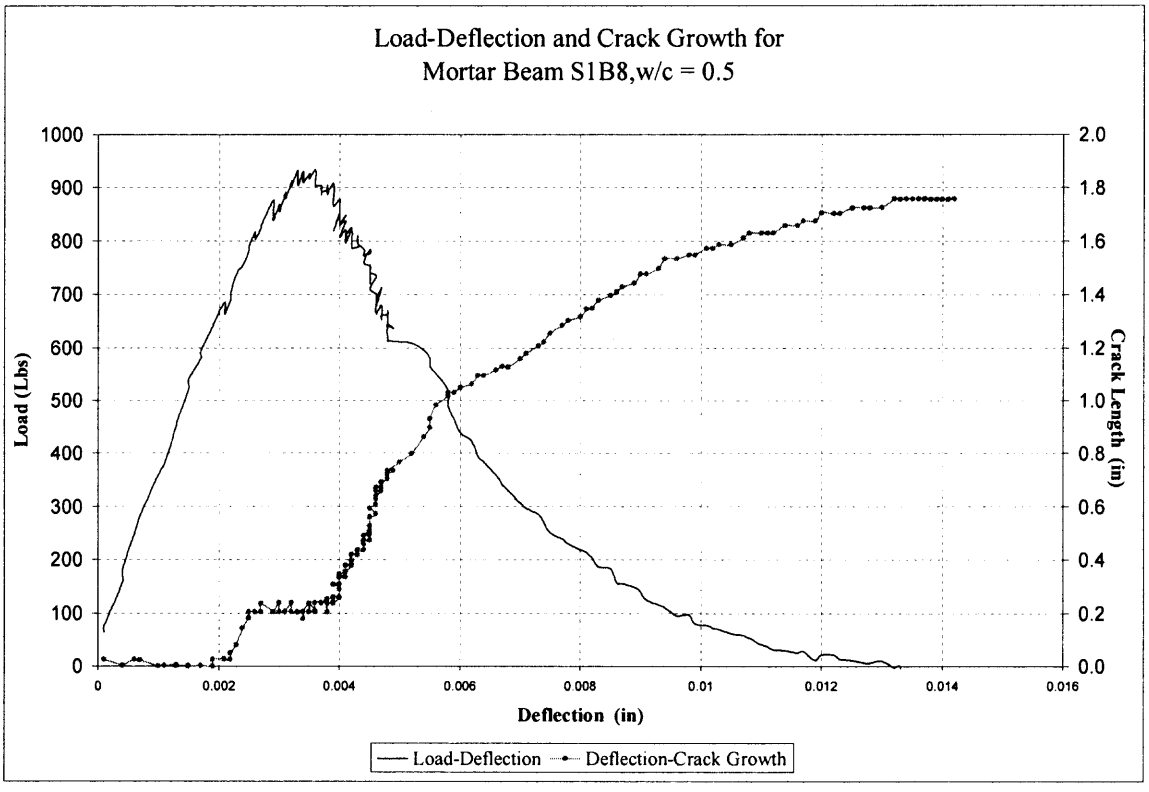

Figure 3.8 Load-Deflection curve with Crack Extension for Mortar Beam S1B8.

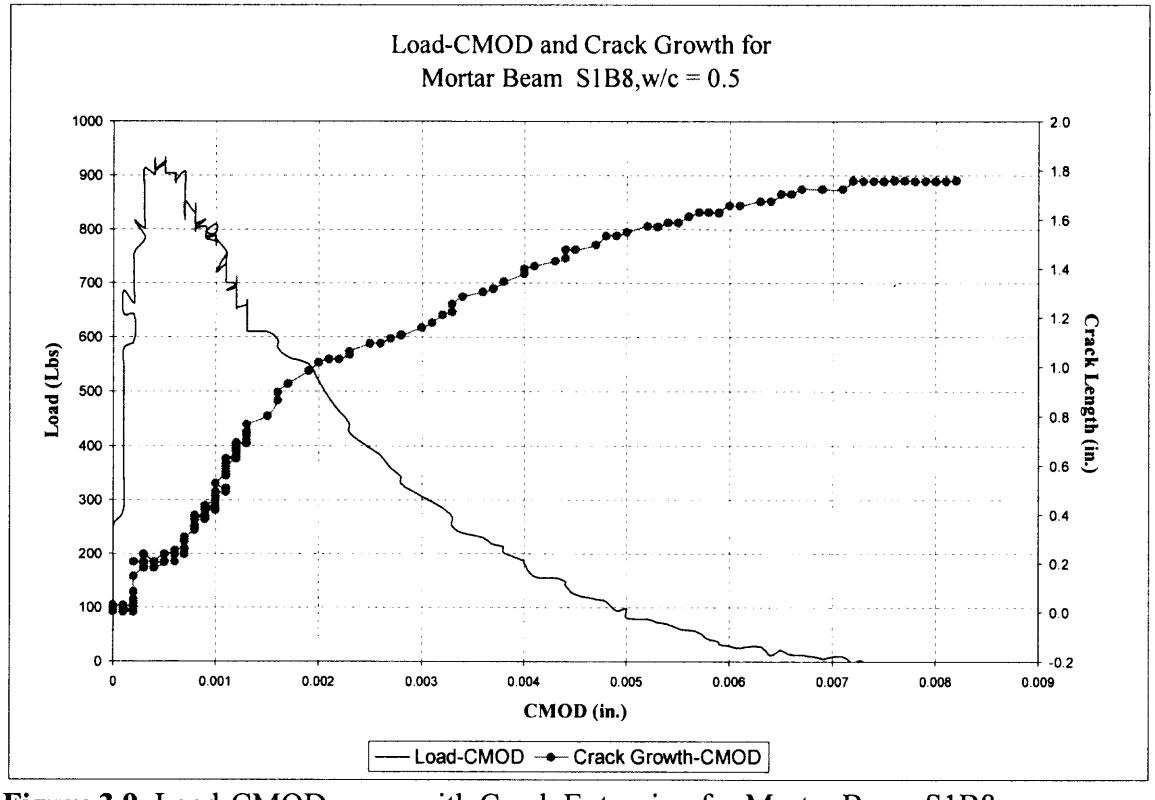

Figure 3.9 Load-CMOD curve with Crack Extension for Mortar Beam S1B8.

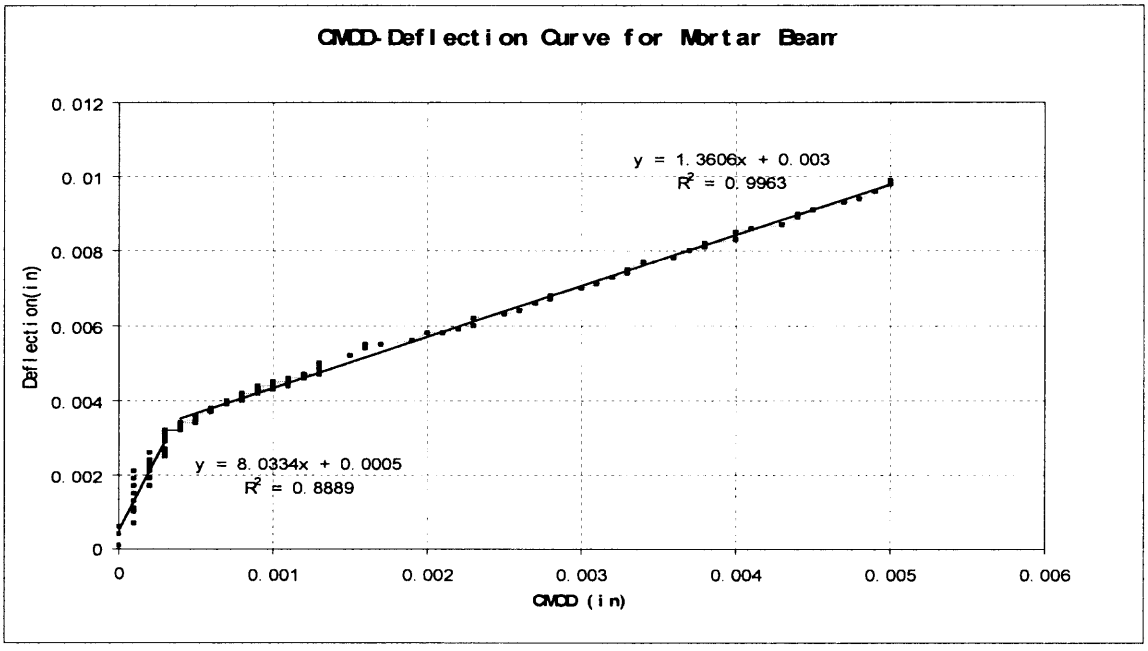

Figure 3.10 Deflection-CMOD Bilinear Relationship for Mortar Beam in Series I.

3.3 Series II Experimental Design and Results

3.3.1 Design of Series II Experiment

Three-point load bending test was introduced by Peterson (1980) and recommended by RILEM (1985) as standard test to investigate concrete fracturing behavior. Some formulas are also available to calculate fracture parameters based on this test setup. Almost all the tests in Series II are three-point load bending test on notched beam to calculate some fracture parameters from proposed model and some other available models (TPFM and Double K), with only one group using 4 point bending test as comparison.

The emphasis is made on testing specimens with different size of specimen and notch length to investigate the size-dependence of fracture paramters. The experiments design details are presented in Table 3.3 and test setup was illustrated by Figure 2.6.

Table 3.3 Series II Experiment Design

Material Mix	C	S	A	W
	1	2	3	0.5
Test Setup	Three-Point-load Bending Test			Pure Bending Test
Group No.	I	II	IV	III
t × b× S (in)	3×4. 5×18	3×3×12	6×6×24	4×4×28
a_0/b	20%, 21%,22%	20%,22%,26%, 37%,38%,48%	21%,23%	25.1%,28.5%

Note: C: cement; S: sand; W: water; A: aggregate; ρ: reinforcement ratio;
t: thickness of specimen; b: width of specimen; S: span; a_0: notch length.

3.3.2 Results of Series II Experimental

The typical load-CMOD curve and Load-Deflection curve from Series II experiments are presented in Figure 3.11 and Figure 3.12.

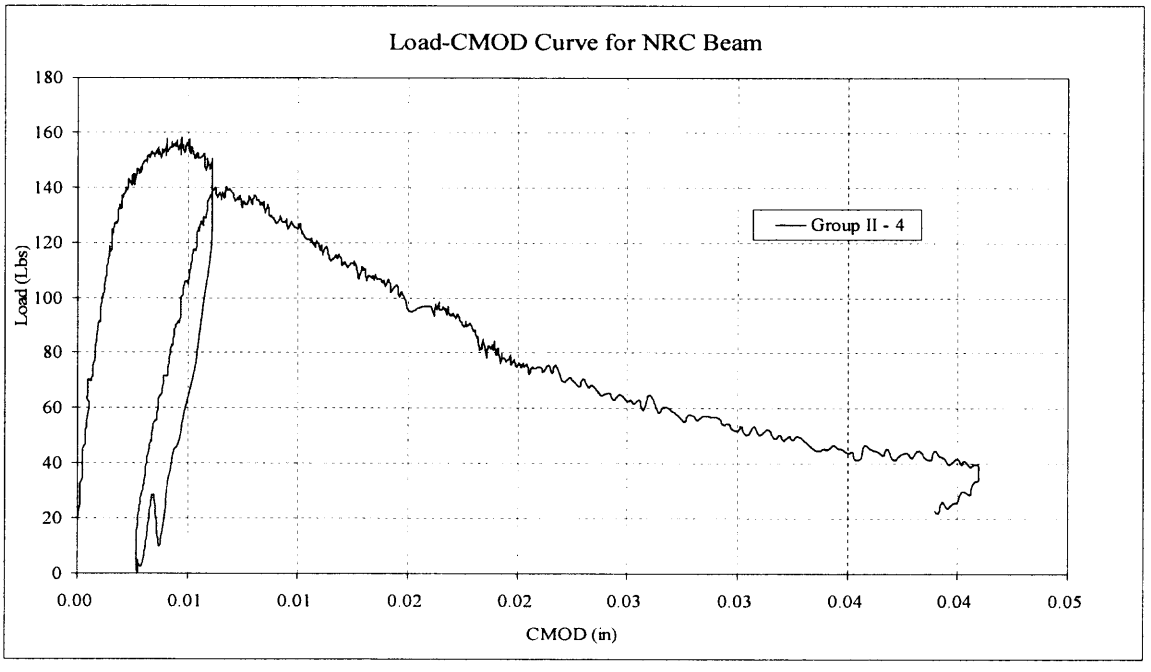

Figure 3.11 Load-CMOD Curve for NRC Beam S2GII B4.
(Thickness × Width× Span = 3×3×12, a_0=1.1 in)

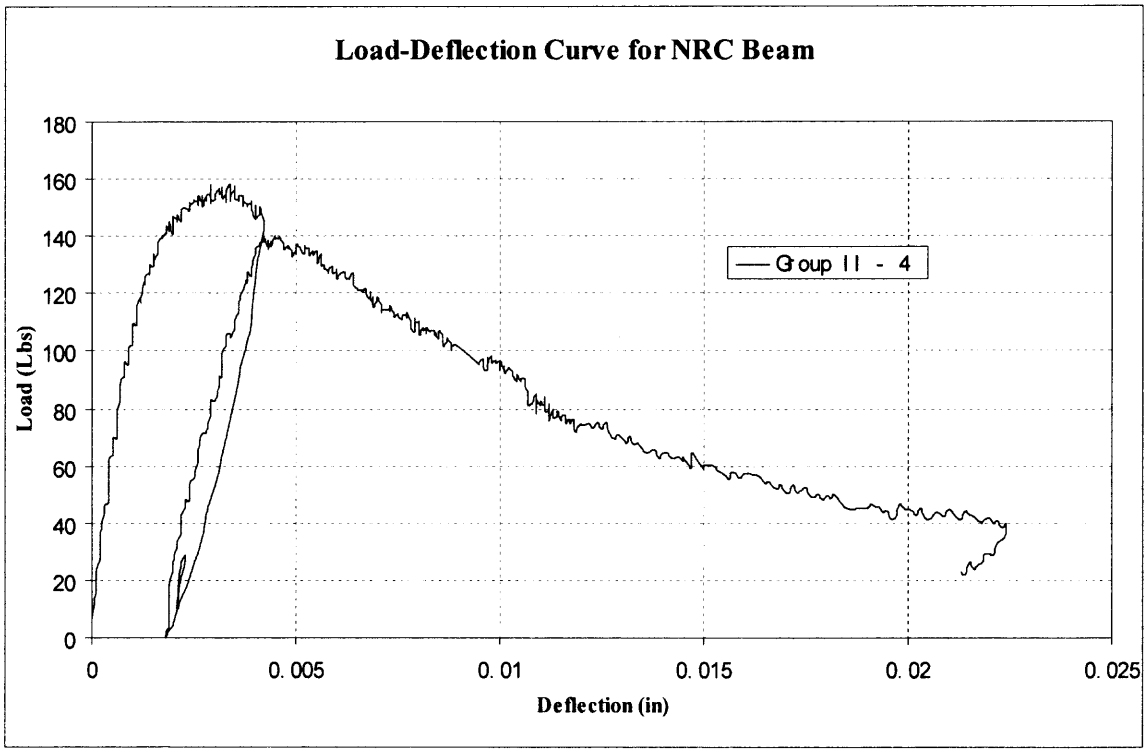

Figure 3.12 Load-Deflection Curve for NRC Beam S2GII B4.
(Thickness × Width× Span = 3×3×12, a_0=1.1 in)

3.4 Series III Experimental Design and Results

3.4.1 Design of Series III Experiment

In series III of experiments, reinforced concrete is mainly of interest. Presence of reinforcement, the tests on RC beams were further complicated. Diagonal tension failure , debounding between concrete and reinforcement are all happened in Series III experiments and can be seen in Figure 3.13, 3.14 respectively. Shear cracks were also observed as shown in Figure 3.15. Since flexure failure is of our primary interests, different methods are tried here to prevent those from happening. In first group tests, CFRP plate was glued on the both side of surface to increase the shear resistance. (Figure 3.17) and its setup can be demonstrated by Figure 3.16. At last, a beam with longer span

was used and stirrup and steel fiber were also applied in the shear portion (Figure 3.18) and its photograph is in Figure 3.19.

Figure 3.13 Bearing Failure during the Test.

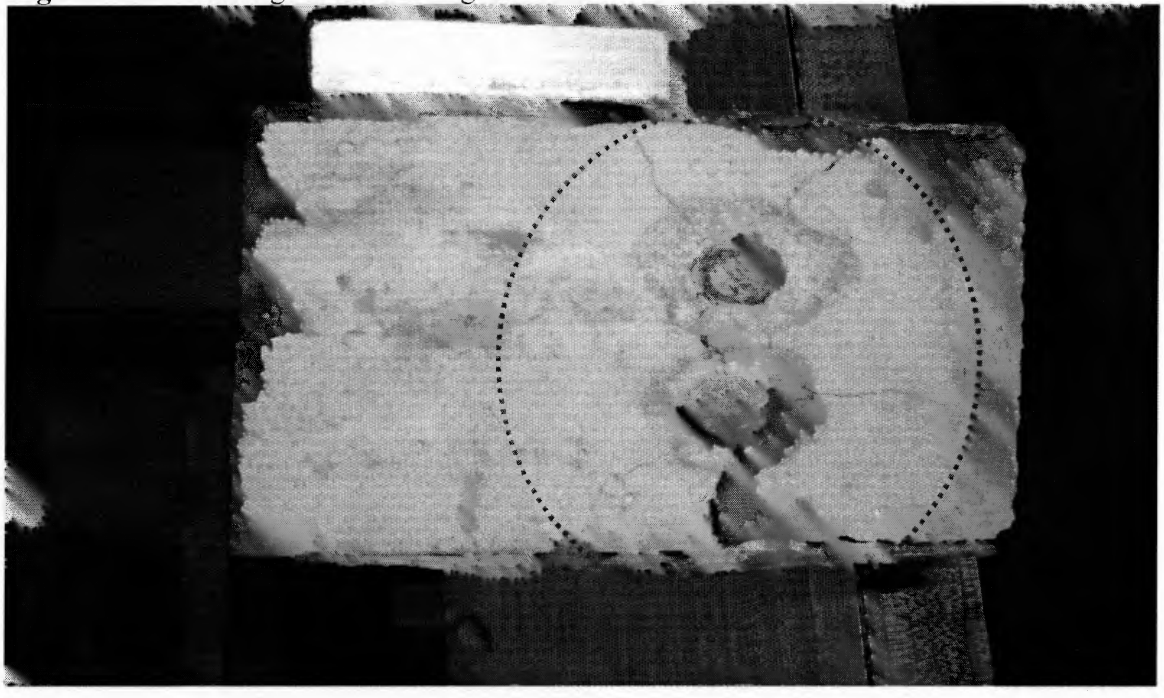

Figure 3.14 Debonding between Concrete and Rebar .

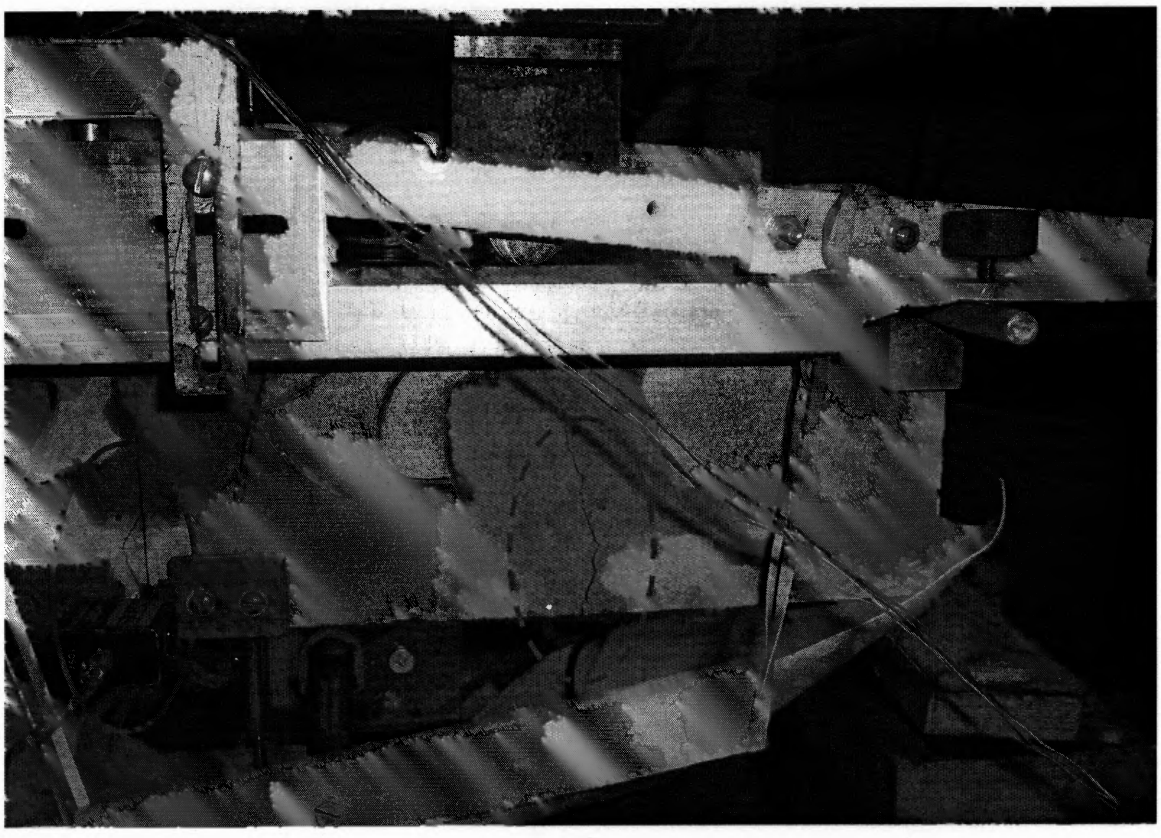

Figure 3.15 Shear Crack and Flexure Crack seen by water ink (circled by solid line is flexure crack and circled by dashed line is shear crack).

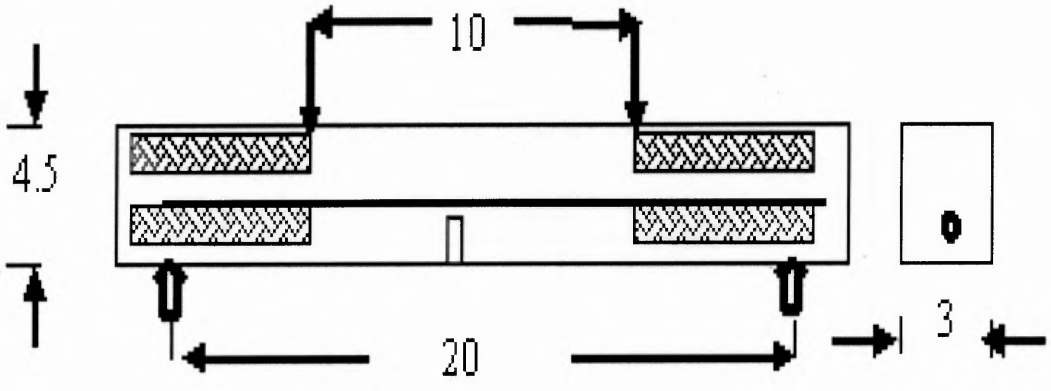

Figure 3.16 Test Setup for 4-Point Load Bending Test with CFRP Enforced on Specimen Surface. (Group I Series III).

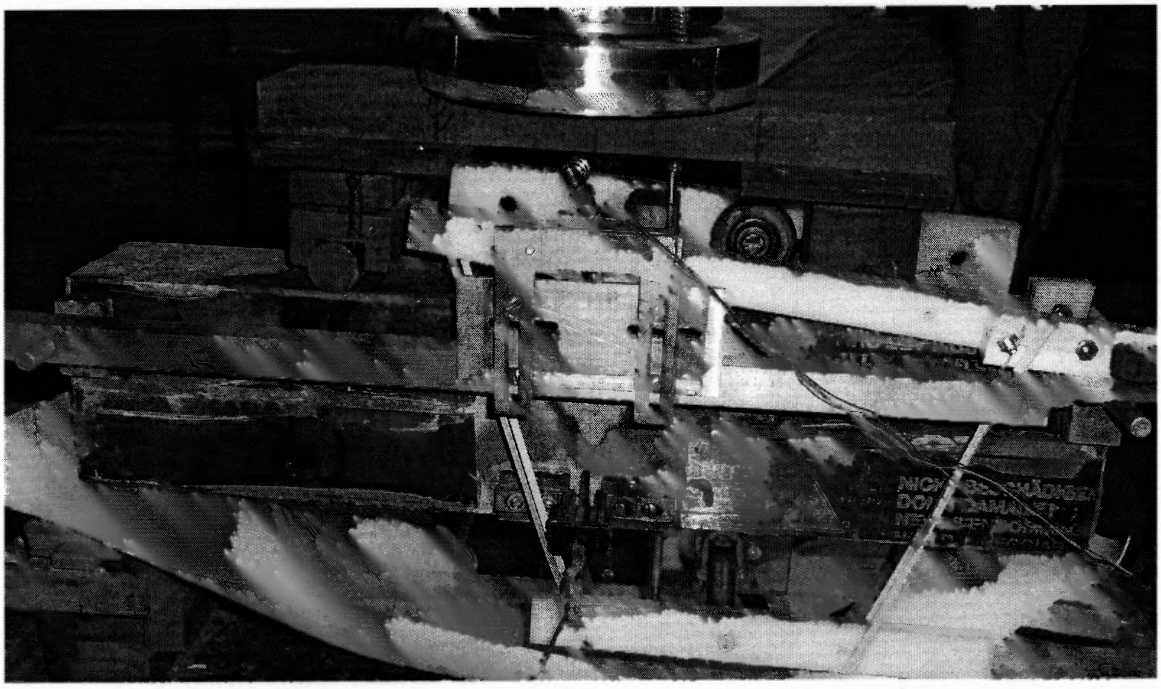

Figure 3.17 Photograph of 4 Point Load Bending Test with CFRP Enforced on Beam Surface (Group I Series III).

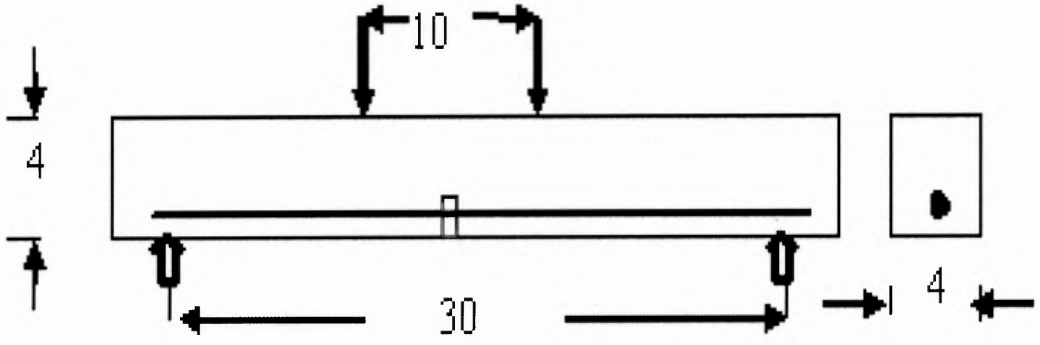

Figure 3.18 Testing Setup for Group III Tests in Series III.

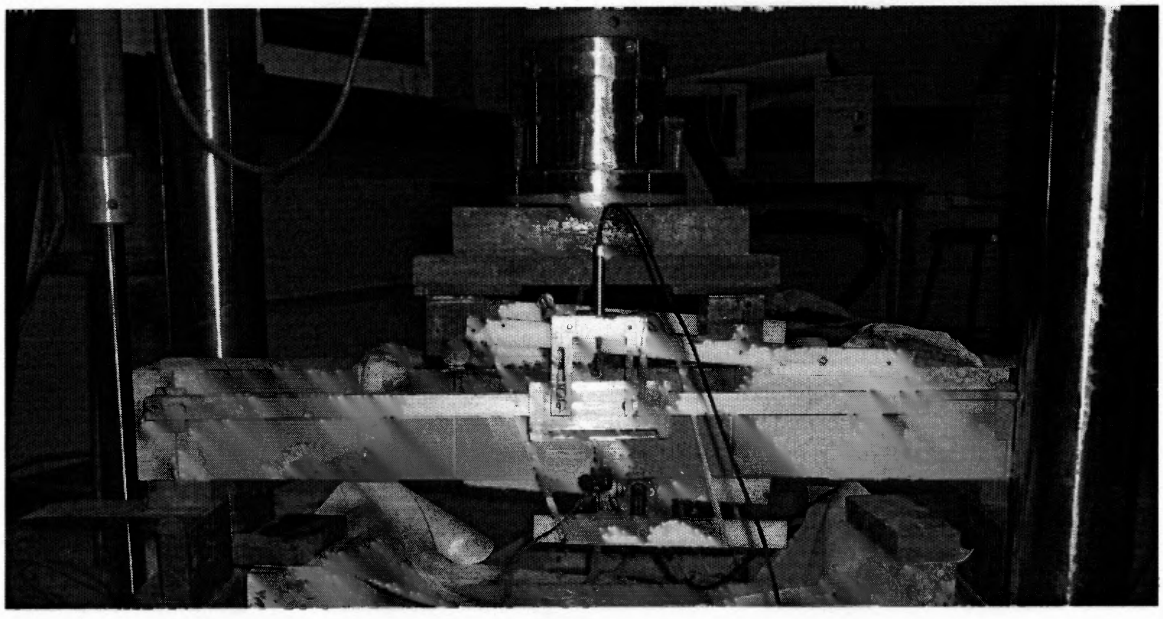

Figure 3.19 Photograph of Testing Setup for Group III in Series III Experiments

During this process, 4 point load bending tests without Ultrasonic device (Group II) were also performed. In this group tests, loading space was as short as 5 inches in order to prevent the beam from being deep beam. Its testing setup is illustrated in Figure 3.21 and its photograph can be seen in Figure 3.22 and Figure 3.23.

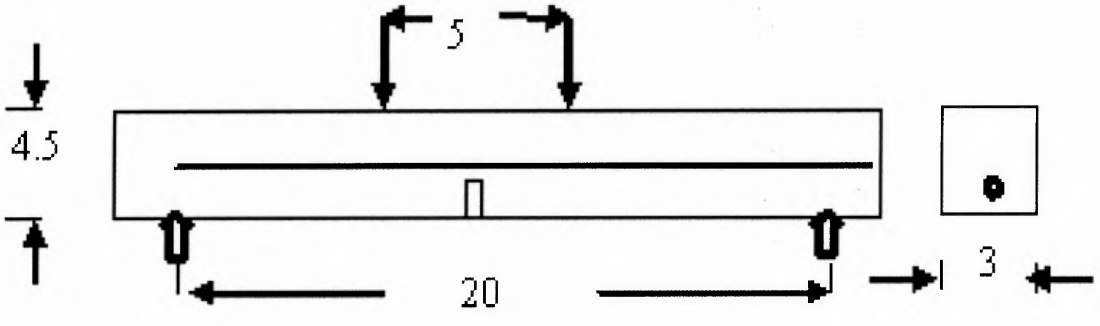

Figure 3.20 4 point load bending test setup without Ultrasonic device (Group II Series III).

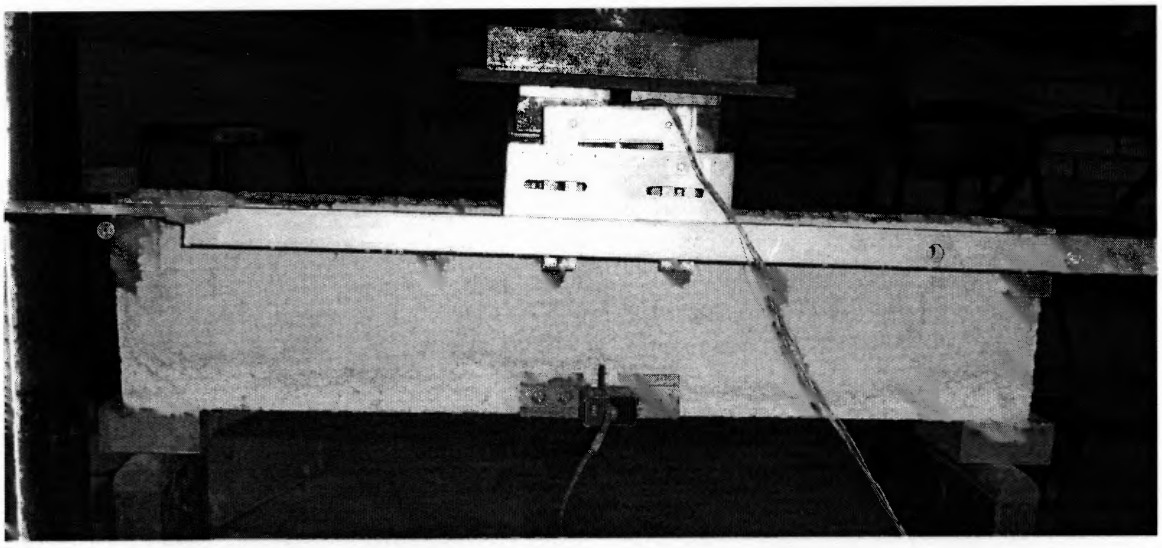

Figure 3.21 Photograph of testing setup for Group II in Series III (Front View).

Figure 3.22 Photograph of testing setup for Group II in Series III (Back View).

The entire series III of experiments are summarized in Table 3.4.

Table 3.4 Summary of Series III Experiments .

	Specimen No.	Specimen Configuration ($H \times t \times S \times a_0$)(in)	Test Age (day)	fc' (Psi)	E (Psi)	As (in^2)	ρ (%)	fy (Psi)
Group I	SIIIGIB1	4.5×3×20×1.0	29	4751		0.110	0.8%	4.00E+04
	SIIIGIB2	4.5×3×20×1.0	29	4751		0.220	1.6%	4.00E+04
	SIIIGIB3	4.5×3×20×1.0	29	4751		0.393	2.9%	6.00E+04
Group II	SIIIGIIB1	4.5×3×20×1.0	98	7045	3.32E+06	0.110	0.8%	4.00E+04
	SIIIGIIB2	4.5×3×20×0.6	103	7045	3.32E+06	0.110	0.8%	4.00E+04
	SIIIGIIB3	4.5×3×20×0.6	92	6914	1.98E+06	0.110	0.8%	4.00E+04
	SIIIGIIB4	4.5×3×20×1.3	98	6914	1.98E+06	0.110	0.8%	4.00E+04
	SIIIGIIB5	4.5×3×20×1.3	98	6914	1.98E+06	0.110	0.8%	4.00E+04
Group III	SIIIGIIIB1	4.5×3×20×1.5	14	5111	2.60E+06	N/A	N/A	N/A
	SIIIGIIIB2	4.5×3×20×1.5	21	5111	2.60E06	N/A	N/A	N/A
	SIIIGIIIB3	4.5×3×20×1.5	28	5100	2.41E+06	N/A	N/A	N/A
	SIIIGIIIB4	4.5×3×20×1.5	28	5890	7.37E+06	0.049	0.3%	3.60E+04
	SIIIGIIIB5	4.5×3×20×1.5	21	5022	6.21E+06	0.110	0.7%	4.00E+04
	SIIIGIIIB6	4.5×3×20×1.5	33	5300	5.33E+06	0.110	0.7%	4.00E+04
	SIIIGIIIB7	4.5×3×20×1.5	28	5598	7.10E+00	0.196	1.2%	6.00E+04
	SIIIGIIIB8	4.5×3×20×1.5	26	5156	4.65E+05	0.307	1.9%	6.00E+04
	SIIIGIIIB9	4.5×3×20×1.5	28	5890	7.37E+06	0.442	2.8%	6.00E+04
	SIIIGIIIB10	4.5×3×20×1.5	28	5399	4.00E+06	0.601	3.8%	6.00E+04

Note: H: Height of specimen; t: thickness of specimen; S: span; a_0: notch length.

3.4.2. Results of Series III Experimental

Typical load-deflection & Crack Growth and load-CMOD & Crack Growth for reinforced concrete can be seen in Figure 3.23 and Figure 3.24.

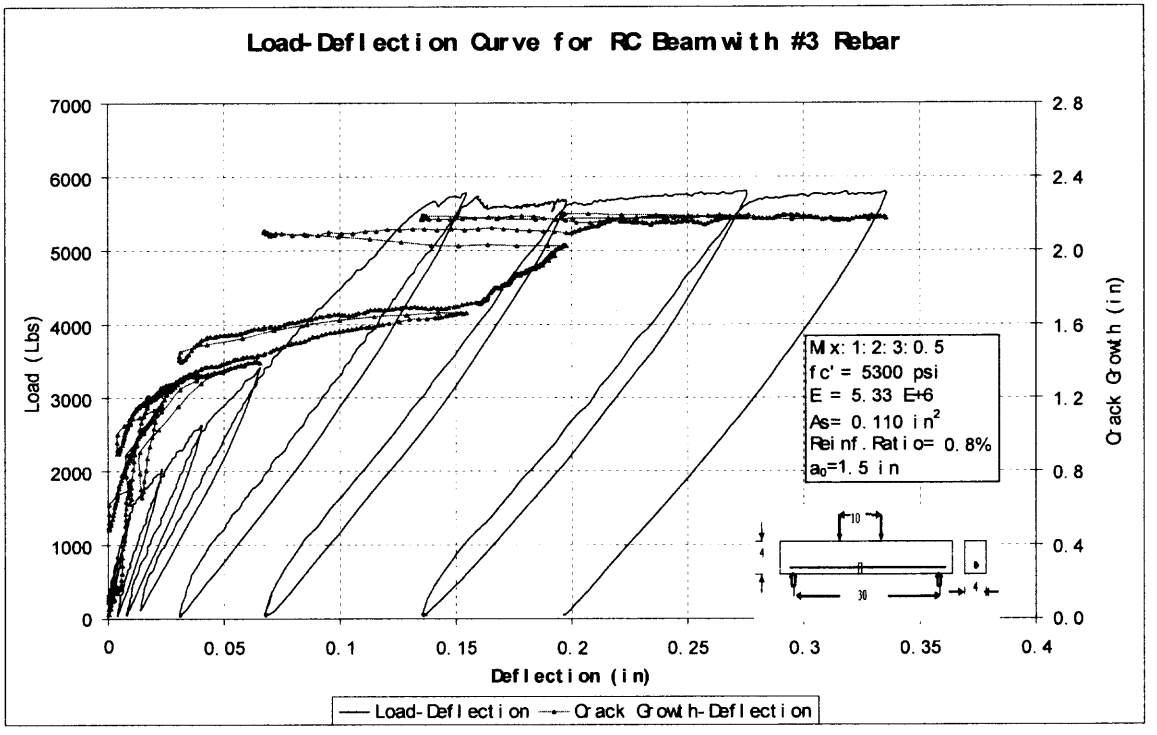

Figure 3.23 Load-Deflection &Crack Growth for NRC Beam S3GIII B6(0922-1025).

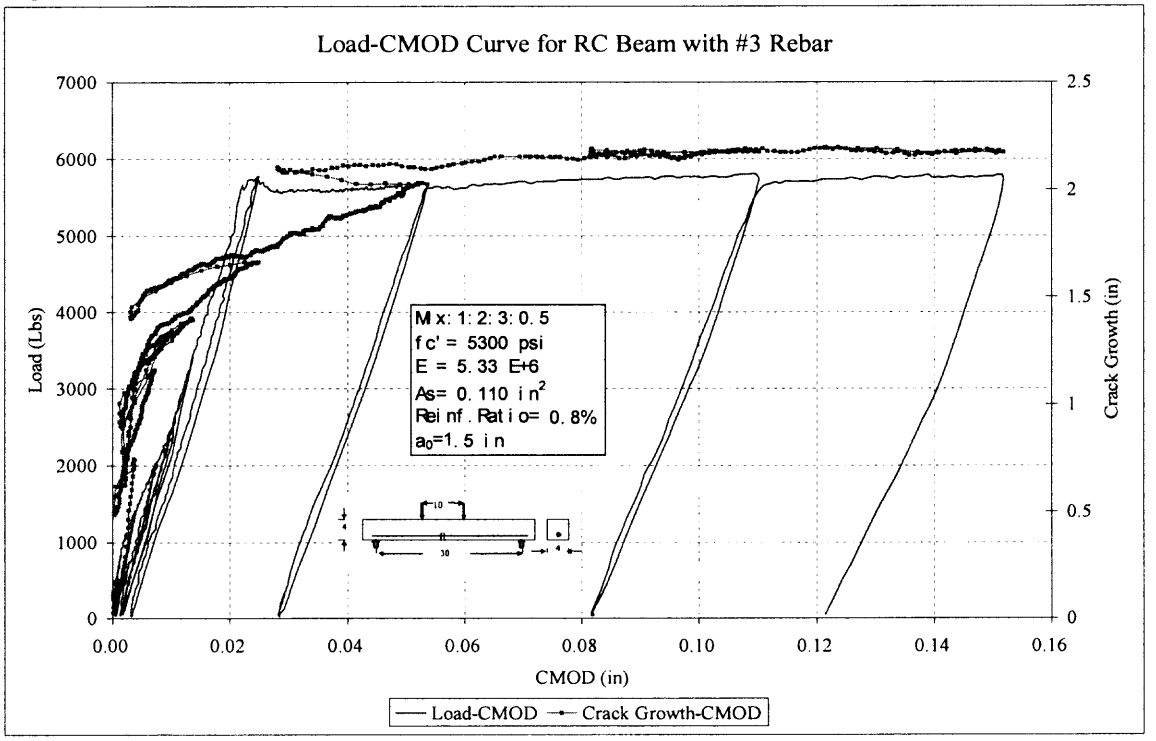

Figure 3.24 Load-CMOD &Crack Growth for NRC Beam S3GIII B6(0922-1025). Further analysis will be performed in Chapter 5.

CHAPTER 4

PROPOSED FRACTURE MODEL,RESULTS AND DISCUSSION

A new nonlinear fracture model, Effective Compliance Fracture Model (ECFM) is presented in this chapter. And experiment results from different sources will be used to evaluate the size-dependence of parameters in this proposed model. Comparison of proposed model with TPFM, Double K model will also be made according to some available experimental results.

4.1 Critical Fracture Toughness on Plain Concrete

4.1.1 Fracture Propagation Process in Concrete and Assumptions

It has been proposed by many researchers that the whole process of fracture propagation in concrete includes crack initiation, stable crack propagation and strain softening stage. It can be illustrated by Figure 4.1 and experimental observation for crack imitation and stable crack propagation prior to maximum load detected by laser speckle interferometry (Shilang xu,1998) is shown in Figure 4.2.

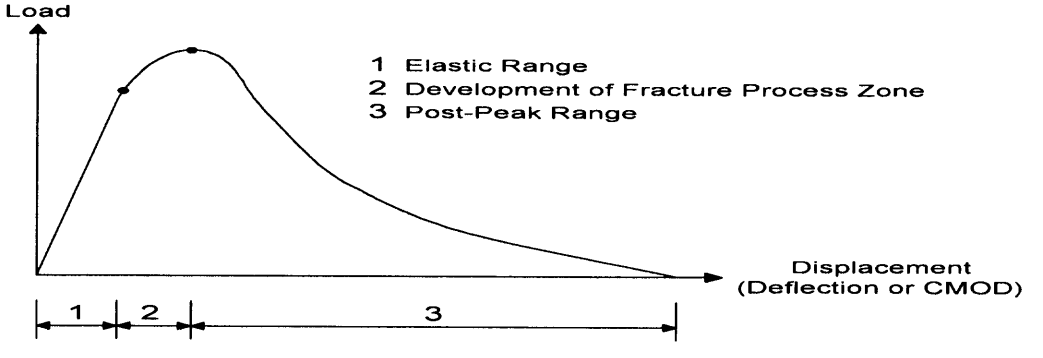

Figure 4.1 Three-Stage Fracturing Process in Concrete Specimen .

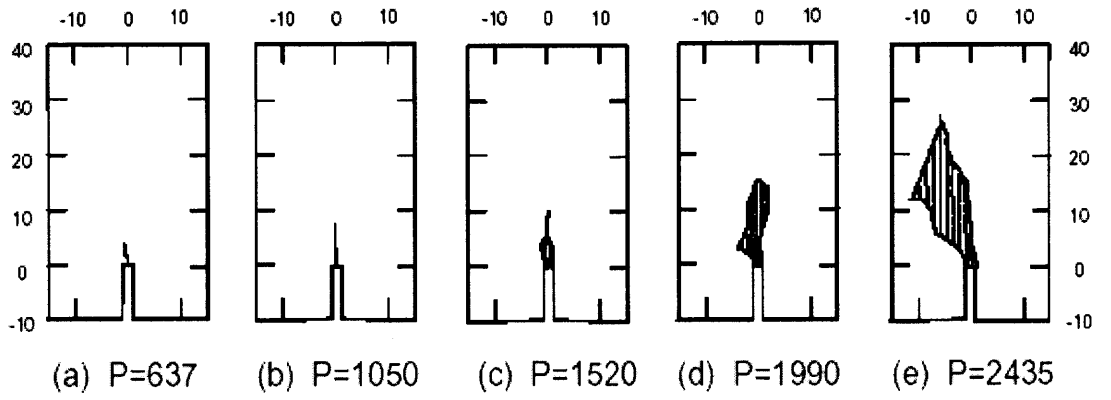

Figure 4.2 Fracture Process Zone developments at different load level.
(Load: Lbs; Dimension: inches)

From the load-displacement curve in Figure 4.1, when specimen is in stage 1, elastic behavior will be demonstrated and at the end of this stage, micro-cracks starts to grow as showed in Figure 4.2 (a). Continuous increases in the level of the load lead to the development of micro-cracks in a narrow strip (Figure 4.2 (b), (c), (d)). And this narrow strip is normally called as "*Fracture Process Zone*". In Figure 4.2 (d), load reaches the maximum value and it is always believed that fracture process zone has been fully developed at the same time and will shift forward with constant size in the post-peak range. Traction-free crack initiates also after the peak load. From micro-crack initiation to the onset of traction-free crack development, it is called stable crack propagation. During the post-peak range, strain-softening will be exhibited which is characterized by displacement increasing and load decreasing. If load control is used in the test, specimen will fail by unstable crack propagation at the end of stage 2.

Consequently, onset of unstable crack propagation, which is corresponding to the point where maximum load occurs become critical for plain concrete. According to

LEFM, fracture toughness could be used to indicate the fracture resistance and its critical value indicate the onset of unstable crack propagation of brittle material. When people attempted to apply this parameter to concrete, its value showed size-dependence for different size specimen. Therefore results from small size specimen can not be extrapolated into large size structural element in practice. Although it is possible to conduct large scale structural tests, they can only be done with limited number of specimens, limited geometries, and limited loading configurations, and with great expense. To overcome this limitation, size-independences of fracture parameters in the fracture model become critical.

Through literature review, it can be found out that even though a huge amount of investigations had been carried out during the past decades to pursue size-independent parameters to indicate fracture resistance of concrete, there are still no final conclusions. This study provides another approach to evaluate the fracturing condition at the peak load based on standard three-point load bending test.

Assumptions about fracture propagation in Concrete based on experimental observations and widely accepted results. Some assumptions were made here:

1. Microcrack initiates at the point and direction where the principle tensile stresses reach maximum or tensile strength ft and the damaged materials with micro-cracks still can transfer stresses and behave strain softening;
2. All the damaged material is enclosed in fracture process zone during the fracture propagation prior to the peak load, outside responses linear elastically;
3. Maximum load capacity of specimen can be indicated by the Critical Stress Intensity Factor (or called as Fracture Toughness) which is calculated at the tip of fracture process zone at the peak load point, which can be considered as material property and independent of specimen size;
4. In the post-peak regime, depending upon the geometry of the specimen, the rate of loading, and the method of loading, further crack growth may occur at a steady

state value as fracture toughness and fracture process zone will also keep constant size and only shift forward until enter the compressive area.

4.1.2 Critical Fictitious Crack length and Compliance Method

According to LEFM, crack length is always required. Therefore how to evaluate the fictitious crack length becomes critical when apply LEFM on concrete. During the past decades, researchers devoted a lot of efforts to investigate the critical fictitious crack length, including:

1. M. Wecharatana and S.P .Shah proposed a regression formula in 1982;
2. Karihaloo and Nallathambi proposed another regression formula in 1986 taking account of aggregate size and load-deflection relationship;
3. Bazant, Z.P. and Pfeiffer, P.A in 1987 proposed size-effect method;
4. TPFM applied a compliance method to evaluate the fictitious crack length and this method was also adopted by Double K model. And this method has also been published By RLEM Committee.

In this work, modified compliance method will be adopted to evaluate the length of critical fictitious crack length. According to Figure 2.7, there are three kinds of compliances we can use: (1) original compliance (C_i), (2) Unloading Compliance (C_u), (3) Secant Compliance (C_s).

When beam is in elastic range (Figure 4.1), LEFM theory is valid and initial compliance from Figure 2.7 can be used in LEFM formula. After micro-cracks initiates from the tip of the pre-molded notch, non-linearity appears in load-displacement curve and compliance varies at different load levels and LEFM formula are not applicable for the damaged concrete beam. In order to simulate this nonlinearity with LEFM theory, TPFM used unloading compliance to extract elastic displacement from the total displacement at the peak load and plug this elastic displacement into LEFM formula to

achieve critical crack length; Bazant and Shilang xu both believed that it was not reasonable to only use elastic displacement since non-elastic part of displacement also contributes to the fracture propagation in concrete specimen. Then Bazant in Size-Effect Model assumed the size of the concrete beam to be infinite to make LEFM valid; Shilang xu suggested using secant compliance based on his proposed linear asymptotic superposition assumption.

4.1.3 Linear Elastic Equivalent Beam

In order to solve those arguments hereinbefore and make LEFM applicable, Linear Elastic Equivalent Beam is proposed as below.

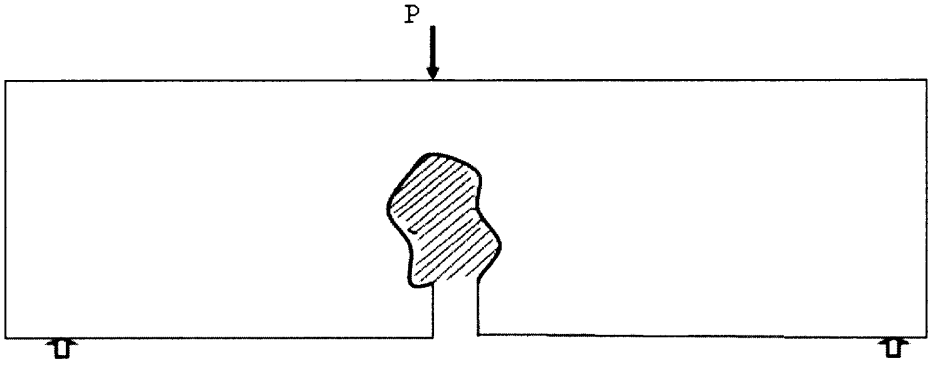

(a) 3 point bending beam with damaged nonlinear fracture process zone

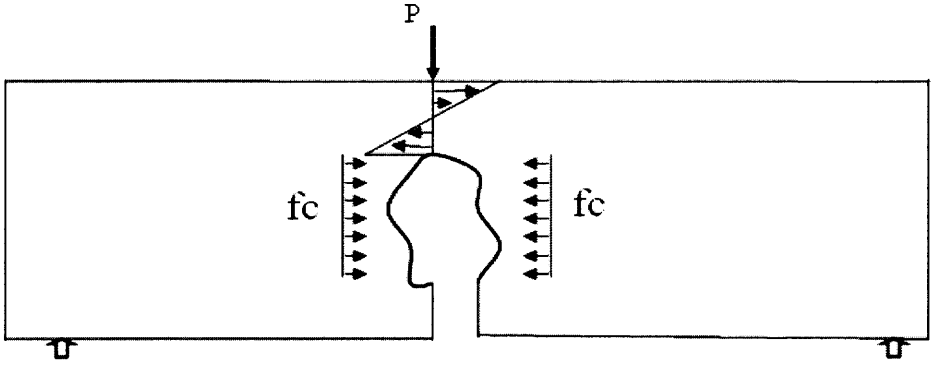

(b) Linear Elastic Equivalent Beam with Extra Uniform Load

Figure 4.3 Schematic Illustration of Linear Elastic Equivalent Beam .

First of all, we have to know what really happened intrinsically during fracture propagation within concrete specimen at the peak load. From Figure 4.3a, we can see a damaged fracture process zone within a concrete beam. According to assumption (2) mentioned above, all the material outside this fracture process zone behaves elastically. Considering if there is no fracture process zone but a traction-free crack, LEFM is applicable here absolutely. Therefore, we isolate this damaged fracture process zone and apply cohesion force along the fictitious Griffith traction-free crack contour which is shown in Figure 4.3b. Under this condition, the stress distribution at the tip of fictitious crack would not be disturbed. In other words, stress intensity factor at the tip of this fictitious crack tip is same as that at the tip of damaged fracture process zone in Figure 4.3a. What is more important is that this equivalent beam satisfies the restriction of LEFM at this moment. As a result, crack propagation of concrete beam in Figure 4.3a can be investigated by LEFM on this linear elastic equivalent beam.

4.1.4 Proposed Effective Compliance Method to Evaluate Critical Fictitious Crack Length

Based on method and procedure proposed by RILEM Technical Committee 89-FMT (1990a), the Young's modulus for original beam can be predicted using the following formula based on Load-CMOD curve:

$$E = \frac{6SV(\alpha)}{C_i d^2 b} \tag{4.1}$$

where S = Specimen loading span; b = width of the beam; d = beam depth.

$$\alpha = \frac{(a_0 + h)}{(d + h)};$$

a_0 = initial notch depth; h = thickness of holder of clip gauge.

$$V(\alpha) = 0.76 - 2.28\alpha + 3.78\alpha^2 - 2.04\alpha^3 + \frac{0.66}{(1-\alpha)^2} \qquad (4.2)$$

C_i = the initial compliance experimentally determined from the load-CMOD curve (See Figure 2.7)

According to compliance method, a_c can be calculated by using E from formula 4.1 and knowing the corresponding compliance at the peak loading condition. The critical crack length a_c here is the total of critical fictitious crack length l_p and notch length a_0. For the elastic equivalent beam, the loads which contribute to the crack mouth opening displacement or CMOD are external concentrate load P and extra distributed cohesion force f_c.

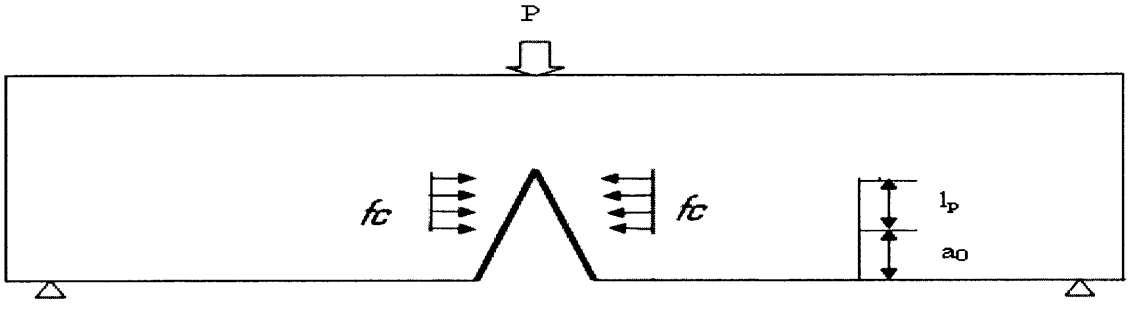

Elastic Equivalent Beam with External Concentrated Load P and Distributed Cohesion Force

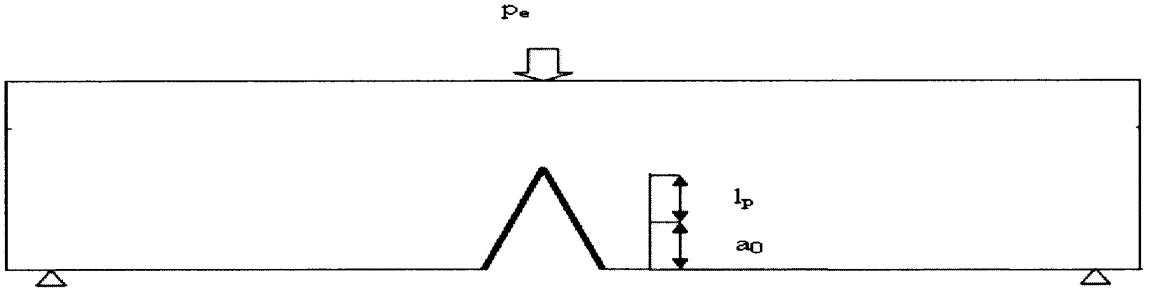

Elastic Equivalent Beam with Only Effective External Concentrated Load *Pe*

Figure 4.4 Superposition Scheme of Effective Loading .

If we only consider external point load P, secant compliance should be used here. If we only consider the elastic part of CMOD, we use unloading compliance. We can see neither condition could reflect the real load condition at this moment.

In fact, formula 4.1 is from LEFM formula calculating the crack opening displacement. Due to the lack of close form solution of CMOD of a beam subjected to distributed cohesion force, the external concentrate load P and the cohesion force are transformed into one effective external concentrated load:

$$p_e = p - \frac{2}{3s}\left(f_t l_p^{\,2} b\right) \tag{4.3}$$

This effective point load P_e have same moment effects at the tip of fictitious crack as that by both external point load and extra distributed cohesion force. The superposition scheme can be illustrated by Figure 4.4.

Using this effective load, it is obvious that the compliance used to calculate the critical length of fictitious crack can be expressed by this formula:

$$C_e = \frac{CMOD_c}{P_e} \tag{4.4}$$

In which $CMOD_c$ is crack mouth opening displacement experimentally determined at the peak load and P_e is effective load determined by formula (4.3).

Plugging in corresponding parameters at the peak load, formula (4.1) is transformed into:

$$E = \frac{6Sa_e V(\alpha_e)}{C_e d^2 b} \tag{4.5}$$

In which a_e is the effective crack length and C_e is the effective compliance calculated by formula (4.4). Trying different a_e to make E calculated by (4.5) equal to E calculated by (4.1), then a_e is the critical fictitious crack length.

4.1.5 Cohesive Force

The distribution of cohesive force within the fracture process zone is determined by selected stress-crack opening displacement relationship. The most reliable stress-displacement relation is supposed to be the one directly obtained from the uniaxial tension test. While conducting a direct tension test to observe the post-peak tensile response of concrete and other brittle materials may seem to be rather difficult, but no impossible, several researchers have successfully employed the closed-loop strain control to observe the post-peak stress-displacement responses. Different empirical stress-displacement relationships have been proposed by Reinhardt, Wecharatana, Cintora and Chiou, Peterson. In this study, the simplest stress-displacement relation proposed and used by Peterson will be applied. The linear stress-displacement function can be written as follows:

$$\frac{\sigma}{f_t} = (1 - \xi) \tag{4.6}$$

where

σ is cohesive force,

f_t is the maximum tensile strength;

ξ represents the ratio of crack opening displacement to maximum crack opening displacement at $\sigma = 0$.

4.1.6 Critical Fracture Toughness Calculation

From the linear elastic equivalent beam in Figure 4.3b, we can see that any stable crack advance will introduce additional cohesion force which is intrinsic crack resistance. A critical length of this fictitious crack indicates the maximum crack resistance for traction-free crack initiation which occurred at the peak load. Beyond that, any fictitious crack

extension will lead to same distance traction-free crack propagation and the length of fictitious crack will keep constant and shift forward as reported by other researchers (Methi Wachiratana, 1982 and Shilang xu in 1998). Due to the difficulties to figure out the magnitude and distribution of cohesion force, indirect method has to be proposed.

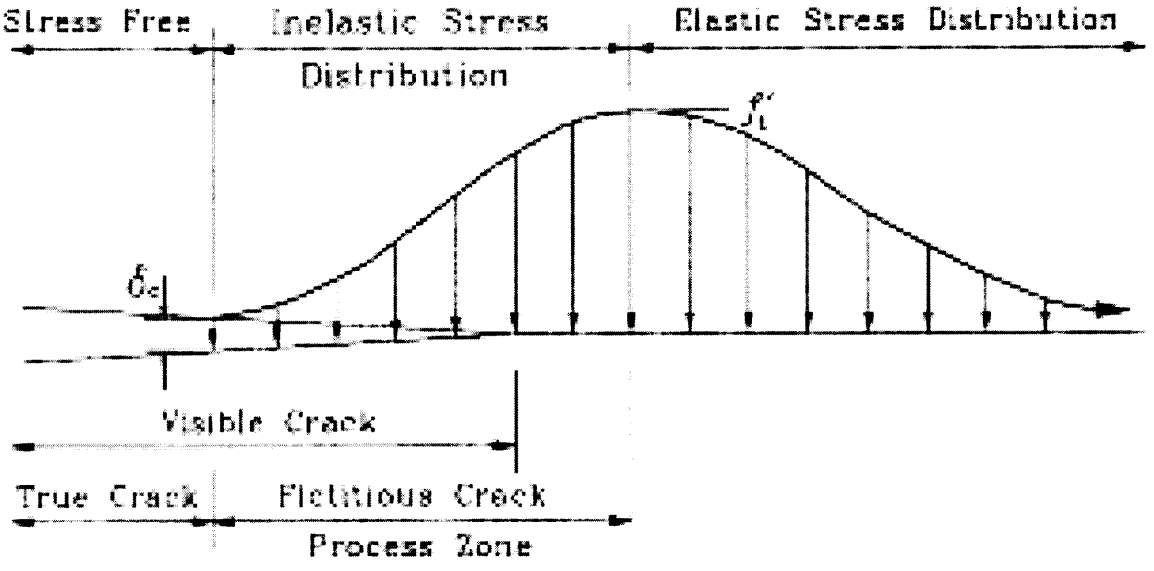

Figure 4.5 Stress Distribution along the Crack Axial During Crack Propagation.

Due to existence of micro-cracks in front of notch tip, stress concentration in front of traction-free crack tip disappeared (Figure 4.5) and, theoretically as a result, stress intensity factors due to external load and internal cohesion force should cancel each other. This condition can be expressed by following formula:

$$K = K_{IP} + K_{IC} = 0$$

Then $$K_{IP} = -K_{IC} \qquad (4.7)$$

Therefore the critical stress intensity factor at the tip of fictitious crack can indicate the crack resistance to create traction-free crack and can be treated as a material parameter and size-independent.

Based on the equivalent beam which responses elastically, its critical stress intensity factor can be calculated by inserting maximum load P_{max}, and effective crack length a_e into the LEFM's formula and can be written as :.

$$K_{Ip} = \frac{3(P_{\max} + 0.5W)S\sqrt{\pi a_e}F(\alpha_e)}{2d^2 b} \tag{4.8}$$

Where

$$F(\alpha_e) = \frac{1.99 - \alpha_e(1-\alpha_e)(2.15 - 3.93\alpha_e + 2.7\alpha_e^{\,2})}{\sqrt{\pi}(1+2\alpha_e)(1-\alpha_e)^{3/2}} \tag{4.9}$$

$a_e = l_p + a_0$, $\alpha_e = \frac{a_e}{d}$; $P_{\max}$ = the measured maximum load; $W = W_0 \frac{S}{L}$;
W_0 = self-weight of the beam; L = length of beam, b= the thickness of beam;

d= the depth of beam .

The maximum errors between obtained by Equation (4.8) and the accurate results by boundary collocations method in (Srawley and Gross , 1972) is less than 2.0 percent. It can meet the accuracy required in practical engineering calculations.

4.2 Critical Fracture Toughness Calculation Procedure

The whole procedure to calculate critical fracture toughness will be listed as follows:

1. Using Formula (4.1) and (4.2) to calculate Young's Modulus of concrete specimen under consideration or using Young's Modulus from Compression Test directly;

2. Try a critical crack length to calculate Young's Modulus using Formula (4.5).

3. Effective compliance in Formula (4.5) is determined by Formula (4.4) and effective load is determined by Formula (4.3) by inserting the tentative critical crack length;

4. Different critical crack length and iteration procedure will be tried until the calculated Young's Modulus using Formula (4.5) is equal to the one from Step (1);

5. Insert the critical crack length from step (4) and maximum load from test into Formula (4.8) to calculate critical stress intensity factor from the external load;

6. The critical stress intensity factor from step (5) is fracture toughness which can indicate the fracture resistance of the plain concrete specimen under consideration;

7. For reinforced concrete, critical stress intensity factor is the resultant of critical stress intensity factor due to concentrate external load and critical stress intensity factor due to the reinforcement tension. The details will be discussed in the future;

8. The prediction of load-CMOD curve of post-peak range will be make using assumption (4) by extension traction-free crack length and keep constant of fictitious crack length. It is also a part of future work.

4.3 Experimental Verification and Parametric Analysis of Proposed Model

As a fracture model on concrete, the corresponding fracture parameters defined in the model are required to be useful in practice and to be measurable in the experiments. The characteristics of them should be only dependent on the material properties for being able to extrapolate into the larger structures.

According to the determination method of the proposed effective compliance model, The measurements of the maximum load P_{max} and the critical crack mouth opening displacement $CMOD_c$ in three-point bending beam tests and Young's modulus and Compressive Strength in Compressive Tests are required to calculate critical fracture toughness. Experiments on three point bending beams had been carried out by various researchers (Jenq and Shah, 1985a,1985b; Nallathambi and Karihaloo, 1986, 1989, 1990; Swartz and Go, 1984; Swartz and Refai,1987a; Refai and Swartz, 1987b; Karihaloo and Nallathambi, 1991; Kim, 1996, Rajen Navaluker 1996, Shilang xu and Reinhardt, 1998).

However, most of published literature did not supply the complete information of P-CMOD curves for all tested beams. Only in the report of Kim's dissertation (1996) and Shilang xu's paper (1998) enclosed complete P-CMOD curves measured from all tested beams and Young's modulus and Compressive strength. So, except the results measured from the experiments of Series II of three-point bending beams, Kim and Shilang xu's experimental data are also utilized to evaluate the proposed effective compliance model. The results of proposed model parameters determined by Series II experiments and Kim's experiments are presented in Table 4.1 and Table 4.2.

It should be noted here is that in Shilang xu's experiments, only one size specimens were tested with variation of notch/depth ratio, so size-independence of fracture parameters in proposed model from specimen size can not be verified. But Kim's experiments and our series II experiments are designed perfectly for specimen size-independence verification.

Table 4.1 Results of Fracture Parameters in Proposed Model Determined using Kim's Experimental Data.

Test No.	Depth (in)	Notch-Depth Ratio (%)	Scant Compliance Cs	Effective Secant Compliance Ce	Calculate Young's Modulus (E) Using Ce	Critical Effective Crack Length ac	ac/d	Critical Stress Intensity Factor Kic
1	2	3	4	5	6	7	8	9
S1	3	20%	1.451E-06	1.473E-06	3.12E6	0.963	0.321	938
S2	3	33%	2.218E-06	2.232E-06	3.12E6	1.202	0.401	909
S3	3	40%	2.865E-06	2.876E-06	3.12E6	1.346	0.449	911
S4	3	50%	4.651E-06	4.665E-06	3.12E6	1.607	0.536	792
M1	4.5	20%	1.349E-06	1.368E-06	3.12E6	1.380	0.307	943
M2	4.5	33%	2.178E-06	2.192E-06	3.12E6	1.787	0.397	940
M3	4.5	40%	2.780E-06	2.789E-06	3.12E6	1.992	0.443	929
M4	4.5	50%	4.690E-06	4.707E-06	3.12E6	2.417	0.537	843
L1	6	20%	1.216E-06	1.228E-06	3.12E6	1.718	0.286	912
L2	6	33%	2.226E-06	2.243E-06	3.12E6	2.405	0.401	915
L3	6	40%	2.826E-06	2.837E-06	3.12E6	2.675	0.446	900
L4	6	50%	4.532E-06	4.545E-06	3.12E6	3.187	0.531	868

Table 4.2 Results of Fracture Parameters in Proposed Model Determined using Wu's Series II Experimental Data.

Test No.	Depth (in)	Notch-Depth Ratio (%)	Scant Compliance Cs	Effective Secant Compliance Ce	Calculate Young's Modulus (E) Using Ce	Critical Effective Crack Length ac	ac/d	Critical Stress Intensity Factor (Kic)
1	2	3	4	5	6	7	8	9
I-2	4.75	20%	4.494E-06	5.409E-06	4184514	2.890	0.608	1963
I-3	4.75	21%	3.316E-06	3.711E-06	4467941	2.650	0.558	1788
I-4	4.75	22%	3.647E-06	4.171E-06	4541796	2.755	0.580	1819
II-1	3	38%	1.396E-05	1.628E-05	3557704	2.208	0.736	2324
II-2	3	48%	1.917E-05	2.341E-05	4139255	2.370	0.790	2216
II-3	3	26%	7.791E-06	8.876E-06	3324562	1.945	0.648	2270
II-4	3	37%	9.905E-06	1.138E-05	4021395	2.123	0.708	2223
II-5	3	22%	6.719E-06	7.984E-06	3337600	1.900	0.633	1926
II-6	3	20%	4.558E-06	5.367E-06	4399543	1.845	0.615	1892
IV-1	6	21%	2.020E-06	2.367E-06	4693743	3.633	0.606	2135
IV-3	6	23%	1.528E-06	1.712E-06	4694417	3.316	0.553	1751

Table 4.3 Results of Fracture Parameters in Proposed Model Determined using Shilang Xu's Experimental Data

Test No.	Depth (in)	Notch-Depth Ratio (%)	Scant Compliance Cs	Effective Secant Compliance Ce	Calculate Young's Modulus (E) Using Ce	Critical Effective Crack Length ac	ac/d	Critical Stress Intensity Factor Kic
1	2	3	4	5	6	7	8	9
102	7.87	20%	7.093E-07	7.205E-07	5500542	2.710	0.344	1544
402	7.87	20%	5.859E-07	5.915E-07	5344436	2.370	0.301	1114
3402	7.87	20%	9.061E-07	9.265E-07	4957246	2.933	0.373	1678
3502	7.87	20%	8.715E-07	8.956E-07	5339683	2.994	0.380	1532
3602	7.87	20%	6.843E-07	6.884E-07	4270023	2.262	0.287	1280
303	7.87	30%	1.149E-06	1.164E-06	4867663	3.249	0.413	1387
2603	7.87	30%	1.215E-06	1.230E-06	4517658	3.220	0.409	1304
2703	7.87	30%	1.134E-06	1.147E-06	5052716	3.283	0.417	1682
2803	7.87	30%	1.233E-06	1.254E-06	4875406	3.362	0.427	1366
2903	7.87	30%	1.313E-06	1.340E-06	4811386	3.441	0.437	1398
3003	7.87	30%	1.290E-06	1.325E-06	5312660	3.570	0.454	1390
705	7.87	50%	2.612E-06	2.623E-06	4729904	4.365	0.555	1468
805	7.87	50%	3.170E-06	3.202E-06	4227498	4.480	0.569	1085
1205	7.87	50%	3.210E-06	3.350E-06	6045978	4.980	0.633	1229
1305	7.87	50%	3.928E-06	4.115E-06	5459566	5.100	0.648	1495
1505	7.87	50%	2.417E-06	2.448E-06	6068837	4.600	0.584	1355
2005	7.87	50%	2.490E-06	2.510E-06	5340952	4.467	0.568	1324
1406	7.87	60%	8.627E-06	9.703E-06	5198855	5.910	0.751	1076
1806	7.87	60%	5.584E-06	5.750E-06	5649265	5.497	0.698	1319
1906	7.87	60%	6.099E-06	6.724E-06	6266222	5.749	0.730	851

4.3.1 Critical Stress Intensity Factor

As expressed by Irwin, crack propagation will occur when the combined effect of stress and crack growth (stress intensity) reaches a critical value commonly referred to as the *critical stress intensity factor*, K_{IC}. This value is also called *Fracture Toughness*, which describes the characteristics of material to deform with crack growth and the energy absorption before and during rupture. Therefore, critical stress intensity factor is a materials parameter and can characterize material's fracture resistance regardless of the geometry of the specimen.

Using proposed approach, critical stress intensity factor was calculated based on the results of Kim's testing Data (1996), series II experiments results and Shilang xu's testing data shown in Table 4.1, Table 4.2 and Table 4.3 respectively and their relationships with specimen depth and notch-depth ratio were plotted in Figure 4.6, 4.7 and 4.8 respectively.

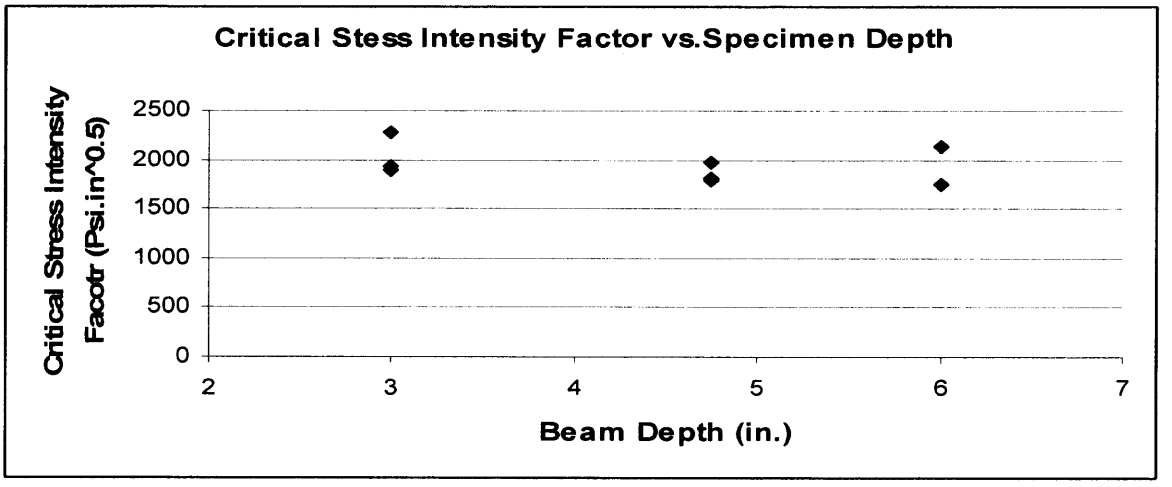

Figure 4.6 Critical Stress Intensity Factor vs. Specimen Depth Using Series II Experiments' Results.

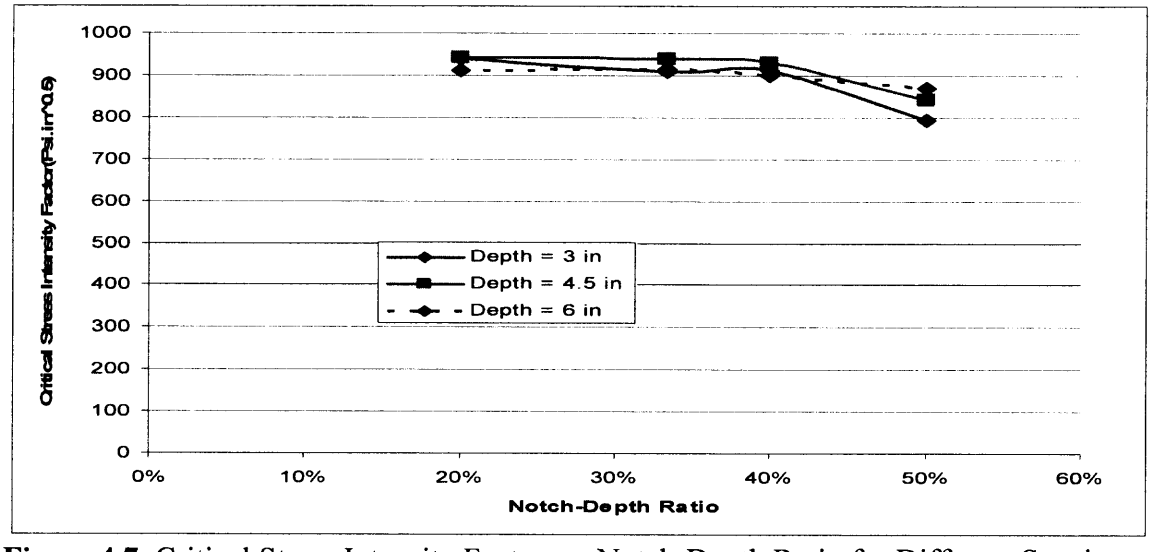

Figure 4.7 Critical Stress Intensity Factor vs. Notch-Depth Ratio for Different Specimen Depth Using Kim's Experiments' Results.

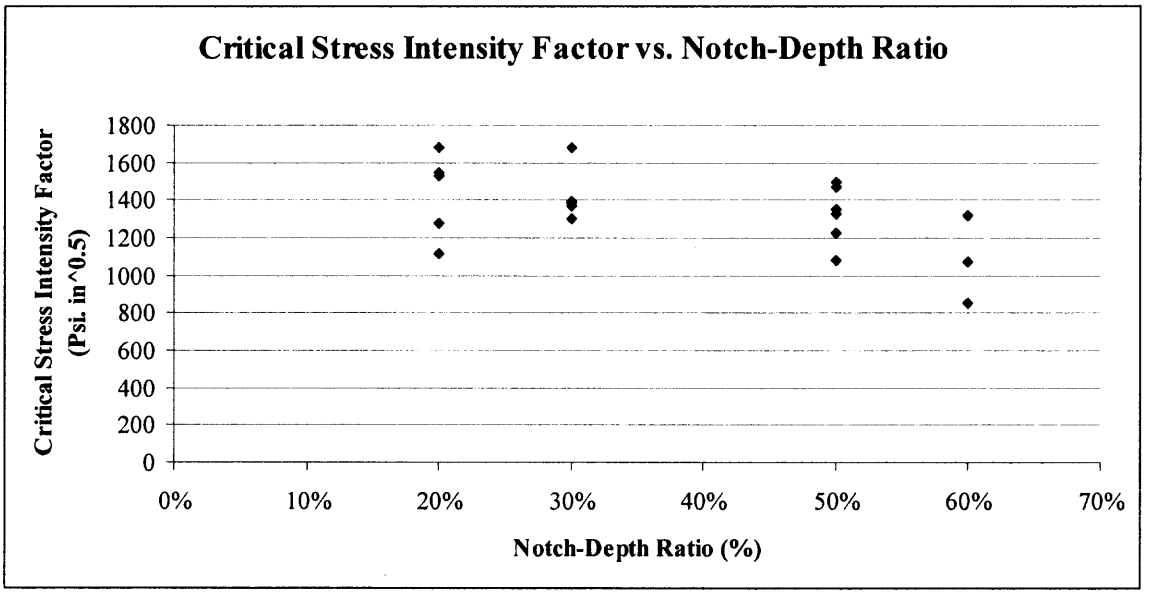

Figure 4.8 Critical Stress Intensity Factor vs. Notch-Depth Ratio Using Shilang xu's Testing Data.

From Figure 4.6 and 4.7, it was manifested that the values of critical stress intensity factor are little dependence on specimen depth. Both Kim's testing data and wu's testing data include 3 inches, 4.5 inches and 6 inches in specimen depth. The calculated values are around 930 $psi\sqrt{in}$ using Kim's Data and are around 2000 $psi\sqrt{in}$ using wu's series II testing data. The discrepancies between two group values can primarily be contributed to the age of testing of material. We tested the specimen at 14 days age and Kim performed the tests at 7 days age instead. It is understandable that 14 days age concrete should have some more potential of fracture resistance than concrete of 7 days age.

From Figure 4.7 and Figure 4.8, we can see before 50% of notch-depth ratio, the calculated critical stress intensity factors are independent from notch-depth ratio but when notch-depth ratio is more than 50%, the results of critical stress intensity factor were decreasing. Both Shilang xu's testing results and Kim's testing results demonstrate this trend. This phenomenon has also been reported by S.P. Shah. (1985). One possible

explanation is that the specimen with a deep notch has a lower load capacity and then is more feasible to fracturing. But it need more work to do on this issue.

Summarily, calculated critical stress intensity factor from proposed fracture model demonstrates its size-independence from specimen thickness and therefore this value can be extrapolated from small size lab specimen into large-size structural beams to indicate fracture resistance of a certain concrete under consideration. And so far we can say this is good for the specimens with notch-depth ratio less than 50%.

4.3.2 Critical Crack Length and Critical Fictitious Crack Length

Critical crack length refers to the total crack length including notch length and crack growth at the peak load. Critical fictitious crack length normally refers to the length of fracture process zone. They are very important fracture parameters in describing the fracturing resistance of concrete since the non-linearity before the peak load in load-displacement curve in 3 point bending notched beam tests is due to the formation of fracture process zone. At peak load, it is believed that fracture process zone will be fully developed and keeps same length shifting forward after the peak load. Some researcher, for instants of B.L.Karihaloo (1995) believed this parameter can indicate fracture resistance. Longer fracture process zone, more energy is required to be absorbed before unstable crack propagation. It supposes to be another material parameter and size-independent.

Wecharatana and Shah (1983) proposed a model to predict the size of the process zone by introducing a crack closing pressure in front of the crack tip. They have successfully predicted the size of the process zone in the notched beam concrete specimens under three-point and four-point bend specimens, making others to realize the

potential significant contribution of microcracking and nonlinearity of concrete materials. In the last decades, different approaches were reported in some non-linear fracture models to predict the length of fracture process zone. (Y.Jenq and S.P.Shah,1985, Z.P.Bazant and P.A. Pfeiffer,1987; Karihaloo and P.Nallathambi,1987; Shilang xu and Reinhardt, 1998)

In this study, predicted critical crack length a_c using different testing data was also reported in column 8 of Table 4.1, 4.2 and 4.3. In Figure 4.9, we plotted the length of fracture process zone predicted by proposed effective compliance model and predicted by M.Wecharatana's regression equation based on Wu's series II testing results and predicted fracture process zone by proposed effective compliance model using Wu's series II testing results.

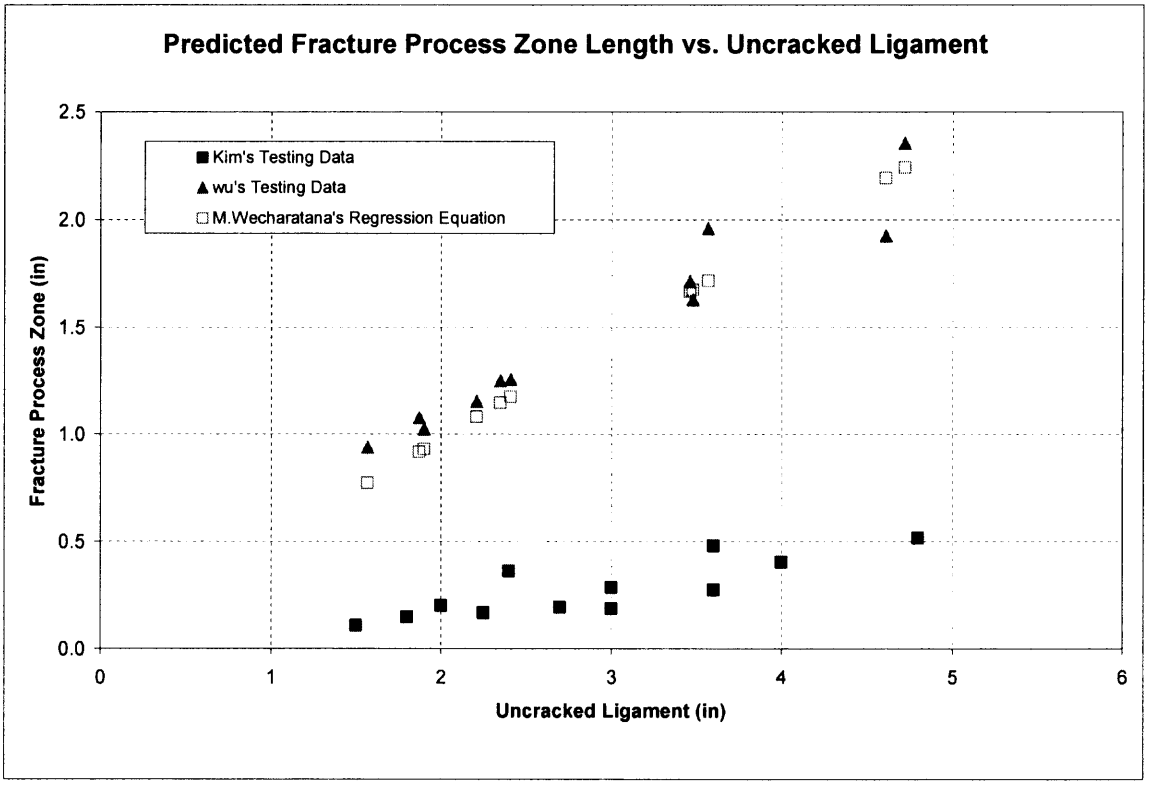

Figure 4.9 Predicted Fracture Process Zone Lengths vs. Uncracked Ligament.

It is very clear that M.Wecharatana's method and proposed method are in a very good agreement based on the Wu's series II experimental results. But fracture process zones using proposed method and Kim's testing data (solid rectangular points) are much smaller than the ones predicted using wu's testing data. Combining the difference of critical stress intensity factors between the results from Kim's testing and wu's testing data, we can guess that fracture process zone is able to provide some information of fracture resistance of the material under consideration. We can not just say that fracture process zone is a geometry parameter or a material parameter. It is a structural parameter. It is the results both of configuration of specimen and material behavior.

Note that the predictions of fracture process zone are based on following rather simplifying assumptions:

1. The fracturing occurs at the maximum load;
2. Effect of shear deformations and mix mode crack propagation are ignored;
3. Neutral axis was assumed at the depth of half depth of uncracked ligament;
4. A straight line crack profile was assumed

4.4 Comparison of Proposed Model, TPFM and Double K Model

The reason to propose a new model is due to some restriction or inaccuracies inherently existing in some other fracture models. Using TPFM, unloading and reloading at about 95% of post-peak range is necessary to predict critical stress intensity factor. Early or later will lead to some prediction errors. The contribution from Double K Model is introducing initial fracture toughness. Since they proposed to use secant compliance directly to calculate critical stress intensity factor, LEFM formula was applied without

any modification to non-linear fracture behavior of concrete. It has been approved not correct.

Proposed non-linear fracture model uses effective compliance to extract non-linearity happening around peak load from its total fracture behavior and then LEFM formula was applied to an equivalent elastic concrete beam. Theoretically, proposed model should have some more advantages than TPFM and Double K model. Shilang xu's testing data and wu's series II testing data, both enclosing some unloading curve at the peak load were utilized on proposed model, on TPFM and Double K model. Calculated different compliance, including initial compliance, secant compliance, unloading compliance and effective compliance, which are useful for Double K model, TPFM and proposed model respectively were presented in Table 4.4 and critical crack length and critical stress intensity factors were presented in table 4.5.

It shows that effective compliance is always in the middle between unloading compliance and secant compliance. It is because secant compliance includes elastic behavior and non-elastic behavior. Through unloading at the peak load, recovered displacement would be elastic portion and unrecovered displacement was treated as plastic. Due to the tortuous surface of crack faces, unloading can not make all the elastic displacement recovered. In another words, unloading compliance overestimates the plastic portion and underestimates the elastic portion. But effective compliance, as discussed above, is calculated based on equivalent elastic beam, therefore it represents the elastic behavior exactly. Critical stress intensity factor calculated based on same material and different approaches were plotted in Figure 4.10 and 4.11.

Table 4.4 Different compliance calculated using Shilang xu and wu's Testing data.

Test No.	Specimen Depth (in)	Notch-Depth Ratio (%)	Initial Compliance C_i (in/Lbs)	Scant Compliance C_s (in/Lbs)	Unloading Compliance C_u (in/Lbs)	Effective Secant Compliance C_e (in/Lbs)
Shilang xu's Testing data						
3402	7.87	20%	3.632E-07	9.061E-07	5.700E-07	9.265E-07
3602	7.87	20%	4.216E-07	6.843E-07	7.314E-07	6.884E-07
2603	7.87	30%	6.955E-07	1.215E-06	1.403E-06	1.230E-06
2703	7.87	30%	6.221E-07	1.134E-06	1.119E-06	1.147E-06
2903	7.87	30%	6.519E-07	1.313E-06	1.524E-06	1.340E-06
3003	7.87	30%	5.913E-07	1.290E-06	1.157E-06	1.325E-06
1305	7.87	50%	1.658E-06	3.928E-06	3.491E-06	4.115E-06
2005	7.87	50%	1.697E-06	2.490E-06	2.441E-06	2.510E-06
1806	7.87	60%	2.897E-06	5.584E-06	5.230E-06	5.750E-06
Xuezeng Wu's Testing Data						
I-4	4.75	22%	5.800E-07	3.647E-06	2.960E-06	4.171E-06
II-2	3	48%	2.550E-06	1.917E-05	1.420E-05	2.341E-05
II-4	3	37%	1.450E-06	9.905E-06	7.810E-06	1.138E-05
II-5	3	22%	7.800E-07	6.719E-06	6.090E-06	7.984E-06
II-6	3	20%	5.240E-07	4.558E-06	4.270E-06	5.367E-06
IV-1	6	21%	2.720E-07	2.020E-06	1.520E-06	2.367E-06
IV-3	6	23%	4.180E-07	1.528E-06	1.490E-06	1.712E-06

Table 4.5 Comparison of TPFM, Double K and Proposed Model based on S.L. Xu's Testing Data.

		TPFM			Double K model				Proposed Model	
Test No.	a_0/d (%)	a_c/d	K_{ic} ($psi\sqrt{in}$)	$CTOD_c$ (in)	a_c/d	K_{un} ($psi\sqrt{in}$)	K_{ic} ($psi\sqrt{in}$)	K_{ini} ($psi\sqrt{in}$)	a_c/d	K_{ic} ($psi\sqrt{in}$)
3402	20%	0.279	1316	1.105E-03	0.37	1658	783	876	0.373	1678
3602	20%	0.298	1316	8.544E-04	0.29	1276	380	896	0.287	1280
2603	30%	0.434	1401	1.008E-03	0.41	1294	429	865	0.409	1304
2703	30%	0.412	1658	1.116E-03	0.41	1668	514	1154	0.417	1682
2903	30%	0.461	1500	1.144E-03	0.43	1386	467	919	0.437	1398
3003	30%	0.428	1291	9.881E-04	0.45	1368	513	854	0.454	1390
1305	50%	0.624	1353	1.103E-03	0.64	1459	670	789	0.648	1495
2005	50%	0.563	1304	6.430E-04	0.57	1318	369	949	0.568	1324
1806	60%	0.686	1243	7.667E-04	0.70	1299	476	823	0.698	1319

Table 4.6 Comparison of TPFM, Double K and Proposed Model based on Wu's Data.

			TPFM			Double K model				Proposed Model	
Test No.	d (in)	a_0/d (%)	a_c/d	K_{ic} ($psi\sqrt{in}$)	$CTOD_c$ (in)	a_c/d	K_{un} ($psi\sqrt{in}$)	K_{ic} ($psi\sqrt{in}$)	K_{ini} ($psi\sqrt{in}$)	a_c/d	K_{ic} ($psi\sqrt{in}$)
I-4	4.75	22%	0.522	1487	2.089E-03	0.56	1680	663	1017	0.580	1819
II-2	3	48%	0.736	1571	2.320E-03	0.77	1923	663	1261	0.790	2216
II-4	3	37%	0.657	1746	2.469E-03	0.69	2033	663	1371	0.708	2223
II-5	3	22%	0.593	1643	2.745E-03	0.61	1729	663	1067	0.633	1926
II-6	3	20%	0.579	1648	2.037E-03	0.59	1715	663	1052	0.615	1892
IV-1	6	21%	0.532	1789	3.090E-03	0.58	2122	663	1459	0.606	2135
IV-3	6	23%	0.529	1614	2.038E-03	0.48	1362	663	700	0.553	1751

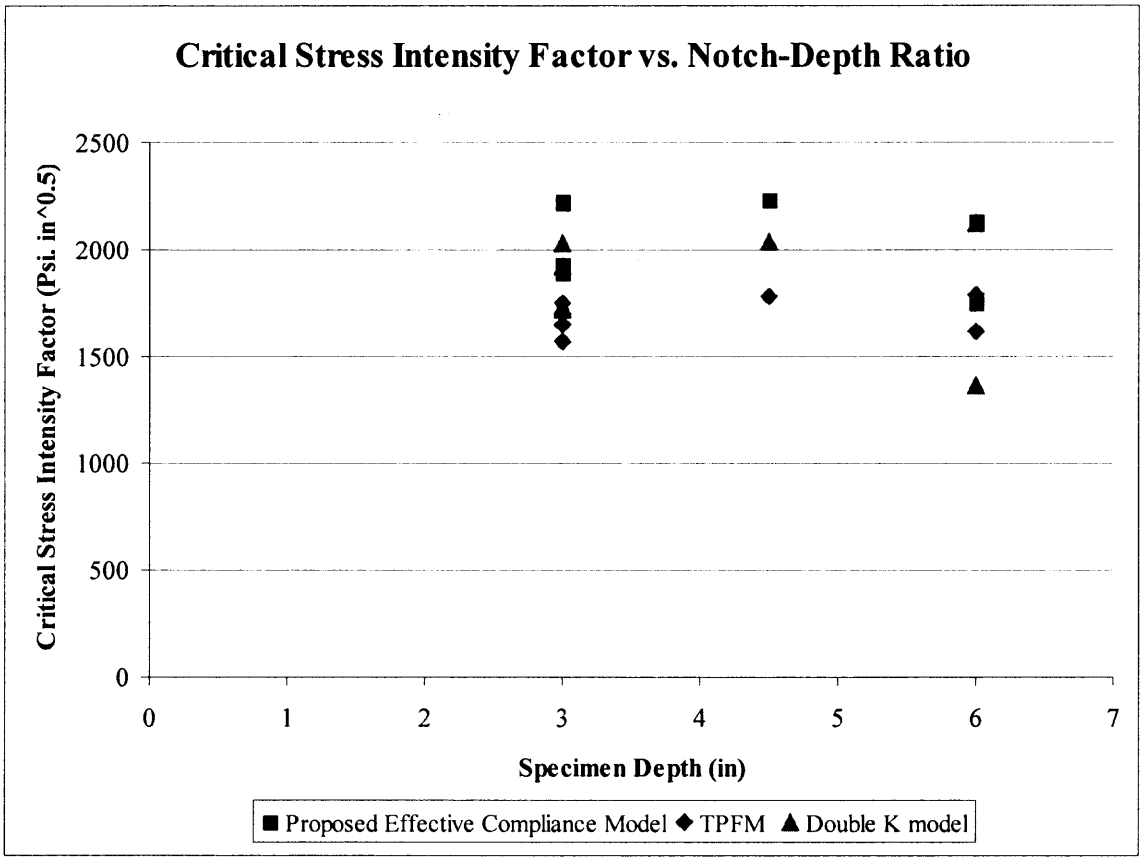

Figure 4.10 Critical Stress Intensity Factor vs. Specimen Depth using Wu's Testing Results.

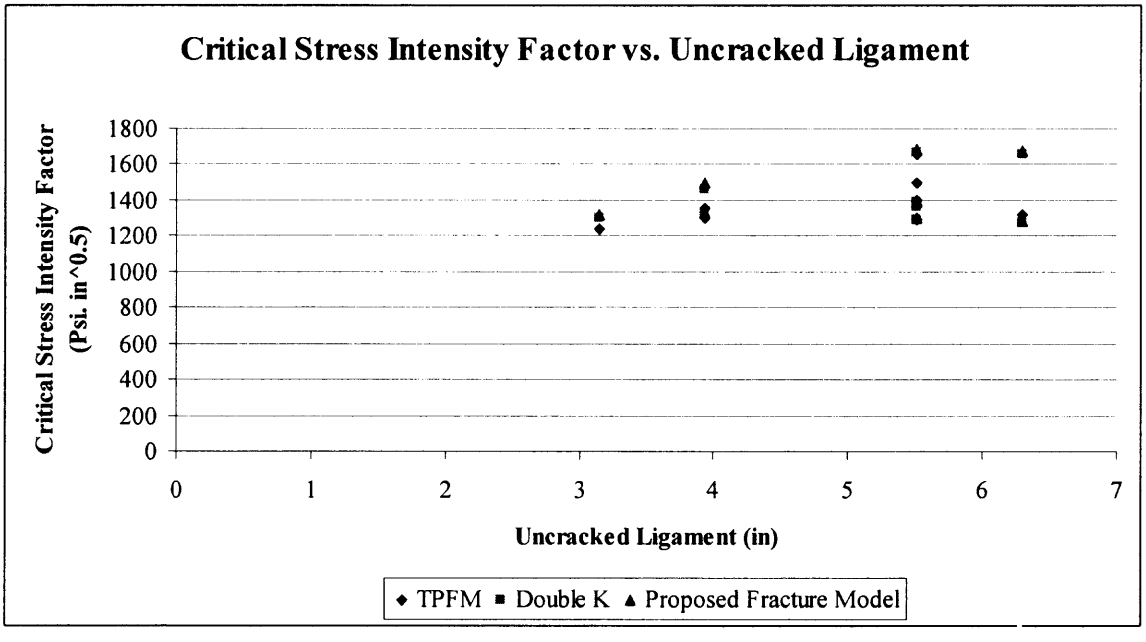

Figure 4.11 Critical Stress Intensity Factor vs. Uncracked Ligament using S.L.Xu's Data.

From S.L.Xu's experimental data, the critical stress intensity factors, predicted using the TPFM, Double K and the proposed models were plotted against the uncracked ligament as shown in Figure 4.11. The proposed model and the TPFM yield similar consistent results, while the Double K model exhibits some degree of variation.

4.5 Conclusion

Through the analysis mentioned above, the following conclusions can be drawn here:

1. Non-linear effective compliance model is developed to predict the length of nonlinear fracture process zone and critical stress intensity factor in concrete which both can subsequently be used to determine the fracture resistance of concrete.
2. The length of fracture process zone depends on material behavior as well as specimen geometry and can be considered as a structural parameter;
3. Proposed model can achieve a size-independent (when $a/w<0.4$) critical stress intensity factor without unloading at peak load which is required by TPFM, thus simplify the experiment.

CHAPTER 5

REMAINING SERVICE LIFE PREDICTION

As many concrete structural elements in the present infrastructure system, such as buildings, bridges and highways, are decaying rapidly, there is an urgency to evaluate these structures non-destructively for cracking and its remaining service life.

Over the last two or three decades, the prediction of remaining service life of concrete structure attracted a lot of attentions and got a considerable development. But most of investigations focus on (1) the concrete deteriorations from steel corrosion, (2) fatigue crack growth behavior.

In practice, even though there is no much steel corrosion or fatigue crack growth does not dominate the structure service behavior, the existence a certain length of crack in concrete member still can indicate this member's service condition. But so far there is no one method available to express this condition. This study will present a method to predict remaining service life on fractured concrete member using the concept of Fracture Energy. And the fracture parameters required by this method will be analysis by proposed fracture model.

5.1 Remaining Service Life Prediction using Fracture Energy Method

The term "Fracture Energy" originally was proposed by Hillerborg in 1976. Figure 5.1 shows a schematic diagram of any beam member subjected to an applied load. The Load-Deflection (load-line deflection) diagram shows the amount of energy absorbed by the beam prior to its failure. The area under the P-δ curve represents the amount of total energy applied to this member.

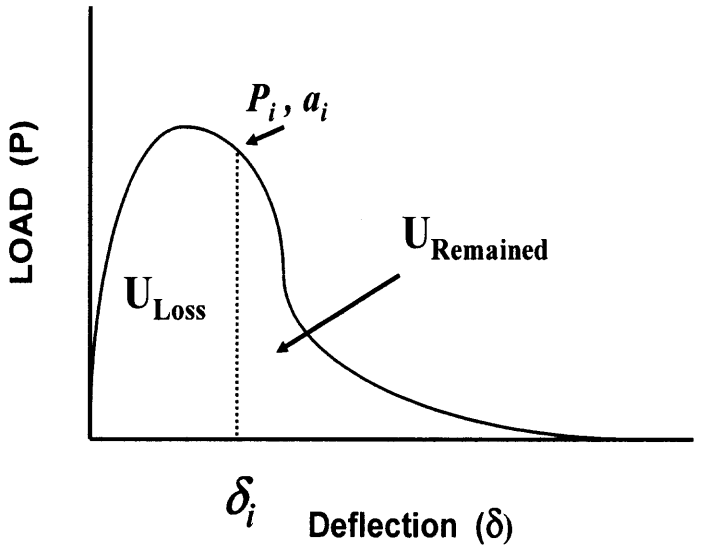

Figure 5.1 Schematic Illustration of Remaining Service Life based on Fracture Energy.

The total amount of energy absorbed by the beam can be determined from the following expression:

$$Utotal = \int_0^{\delta} Pd\ \delta \tag{5.1}$$

At point *i* on the P-δ curve, the corresponding load, load-line deflection and crack growth are P_i, δ_i and a_i respectively. The amount of energy used to create a crack of a_i is equal to U_{loss} whereas the remaining energy that the beam can withstand is $U_{remained}$. As crack, *a*, continues to propagate, the amount of $U_{remained}$ decreases, so as the uncracked ligament of the member, (*d*-*a*), where *d* is the total depth of the beam. It becomes obvious that the remaining service life of any member subjected to crack growth is proportional to the ratio of the $U_{remained} / U_{total}$ and the crack over depth ratio, *a*/*d* , or the uncracked ligament over depth ratio, (*d*-*a*)/*d*. Thus, one can predict the remaining service life of a cracked member by simply using the normalized energy remained versus the crack over

depth ratio of the member. Therefore, the remaining service life can be expressed as follows:

$$\text{Remaining Service Life} = \frac{Uremained}{} = 1 - \frac{Uloss}{Utotal} \qquad (5.2)$$

In order to investigate this method, two series of experiments were carried out in 2003 and 2004. Tables 1, 2 and 3 summarize results of the beam test in series 1 (w/c =0.5) of this study for three types of cementitious materials, namely, reinforced concrete, concrete and mortar. All are with a water to cement ratio of 0.5. All beams have a dimension of 4.75 in. width (B), 3 in. depth (d) and with the initial notched depth (a_o) of 3/8 in. and ¼ in. (for mortar only). The values of fracture energy, G_F, for mortar, concrete and reinforced concrete were found to be 0.361, 0.969 and 3.272 lb/in., respectively. The presence of steel reinforcement significantly increases the fracture energy of the composite. The larger the crack opening displacement (CMOD) increases, the more the contribution that the reinforcement provides. The value of G_F for concrete is also larger than that of mortar since larger aggregate size leads to a bigger process zone as cracks and microcracks have to pass around strong aggregates. Also listed in these Tables are the measured crack growth using ultrasonic equipment, peak load and the corresponding load-line displacement, CMOD, and energy used.

Tables 4, 5 and 6 show results of the beams tested in the second series (w/c = 0.4), which also consists of mortar, plain concrete and reinforced concrete. The results in both series have similar trends and lead to the same conclusions of fracture energy, energy used and the remaining service life at each stage of crack growth.

Table 5.1 Service Life of Reinforced Concrete Beam (Group I).

	P peak	δ peak in.	CMOD peak	U to peak	U total	G_F	%U loss	%U remain	Δa	Δa d-a_0
Test #7 RC W/C = 0.5	1285.7	0.0470	0.0266	3.61	40.80	3.27	-	-	-	0
							5.8	94.2	0.27	0.1
							8.8	91.2	0.52	0.2
							11.9	88.1	0.83	0.3
							14.4	85.7	1.03	0.4
							20.2	79.8	1.32	0.5
							25.7	74.3	1.60	0.6
							58.7	41.3	1.84	0.7
							100.0	0	-	0.8
							100.0	0	-	0.9
							100.0	0	-	1.0

Table 5.2 Service Life and Fracture Energy of Concrete Beam (Group I).

	P peak	δ peak in.	CMOD peak	U to peak	U total	G_F	%U loss	%U rema	Δa	Δa d-
Test # 5 NRC W/C = 0.5	1373.9	0.0297	0.0159	2.75	12.08	0.969	-	-	-	0
							23.9	76.1	0.25	0.1
							29.4	70.6	0.51	0.2
							36.7	63.3	0.77	0.3
							44.9	55.1	1.05	0.4
							60.2	39.8	1.30	0.5
							82.0	18.0	1.57	0.6
							91.4	8.6	1.83	0.7
							99.97	0.03	2.06	0.8
							100.0	0	-	0.9
							100.0	0	-	1.0

Table 5.3 Service Life and Fracture Energy of Mortar Beam (Group I).

	P peak	δ peak (in.)	CMOD peak	U to peak	U total	G_F	%U loss	%U remain	Δa	Δa d-a_0
Test # 8 Mortar W/C = 0.5	934.1	0.0142	0.0082	2.04	4.68	0.358	-	-	-	0
							55.9	44.1	0.256	0.1
							63.6	36.4	0.524	0.2
							72.6	27.4	0.752	0.3
							88.3	11.7	1.044	0.4
							95.9	4.11	1.318	0.5
							99.5	0.47	1.578	0.6
							100.	0	-	0.7
							100.	0	-	0.8
							100.	0	-	0.9
							100.	0	-	1.0

Table 5.4 Service Life of Reinforced Concrete Beam (Group II).

	P peak	δ peak in.	CMOD peak	U to peak	U total	G_F	%U loss	%U remain	Δa	Δa d-a_0
Test #15 RC W/C = 0.4	1593.7	0.0322	0.0127	2.640	35.08	2.813	-	-	-	0
							8.5	91.5	0.265	0.1
							11.1	88.9	0.521	0.2
							12.2	87.8	0.787	0.3
							17.7	82.3	1.055	0.4
							24.6	75.4	1.316	0.5
							45.9	54.1	1.576	0.6
							100.0	0	1.754	0.7
							100.0	0	-	0.8
							100.0	0	-	0.9
							100.0	0	-	1.0

Table 5.5 Service Life and Fracture Energy of Concrete Beam (Group II).

	P peak	δ peak in.	CMOD peak	U to peak	U total	G_F	%U loss	%U remain	Δa	Δa d-a_0
Test # 16 NRC W/C = 0.4	1298.2	0.0310	0.0174	3.394	13.11	1.051	-	-	-	0
							22.7	77.3	0.269	0.1
							28.8	71.2	0.520	0.2
							40.1	59.9	0.799	0.3
							41.6	58.4	1.059	0.4
							62.9	37.1	1.317	0.5
							81.0	19.0	1.576	0.6
							95.9	4.2	1.832	0.7
							100.0	0	-	0.8
							100.0	0	-	0.9
							100.0	0	-	1.0

Table 5.6 Service Life and Fracture Energy of Mortar Beam (Group II).

	P peak	δ peak (in.)	CMOD peak	U to peak	U total	G_F	%U loss	%U remain	Δa	Δa d-a_0
Test # 17 Mortar W/C = 0.4	957.3	0.0119	0.0052	1.294	4.503	0.361	-	-	-	0
							36.4	63.6	0.263	0.1
							75.8	24.2	0.522	0.2
							87.4	12.7	0.803	0.3
							97.5	2.5	1.054	0.4
							100.0	0	1.262	0.5
							100.0	0	-	0.6
							100.0	0	-	0.7
							100.0	0	-	0.8
							100.0	0	-	0.9
							100.0	0	-	1.0

Table 1, 2 and 3 can be used to project the remaining service life of the three concrete beams. To illustrate its applications, if a specific crack length was detected in these beams, the crack over depth ratio (*a/d*) gives us the critical parameter that will project the remaining service life of the beam. For example, if the crack found in these beams gives the a/d equals to 0.3, Tables 1, 2 and 3 shows that there will be 27.4, 63.3

and 88.1 percent of energy remained in the mortar, concrete and reinforced concrete beam respectively. These numbers represent the remaining service life of the members.

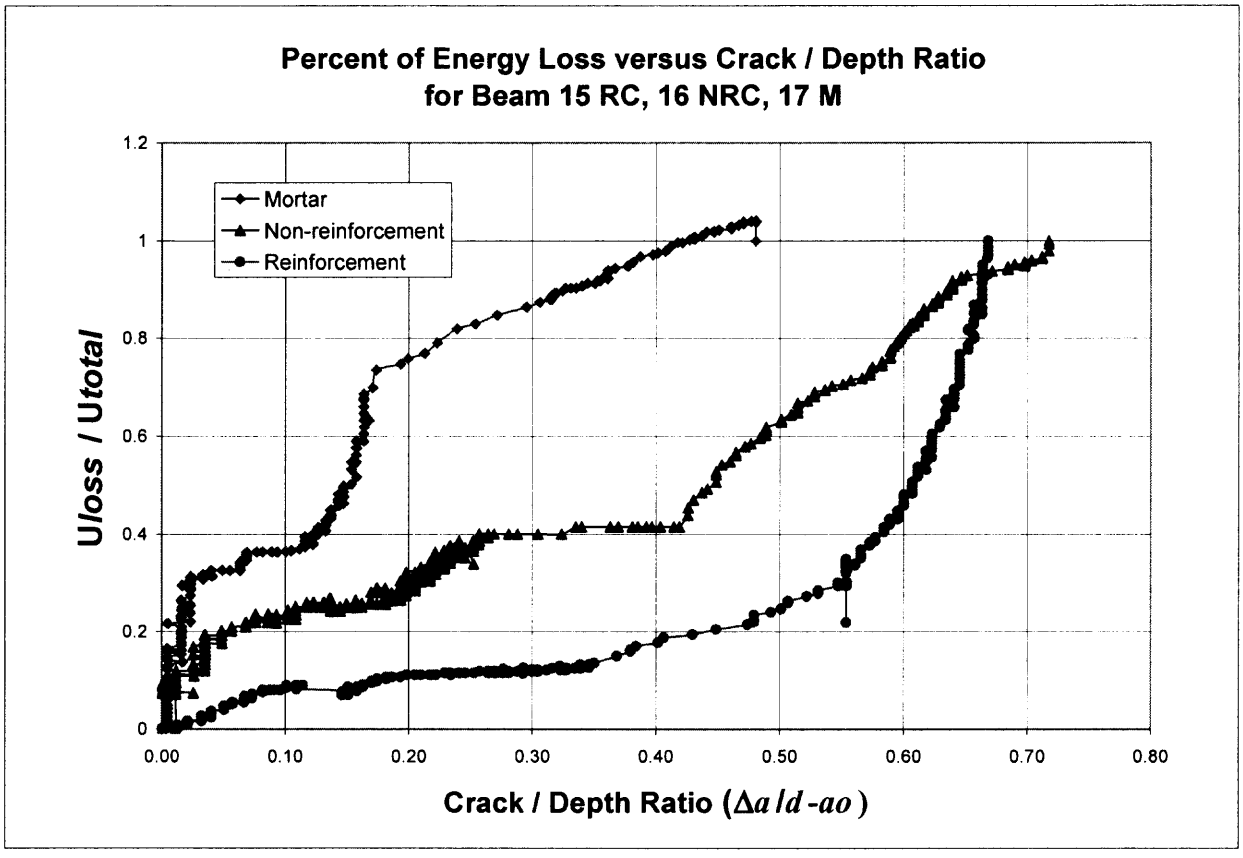

Figure 5.2 Energy Loss versus Crack over Depth Ratio of Reinforced and Non-reinforced Concrete Beam.

Figure 5.2 compares the energy loss (or inversely the remaining capacity) versus the crack over depth ratio of another series (Series 2) of mortar, concrete (non-reinforced) and reinforced concrete (Test No. 15, 16 and 17), which all have a water to cement ratio of 0.4. It clearly shows that reinforced concrete is the strongest, representing by the lowest curve, followed by concrete and mortar. The steep slope toward the end of the reinforced concrete sample is primarily the contribution of the reinforcement. For a crack growth of 30% of the depth in these three members, the remaining service lives are 12.7, 60.0 and 88.9% of the total capacity. As the energy loss ratio approaches 1.0, the beam

fractures. The instance of instability should theoretically coincide with the total cracking of the section, i.e., *a/d* equals 1.0. The results, however, indicate that most failures occur earlier, which could be attributed to the effect of the compression zone and interlocking between the aggregates.

Table 4, 5 and 6 summarize the critical parameters for the beam series of concrete with a water to cement ratio of 0.4. The percent energy loss at various stages of crack growth was listed for all three types of materials, namely, mortar (Test #17), concrete (Test #16) and reinforced concrete (Test #15). These tables again can be used to predict the remaining service life of concrete beams with and without reinforcement. In general, the results are in good correlation with those reported for the other series, which the mix-proportion has a w/c ratio of 0.5.

5.2 Fracture Energy Prediction Using Load-CMOD Curves

As mentioned before, fracture energy should be predicted based on Load-Load line deflection curve, but according to Kim and R.K.Navarlurker's research results, Load-CMOD curve and Load-Load line deflection curve has a very good bi-linear relationship. Figure 5.3 demonstrates the typical bi-linear relationship of CMOD and load line deflection for mortar. Using this bi-linear relationship, fracture energy or remaining service life can be predicted using load-CMOD curves.

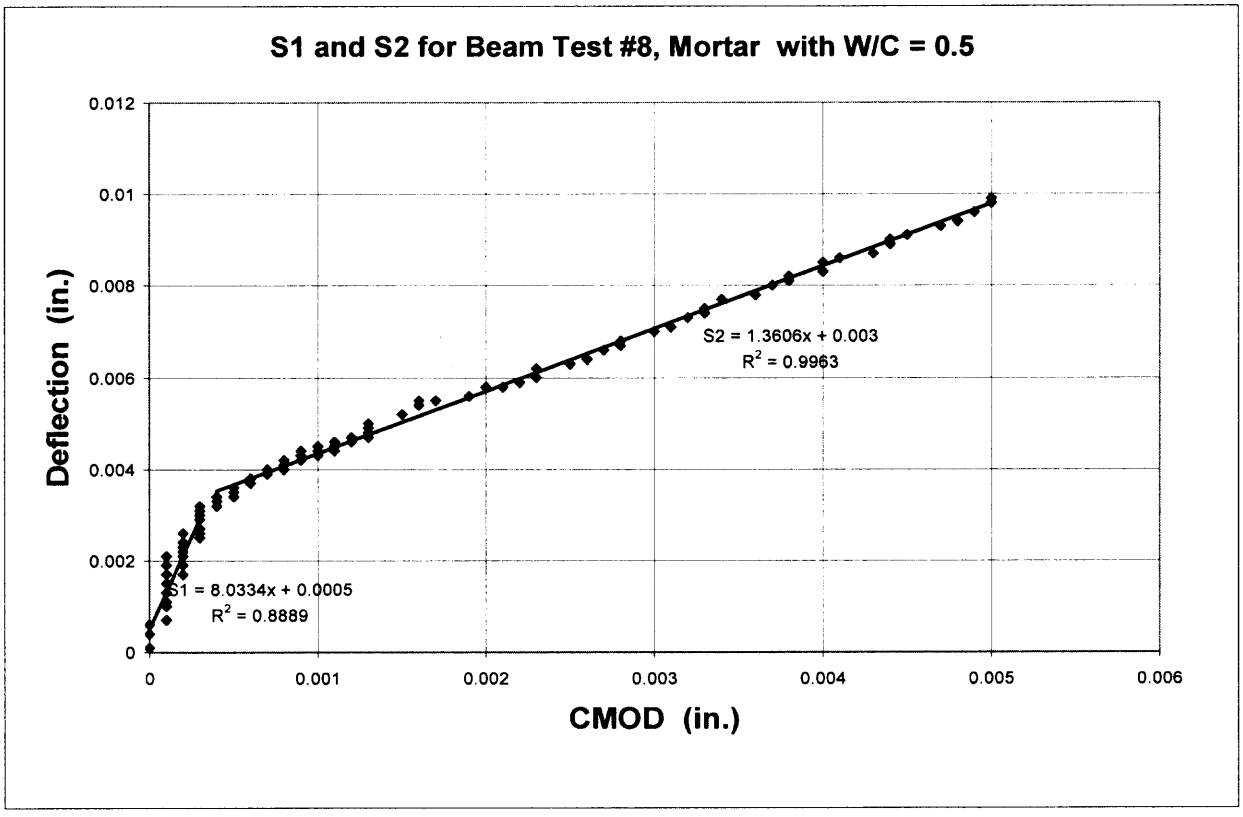

Figure 5.3 Bi-linear Relationships between Load-line Deflection and CMOD of Mortar.

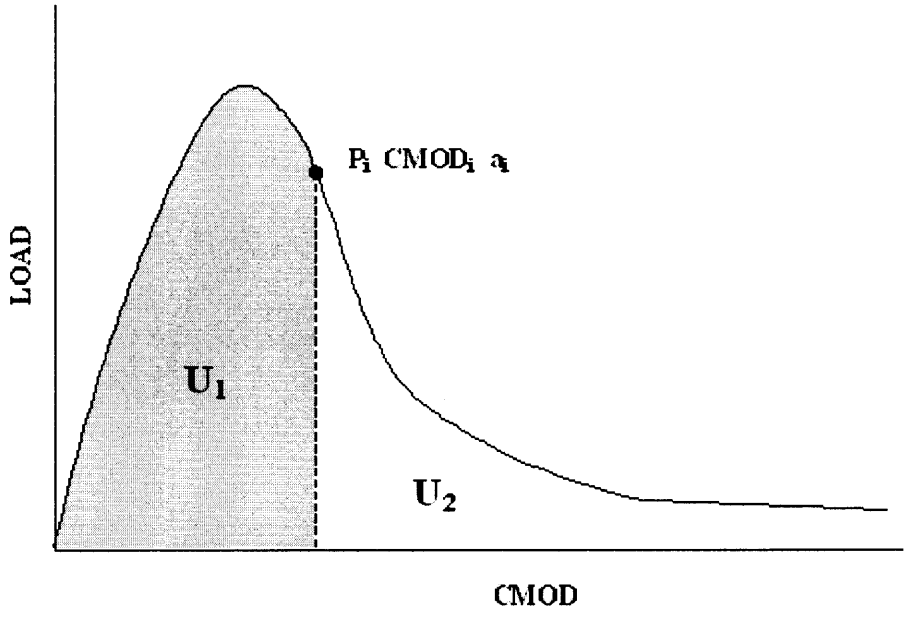

Figure 5.4 Schematic Diagram of a Typical Load-CMOD Response.

Figure 5.4 presents a typical load-CMOD response of a notched beam test. For any point *i* along the descending branch of the curve, one will have the load (P_i), Crack Mouth Opening Displacement ($CMOD_i$), and the measured crack growth (a_i). The energy used to generate crack a_i is U_{loss} (as shown in Figure 5.1) whereas the remaining energy capacity of the beam at that instance is $U_{remained}$ (see Figure 5.1). The area under the load-CMOD curve, U_1, can be related to U_{loss} with the use of S_1 and S_2 in accordance with Equation5.3. Similarly, U_2 can also be used to determine $U_{remained}$ of the beam using the same conversion factors.

$$G_F B \int_0^{\Delta a} d\Delta a = \int_0^{\delta} P d\delta = S_1 \int_0^{CMOD_P} P dCMOD + S_2 \int_{CMOD_P}^{CMOD} P dCMOD \tag{5.3}$$

Considering both equation 5.2 and equation 5.3, remaining service life can be expressed by following equation if we ignore the elastic energy loss:

$$\textbf{Remaining Service Life} = Uremained = 1 - \frac{U_{loss}}{U_{total}}$$

$$= 1 - \frac{\int_0^{CMOD_i} P dCMOD}{\int_0^{CMOD_f} P dCMOD} \tag{5.4}$$

In which $CMOD_i$ refers to any CMOD value on the P-CMOD curve and $CMOD_f$ refers to CMOD value when unstable fracture propagation occurs.

Therefore it is not necessary to figure out conversion factors between CMOD and load line deflection to predict remaining service life.

A summary of these remaining service life prediction curves for non-reinforced (mortar, concrete) and reinforced concrete based on Series I experimental data are presented in Figure 5.5. The diagram shows performance of mortar beam (green label) to have a shortest service life as compared to concrete (blue) and reinforced concrete (red). This diagram can easily be used to predict the remaining service life of any cracked concrete beam members by simply inputting the crack over depth ratio. Figure 5.5 has demonstrated a simple and practical concept to predict the remaining service life of a concrete member under service condition.

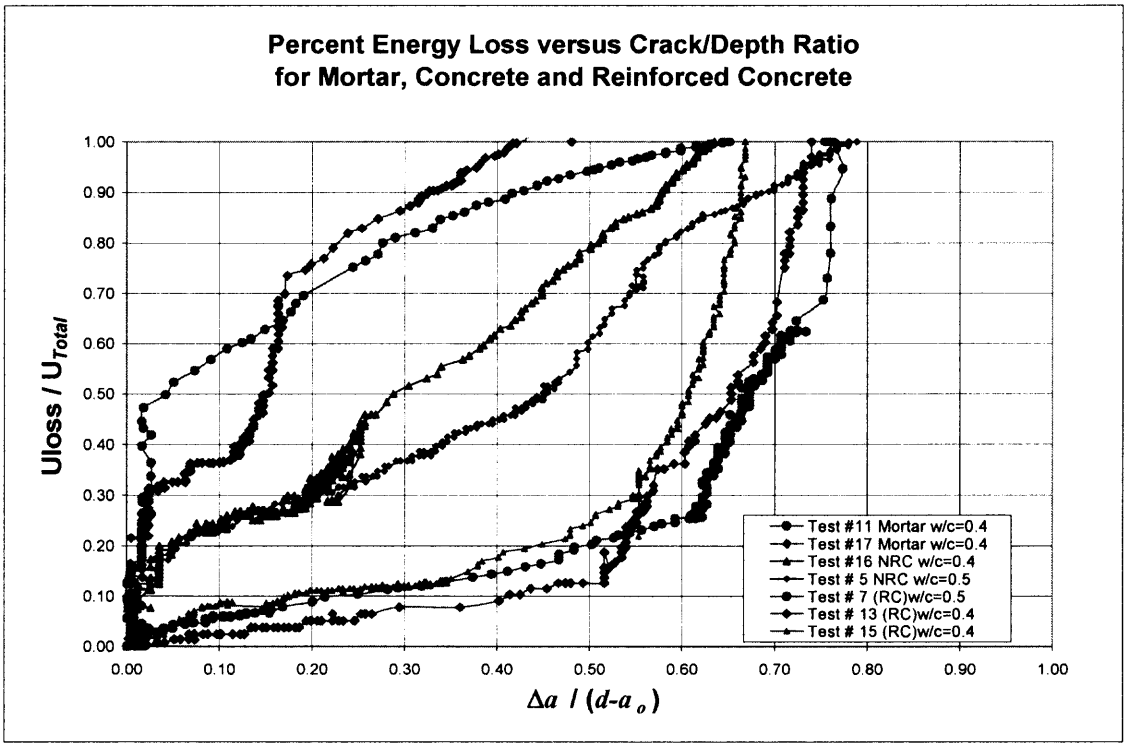

Figure 5.5 Remaining Service Life: Normalized Energy versus Crack-Depth Ratio for Mortar, Concrete and Reinforced Concrete (w/c = 0.4, 0.5).

CHAPTER 6

FRACTURE BEHAVIOR OF REINFORCED CONCRETE AND REMAINING SERVICE LIFE PREDICTION

Cracking commonly exists in most reinforced concrete structural members; special interest is thus given to reinforced concrete in this study.

Theoretically, even though the onset of unstable crack propagation, which can be analyzed using the proposed effective compliance fracture model, does not occur in reinforced concrete members due to the presence of steel reinforcement, the existing of crack growth in the concrete matrix generally reduces the load carrying capacity of the whole member. Predicting fracture behavior of a cracked concrete elements depends not only on the strength of the matrix, but also the size of the cracks. Accurate measurement and prediction of crack growth and its associated microcracking are therefore critical to any facture analysis.

For this purpose, series III experiments were designed and carried out to study fracture and crack growth characteristics of reinforced concrete members. Crack growth behavior at any stage of loading was analyzed from the signals detected by the ultrasonic instrument. And a new model using the relationship between external load and the relative rotation of the crack front, also known as "constant fracture angle", derived by Okamura (1975), to predict crack propagation was proposed here. For simplicity, an elastic-plastic behavior was assumed for the steel reinforcement, which enables this method to predict crack growth at any stage of loading prior to the yielding and debonding of the reinforcement.

Finally, the remaining service lives of reinforced concrete beams are presented using the method as illustrated in Chapter 5.

6.1 Measured Crack growth Characteristics of Reinforced Concrete

6.1.1 General

It is generally known that RC beams with different reinforcement ratios demonstrate different mechanical behaviors. Figure 6.1 illustrates the conceptual load-displacement curves for RC beams with different reinforcement ratios. When its reinforcement ratio is below the minimum reinforcement ratio as required by ACI code, (as shown in Figure 6.1 -1), RC beam performs close or similar to plain concrete, i.e., with softening response. As the amount of reinforcement increases, RC beam becomes more ductile and exhibits a plateau after the yielding of steel. The range of reinforcement ratio is commonly used for design purpose and is generally known as "under-reinforced". As additional reinforcement continuous to increase the ductility of the RC member, there is stage where steel yields while concrete reaches crushing, an optimum stage commonly known as "balanced condition" (see Figure 6.1-3). The beam under balanced condition usually fails in a ductile manner. Overly reinforced RC members, beyond the balanced condition ($\rho > \rho_{balance}$), tend to fail in a brittle manner, i.e., abruptly at the crushing of top layer of concrete (see Figure 6.1-4).

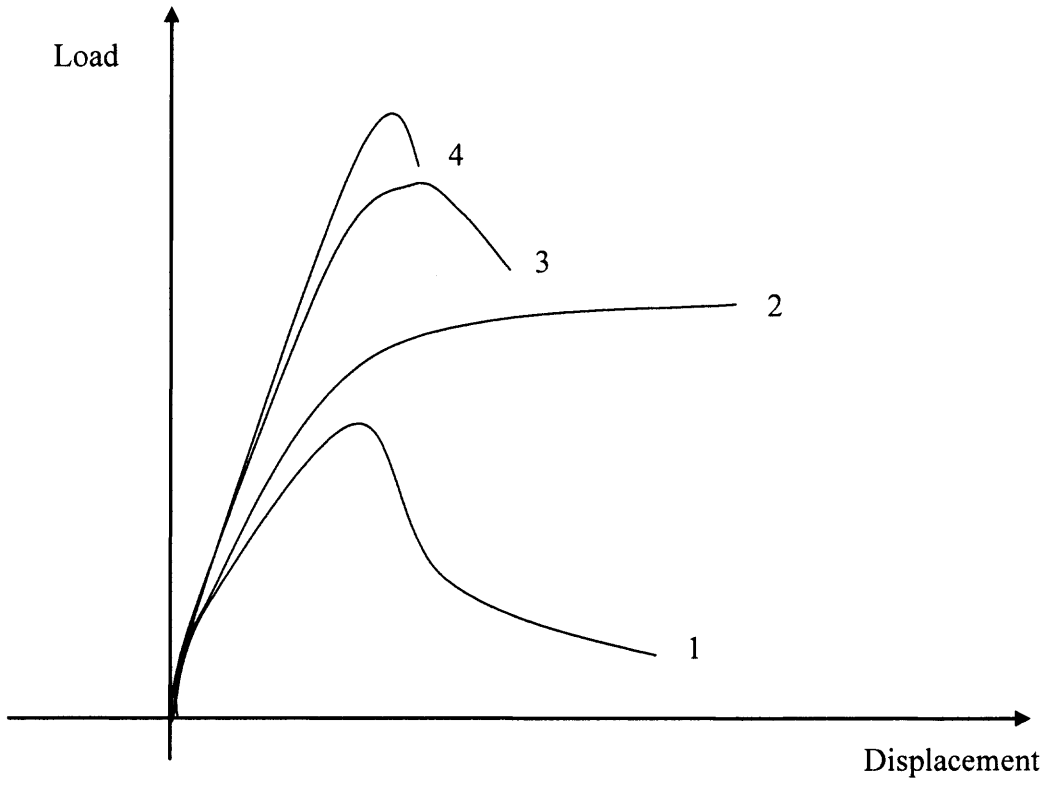

Figure 6.1 Performances of RC Beams with Different Reinforcement Ratio.

In the series III experiments, reinforced concrete beams with different amount of reinforcement ratio were tested to investigate their fracture behaviors. Details of the testing setup are presented in Chapter 3. The beams with reinforcement ratio of 0.3%, 0.7% and 3.8%, which represent under-reinforced, balanced , and over-reinforced condition, are shown in Figure 6.2- 6.7. For each beam, there are two load-deformation curves, which comprise the typical load-deflection response and a more disparate load-CMOD relationship. The former commonly provides the amount of energy spent during the fracture process while the latter represents the actual crack opening characteristics,

which are not affected by any error due to testing configuration such as support crushing. In each figure, there are two curves: the unmarked curve shows the load-deformation relationship whereas the marked one represents crack growth. In each test, multiple unloadings and reloadings were performed in order to use the ultrasonic technique to detect the fracture process zone. Test setup and some key parameters for the test were also shown in the figure.

The under-reinforced beam in Figure 6.2 and 6.3 with reinforcement ratio less than the minimum reinforcement required by ACI code exhibits similar behavior as plain concrete showing strain softening in the post-peak range. Typical under-reinforced concrete beam, illustrated in Figure 6.4 and 6.5, shows a ductile behavior. According to the load-CMOD curve, the load carring capacity seems to reach a steady state of 6000 lbs as the reinforcement yields when CMOD is about 0.0037. This load was maintained up to the CMOD of 0.117. The over-reinforced beam in Figure 6.6 and 6.7 fails abruptly in a brittle mode. During the unloading and reloading cycles after the peak load in over-reinforced beam, deformation was almost fully reversed, indicating that reinforcement is still in the elastic range. As for the under-reinforced concrete beam, unloading curve during the steady state reveals similar compliance as the initial slope. Plastic deformation is clearly visible, conforming that steel has reached yielding at these instances.

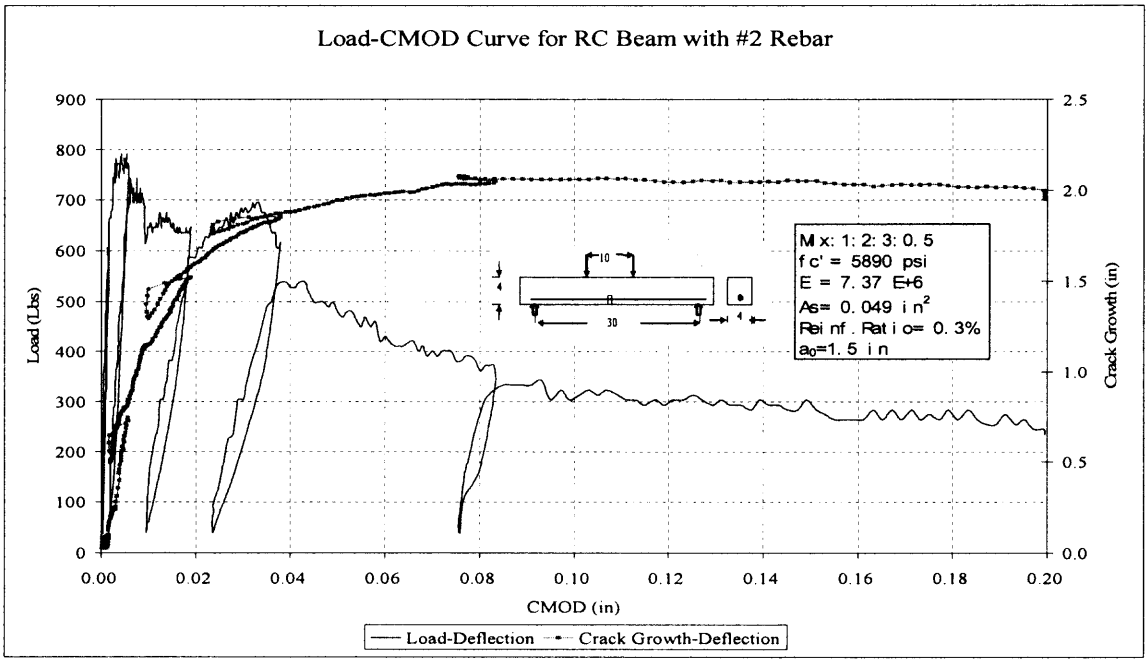

Figure 6.2 Load-CMOD &Crack Growth for Reinforced Concrete Beam with the Reinforcement Less Than ACI Required Minimum Reinforcement.
(Minimum Reinforcement = 0.63%)

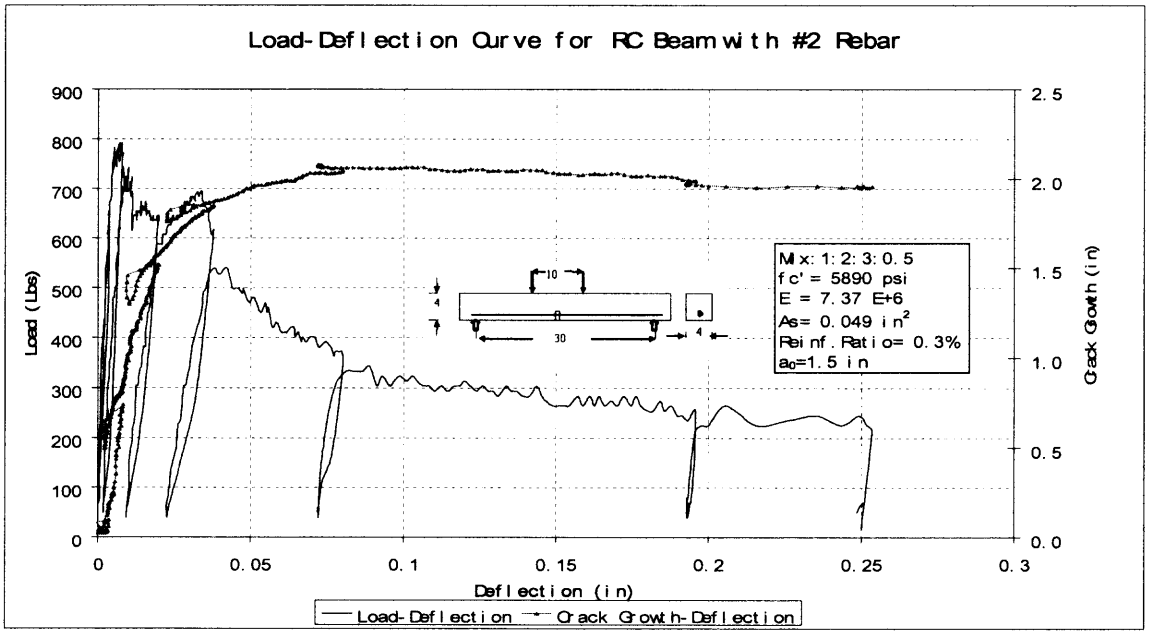

Figure 6.3 Load-Deflection &Crack Growth for Reinforced Concrete Beam with Reinforcement less than ACI Required Minimum Reinforcement.
(Minimum Reinforcement = 0.63%)

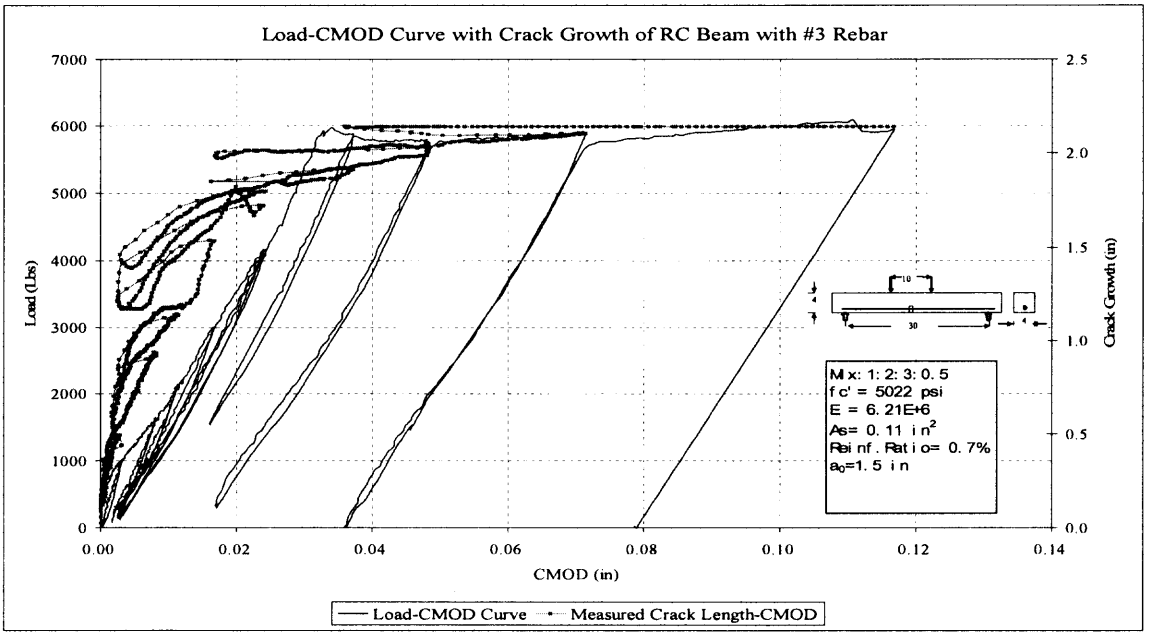

Figure 6.4 Load-CMOD &Crack Growth for Under-reinforced Concrete Beam. (Maximum Reinforcement =4.38% and Minimum Reinforcement =.053%)

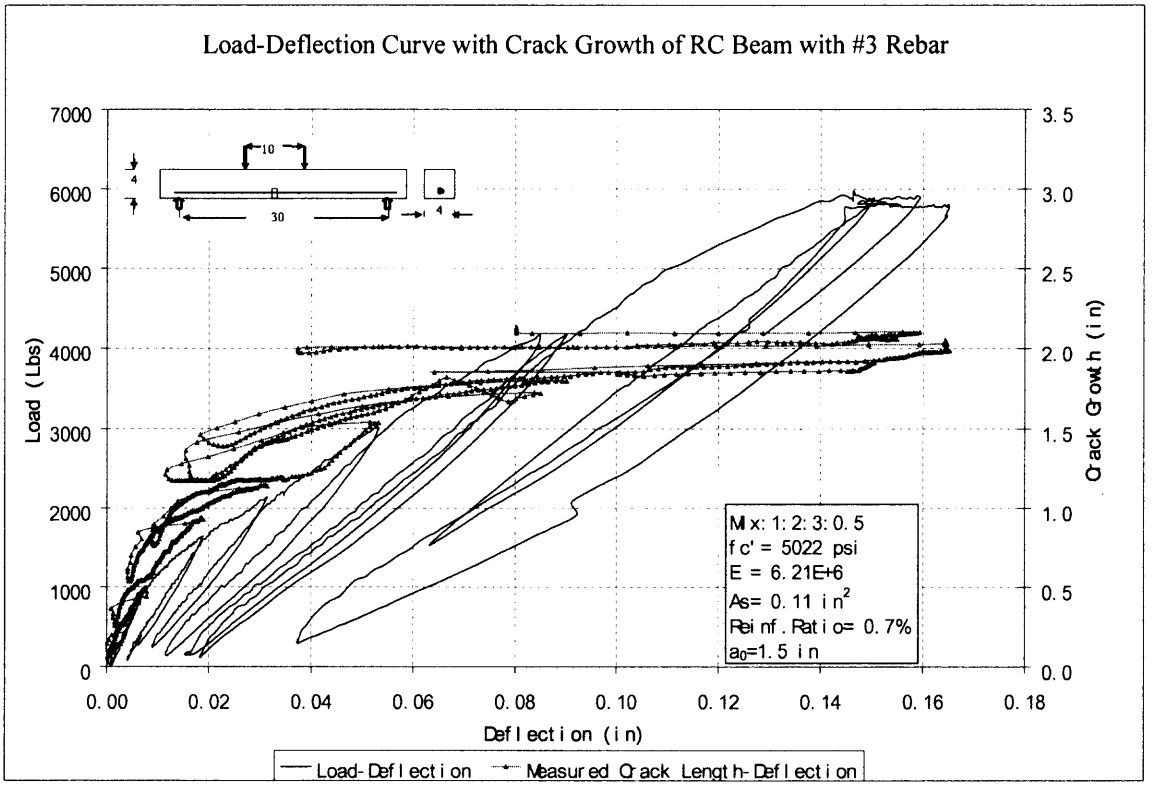

Figure 6.5 Load-Deflection &Crack Growth for Under-reinforced Concrete Beam. (Maximum Reinforcement =4.38% and Minimum Reinforcement =.053%)

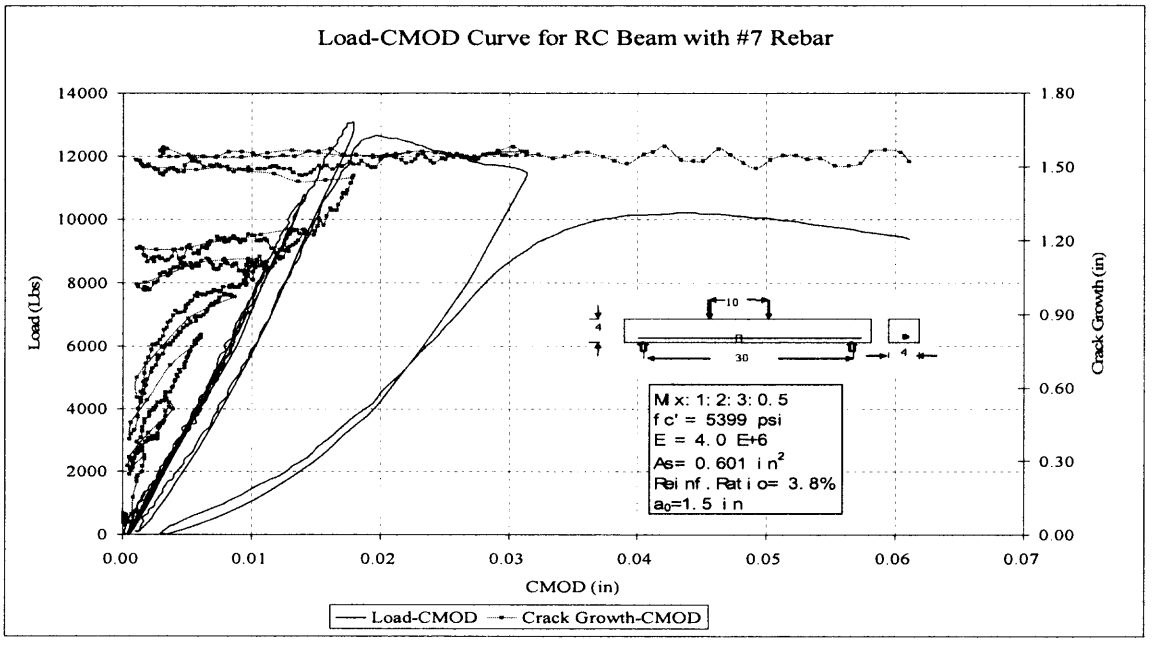

Figure 6.6 Load-CMOD &Crack Growth for Over-reinforced Concrete Beam. (Maximum Reinforcement =2.6 %)

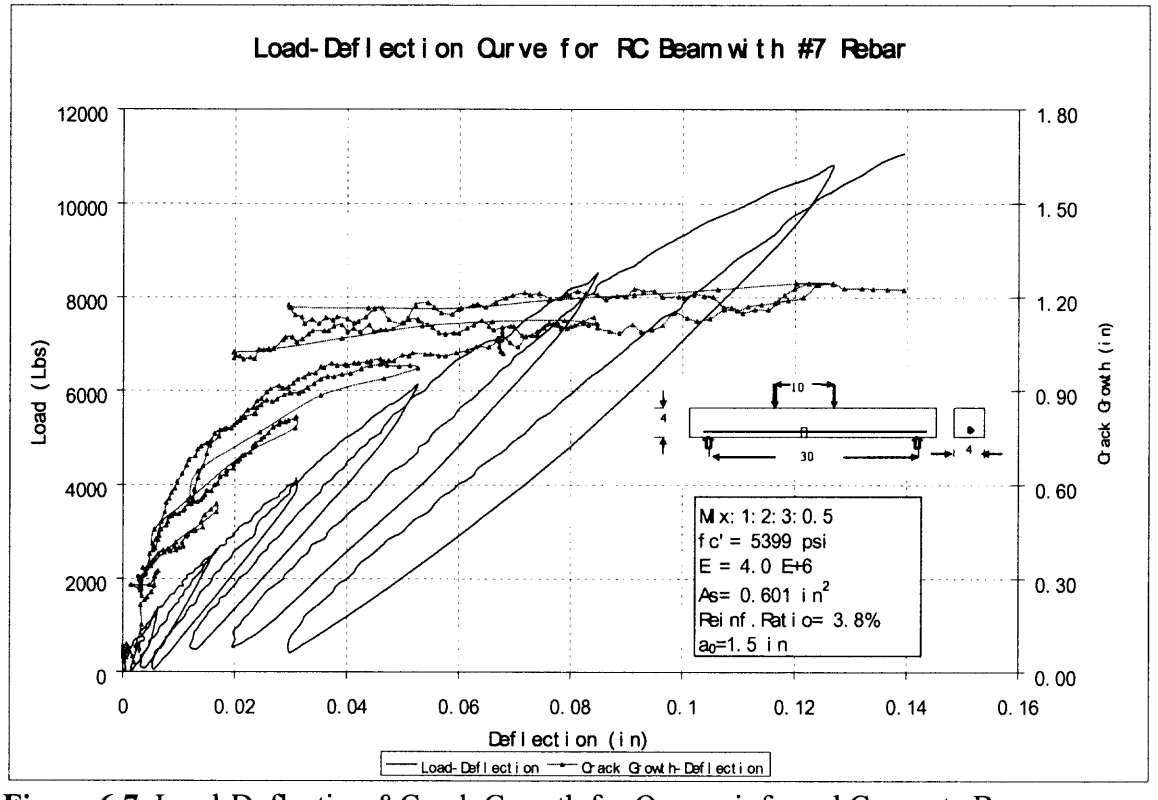

Figure 6.7 Load-Deflection &Crack Growth for Over-reinforced Concrete Beam. ((Maximum Reinforcement =2.6 %)

In over-reinforced concrete beams, crushing of the top layer of concrete was clearly observed (as shown in Figure 6.8 (a)). On the contrary, for the concrete beam with reinforcement less than minimum reinforcement, there was no clear crushing at the top(see Figure 6.8 (b)).

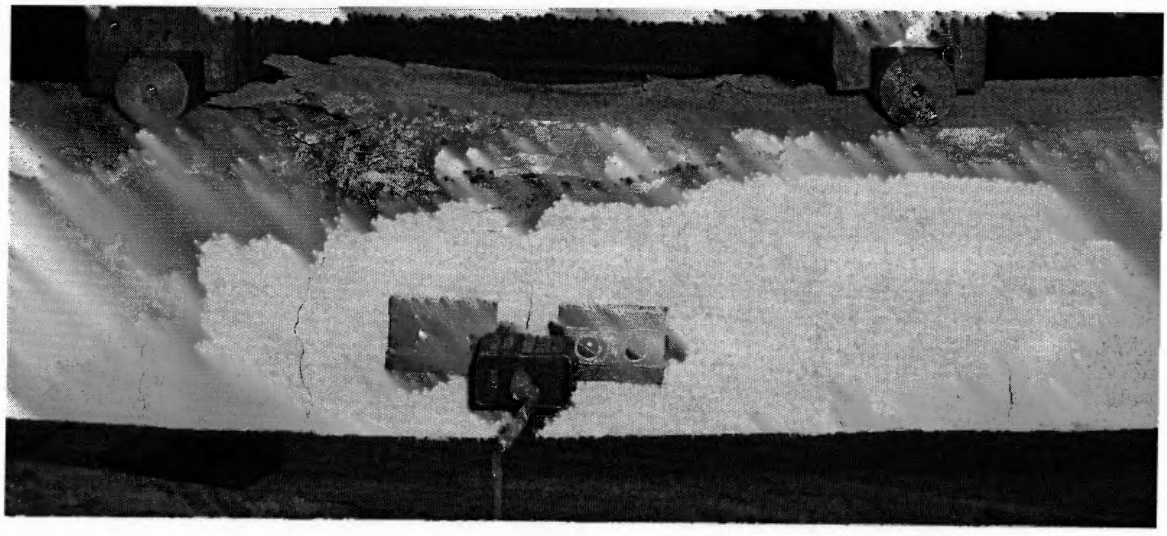

(a) Failure of Over-reinforced concrete

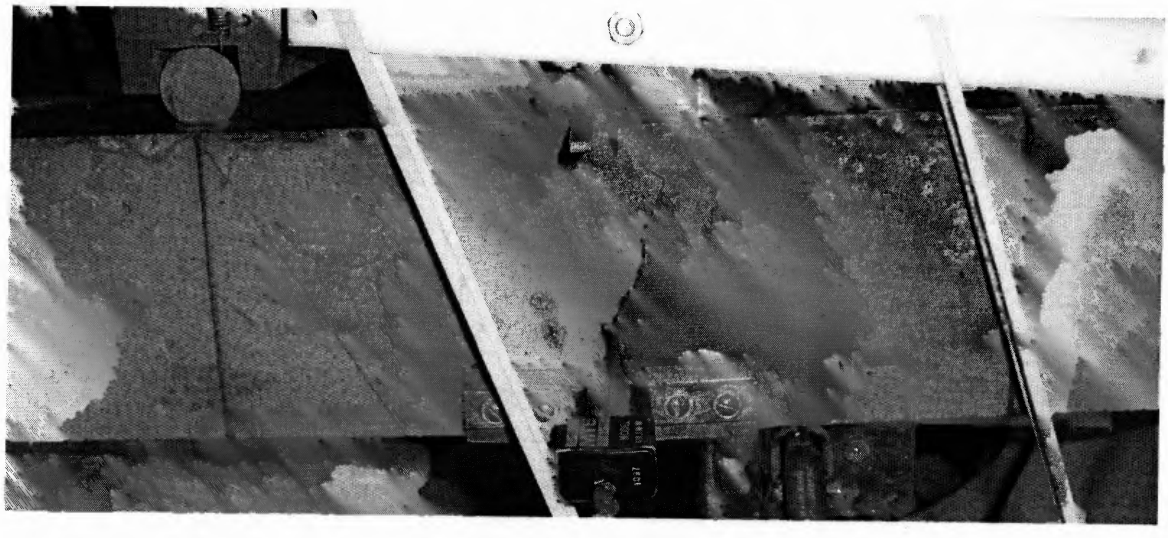

(b) Failure of RC Beam with Reinforcement Less Than Minimum Reinforcement.

Figure 6.8 photos for Concrete Beam with Reinforcement Less Than Minimum Reinforcement and Over-reinforced Concrete beams.

In order to compare between plain concrete and reinforced concrete, two plain concrete beams were also tested in the series III experiments. The results of these comparisons are shown in Figures 6.9 and 6.10. The curve with marks is crack growth versus CMOD response of RC beam whereas the small curve at the bottom is from plain concrete beam. It can be seen that reinforcement contributes significantly to the load capacity of the whole system. It should be noted that before cracking occurs, the whole RC structural system has a higher stiffness. As the NRC beam approaches the strain softening range, crack tends to grow quickly, and stiffness of the whole RC beam decreased accordingly, indicated by changing the slope of the load-displacement curve. And when this change takes place, crack propagation in RC beam become faster as more energy is absorbed by the member.

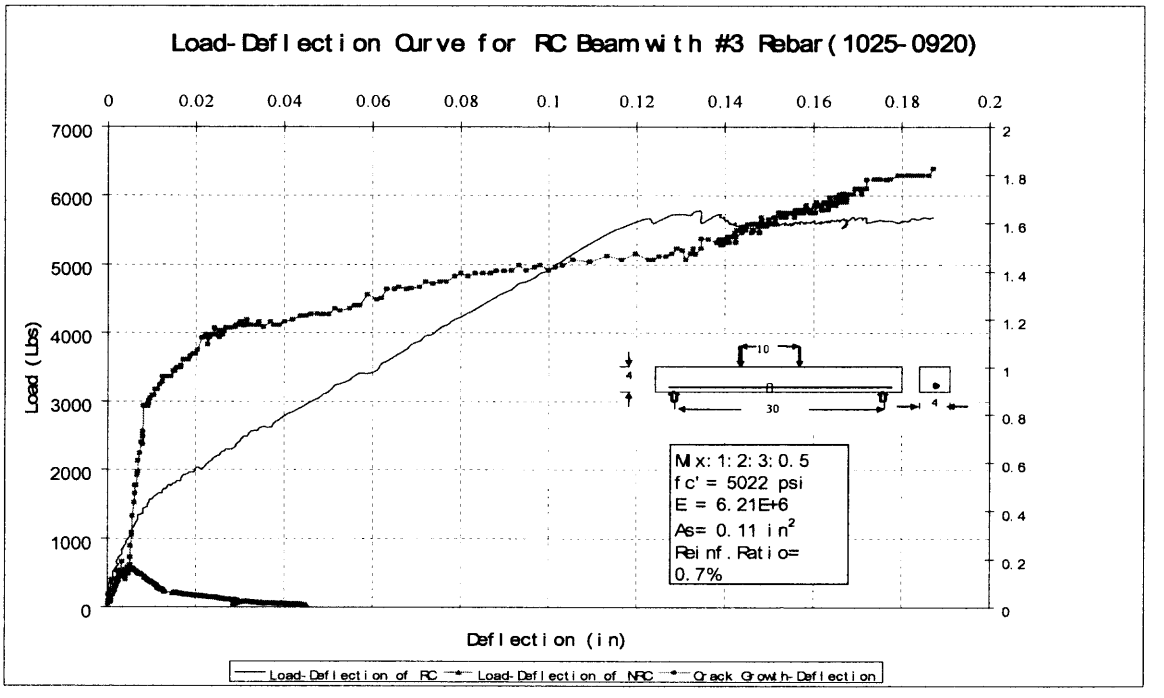

Figure 6.9 Comparison of Load-Deflection Curve for RC Beam and NRC Beam.

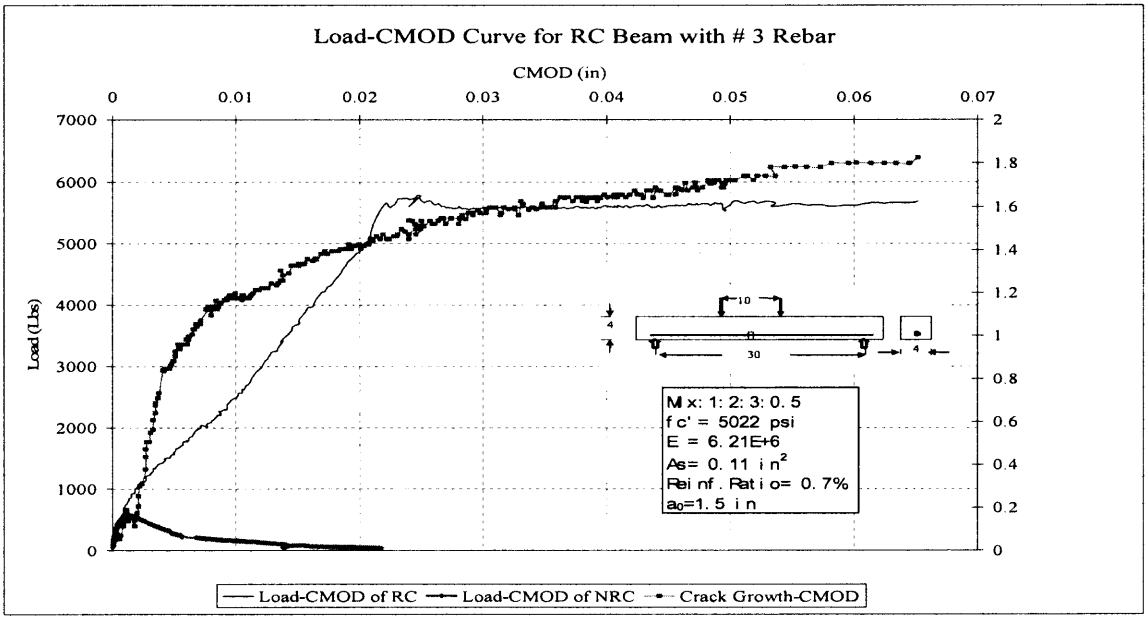

Figure 6.10 Comparison of Load-CMOD for RC Beam and NRC Beam.

6.1.2 Fracture Process Zones in RC Beams

As shown in series I experiments, the ultrasound technique was able to detect the extent of the fracture process zone by performing unloading and reloading. Figure 6.11 (a) and (b) show the load-deflection and crack growth relationships of plain concrete specimens. It was observed that the fracture process zone has fully developed prior to peak load and crack propagation started just before the peak load and continue to grow in the post-peak region. Eventually, crack growth came to a stop as it approached the confinement of the compression zone. Since the traction free portion of the crack has completely separated, such damage is irreversible. However, the microcracks in the process zone (bridging zone), on the other hand, only weaken the system, and thus remain intact. As can be seen in Figure 6.11 (b), during the loading-reloading process, the observed crack growth reversed with a small change in length, representing the size of the process zone as microcracks close during unloading. During reloading, these microcracks reopen and

crack growth proceeds as loading continues. This is undoubtedly the first time ever that microcracking has physically been detected and measured.

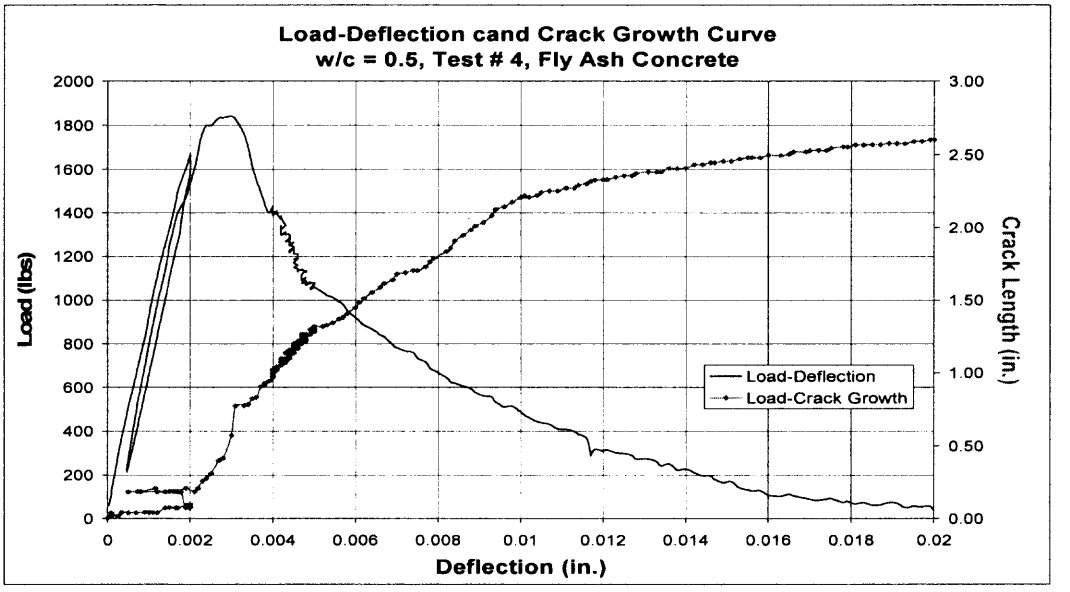

Figure 6.11 (a) Crack Growth prior to Peak Load Detected in NRC Beam using Ultrasound Technique.

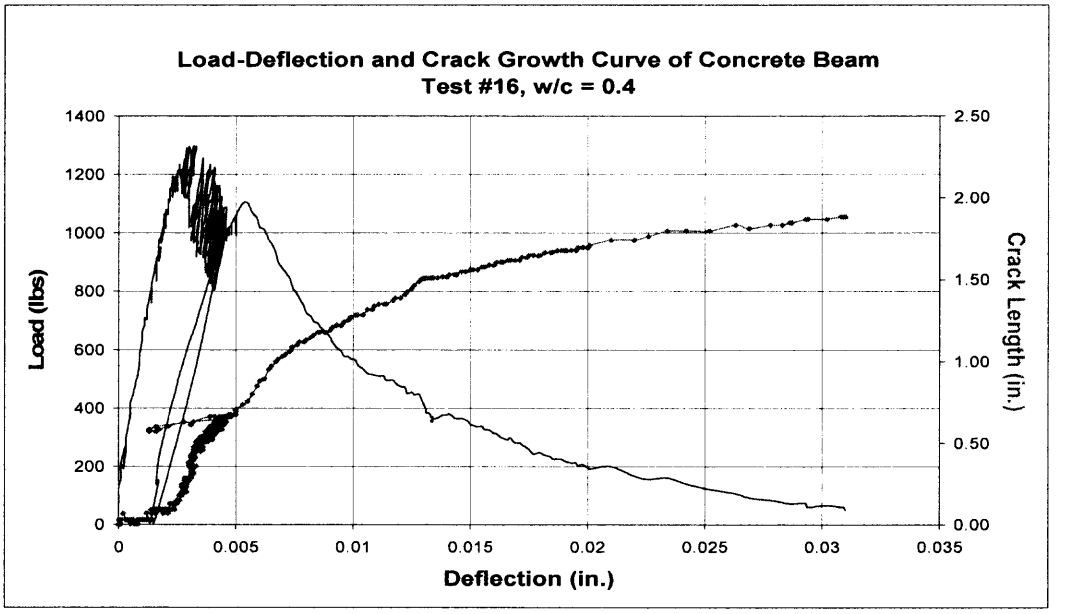

Figure 6.11 (b) Crack Growth in Post-peak Region of NRC Beam Detected by Ultrasonic Technique.

When the unloading-reloading cycle was performed in the elastic range (or within the proportional limit) prior to peak load where cracking has not yet occurred, the crack growth response retracts horizontally with the unloading-reloading process, showing no crack extension. This physically demonstrates that no microcracks or process zone occurs within the elastic range.

In series III experiments, further investigations were carried out on RC beams to observe the fracture process zone by peforming several unloading and reloading cycles during the tests (see Figure 6.2~ 6.7). Figure 6.12 illustrates the whole process of fracture process zone development in a balanced reinforced concrete beam with #5 rebar. When concrete is in the elastic range, there is no damage or process zone in front of the notch tip. With the increases of the external applied load, the fracture process zone grows. Due to the presence of the reinforcement, the whole RC system behaves linearly as the process zone develops. Once it is observed that that some non-linearity appears in the load-displacement curve, it is an indicator that the process zone is fully developed, which corresponds to about 80% of the peak load. The size of fracture process zone drops dramatically as steel reinforcement reaches yielding.

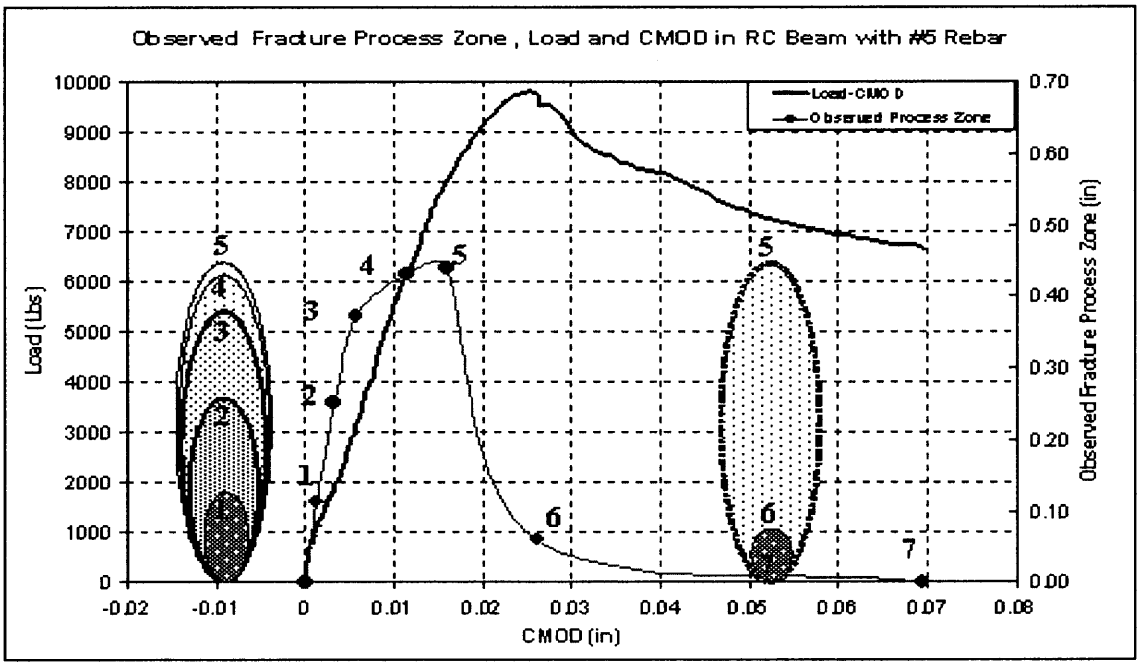

Figure 6.12 Development of Fracture Process Zone with load and CMOD in RC Beam with #5 rebar.

It should be noted that the fracture process zone is growing simultaneously with the extension of the traction-free crack. Figure 6.13 shows the evolution of the traction-free crack as compared to the total crack length, which is in the same RC beam of Figure 6.12. The difference between the two curves is the size of the process zone at that instance.

Variation of the fracture process zone size as observed from the ultrasonic technique for all the tested RC beams and plain concrete are presented in Figure 6.14-a. For plain concrete or unreinforced concrete members, the maximum process zone size was found to be between 0.15-0.2 in., whereas for normal reinforced concrete (under-reinforced through over-reinforced) the size varies from 0.3 to 0.5 in.

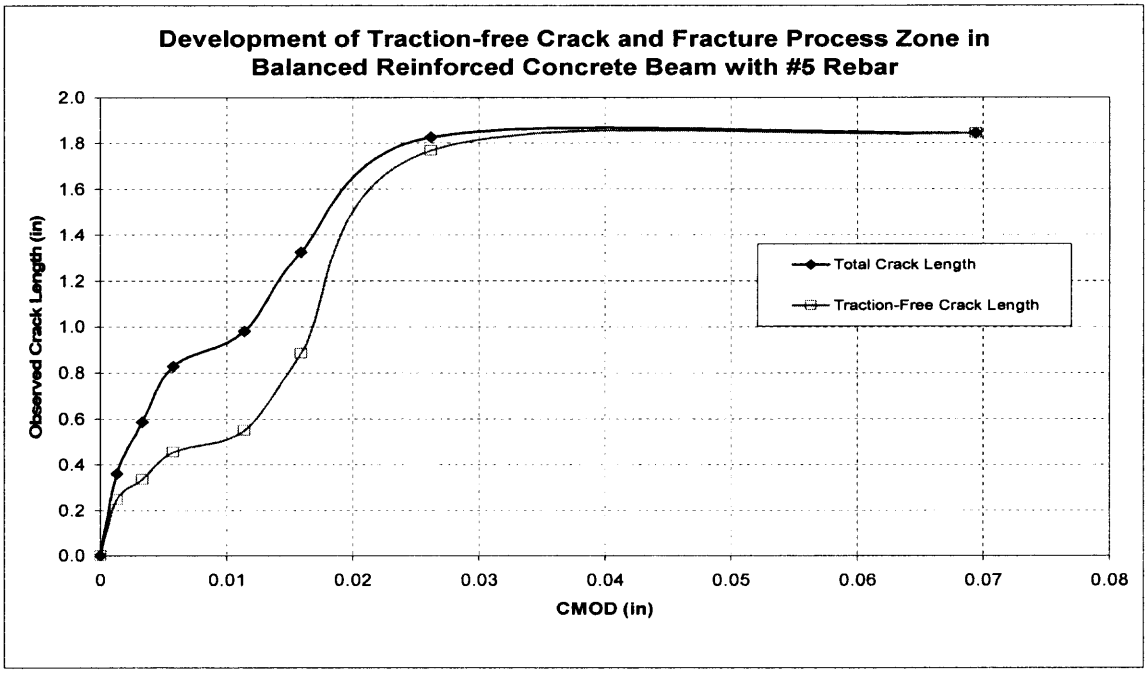

Figure 6.13 Development of Traction-free Crack vs. Fracture Process Zone.

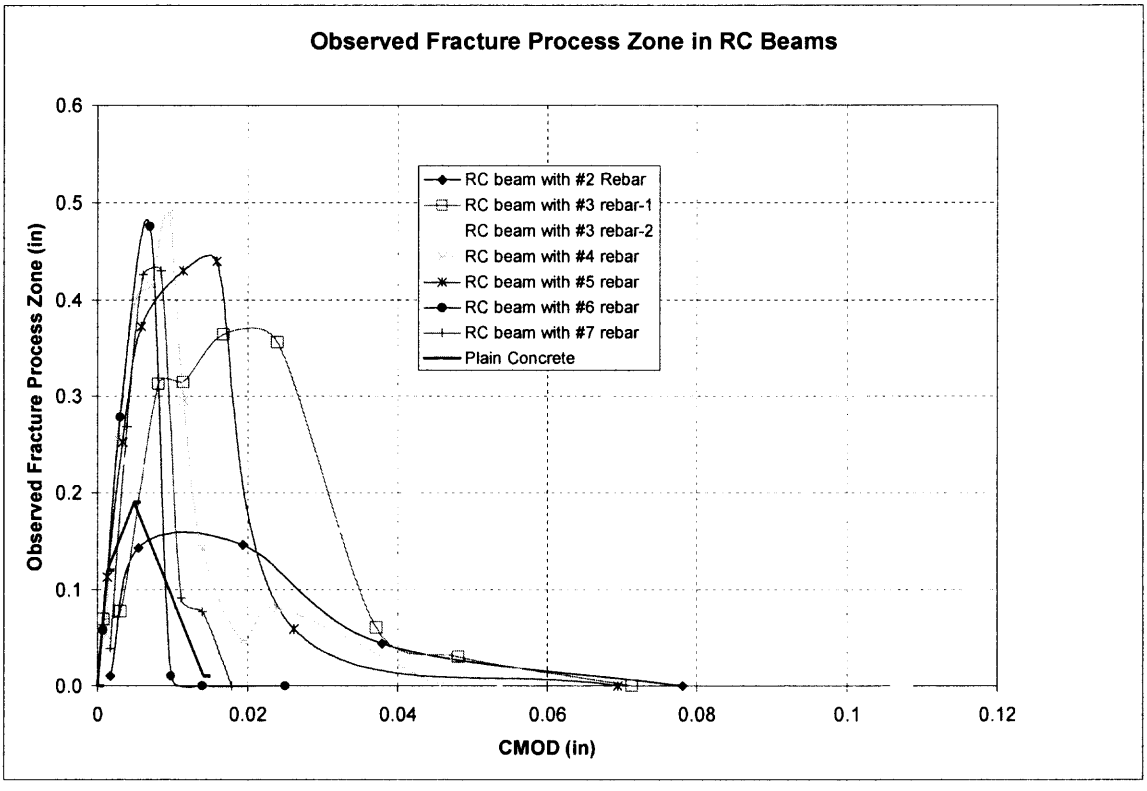

Figure 6.14a Measured Fracture Process Zone in NRC and RC Beams.

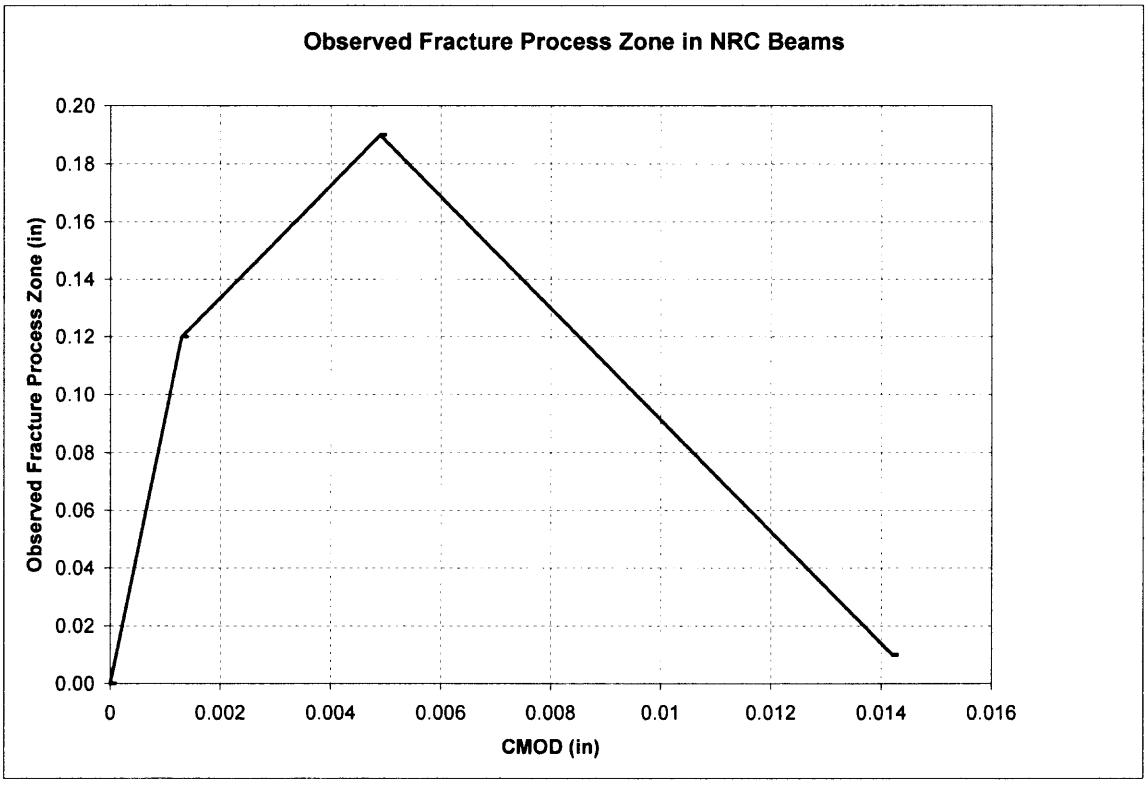

Figure 6.14b Measured Fracture Process Zone in NRC Beams.

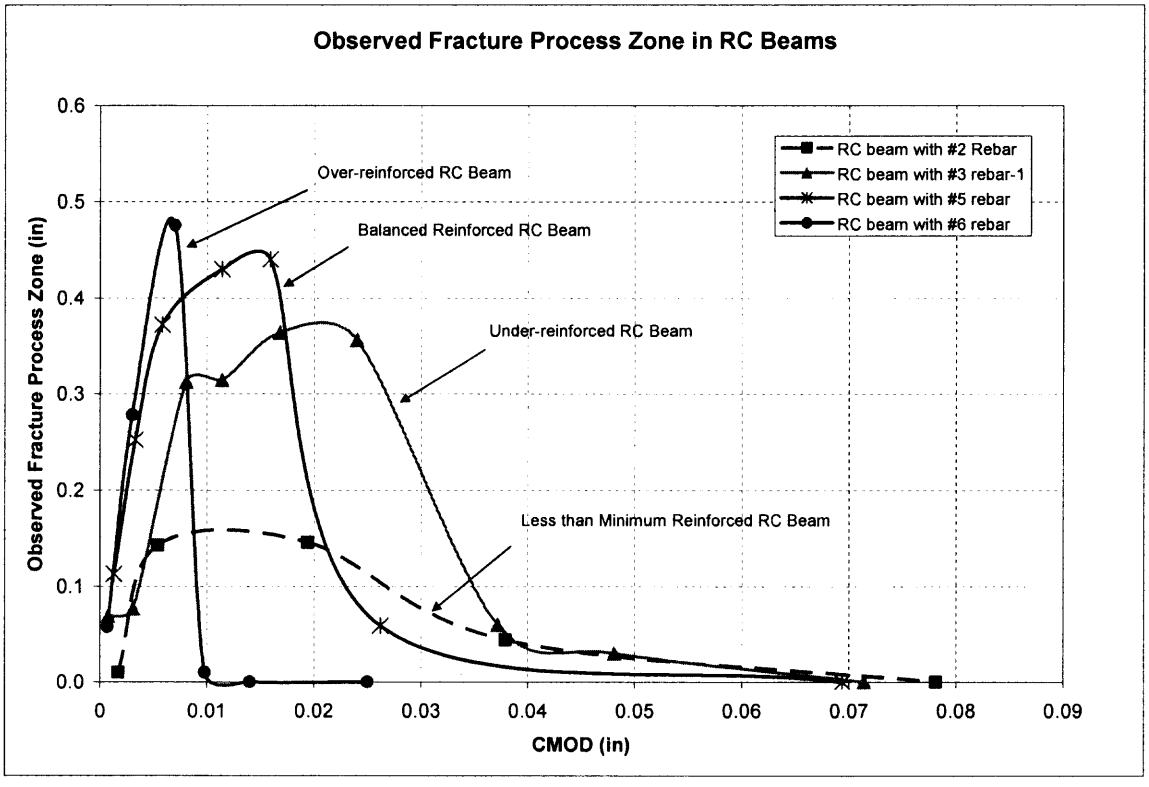

Figure 6.14c Observed Fracture Process Zone in RC Beams.

To clarify the results shown in Figure 6.14a, variation of the fracture process zone size observed from the non-reinforced concrete (or plain concrete) beam is presented in Figure 6.14b. The process zone slowly grows to a size of 0.2 inch and thereafter decreases to nearly zero as CMOD reaches 0.014 inch. Figure 6.14c compares the measured fracture process zone sizes of RC concrete beams with over-, balanced and under-reinforcement. In addition, the observed fracture process zone sizes in the beam reinforced with less than minimum reinforcement are also presented. It can be seen that the size of fracture process zone increases as the amount of reinforcement increases, but with not much variation between under- , balanced and over-reinforcement.

Measurement of crack growth could be one of the most difficult tasks encountered in most fracture tests of concrete and reinforced concrete. The presence of microcracks in the process zone further complicates the measurement process as the exact crack tip is not easily defined since concrete is an opaque material, in which exact tortuous crack front is invisible from outside. Use of ultrasonic technique has overcome this limitation.

In this study, by performing unloading and reloading during testing, the fracture process zones in RC beams were successful measured using ultrasound technique.

6.2 Theoretical Analysis of Fracture Propagation in Reinforced Concrete Beam

Carpinteri (1984) and later Bosco & Carpinteri (1992) proposed an approximate analysis approach to predicting flexural failure in which the concrete and steel actions are coupled. The change in rotation of the beam resulting from the bending moment and reinforcement constrain can be calculated from the relations derived by Okamura,et,al. (1975). Due to the difficulties of estimating the contribution of steel-concrete interaction,

for f_s below a certain load, perfectly rigid-plastic behavior of reinforcement was assumed. This meant that before the yielding or slippage of reinforcement, there is no rotation of the beam. In fact, crack propagation is shown to have happened before the yielding of reinforcement or debonding has occurred. In order to accommodate the presence of reinforcement in concrete, Carpinteri's method was modified and extended to be able to include crack growth before yield or slippage by assuming elastic-plastic behavior of reinforcement. The predicted value using this model was found to be in good agreement with the ultrasound measurement.

6.2.1 Superimposed Effect of Bending and Axial Force on the Deformation of Cracked RC Beam

A reinforced concrete beam specimen with rectangular cross-section of thickness t and depth w is shown in Figure 6.15. The steel reinforcement is at a distance h from the external surface. A through-thickness edge crack of depth $a > h$ is assumed to exist in the stretched position. The cracked concrete beam element is subjected to the bending moment, M and the eccentric axial force, F.

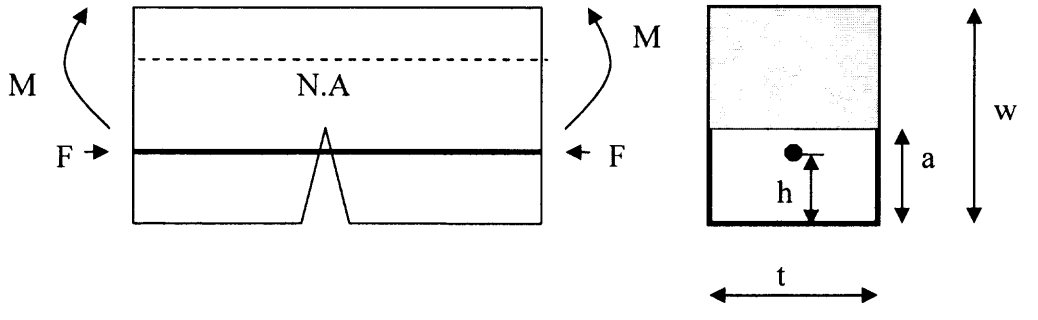

Figure 6.15 Cracked Reinforced Concrete Beam Subjected to Pure Bending Moment.

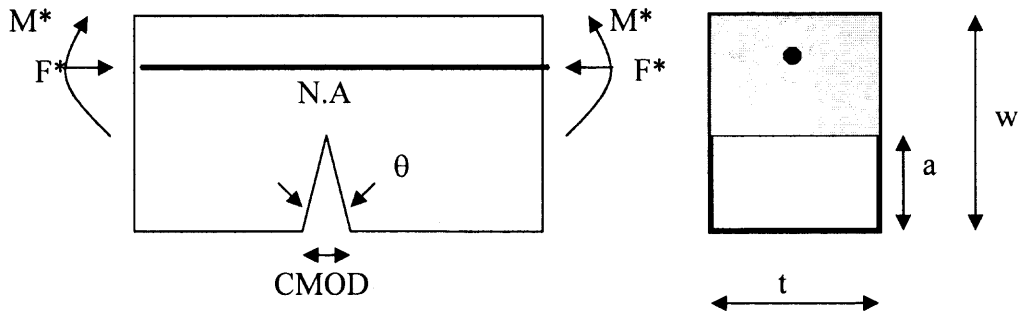

Figure 6.16 Local Rotations in Cracked Beam.

According to the analysis of Okamura, et, al. (1975), considering the cracked beam element subjected to the bending moment, M^* and a concentric axial force, F^*, shown in Figure 6.16, for $\zeta = a/w \leq 0.7$, the local rotation produced by bending moment M^* and axial tensile force F^* can be expressed by equation (6.1):

$$\theta = \lambda_{MM} M^* - \lambda_{MF} F^* \tag{6.1}$$

In which λ_{MM} and λ_{MF} are the increments of compliances caused by the presence of a crack a, and are give by:

$$\lambda_{MM} = \frac{12}{tEW} \int_0^{\zeta} \zeta Y_F(\zeta) Y_M(\zeta) d\zeta \tag{6.2}$$

$$\lambda_{MF} = \frac{72}{tEW^2} \int_0^{\zeta} \zeta Y^2{}_M(\zeta) d\zeta \tag{6.3}$$

in which

$$Y_F = 1.99 - 0.41\zeta + 18.70\zeta^2 - 38.48\zeta^3 + 53.85\zeta^4 \tag{6.4}$$

$$Y_M = 1.99 - 2.47\zeta + 12.97\zeta^2 - 23.17\zeta^3 + 24.80\zeta^4 \tag{6.5}$$

The uncracked section acts as a perfectly fixed joint, as ζ . =0, the local rotation would be zero. That is the boundary condition for formula (6.1).

For the statically indeterminate system in Figure 6.13, the total moment is

$$M^* = M - F(\frac{w}{2} - h) \tag{6.6}$$

While the axial force is

$$F^* = F \tag{6.7}$$

From Figure 6.16, for a given value of CMOD and the length of the total crack, a, which includes the initial notch ,a_0 , and a value of crack growth Δa, the value of θ from equation (6.1) is determined by CMOD/a. Therefore, by substituting the value of θ, determined by CMOD and crack length, into Equation 6.1, a relation between crack length and the external applied load can be established. It is evident from Equation 6.1 that further progress is not possible until we estimate the contribution from the steel-concrete interaction F at each load level.

Since Carpinteri assumed perfectly rigid-plastic behavior of steel, hence, until the steel begins to yield or slip, the global rotation due to bending moment M^* and the closing force F^* is zero. This assumption was used to calculate the closing force contributed by steel reinforcement. It is obvious that this assumption did not conform to the actual condition in tests. From Figures 6.1-6.6, it is clear that some displacements, namely CMOD or deflection, already took place before the yielding of steel. Additionally, the necessity of determining the steel closing force is that it is needed for calculating the local rotation. However, if the local rotation is zero , then there is no need to find the steel closing force.

In literature, Jenq & Shah (1989), So & Karihaloo (1993) and Reinhardt & Van (1992) investigated this closing force based on the behavior of a reinforcing bar when it

was pulled out of concrete. However, these methods are very complex and too many factors inside their formula, making their results undependable.

It is no doubt that before yielding, reinforcing bar behaves linear elastically and therefore internal stress of the reinforcing bar is proportional to the strain or displacement of the steel. Since we assume that there is no slippage before the yielding of steel, so the internal stress of reinforcing bar should have linear correlation with the CMOD. Knowing the CMOD at the yielding point at which the internal stress of reinforcing bar is f_y , the internal stress of reinforcing bar can then be expressed at each load level by:

$$f_s = \frac{f_y}{CMOD_y} CMOD_i \tag{6.8}$$

It should be noted here that for over-reinforced concrete beam, since steel does not yield, this method is not applicable. And since Equations (6.4) and (6.5) are only valid for $\zeta \leq 0.7$, which is when crack develops over 70% of the beam depth, this method will not be accurate.

6.2.2 Comparing Predicted Crack Length with the Measured value from the Ultrasonic Device

Using the proposed approach, crack length was predicted based on the test results from Series III. Comparison of the predicted and the measured values are presented in Figure 6.17-6.20 for #3, #4 and #5 reinforcing bar, respectively. These are two specimens with #3 rebar which were tested at different ages, in this study.

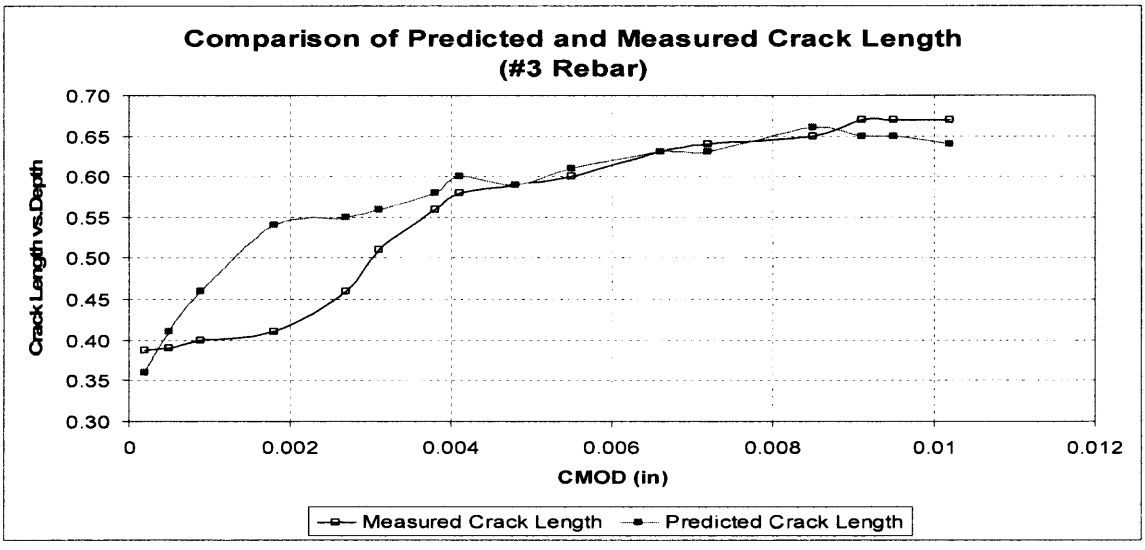

Figure 6.17 Comparison of Predicted and Measured Crack Length for RC Beam with #3 Rebar (tested in 10/25/05).

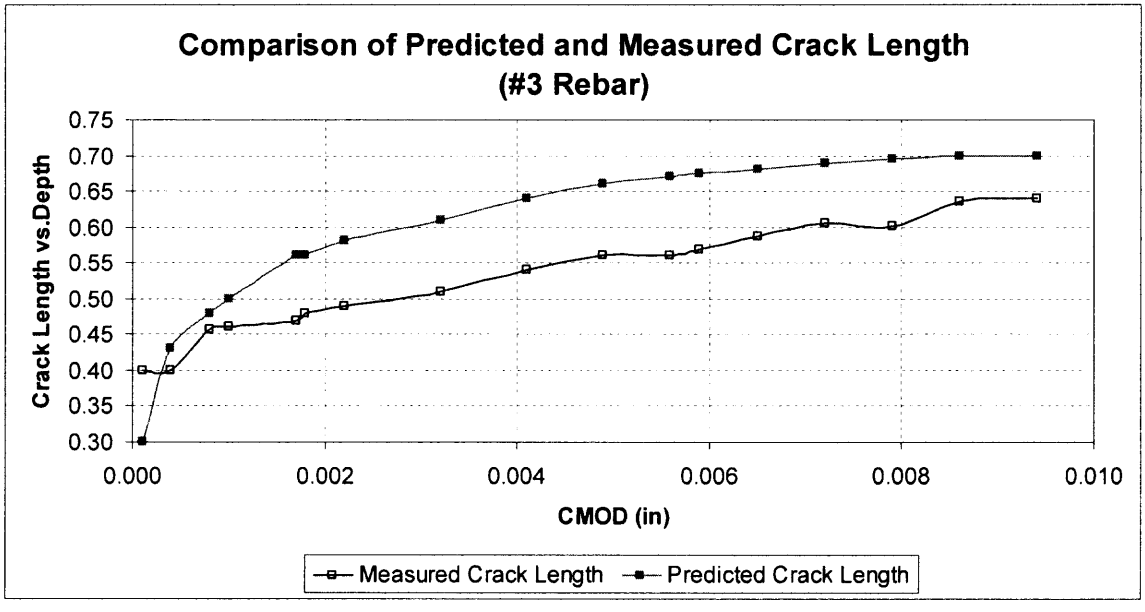

Figure 6.18 Comparison of Predicted and Measured Crack Length for RC Beam with #3 Rebar (tested in 10/10/05).

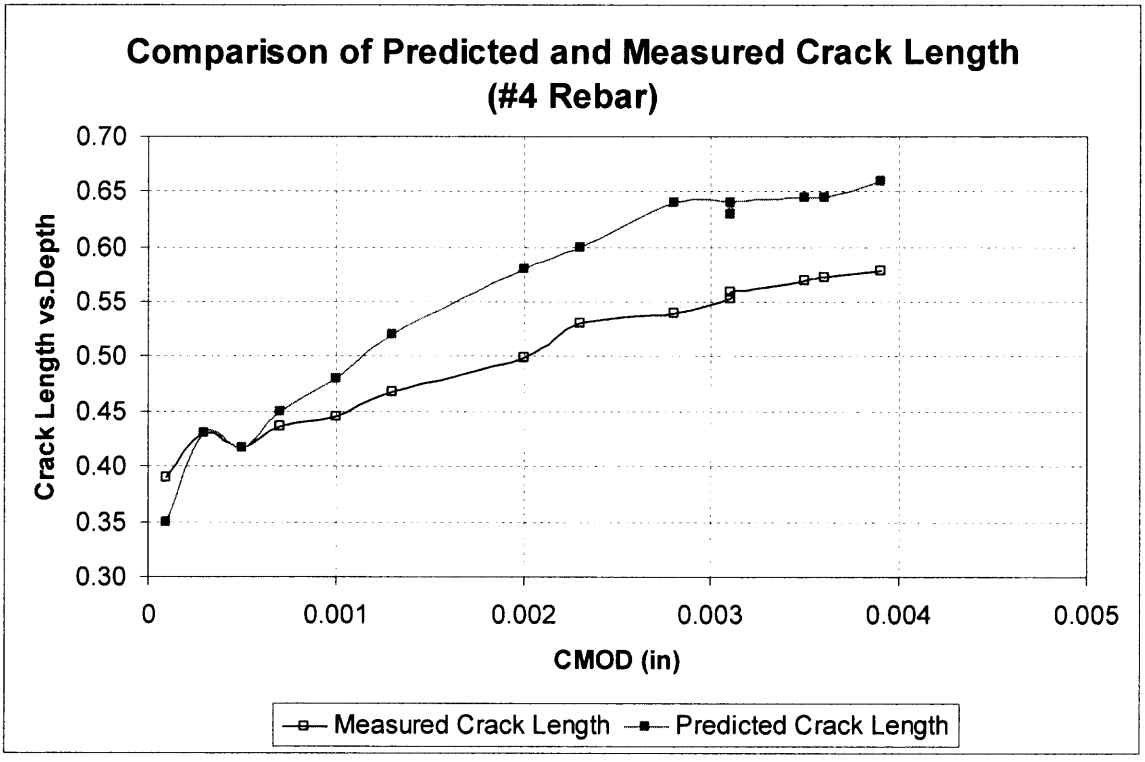

Figure 6.19 Comparison of Predicted and Measured Crack Length for RC Beam with #4 Rebar (tested in 10/18/05).

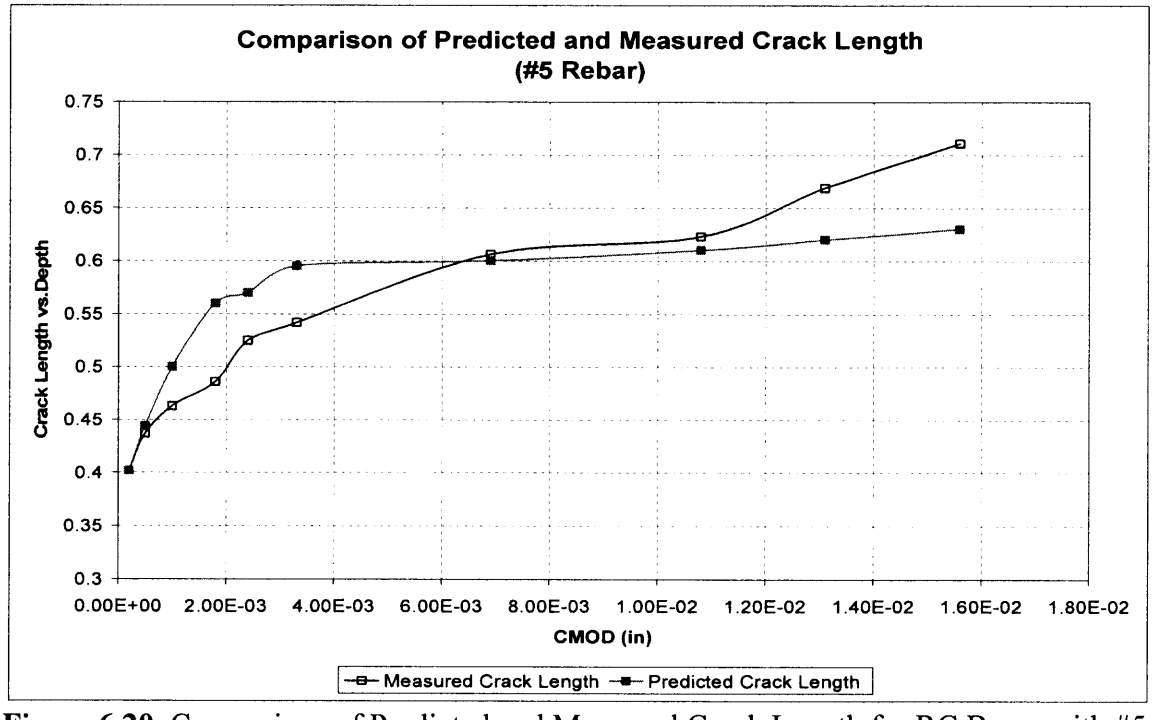

Figure 6.20 Comparison of Predicted and Measured Crack Length for RC Beam with #5 Rebar (tested in 10/18/05).

From these figures, it can seen that predicted crack lengths using the proposed method are in good agreement with the measured results obtained from the ultrasonic technique. Discrepancies between these two values can be attributed to the following factors:

1. In our experiments, there are always some "noise" in the ultrasonic signal which has some influence on the accuracy of the results;
2. The notch in the specimen was pre-molded so its behavior was different from the actual fractured crack;
3. The damage of top layer concrete was also detected by the ultrasonic device and automatically included into the measured crack length by ultrasonic device.

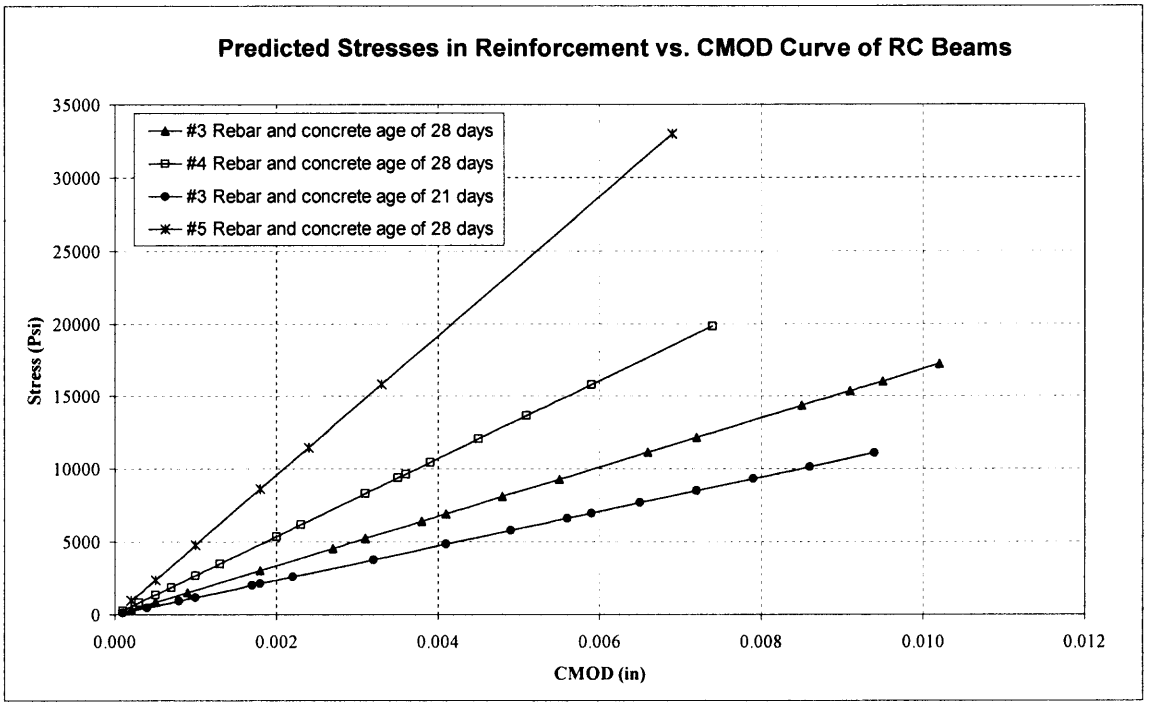

Figure 6.21 Predicted Stresses in Reinforcement vs. CMOD in RC Beams.

The predictions of forces in the reinforcement, used for crack growth prediction are presented in Figure 6.21. Since cracks in the test specimens were arrested before the steel reached yielding, steel stresses predicted in Figure 6.21 therefore do not reach the

yield strength. It can be noted that the larger the bar size, the higher is the stressed in the reinforcement steel, which is directly related to the bond strength between cement matrix and the reinforcement.

6.2.3 Parametric Study

In the above theoretical analysis, the yield point in the load-displacement curve is required for calculating the stress in the rebar at any given load level. Since specimens with #6 and #7 rebar are over reinforced, thus yielding of steel could not be reached and #2 steel used in this study was a round bar, which tends to affect bonding, a parametric study was then performed to investigate the influence of steel stress on the prediction of crack growth in these beams.

By varying the stress in the steel, the crack length was calculated using the method proposed and compared with the measured values. The results are shown in Figures 6.22 and 6.23 for specimens reinforced with #6 and #7 steel bar, respectively.

As can be seen from this parametric analysis, the predicted crack lengths in these two beams show similar trend as the measured values. It should be noted that the predicted values show a larger discrepancy with the measured values when the stress in steel is included. At the end of predicted curve, the crack length vs. beam depth ratios tends to decrease slightly. This is probably due to the presence of multiple crackings, which redistributed fracture energy and CMOD, causing the predicted crack growth into retraction.

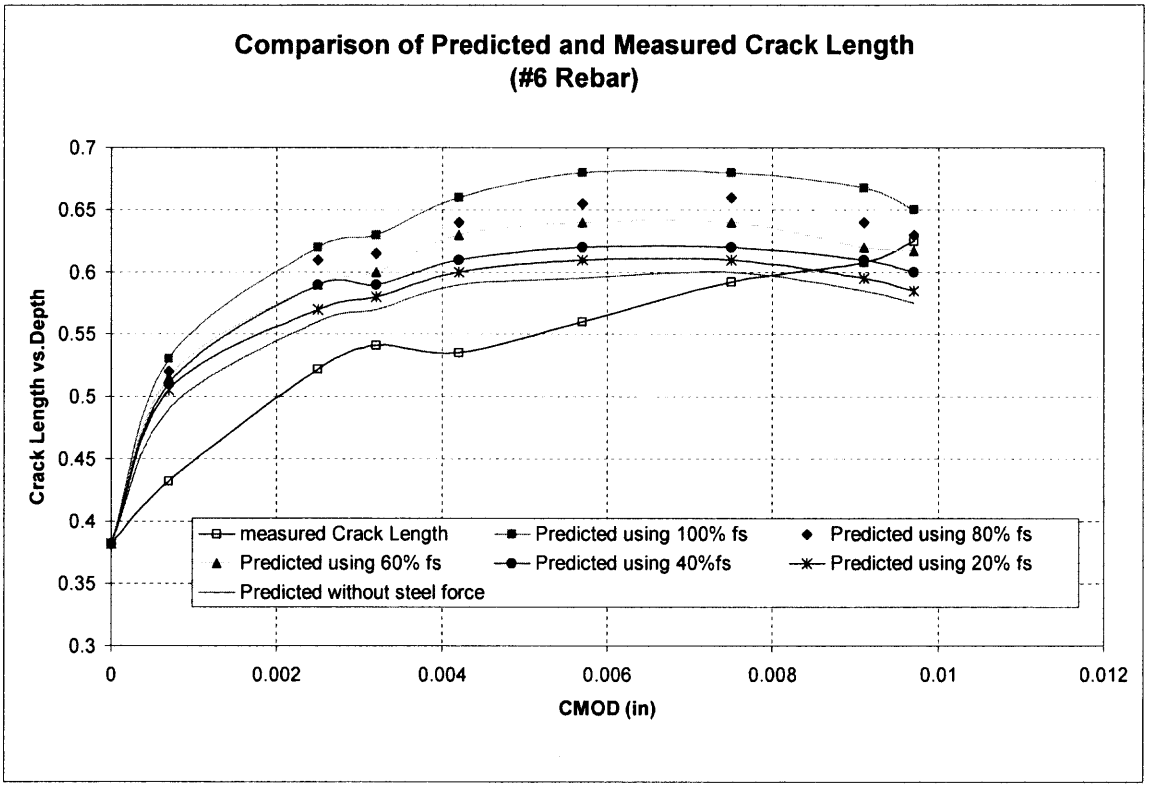

Figure 6.22 Crack Length Prediction Using Different Percentage of Steel Stresses in the #6 Rebar.

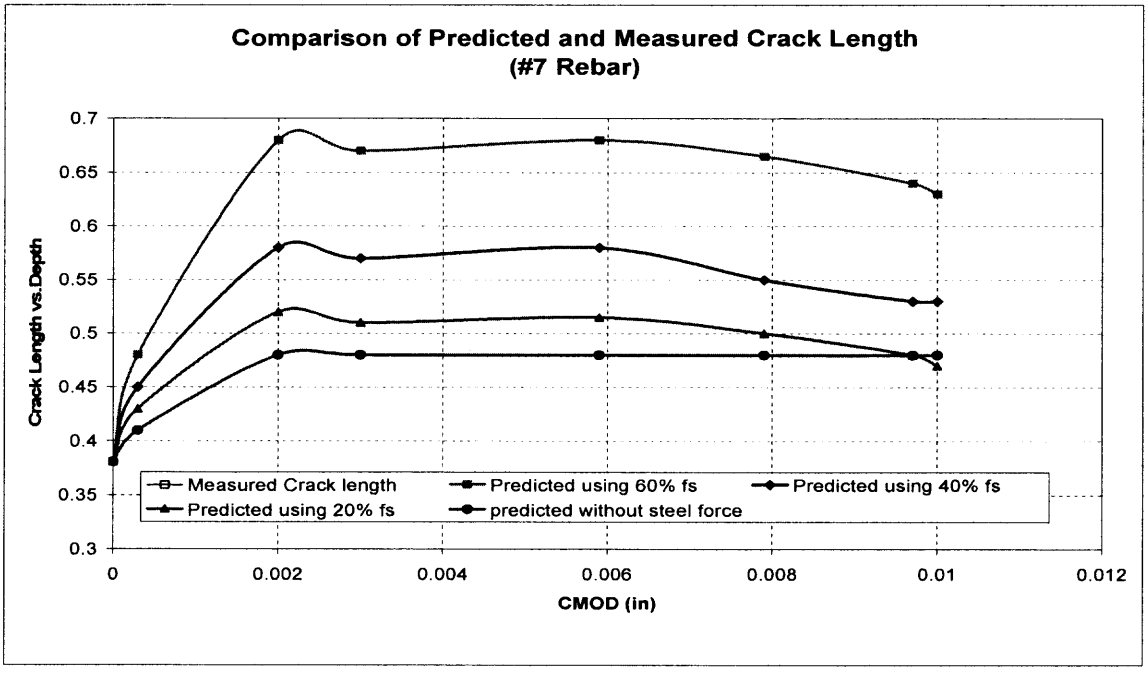

Figure 6.23 Crack Length Prediction Using Different Percentage of Steel Stresses in the #7 Rebar

6.2.4 Summary

Even though some discrepancies exist in the predicted results, it is believed that the proposed approach provides sufficient accuracy for engineering practice. As no other approach is presently available, proposed approach serves as a preliminary tool to analysis cracked reinforced concrete beams.

6.3 Remaining Service Life Prediction of Plain Concrete and RC Beams

As proposed in Chapter 5, the remaining service life of fractured concrete elements can be predicted in terms of fracture energy from a normalized crack growth. Preliminary results of mortar, plain concrete and reinforced concrete have been presented in Figure 5.5. Provided that crack growth can be successful predicted using the proposed approach in Section 6.2, the remaining service life can be estimated without tedious measurement of crack length. For RC beams with under-, balanced and over-reinforcement, both the predicted remaining service life and the measured remaining service life curves were generated and shown in Figures 6.24-6.26 for beams with #3, #5 and #6 rebar, respectively.

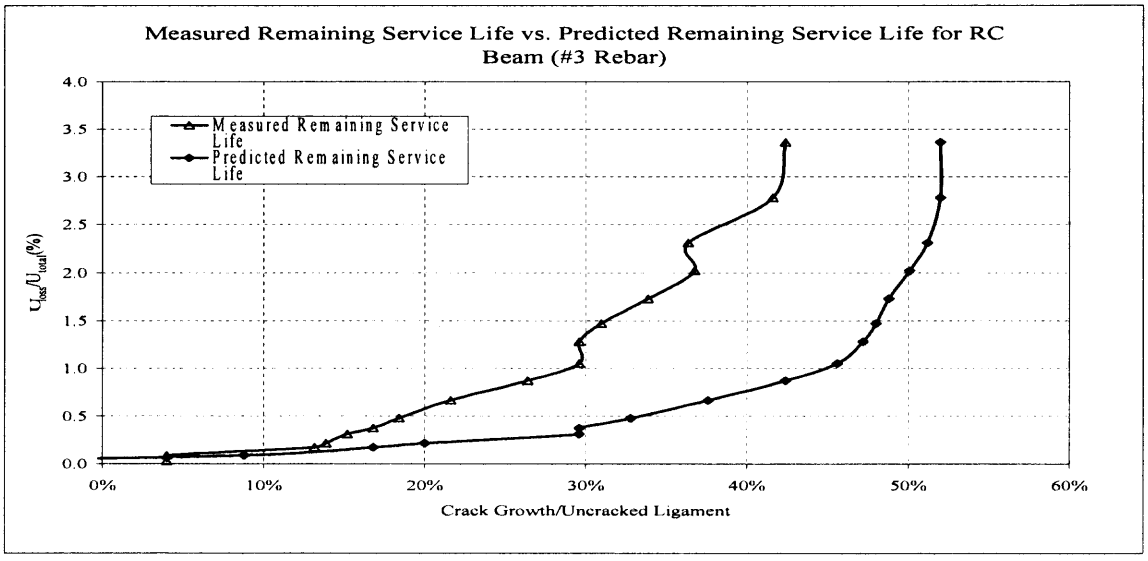

Figure 6.24 Measured Remaining Service Life vs. Predicted Remaining Service Life for Under-reinforced Concrete Beam.

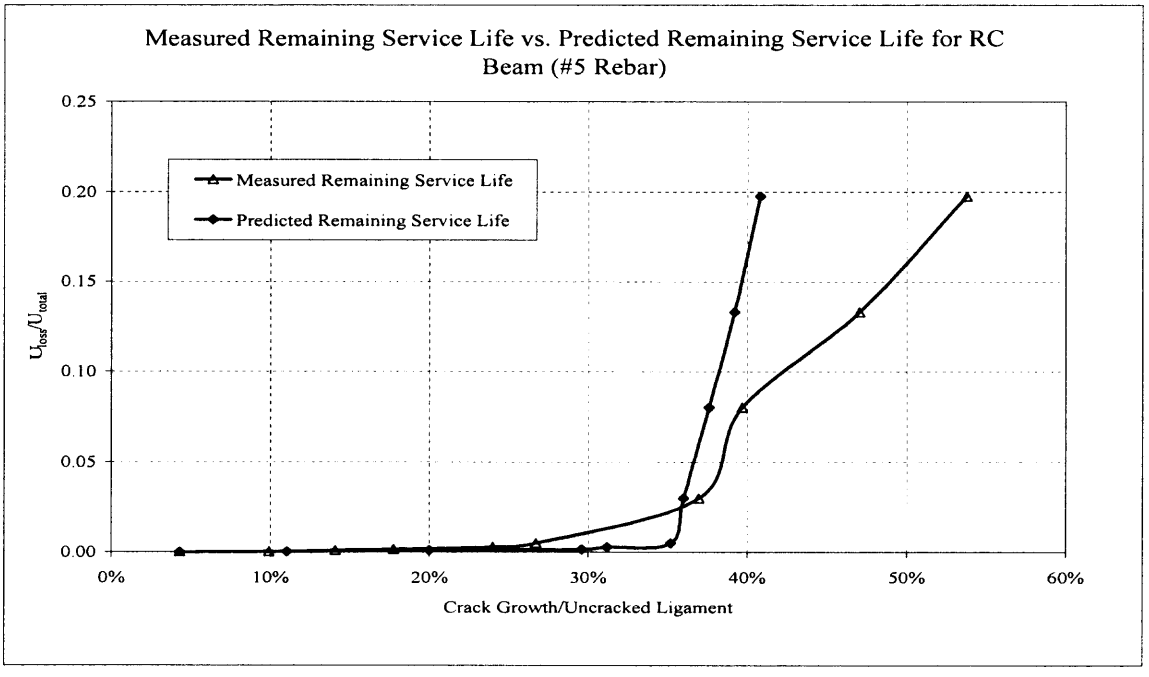

Figure 6.25 Measured Remaining Service Life vs. Predicted Remaining Service Life for Balanced RC Beam.

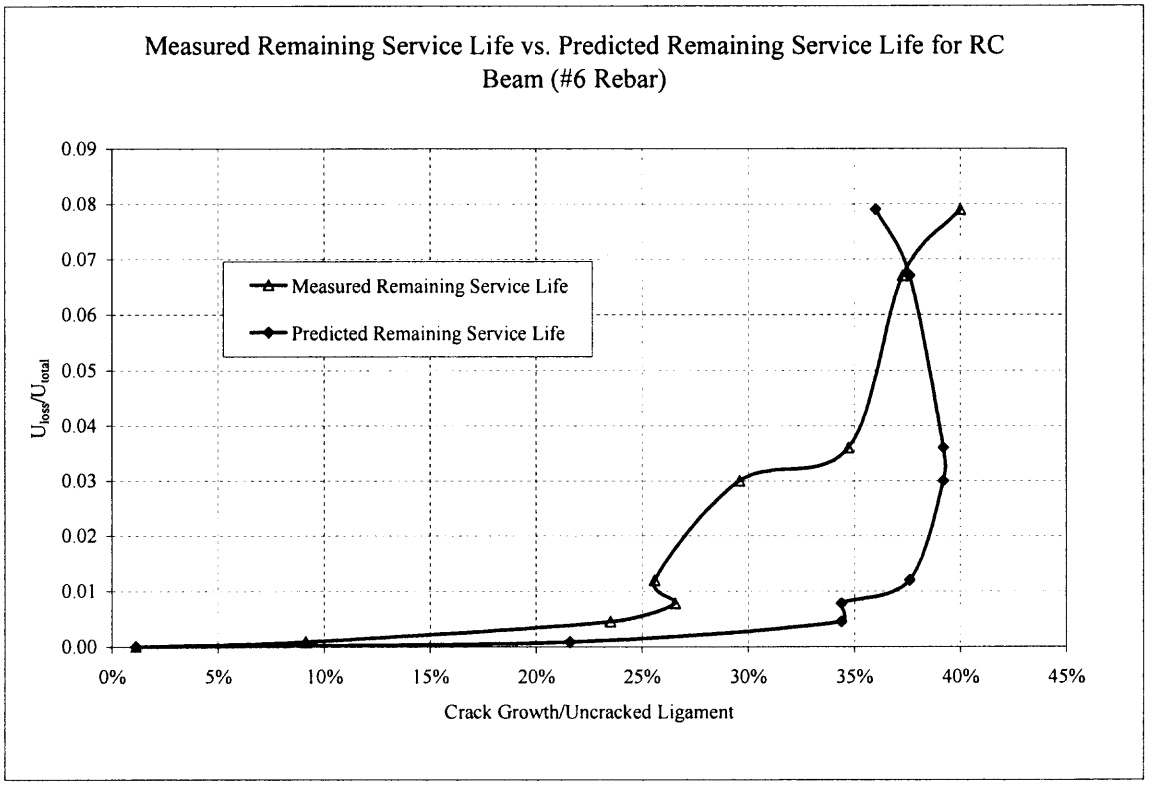

Figure 6.26 Measured Remaining Service Life vs. Predicted Remaining Service Life for Over-reinforced Concrete Beam.

In general, the predicted normalized energy loss versus crack growth relationships show a similar trend with the experimentally measured values. Discrepancies in over-reinforced RC beam can be attributed to the existence of multiple cracks along the specimen as the load increases and the energy released to other cracks causes some small retraction of the observed primary crack. While ultrasound device can detect damage both from crack propagation and crushing in the compression zone, the measured value of crack growth would actually be larger than the exact value. Another critical factor which should be noted here is that the present ultrasonic test setup is only capable of monitoring a single crack, thus rendering some degree of inaccuracy once multiple crack occur.

In short, it can be stated that the remaining service of fractured concrete members can be predicted using the proposed approach in terms of fracture energy without the measurement of crack growth. Noted that accuracy of the proposed approach for predicting crack growth is not reliable when crack vs. beam depth ratio exceeds 70%, nonetheless, under the normal service condition, no one concrete structural element will remain in service at this extreme crack over beam depth ratio. Thus, this proposed approach should be still be usable in assessing the damaged concrete structures.

In this study, in order to provide the complete curves of the remaining service life of fractured cementitious concrete structural elements, the measured value of crack lengths were used here to predict all the remaining service lives. The chart was generated using the load-CMOD curve and the ultrasonic measured crack length.

While Figure 6.27 presents the stage of energy loss of concrete members versus its corresponding observed crack growth, to predict the remaining service life (or load carrying capacity) of a damaged concrete structure, a plot of energy remained versus crack growth should be used instead. This relationship is shown in Figure 6.28 and the diagram can directly be used in practice to assess the remaining load carrying capacity of any cracked concrete members.

It is shown in the diagram that the performance of NRC beams (unfilled label) have the shortest service life as compared to RC members. For any given crack growth ratio, the percentage of energy loss of the NRC beams is much more than the RC ones. Among all the RC beams, over-reinforced concrete members exhibit a shorter service life than the balanced and the under-reinforced concrete beams. Generally, the presence of reinforcement in a concrete beam, no matter how small it is, should lead to the increase of

its remaining service life (see the comparison between the specimen with #2 rebar versus plain concrete members).

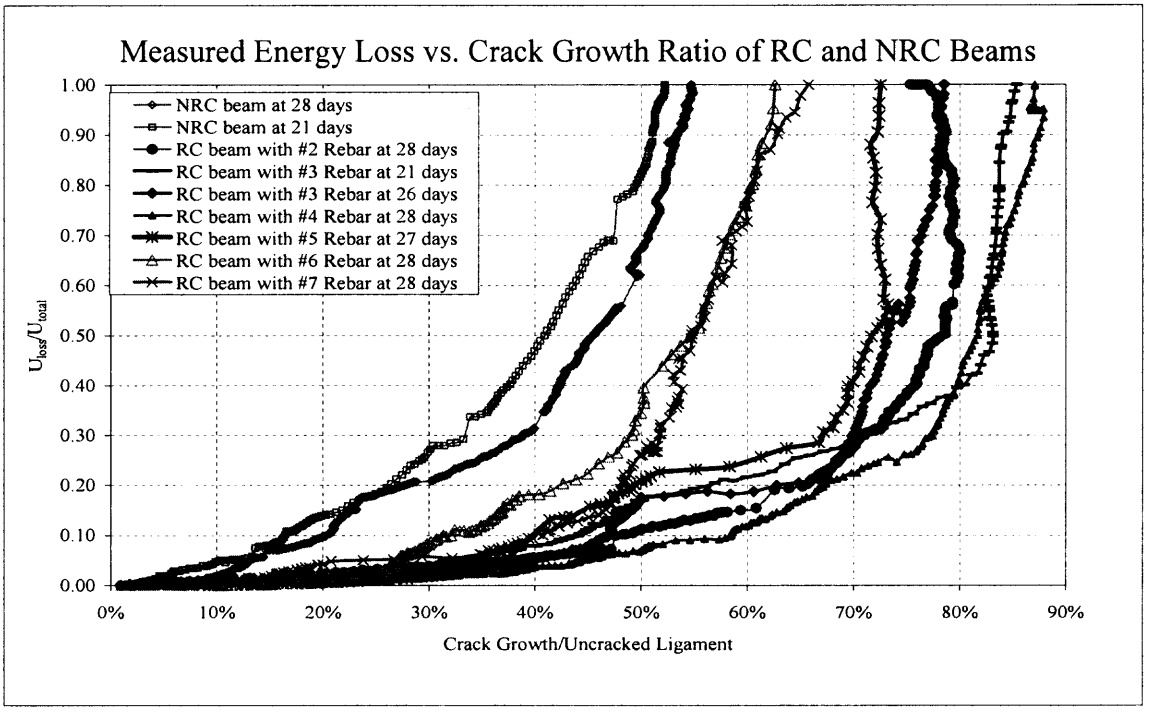

Figure 6.27 Measured Energy Loss versus Crack Growth Ratio of RC and NRC Beams.

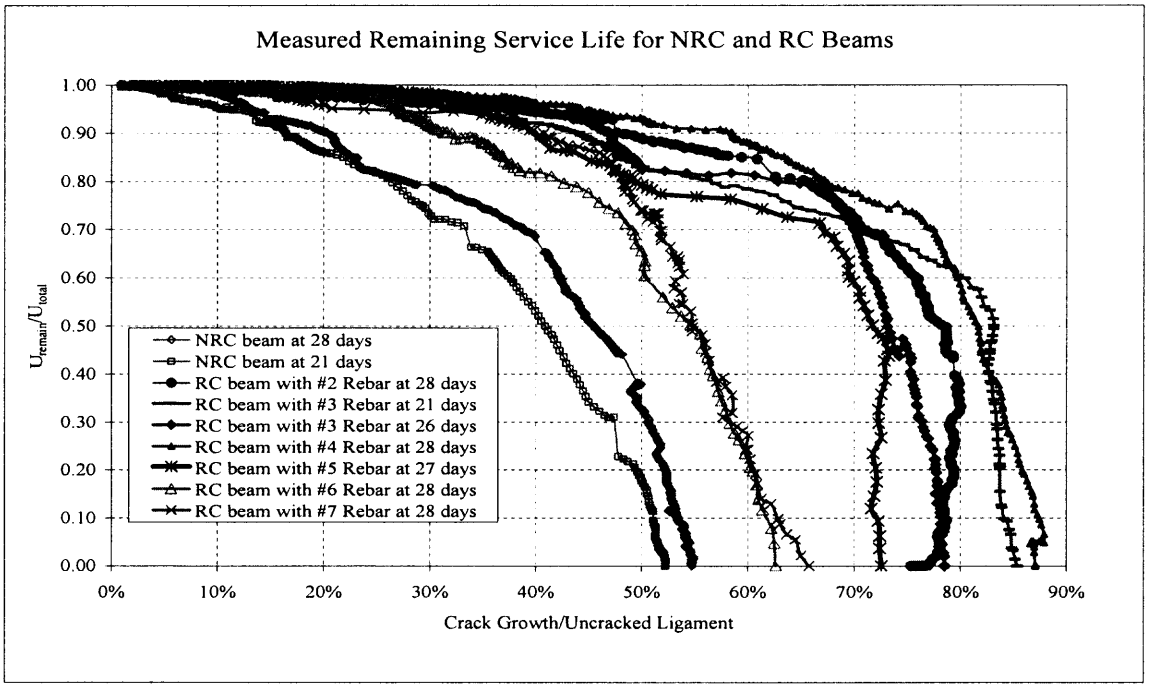

Figure 6.28 Measured Remaining Service Life Chart on RC and NRC .

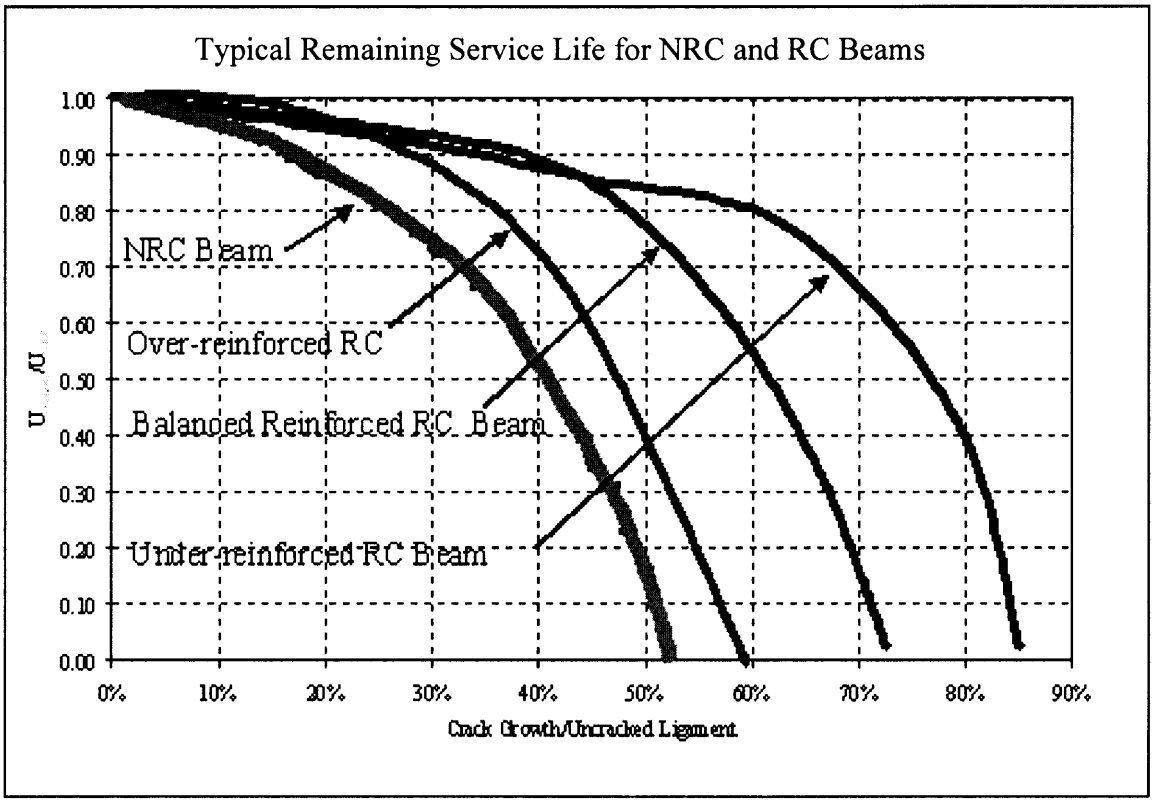

Figure 6.29 Typical Normalized Energy loss versus Crack Growth for NRC and RC members.

Typical normalized energy remained versus crack growth relationships of cementitious composite members should behave as illustrated in Figure 6.29. Due to the brittle nature of plain concrete, the unreinforced concrete (NRC) beam should have the shortest remaining service life as compared with reinforced concrete (RC) beams. The presence of reinforcement in unreinforced concrete matrix provides ductility to the member, thus enhancing the service life of the concrete member. Typical reinforcement used in practice in conventional concrete beams is between 0.5%~2.0%, a range commonly known as "Under-reinforced" ensuring a ductile failure of the overall member. In Figure 6.29, under-reinforced RC beam shows the best overall performance, or in other words, has the longest service life under the same cracking condition. As the amount of

steel increases, the RC beam will reach a stage called "Balanced Condition", where reinforcement reaches yielding (f_s=f_y) and simultaneously concrete approaches crushing (ε_{cu}=0.003). RC beams with balanced reinforcement tends to be more brittle thn under-reinforced RC members (see Figure 6.29), indicating a shorter service life. Ironically , over-reinforced RC beams are rather brittle and exhibit failure characteristic similar to those of plain, unreinforced concrete members. Interesting , over-reinforced RC beams may have higher load carrying capacities than other RC beams as discussed early, as steel reinforcement serves to be the primary load-carrying component of the composites, its failure, once reaches, is abrupt and brittle. Thus, as shown in Figure 6.29 , the over-reinforced concrete beams exhibit a much shorter service life than expected. Experimental results from this study confirm these failure characteristics of plain and reinforced concrete members (see Figure 6.28). The brittle and ductile load-deformation behaviors of unreinforced and reinforced RC beams of different amount of reinforcement was illustrated early in Figure 6.1. These findings further justify ACI recommendations to only use "Under-reinforced" beams in practice.

CHAPTER 7

CONCLUSIONS, RECOMMENDATIONS FOR FUTURE WORK

7.1 Summary and Conclusions

In this work, studies of the experimental and theoretical fracture behavior of Portland cement concrete notched beams were undertaken. Totally 46 concrete beams, in a variety of testing geometries and setups, were tested. A novel nondestructive testing method, ultrasonic acoustic shadowing, not previously utilized in any concrete studies, was used to measure the extent of crack propagation to a level of accuracy never before achieved. The investigations showed the fracture behaviors of un-reinforced and reinforced concrete as follows:

1. There are three stages within the whole process of crack propagation in concrete beams: (1) elastic region; (2) the stage of stable crack propagation before the peak load and (3) unstable fracture propagation after the peak load.
2. RC beams with different reinforcement ratio demonstrate different bending failure modes and the lengths of fracture process zones in RC members tend to vary at different load level. At about 80% of peak load, fracture process zones had fully developed.
3. Multiple cracks appeared along the whole RC beam during testing even though a notch was pre-molded over the level of the reinforcement.

These observations have led to the development of the Effective Compliance Fracture Model (ECFM), which show significant improvement over previous nonlinear fracture models. A large-scale fracture process zone is incorporated employing a superposition approach, and an equivalent elastic beam concept is then used to evaluate the fracture toughness in terms of the stress intensity factor. The values of fracture parameter, K_{IC}^{e}, obtained from specimens of different sizes, showed to be size-

independence when crack growth over beam depth ratio is less than 0.4. Since unloading and reloading is not required, the proposed model has some advantages over the TPFM model proposed by Jenq and Shah (1985).

Considering that all cement concrete structural elements in practice are reinforced, crack propagations in reinforced concrete beams were investigated theoretically based on the series III experiments. By superimposing the effects of bending and an axial force from the reinforcement, a new approach was proposed to predict crack propagations at any load level in RC beam tests. Elastic and perfectly plastic behavior of reinforcing steel was assumed and thus the approach is able to predict crack growth before yielding or debonding occurs. The predicted values of crack growth are in good agreement with those measured by ultrasonic instrument. This is the first time that fracture mechanics theory has been successfully applied to RC beam, taking into account of the influence of reinforcement on crack resistance of RC beam. The proposed approach employs the basic concept of fracture mechanics and simple structural mechanics theorems, which allows structural engineers to apply fracture mechanics to engineering practice.

In order to evaluate service condition of fractured concrete elements, analysis of the remaining service life in terms of normalized fracture energy based on load-displacement curve was proposed. Kim and Navalukar's work on the bi-linear relationship of load-line deflection and CMOD, fracture energy, which was calculated using load-deflection curve initially proposed by Peterson (1985), are the basis of this idea. A load-CMOD curve is used in this study to measure the fracture energy since CMOD reflects local behavior of crack propagation and therefore not affected by any possible support crushing due to the test setup.

A summary of these remaining service life prediction curves for non-reinforced (concrete) and reinforced concrete members are presented in Figure 6.28. The diagram shows performance of non-reinforced concrete beam to have the shortest service life as compared to reinforced concrete whereas RC beams with under-reinforcement exhibits the longest service life. This diagram can easily be applied in practice to predict the remaining service life of any cracked concrete beams by inputting crack growth over uncracked ligament ratio and reinforcement ratio.

7.2 Recommendations for Future Work

1. Influence of shear stresses on crack propagation in beams is often neglected in many fracture models. But in practice, most cracks appear under the mix-mode loading condition. It will be interesting to investigate crack propagation in RC beams incorporating the effects of shear stress;

2. So far, ultrasonic technique can only detect single crack propagation but in practice multiple cracks appeared in most tests. The technique needs further development so the effect of multiple cracking can be detected.

3. It was found in this study that age of concrete specimens might have some influences on the crack resistance of concrete. Additional study should be carried out to understand their influences since most reinforced concrete members in service are old and have been through years of serviceability.

APPENDIX A

RESULTS OF FIRST SERIES OF EXPERIMENTS

In this series test, 14 beam specimens were tested on Mortar, Plain Concrete and Reinforced Concrete in March, 2003. The relationships between Load, Load line deflection, CMOD and Crack Growth were measured and recorded using MTS and Ultrasonic Device. Totally

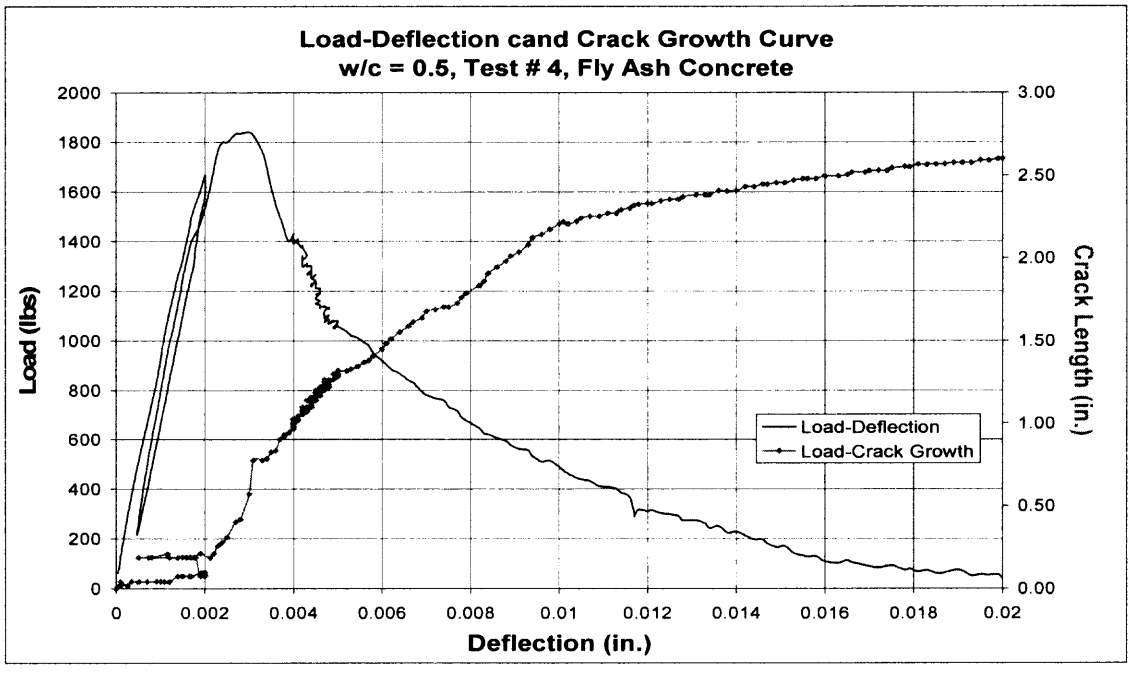

Figure A4a Load-Deflection with Crack Growth of Fly Ash Concrete Beam SIB4

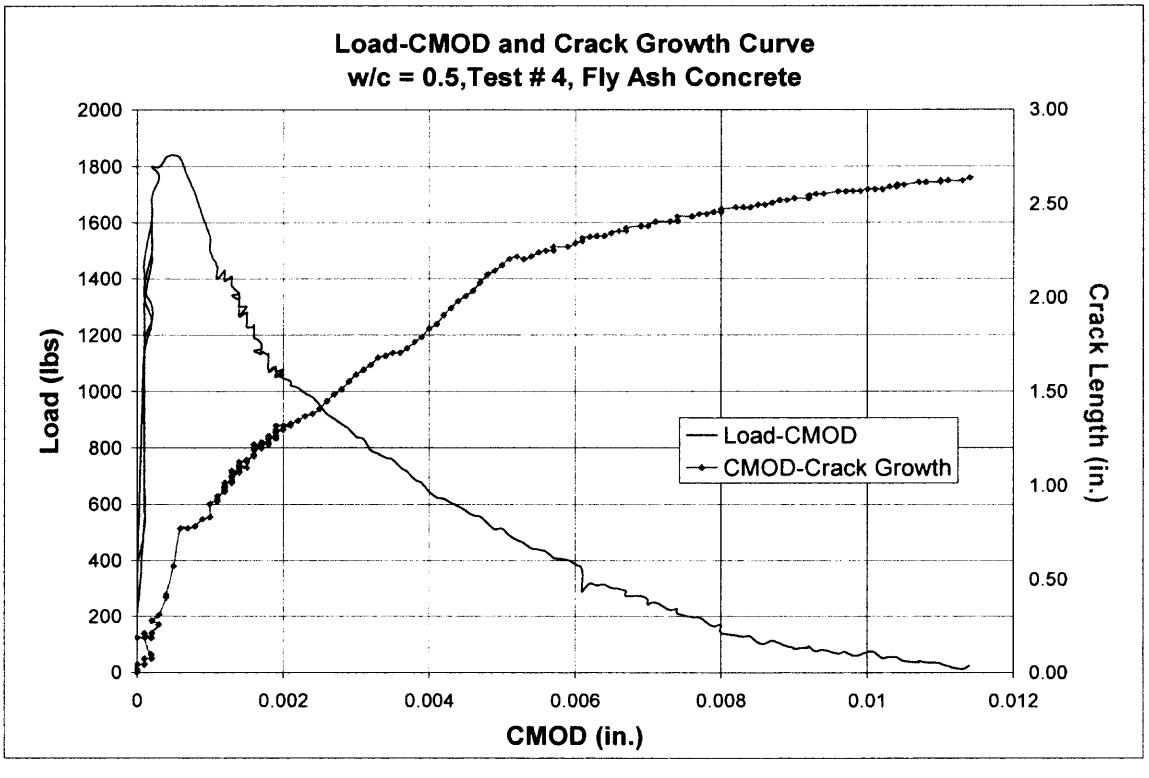

Figure A4b Load-CMOD with Crack Growth of Fly Ash Concrete Beam SIB4

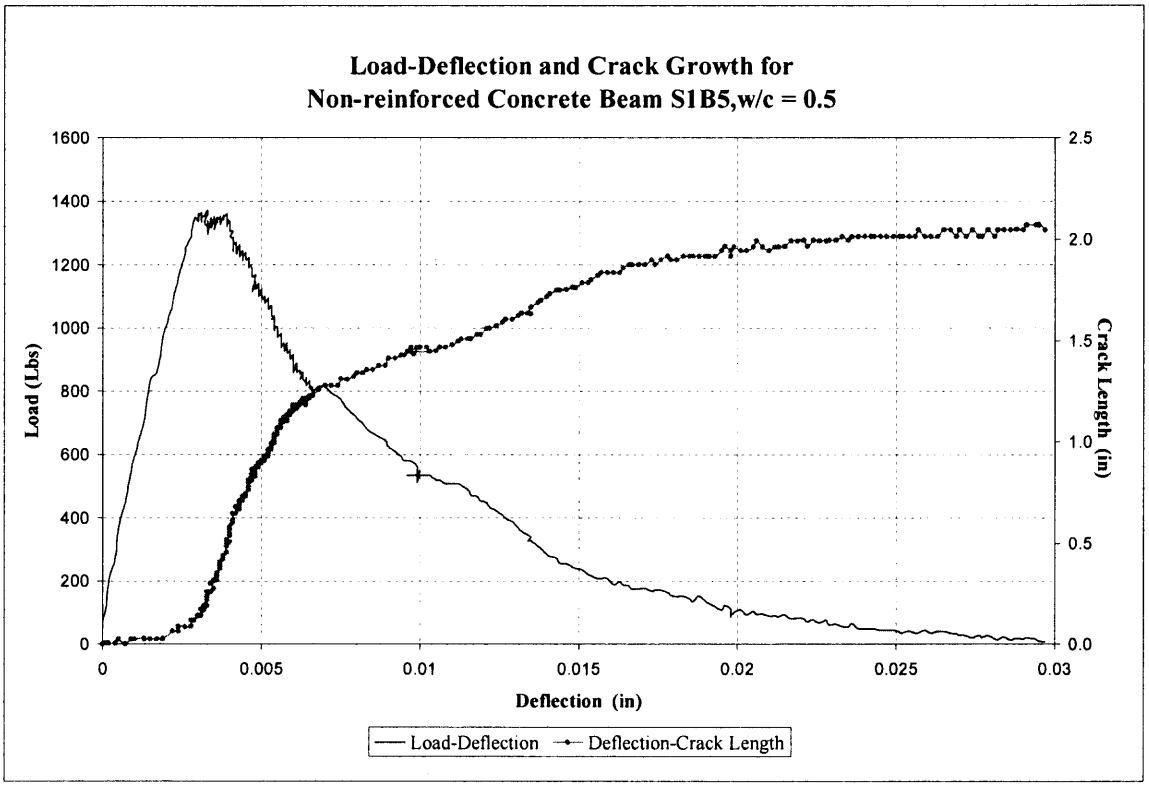

Figure A5a Load-Deflection and Crack Growth of Concrete Beam SIB5

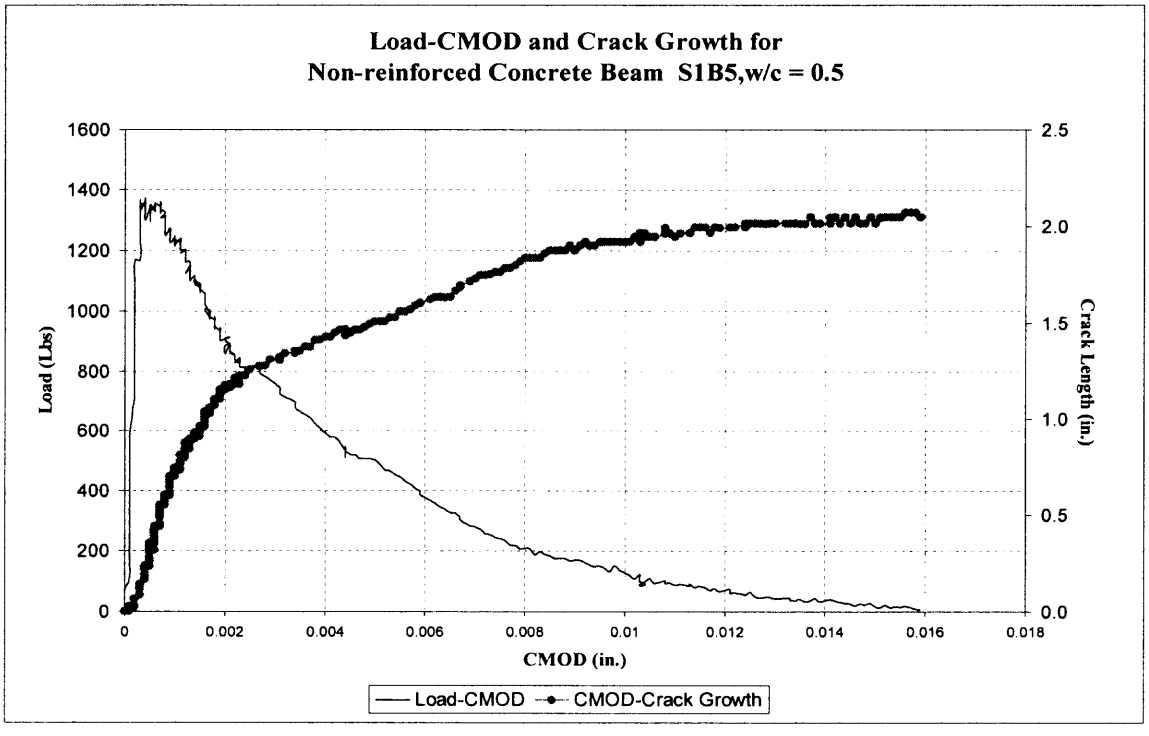

Figure A5b Load-CMOD and Crack Growth of Concrete Beam S1B5

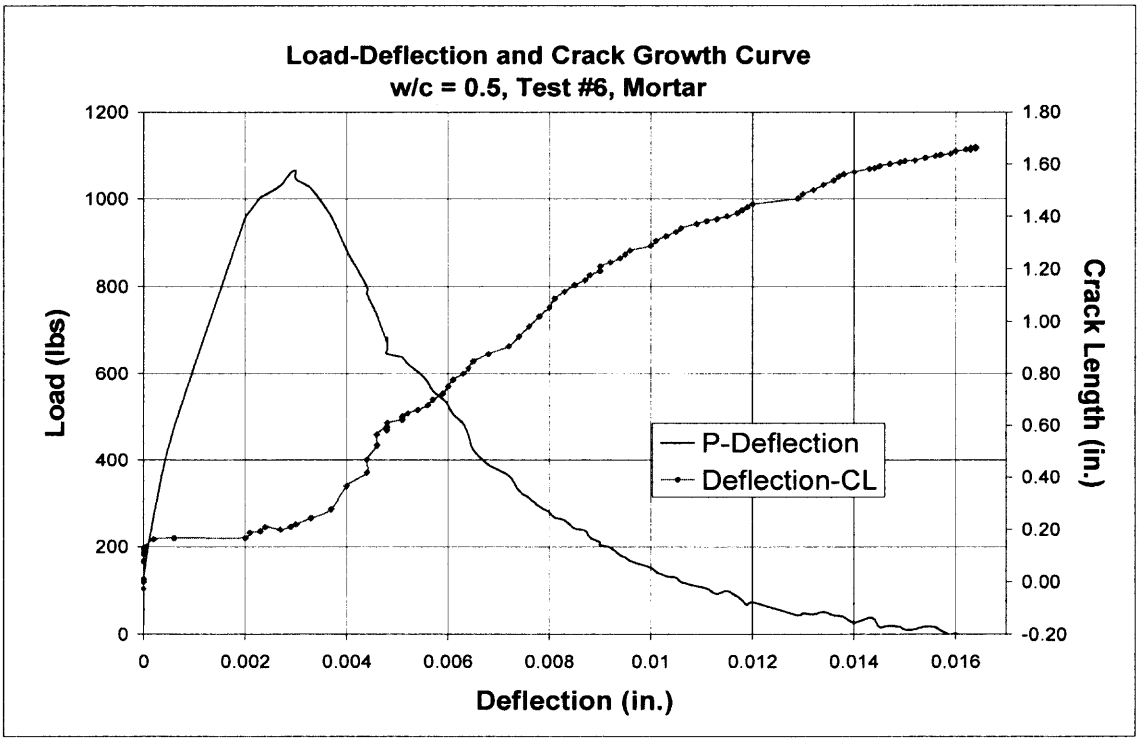

Figure A6a Load-Deflection with Crack Growth of Mortar Beam SIB6.

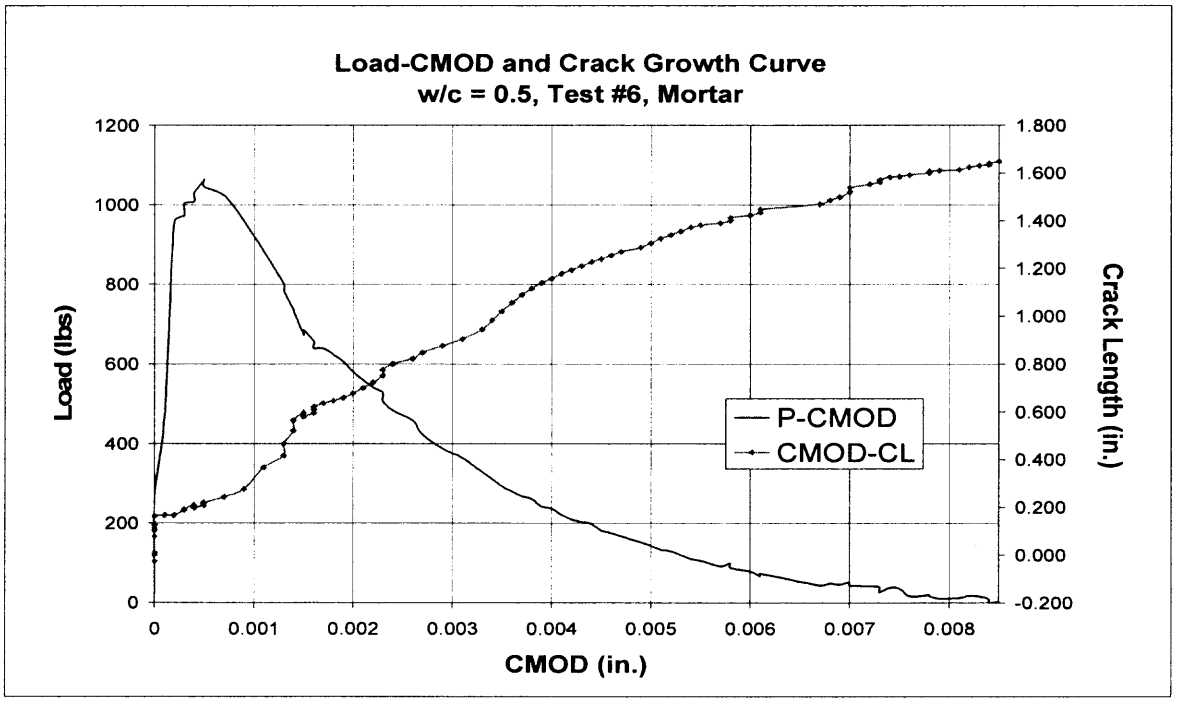

Figure A6b Load-CMOD with Crack Growth of Mortar Beam SIB6.

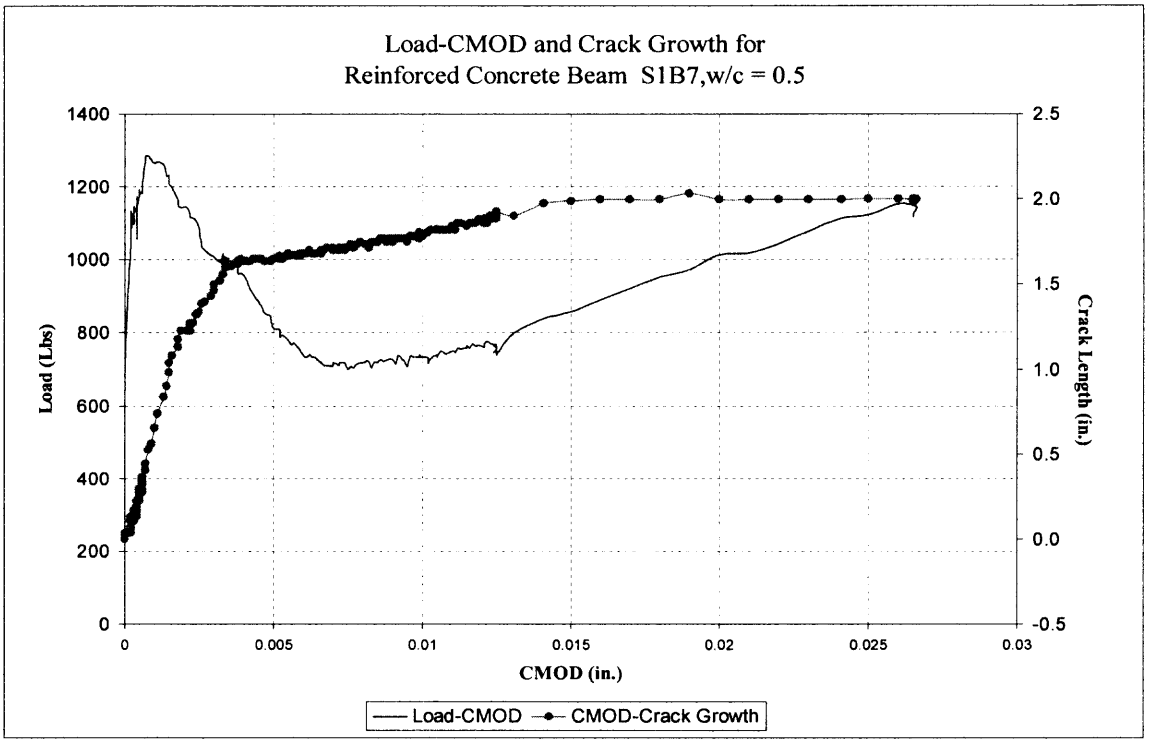

Figure A7a Load-CMOD and Crack Growth of Reinforced Concrete Beam S1B7

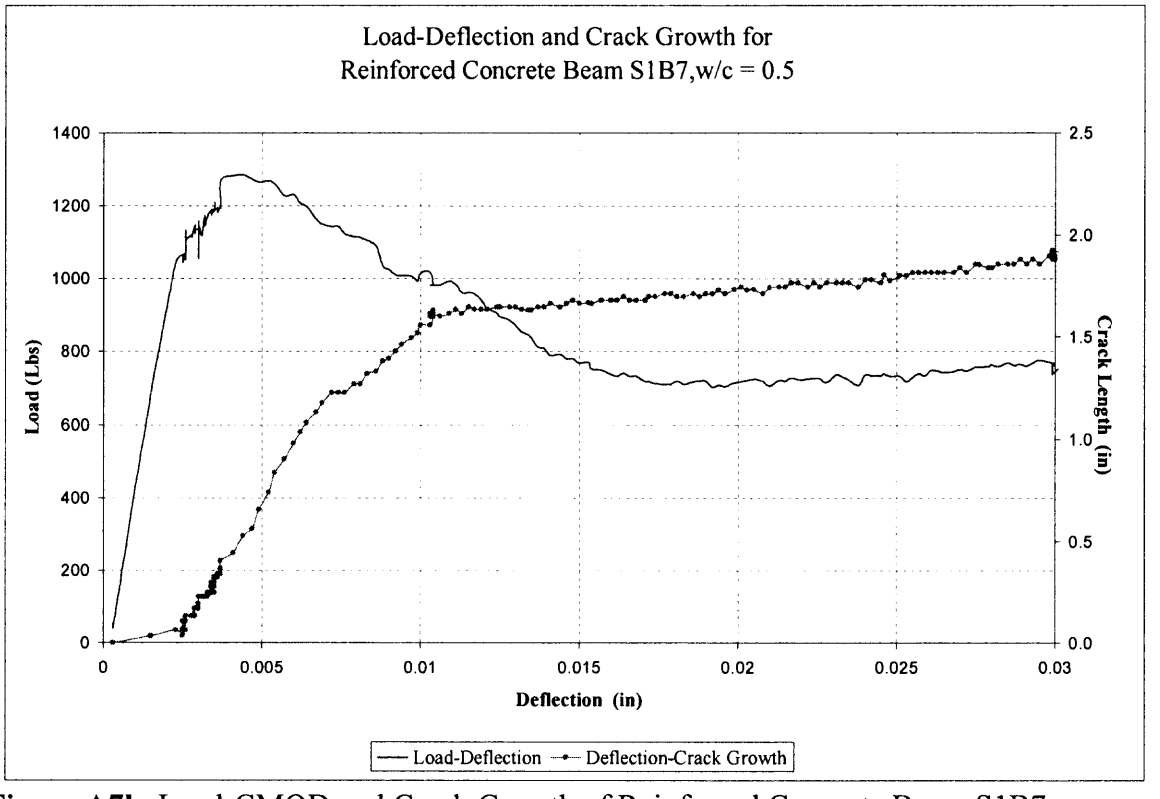

Figure A7b Load-CMOD and Crack Growth of Reinforced Concrete Beam S1B7

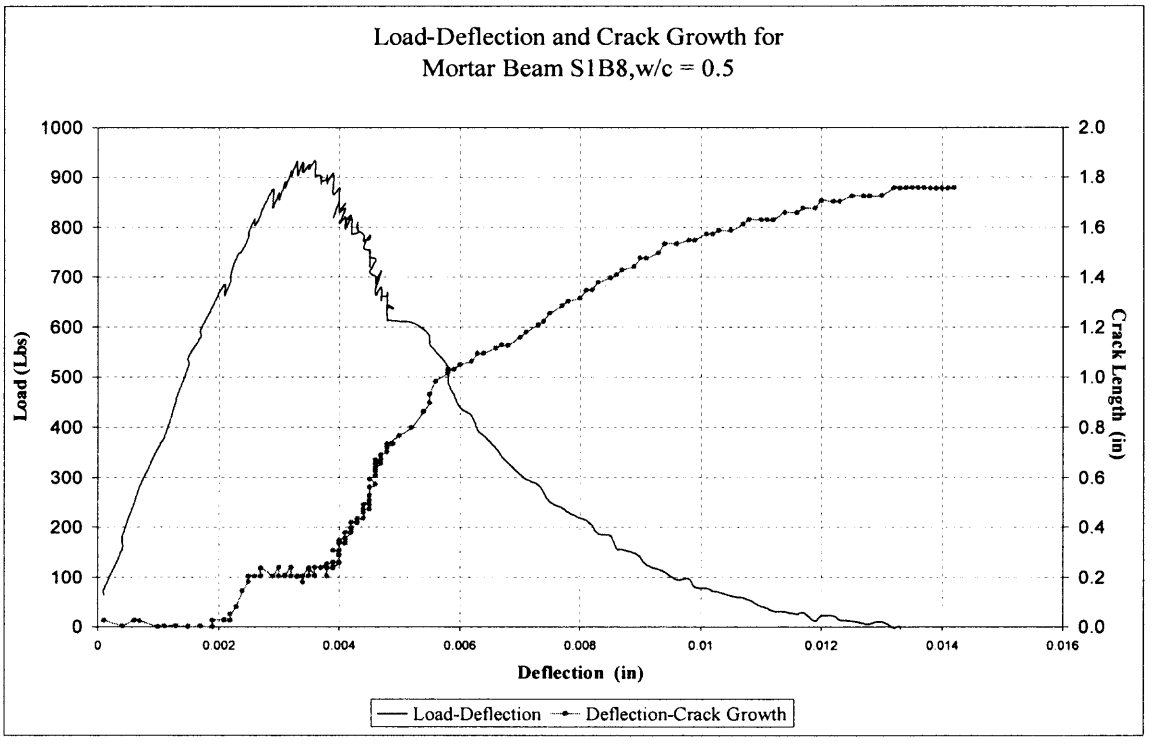

Figure A8a Load-Deflection curve with Crack Extension for Mortar Beam S1B8

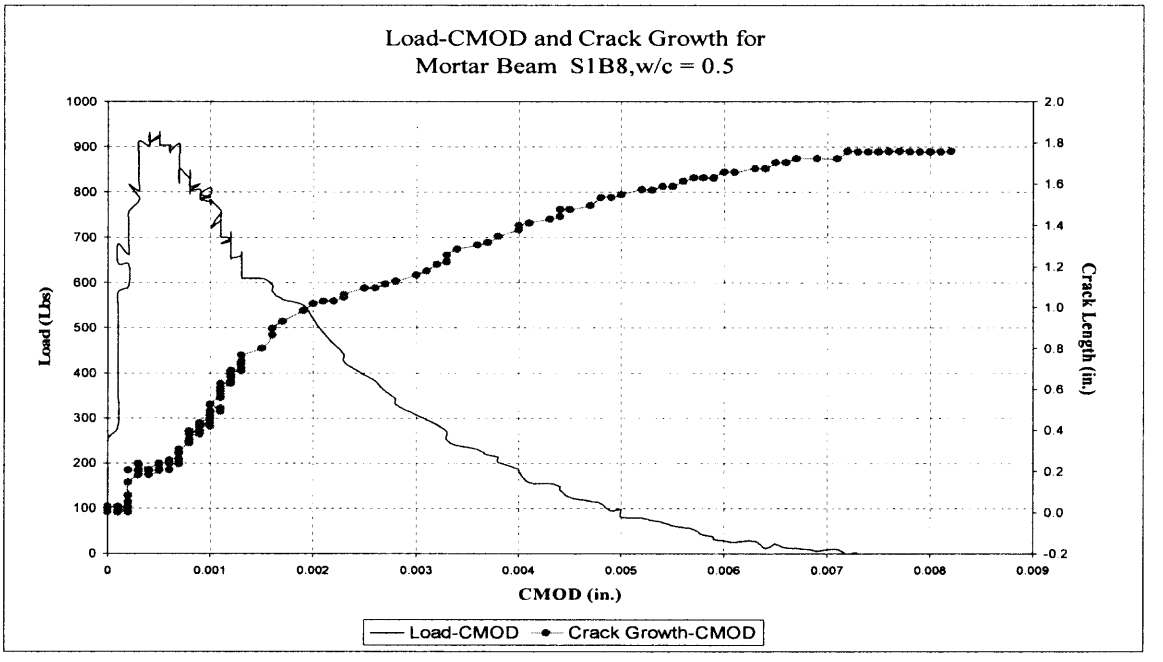

Figure A8b Load-CMOD curve with Crack Extension for Mortar Beam S1B8

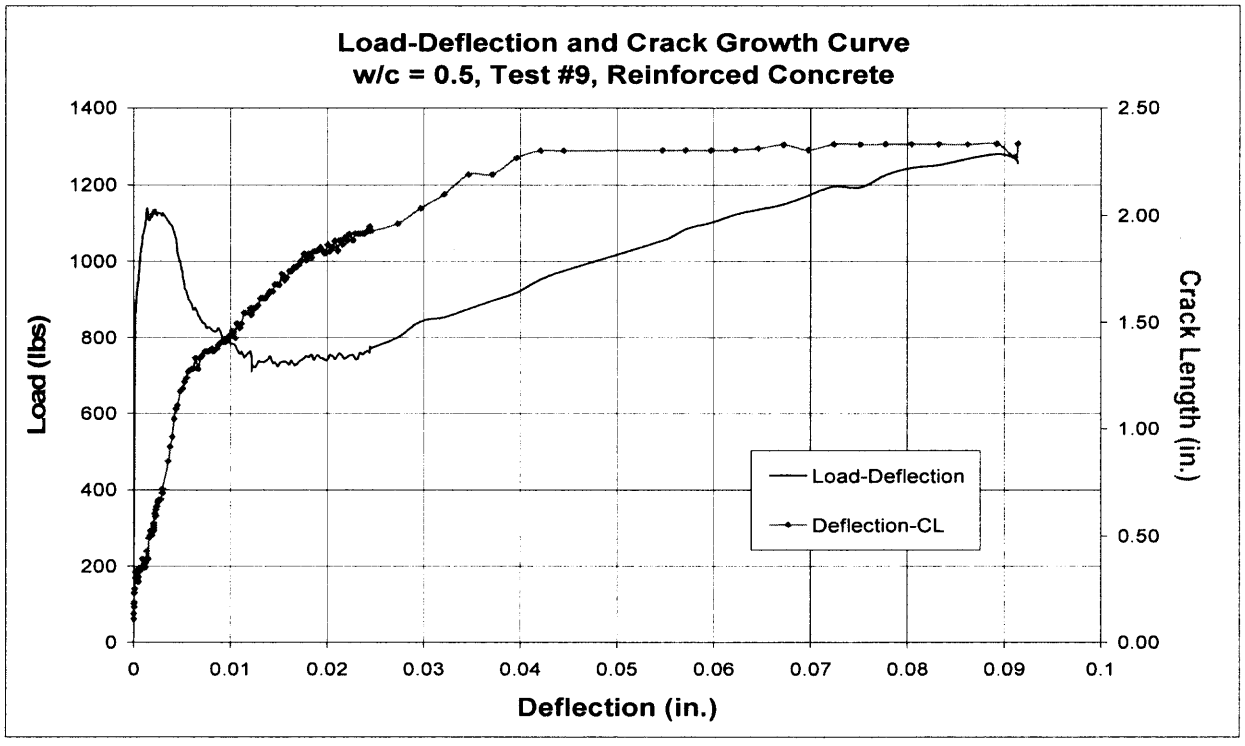

Figure A9a Load-Deflection curve with Crack Extension for Mortar Beam S1B9

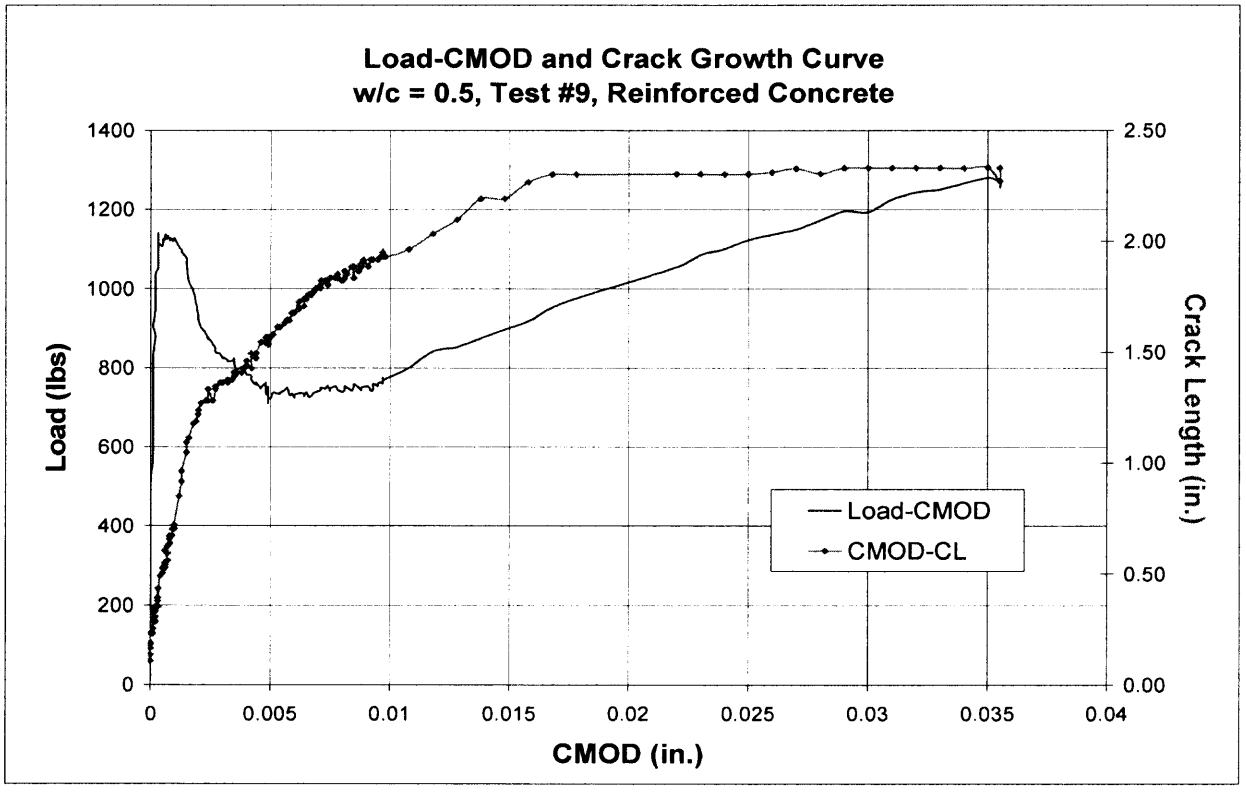

Figure A9a Load-CMOD curve with Crack Extension for Mortar Beam S1B9

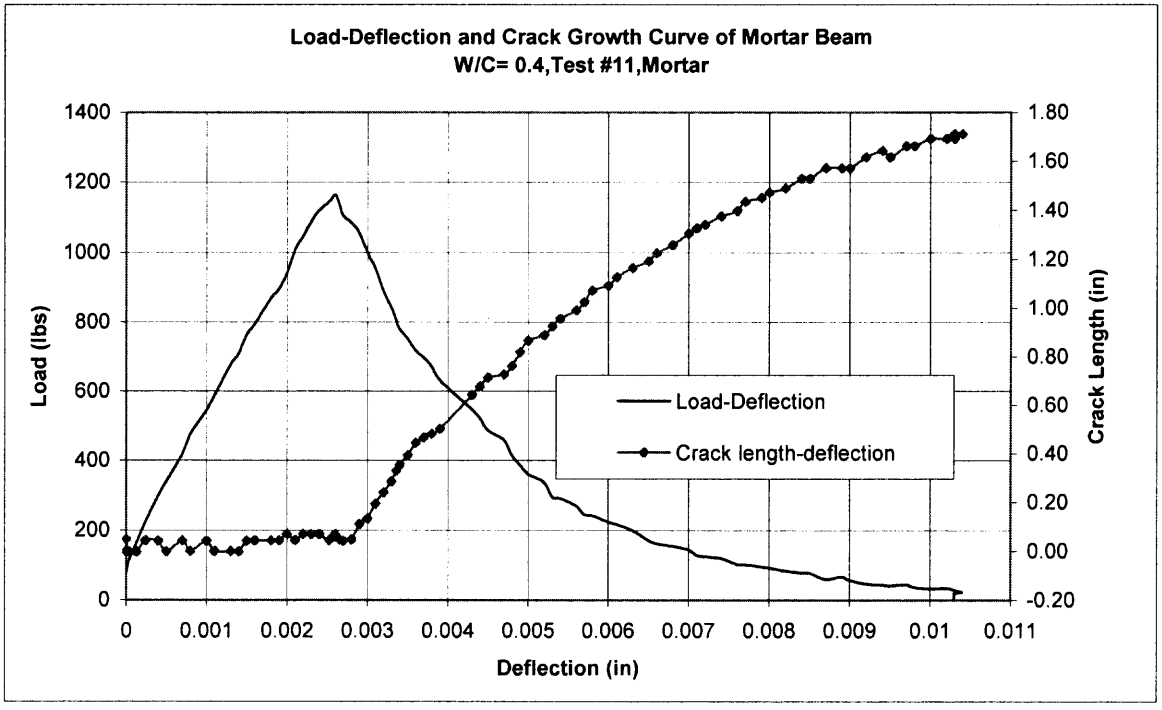

Figure A11a Load-Deflection curve with Crack Extension for Mortar Beam S1B11

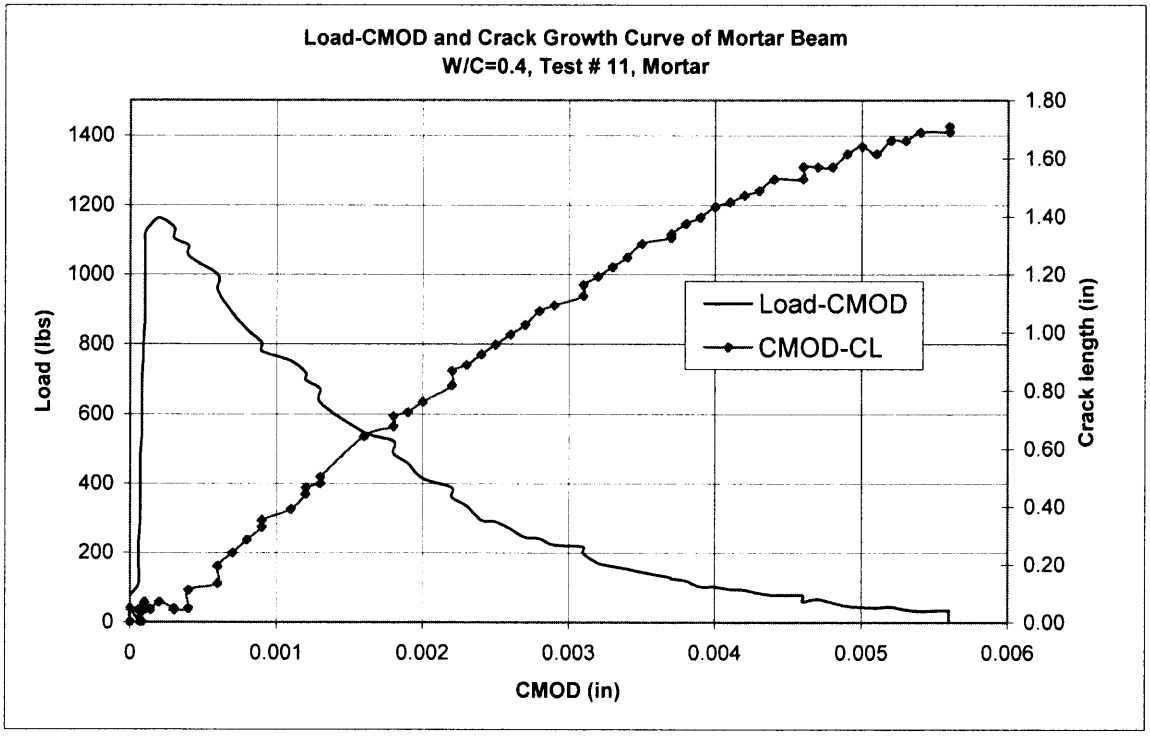

Figure A11a Load-CMOD curve with Crack Extension for Mortar Beam S1B11

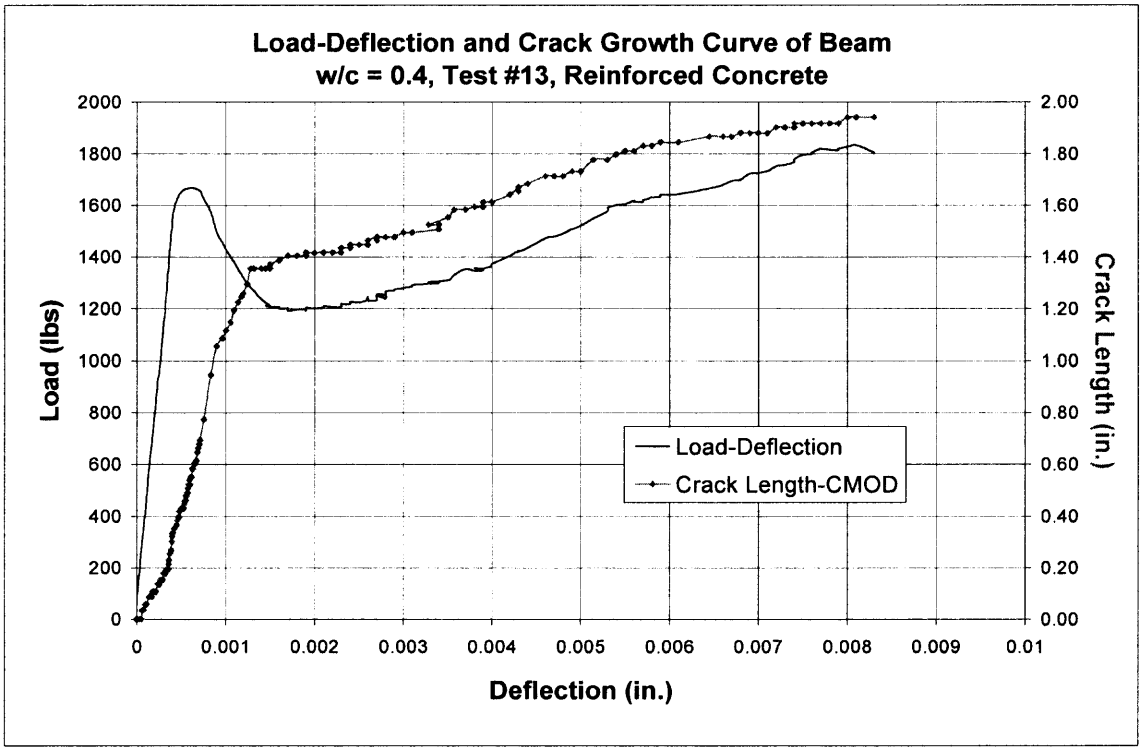

Figure A13a Load-Deflection curve with Crack Extension for Mortar Beam S1B13.

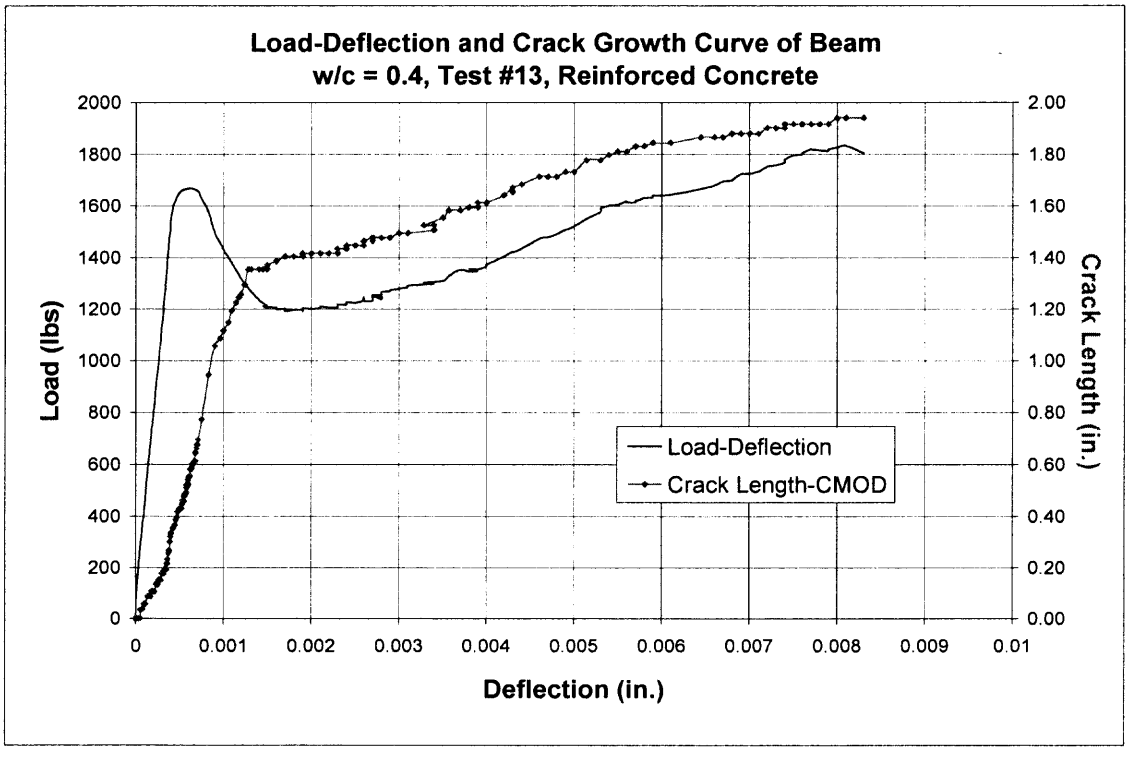

Figure A13a Load-Deflection curve with Crack Extension for Mortar Beam S1B13

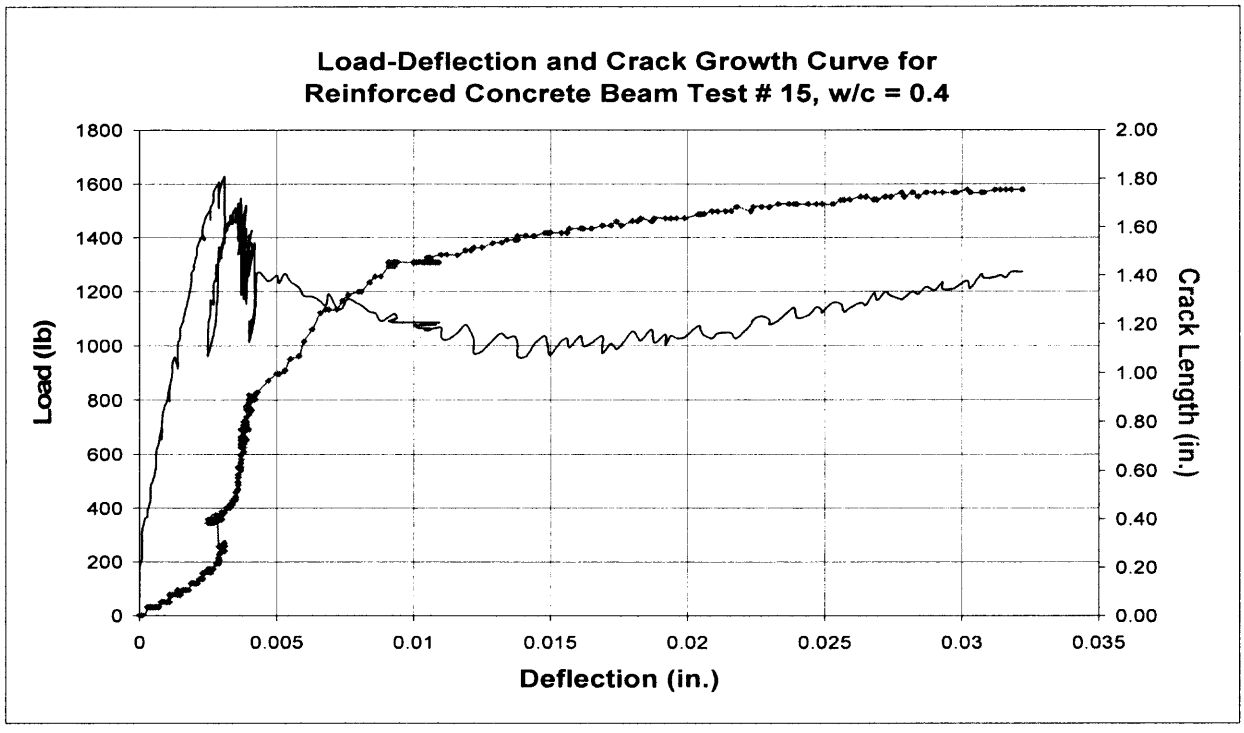

Figure A15a Load-Deflection curve with Crack Extension for Mortar Beam S1B15

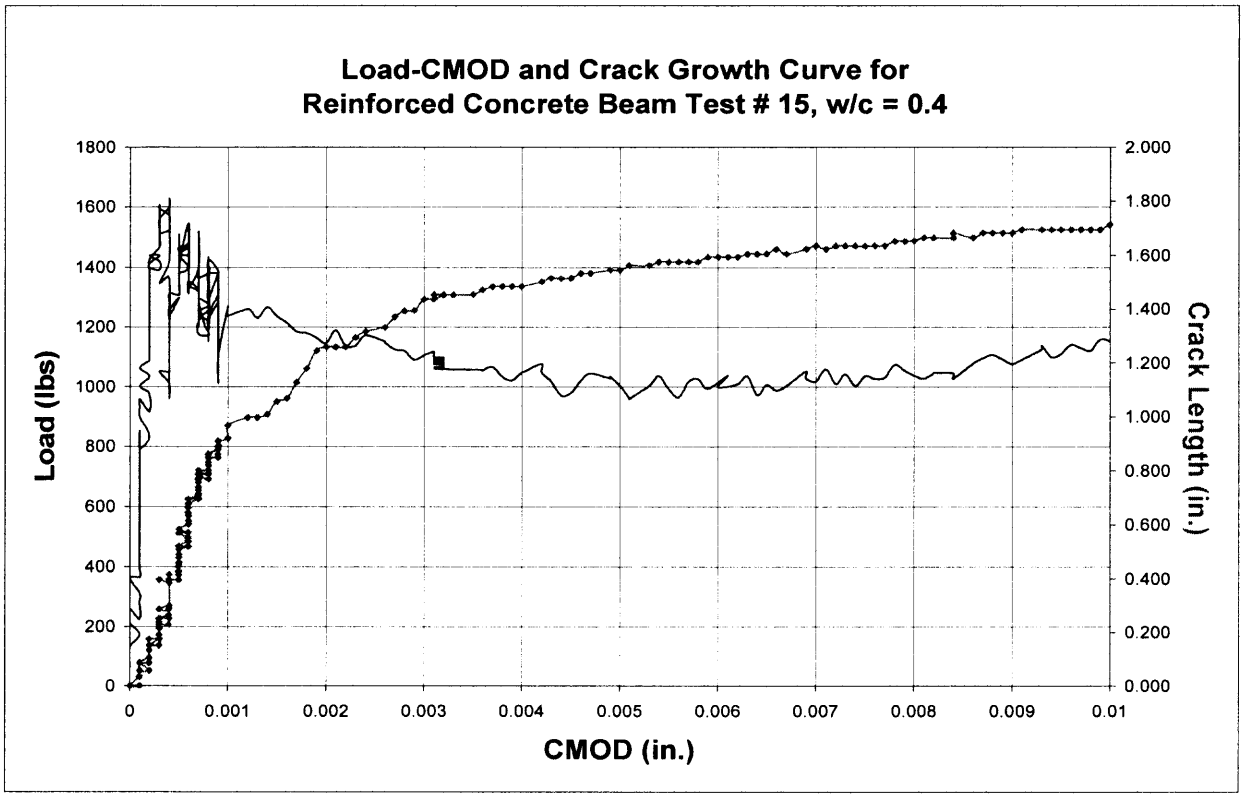

Figure A15a Load-CMOD curve with Crack Extension for Mortar Beam S1B15

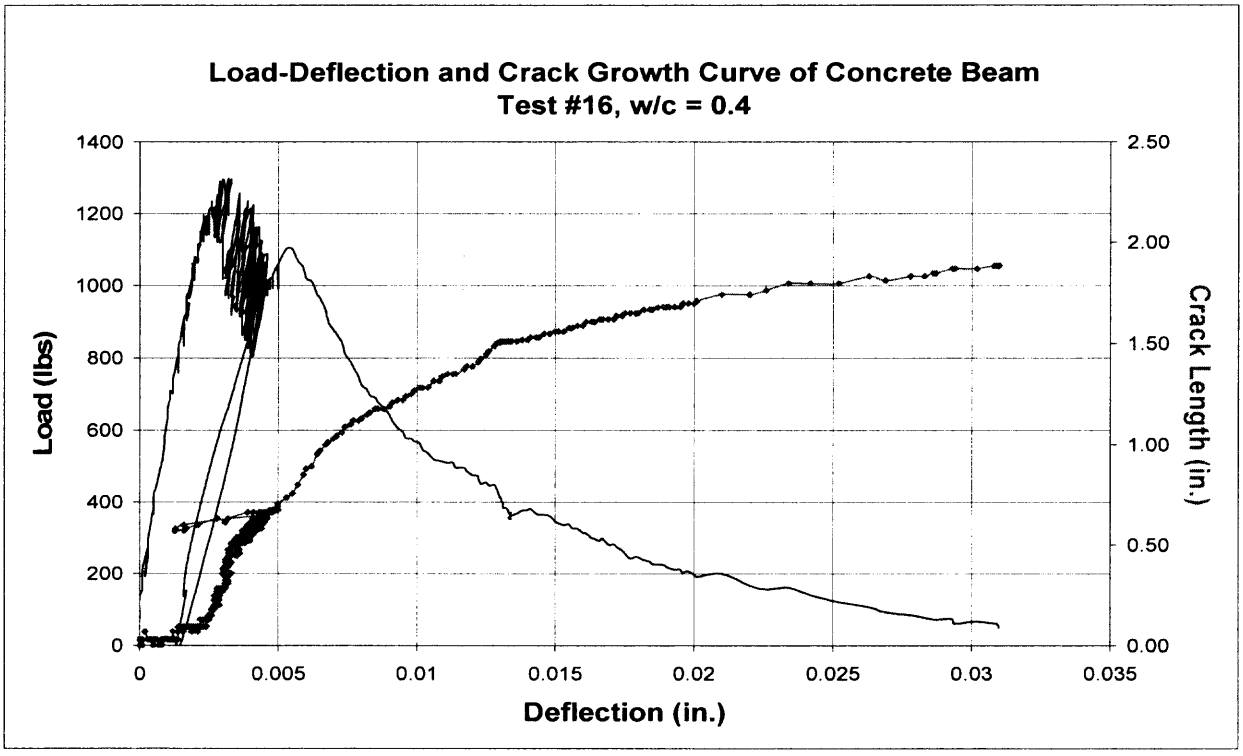

Figure A16a Load-Deflection curve with Crack Extension for Mortar Beam S1B16.

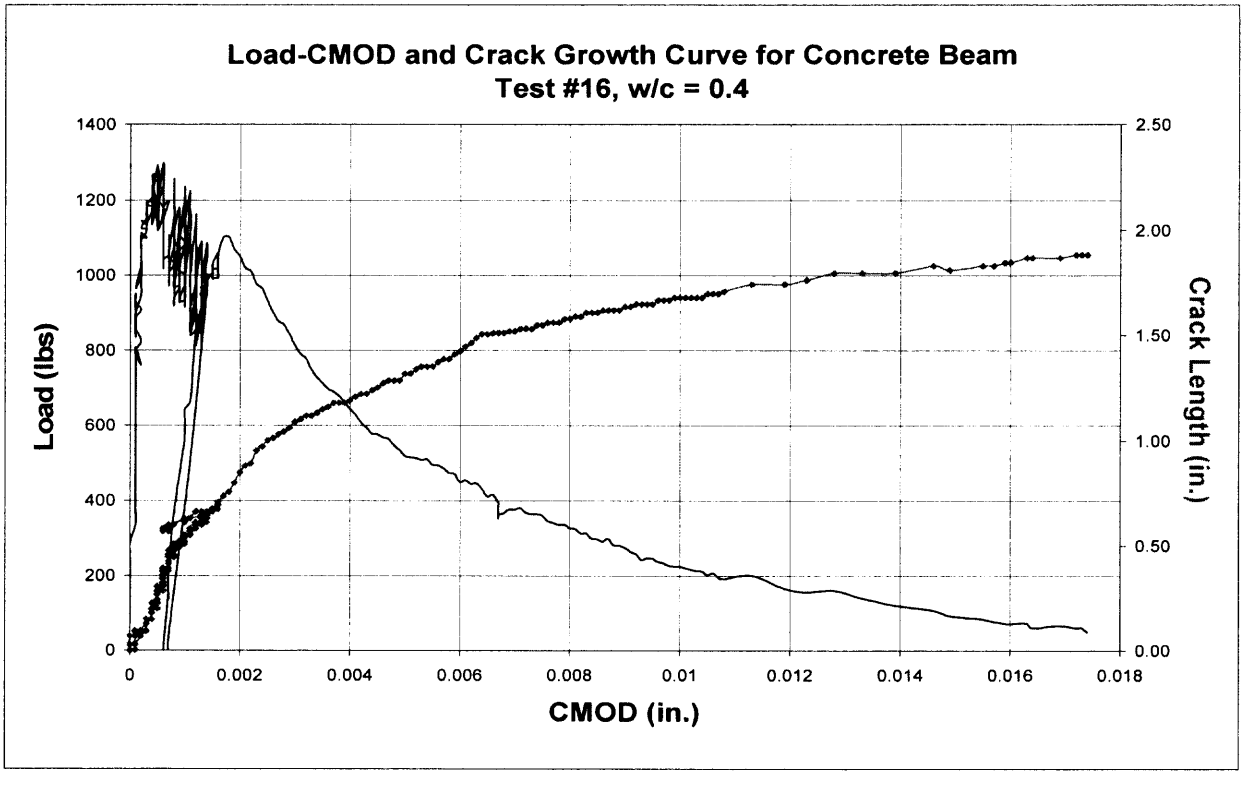

Figure A16a Load-CMOD curve with Crack Extension for Mortar Beam S1B16.

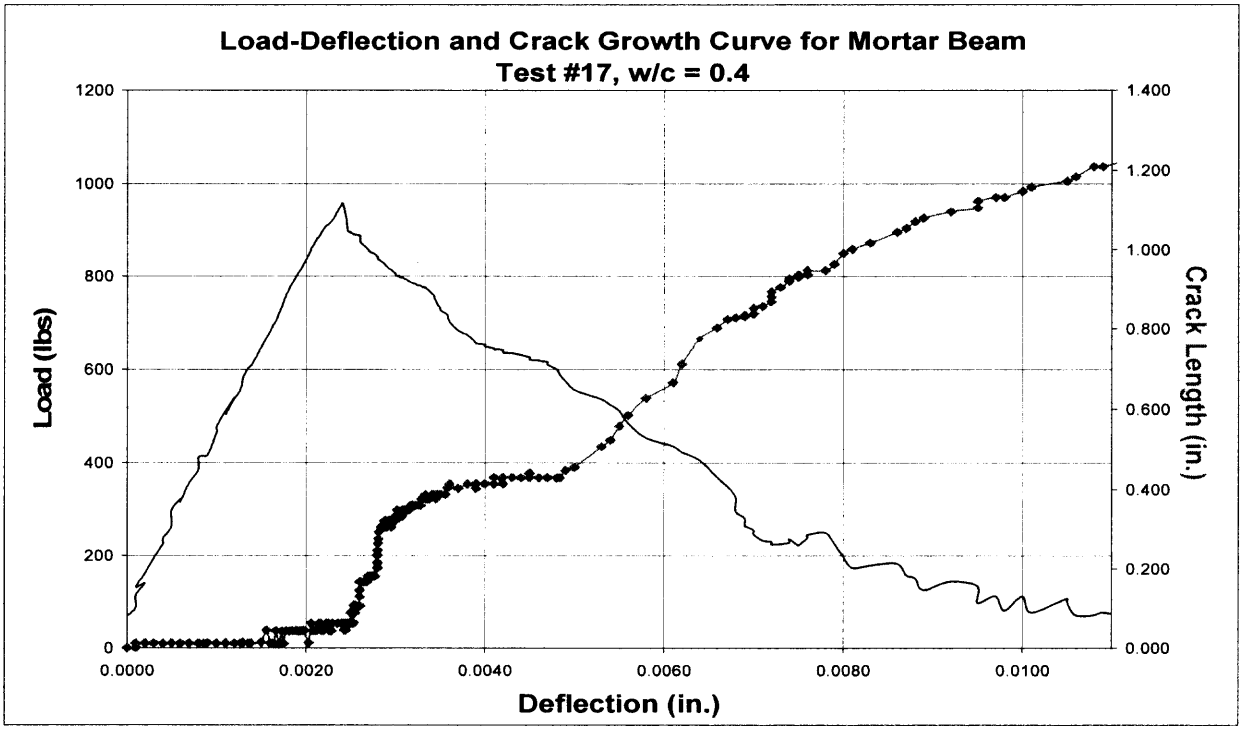

Figure A17a Load-Deflection curve with Crack Extension for Mortar Beam S1B17.

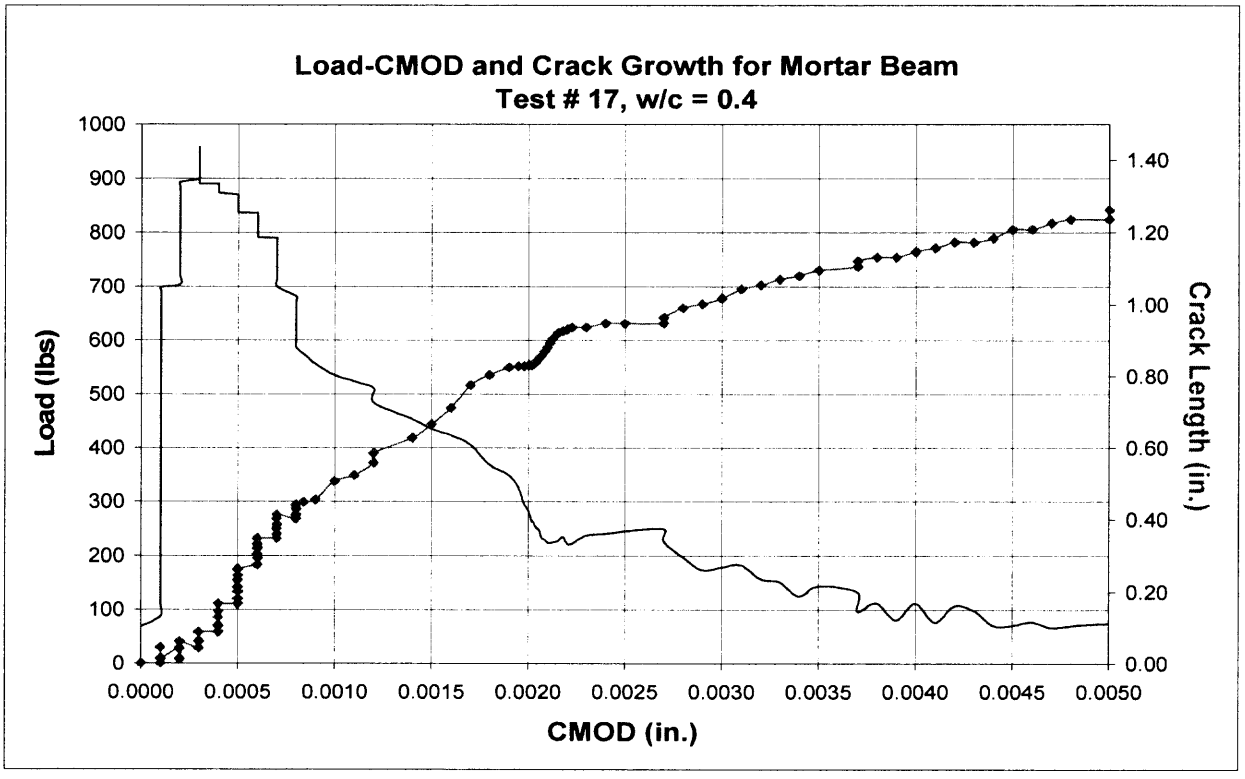

Figure A17a Load-Deflection curve with Crack Extension for Mortar Beam S1B17.

APPENDIX B

RESULTS OF THE SECOND SERIES OF EXPERIMENTS

In this series test, total 16 beam specimens were tested on Concrete in January, 2004. The relationships between Load, Load line deflection, CMOD and Crack Growth were measured and recorded using MTS and Ultrasonic Device.

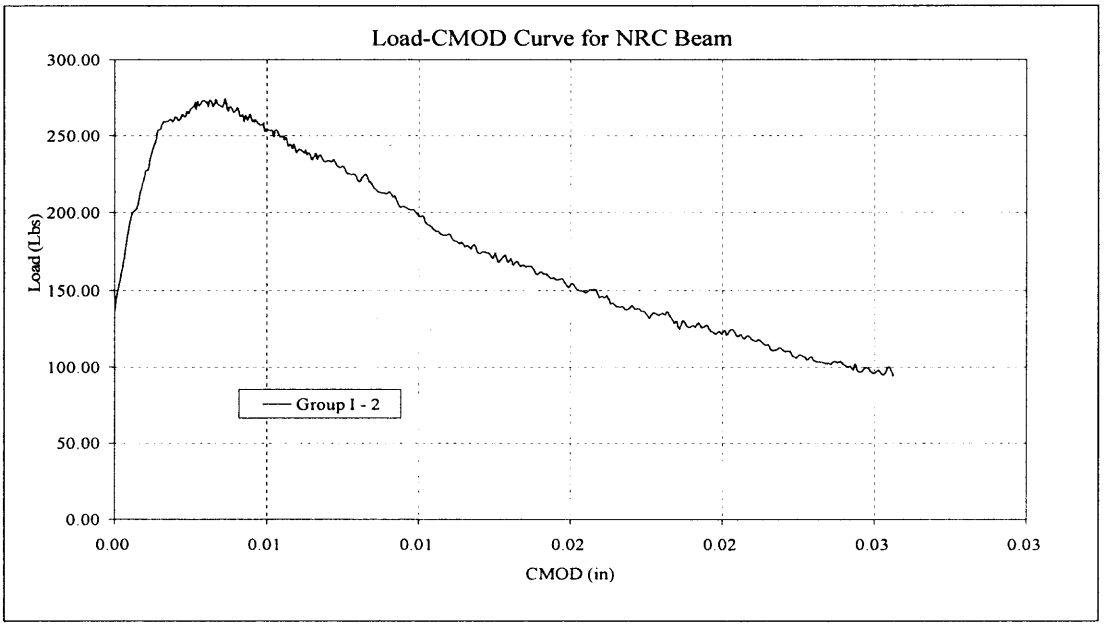

Figure B1a Load-CMOD Curve for NRC Beam S2G1B2
(Thickness × Width× Span = 4.5×3×18)

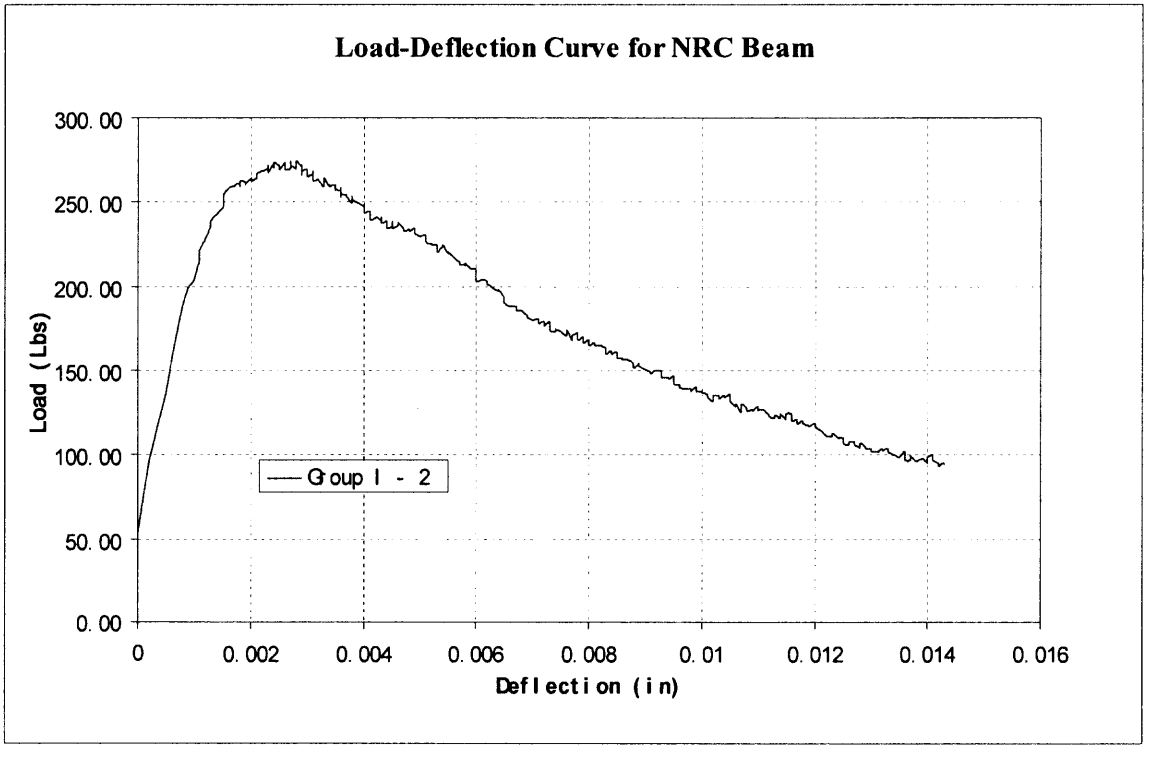

Figure B1b Load-Deflection Curve for NRC Beam S2G1B2
(Thickness × Width× Span = 4.5×3×18)

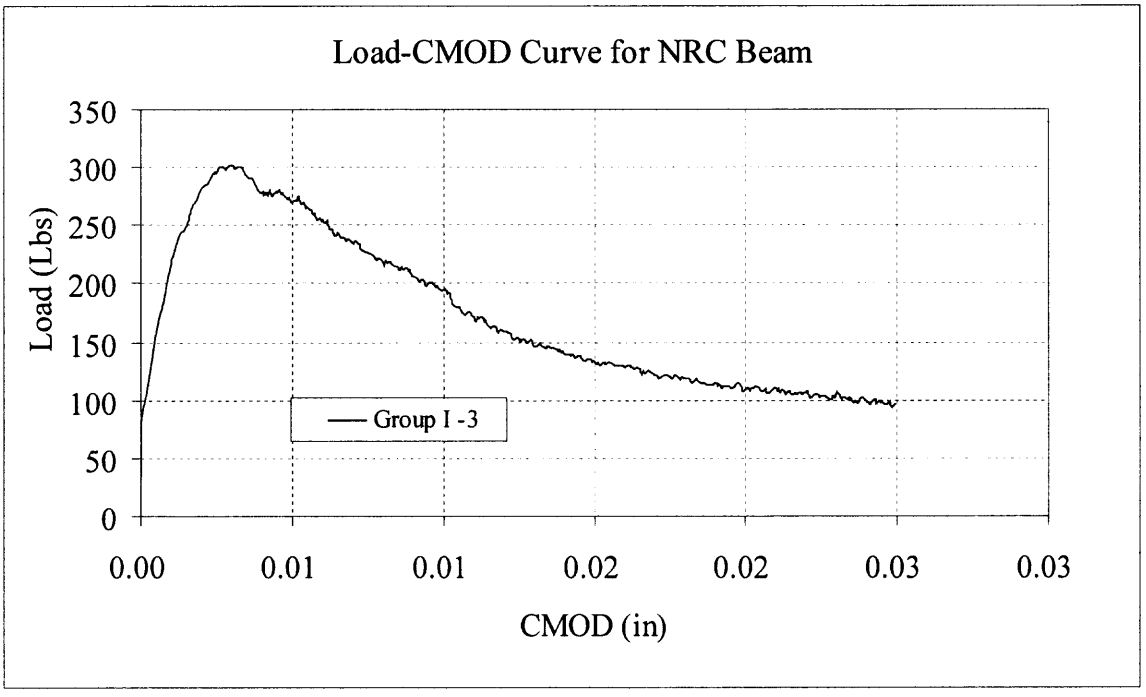

Figure B2a Load-CMOD Curve for NRC Beam S2G1B3
(Thickness × Width× Span = 4.5×3×18)

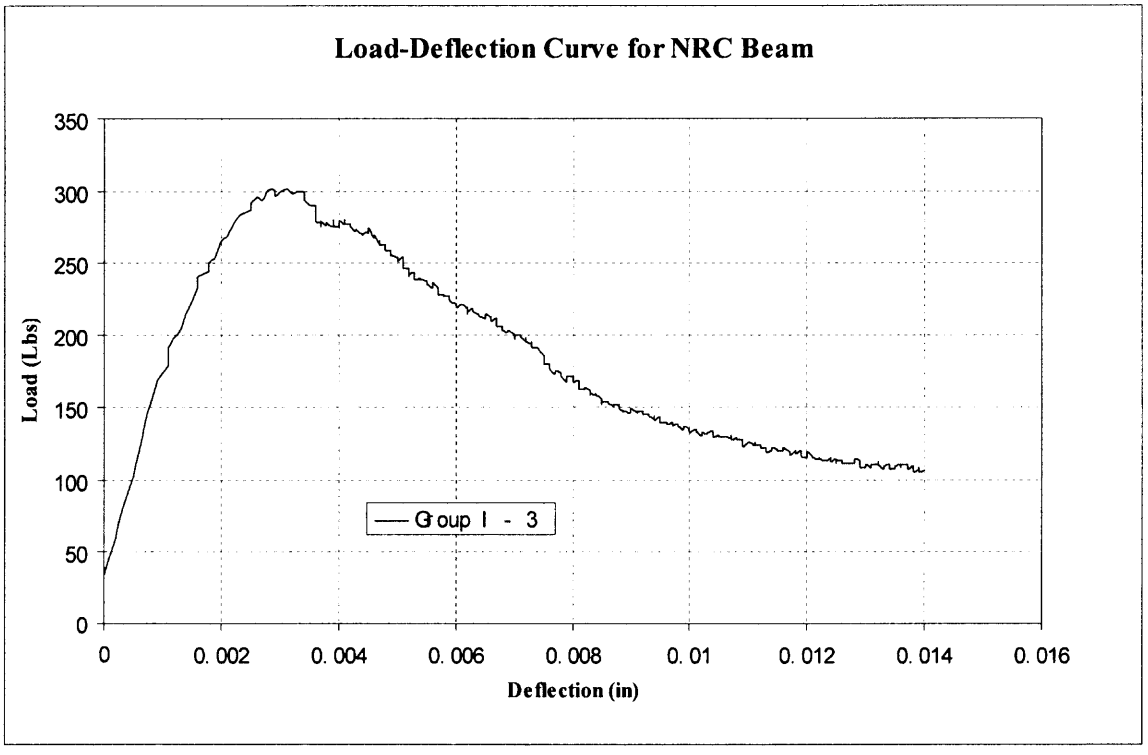

Figure B2b Load-Deflection Curve for NRC Beam S2G1B3
(Thickness × Width× Span = 4.5×3×18)

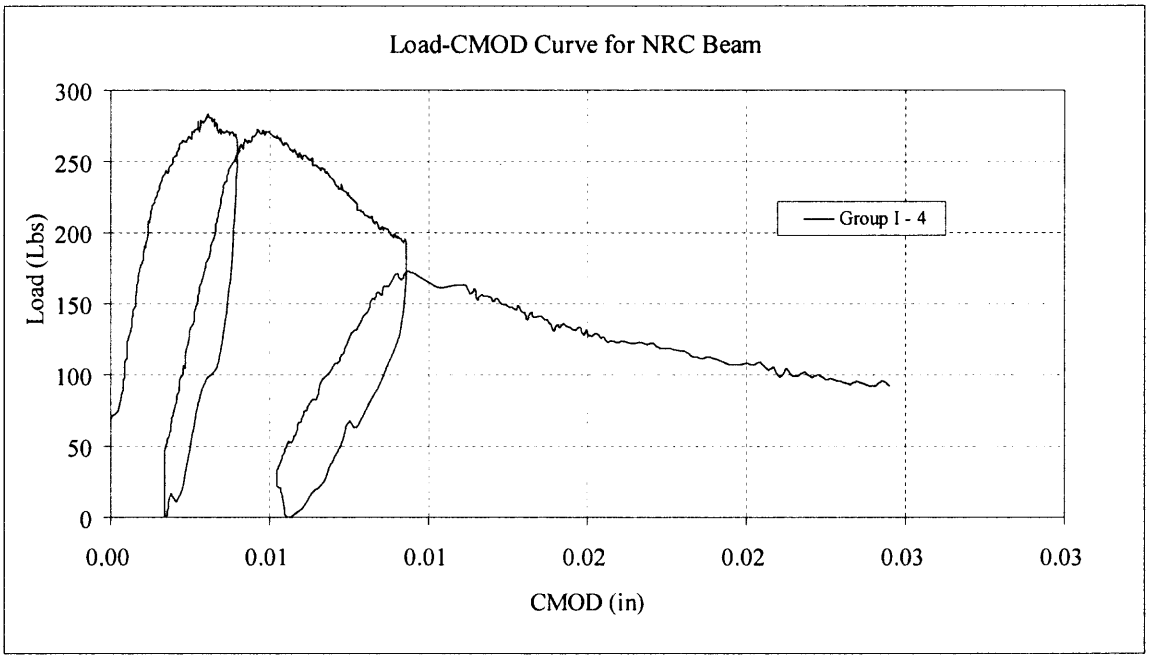

Figure B3a Load-CMOD Curve for NRC Beam S2G1B4
(Thickness × Width× Span = 4.5×3×18)

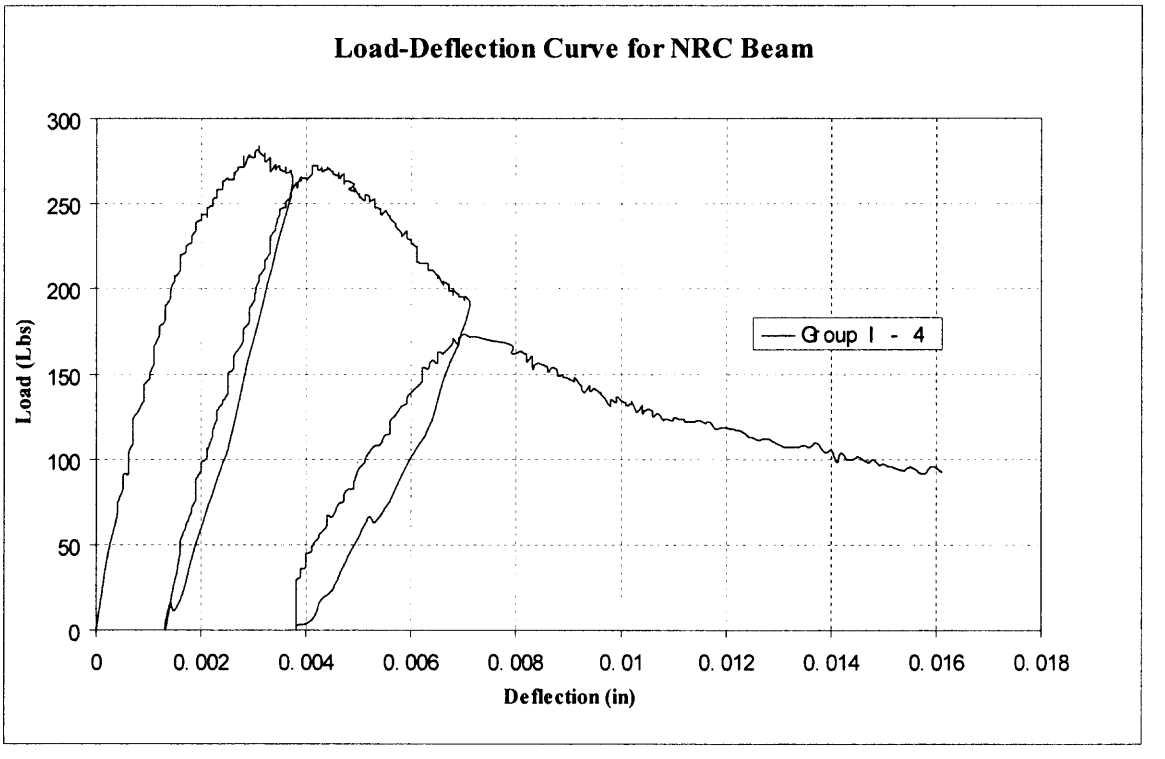

Figure B3b Load-Deflection Curve for NRC Beam S2G1B4
(Thickness × Width× Span = 4.5×3×18)

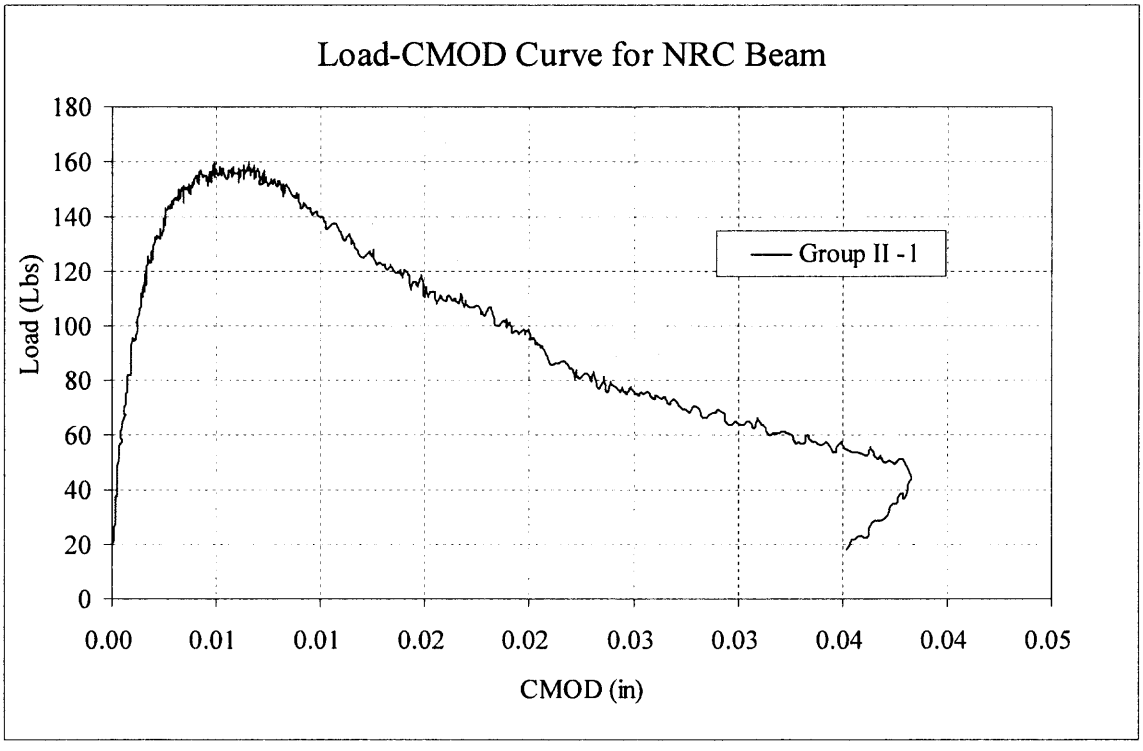

Figure B4a Load-CMOD Curve for NRC Beam S2GII B1
(Thickness × Width× Span = 3×3×12,a_0=1.1 in)

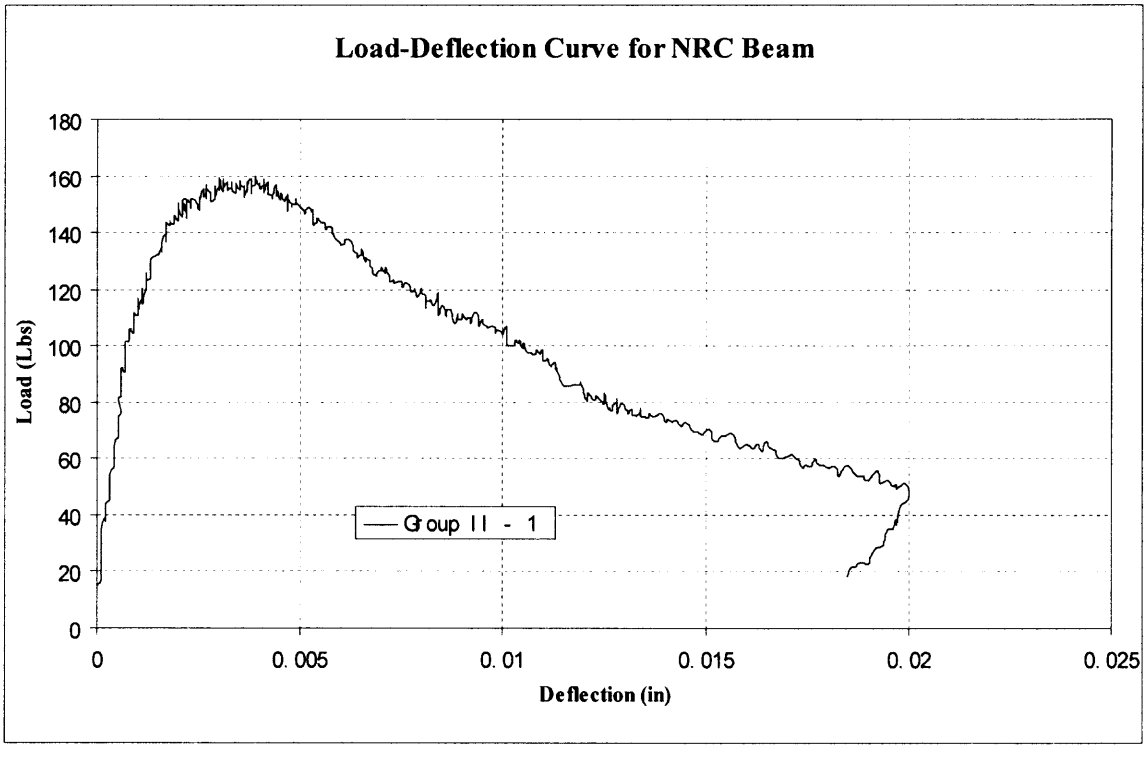

Figure B4b Load-Deflection Curve for NRC Beam S2GII B1
(Thickness × Width× Span = 3×3×12, a_0=1.1 in)

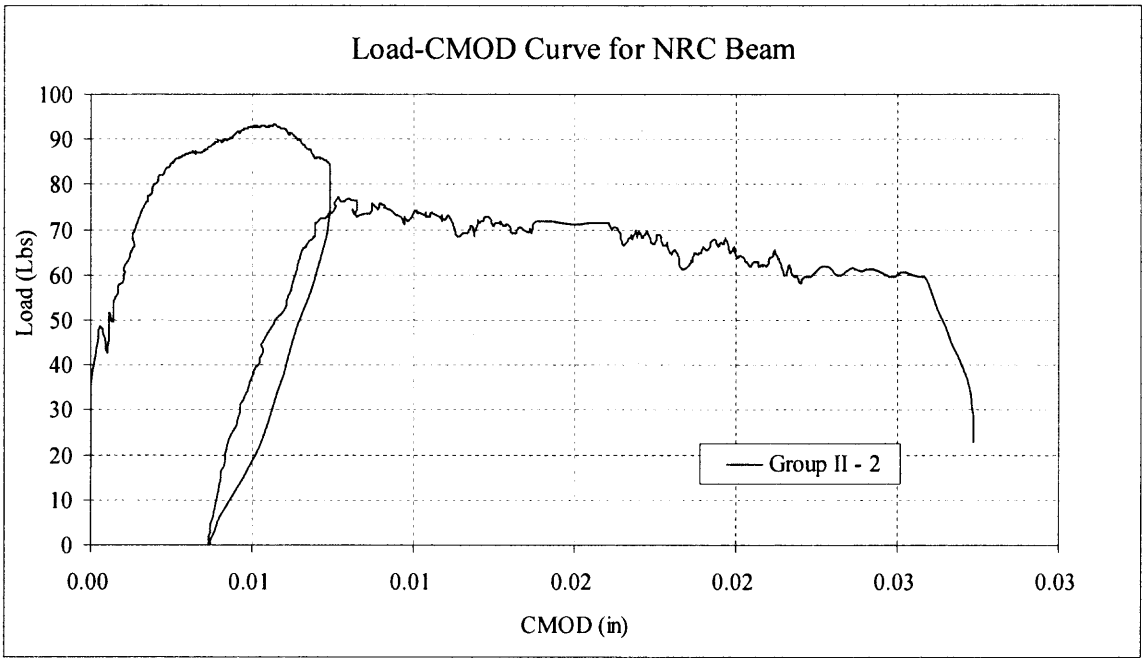

Figure B5a Load-CMOD Curve for NRC Beam S2GII B2
(Thickness × Width× Span = 3×3×12, a_0=1.4 in)

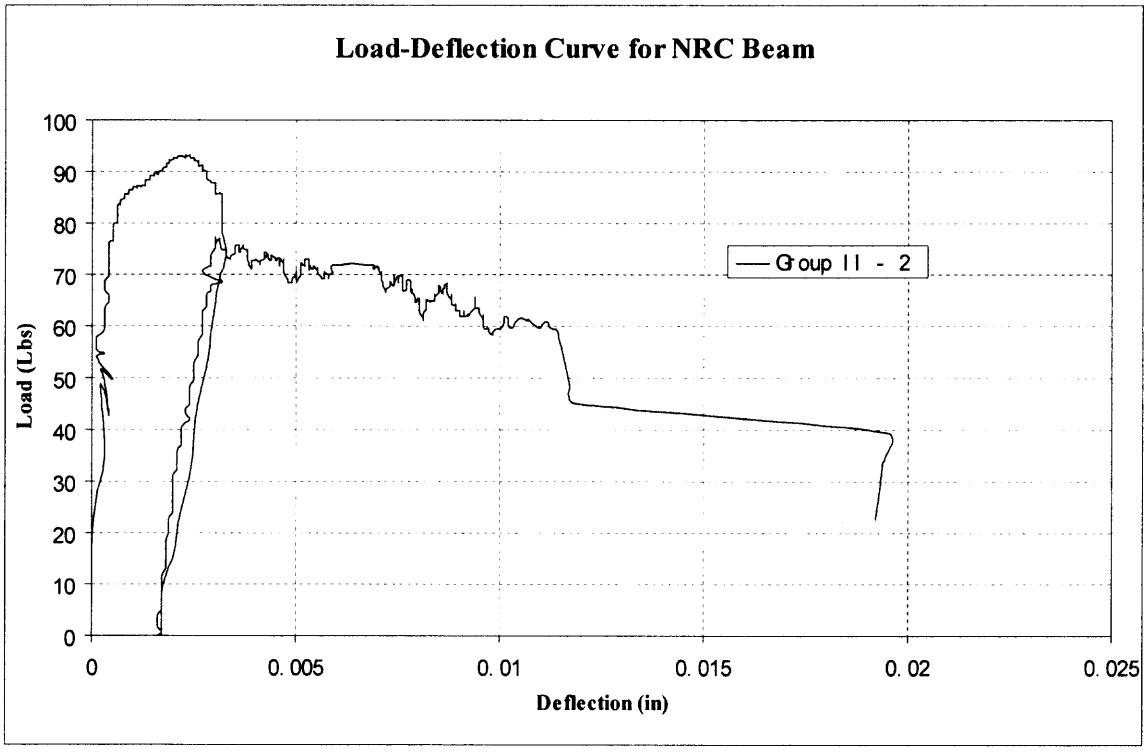

Figure B5b Load-Deflection Curve for NRC Beam S2GII B2
(Thickness × Width× Span = 3×3×12, a_0=1.4 in)

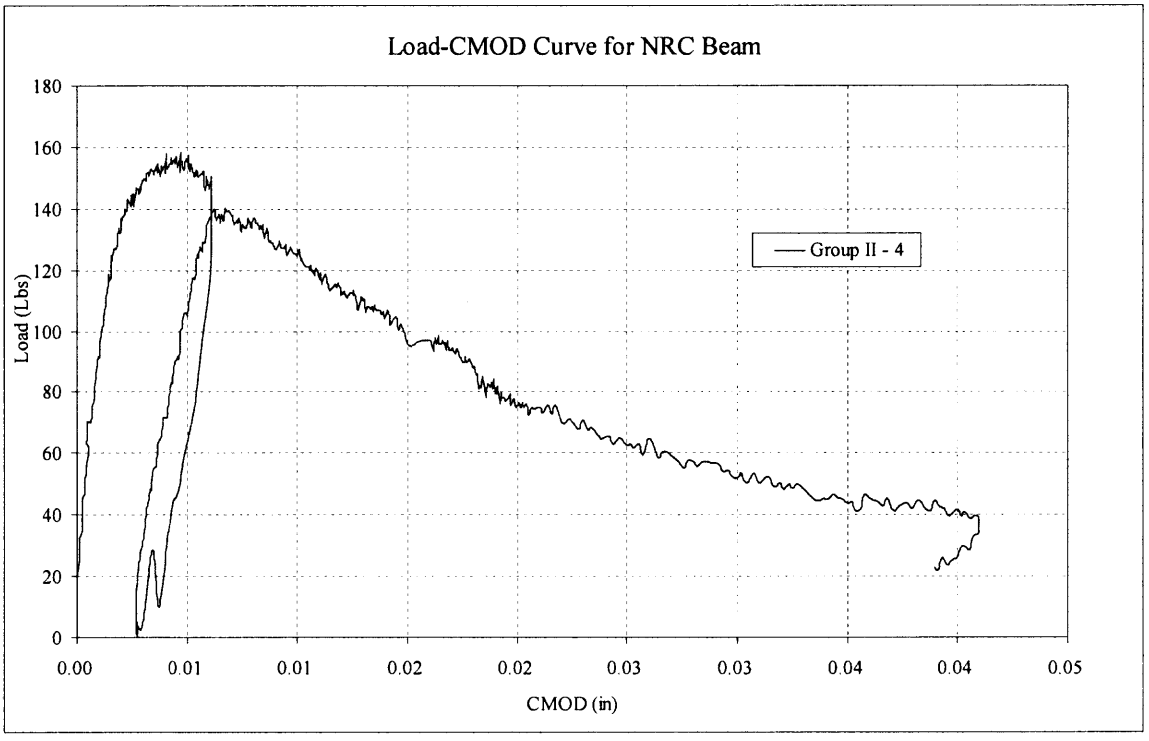

Figure B6a Load-CMOD Curve for NRC Beam S2GII B4
(Thickness × Width× Span = 3×3×12, a_0=1.1 in)

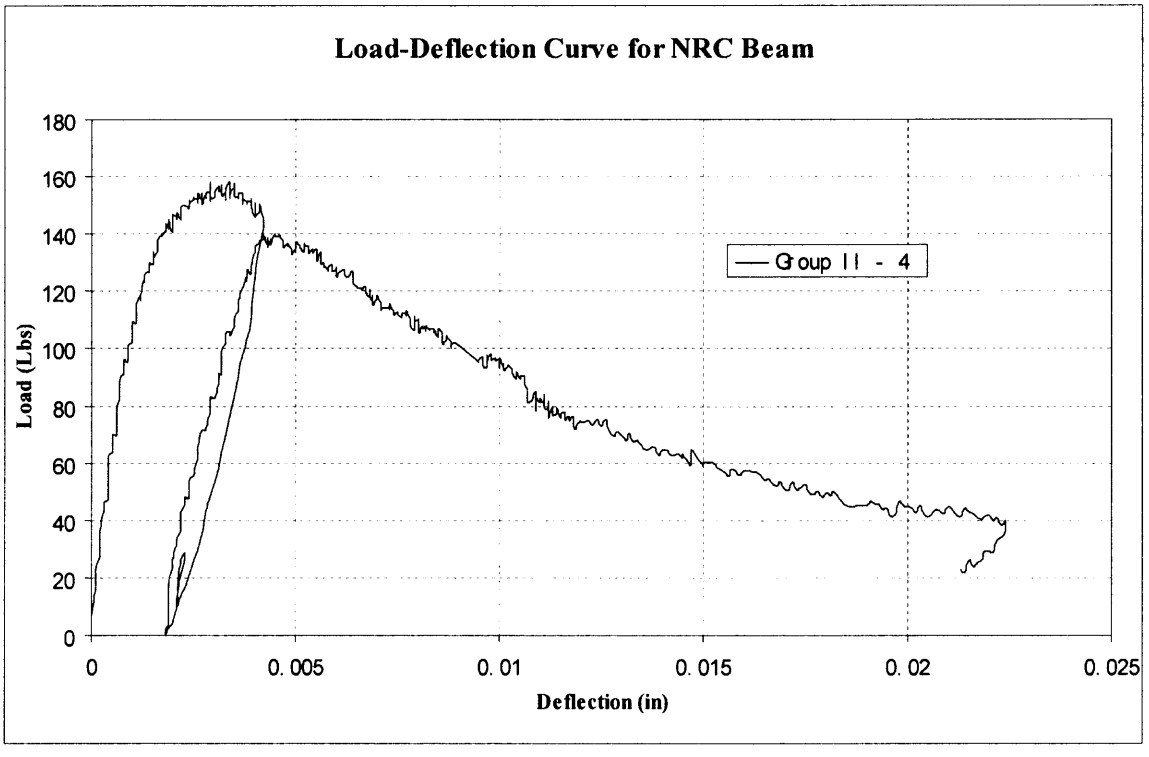

Figure B6b Load-Deflection Curve for NRC Beam S2GII B4
(Thickness × Width× Span = 3×3×12, a_0=1.1 in)

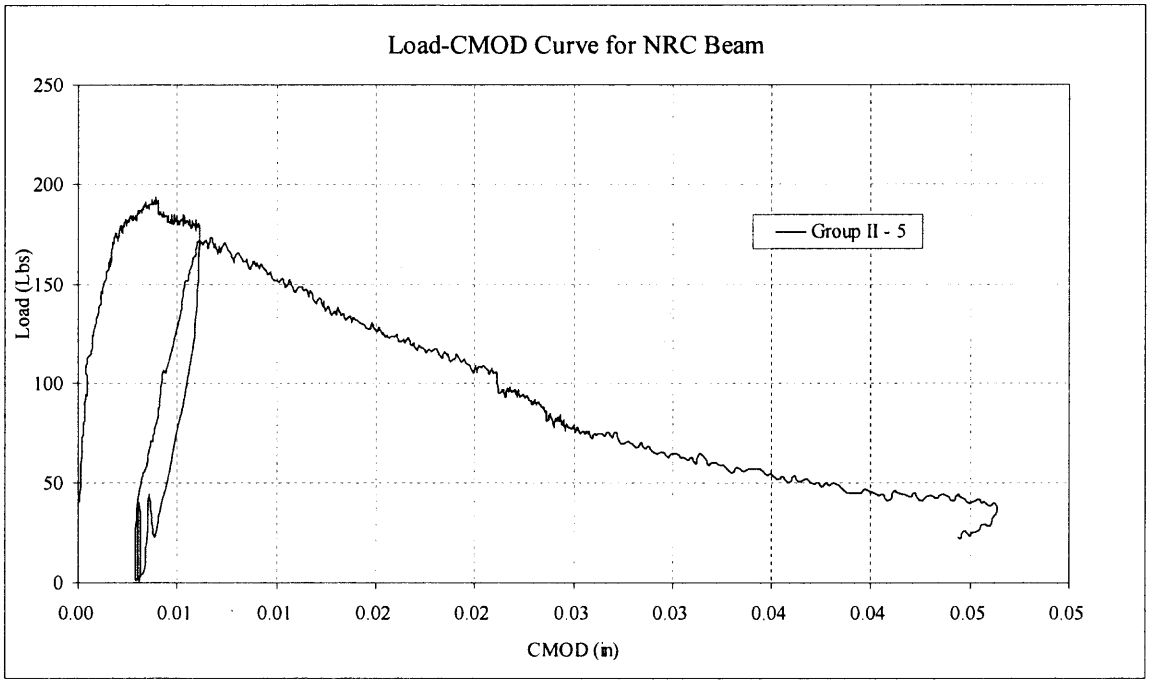

Figure B7a Load-CMOD Curve for NRC Beam S2GII B5
(Thickness × Width× Span = 3×3×12, a_0=0.65 in)

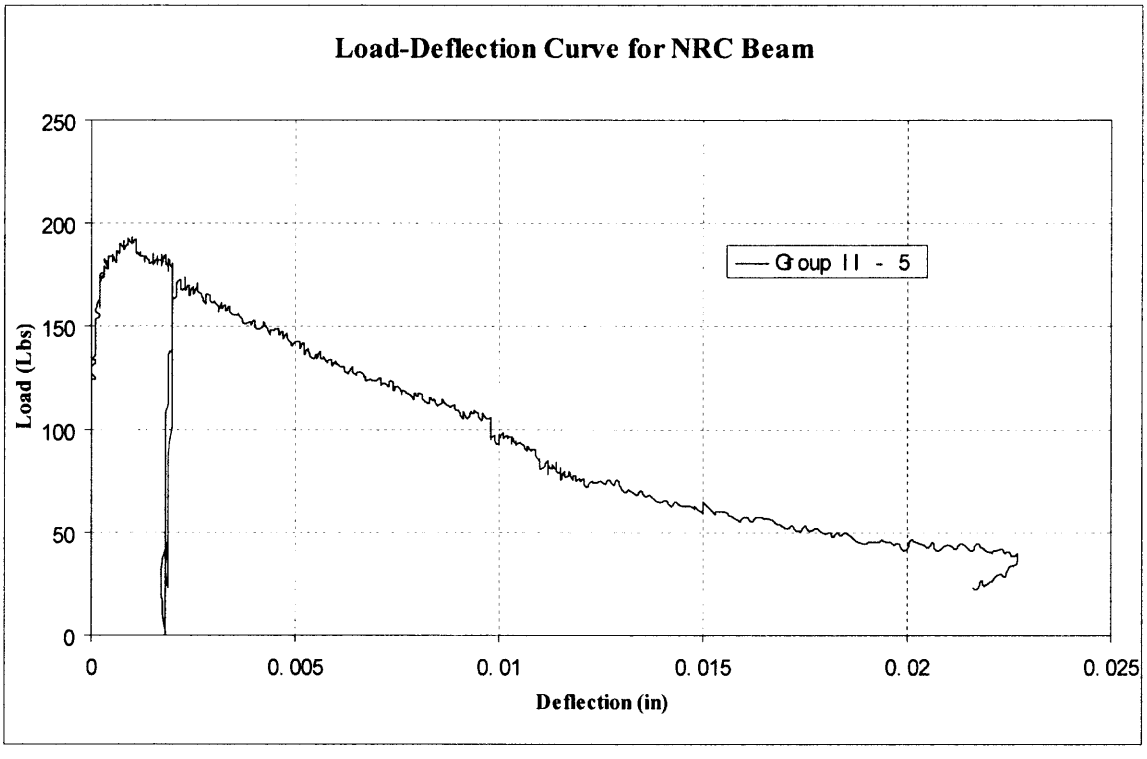

Figure B7b Load-Deflection Curve for NRC Beam S2GII B5
(Thickness × Width× Span = 3×3×12, a_0=0.65 in)

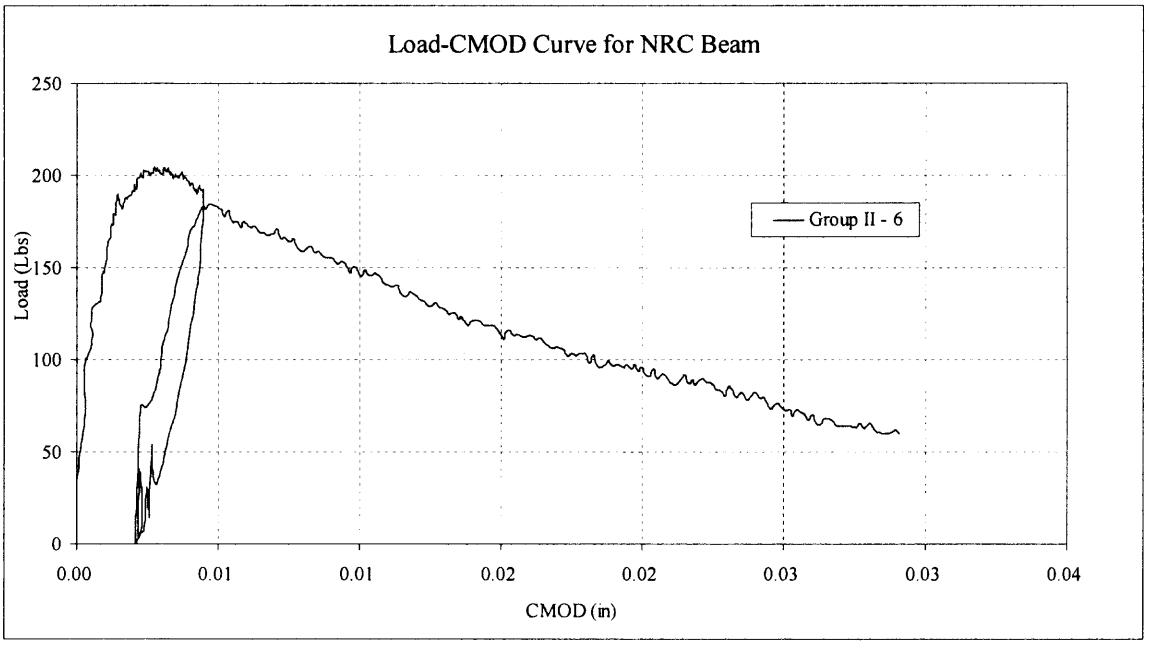

Figure B8a Load-CMOD Curve for NRC Beam S2GII B6
(Thickness × Width× Span = 3×3×12, a_0=0.60 in)

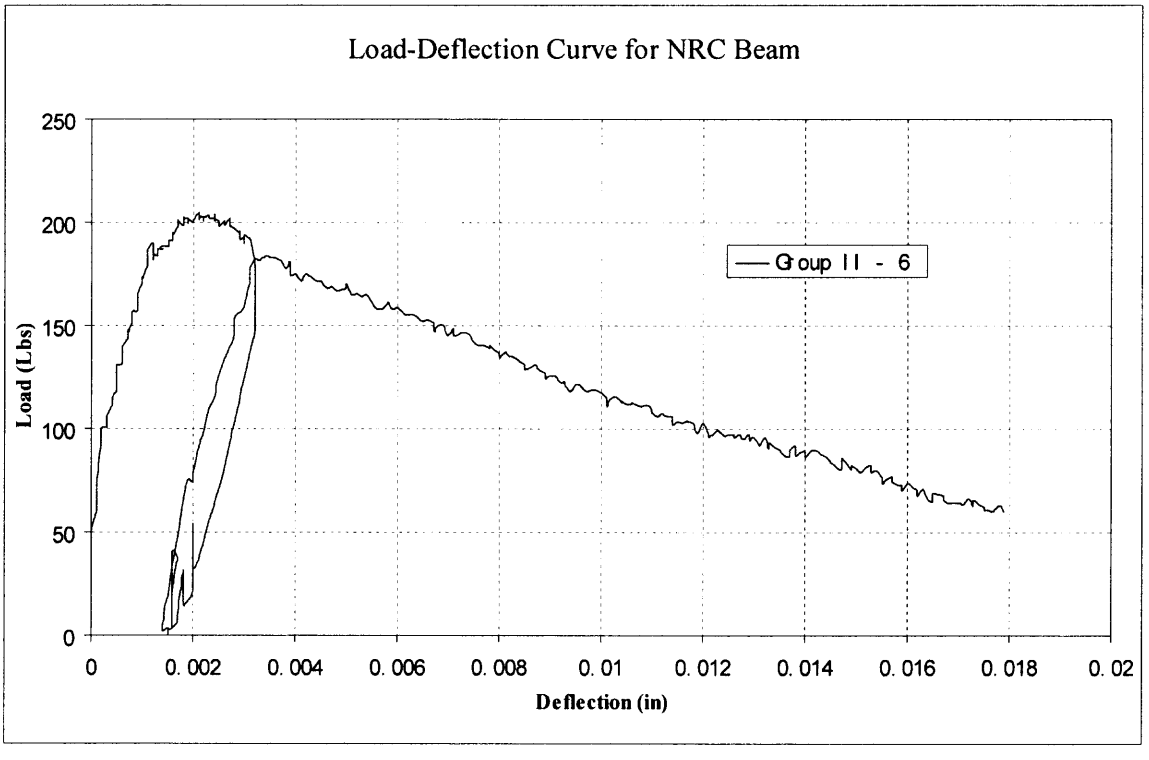

Figure B8b Load-Deflection Curve for NRC Beam S2GII B6
(Thickness × Width× Span = 3×3×12, a_0=0.60 in)

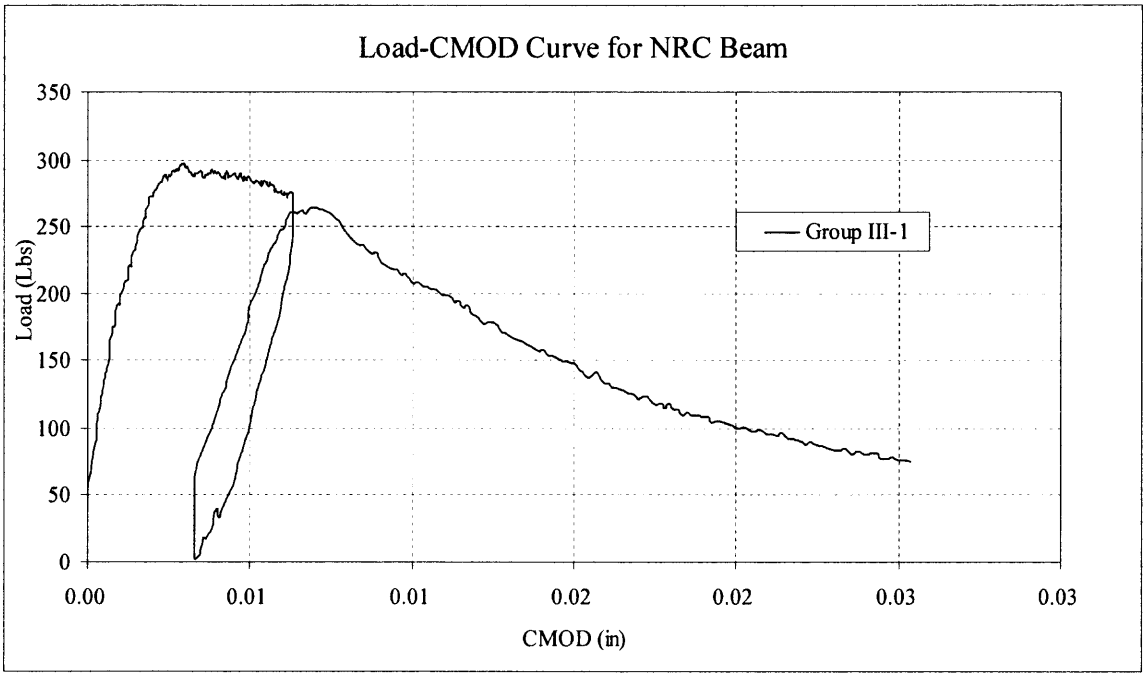

Figure B9a Load-CMOD Curve for NRC Beam S2GIII B1
(Thickness × Width× Span = 4×4×30, a_0=1.0 in)

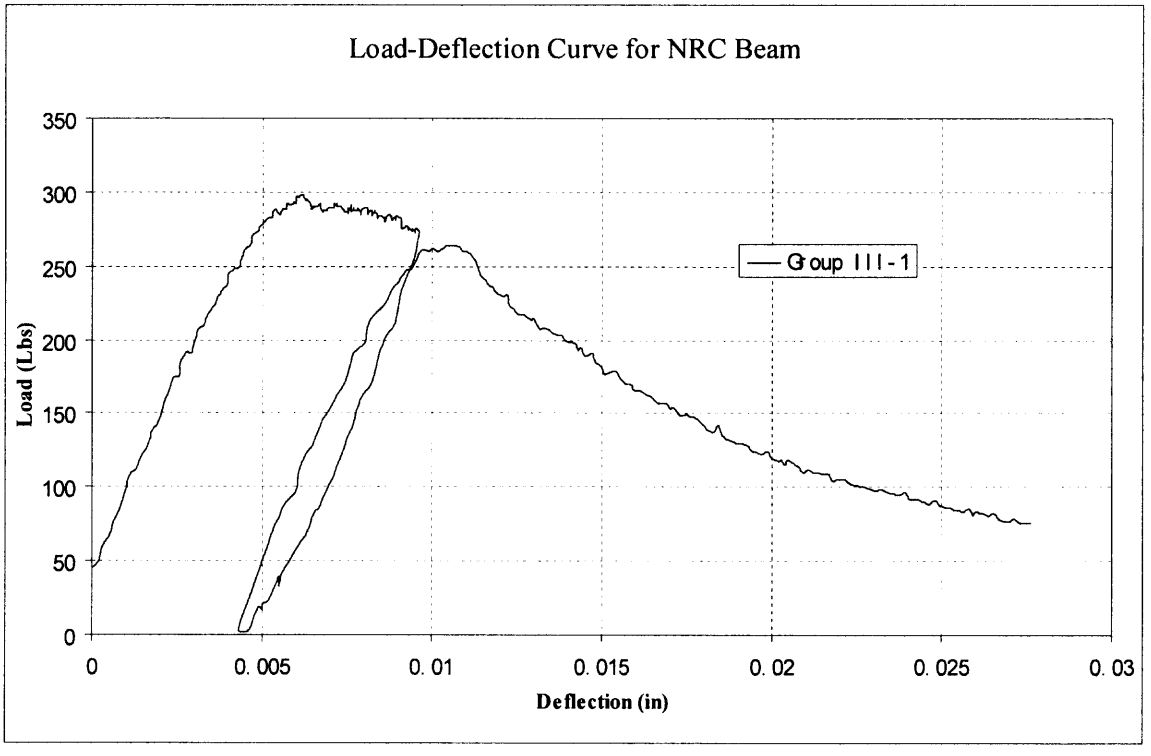

Figure B9a Load-CMOD Curve for NRC Beam S2GIII B1
(Thickness × Width× Span = 4×4×30, a_0=1.0 in)

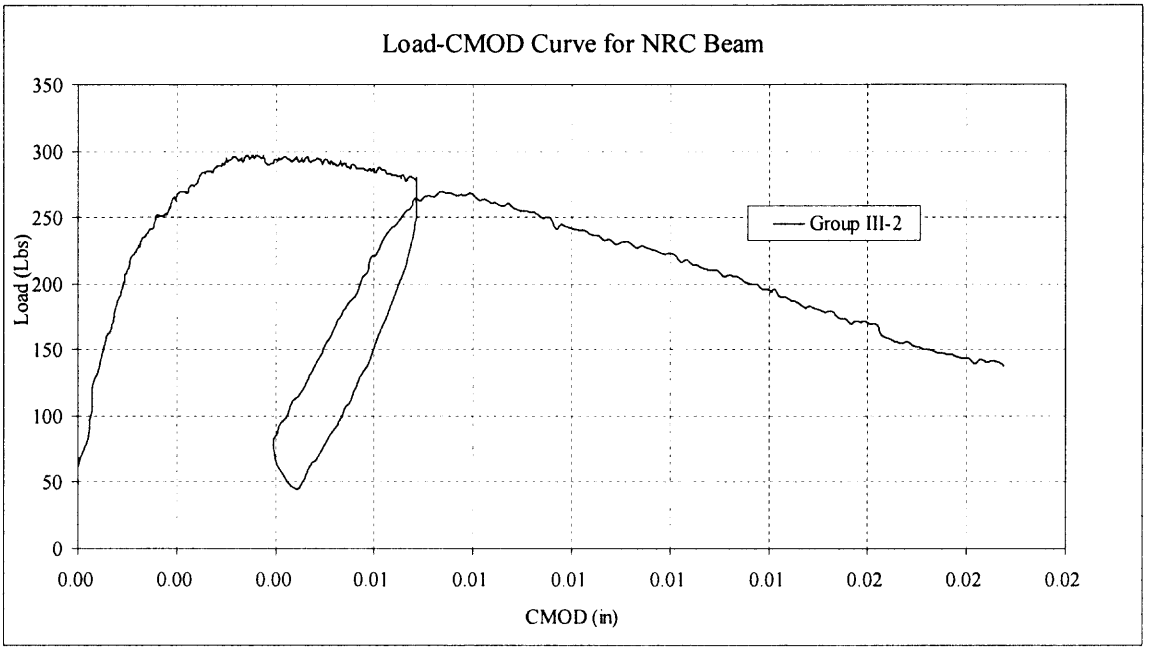

Figure B10a Load-CMOD Curve for NRC Beam S2GIII B2
(Thickness × Width× Span = 4×4×30, a_0=0.93 in)

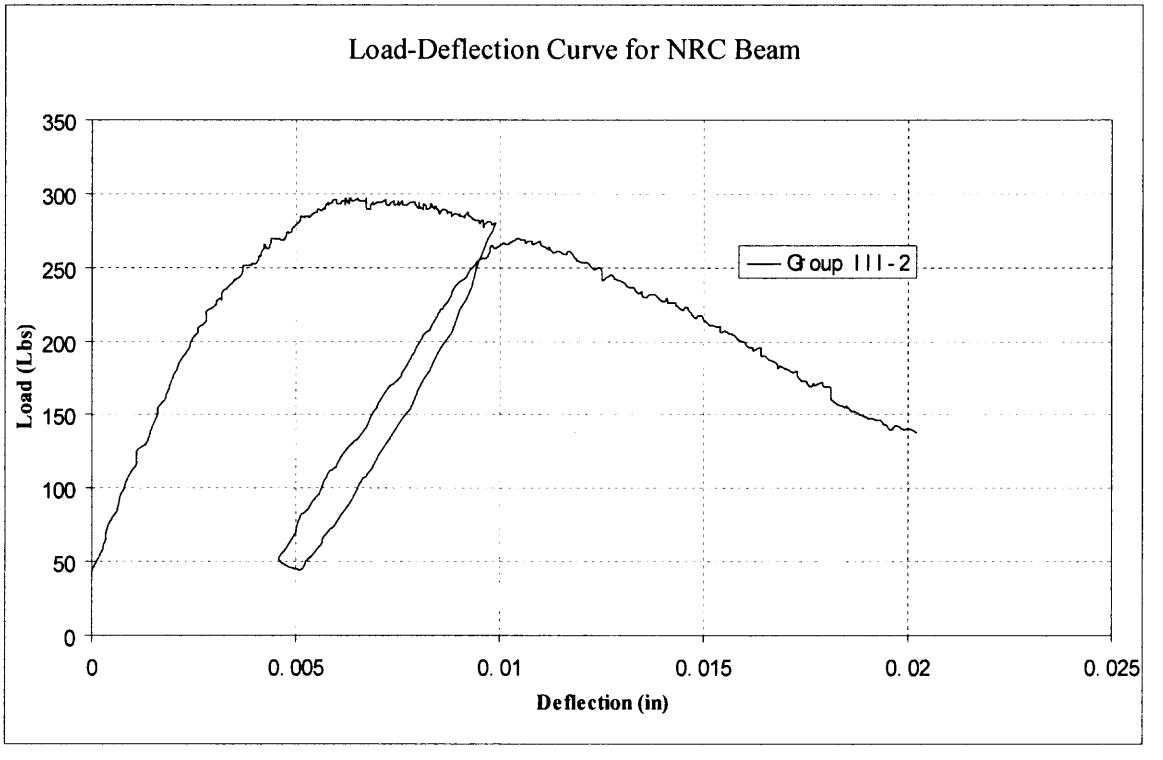

Figure B10a Load-Deflection Curve for NRC Beam S2GIII B2
(Thickness × Width× Span = 4×4×30, a_0=0.93 in)

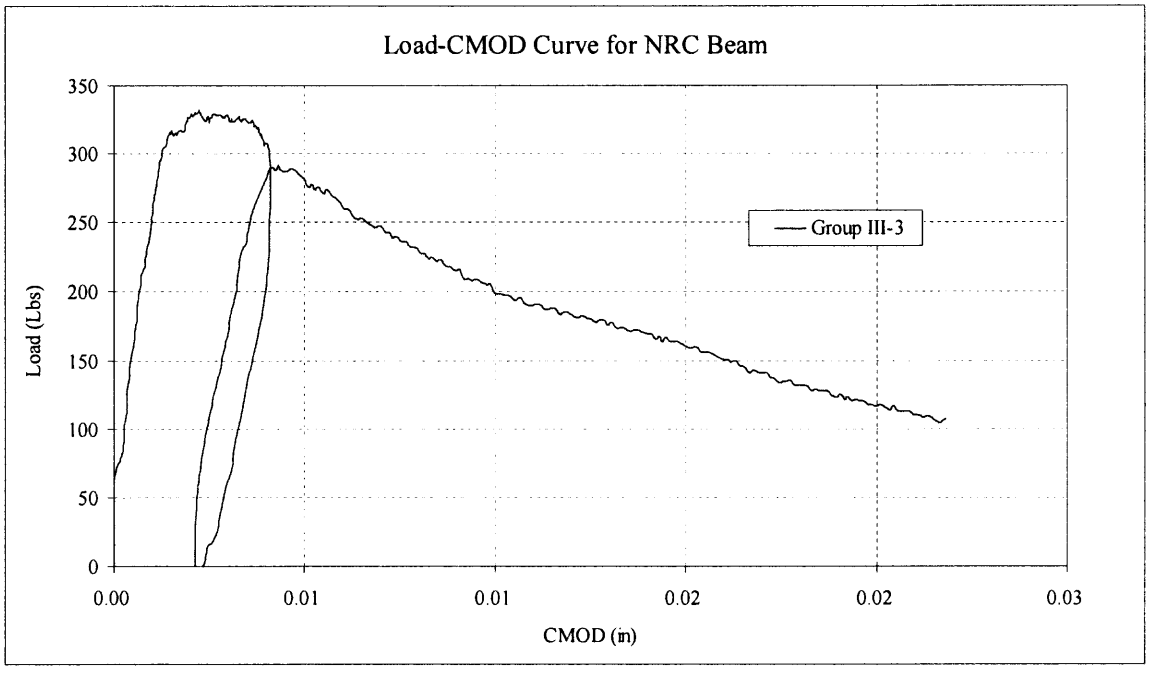

Figure B11a Load-CMOD Curve for NRC Beam S2GIII B3
(Thickness × Width× Span = 4×4×30, a_0=1.0 in)

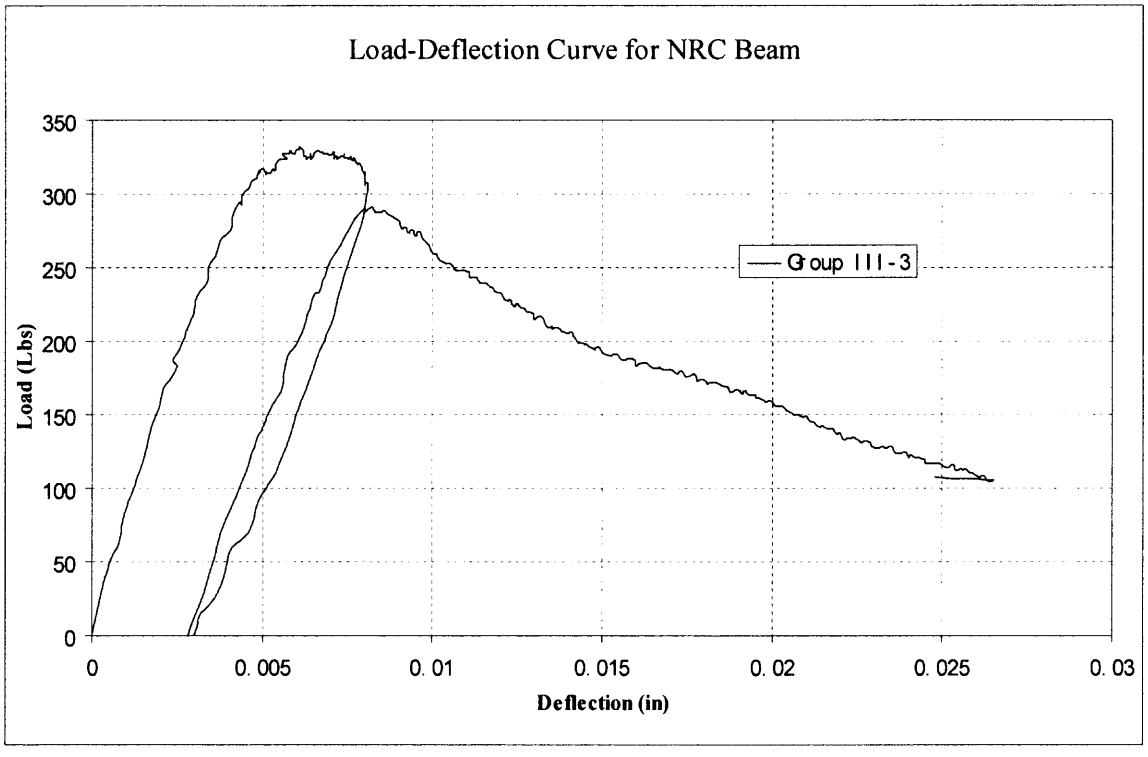

Figure B11a Load-Deflection Curve for NRC Beam S2GIII B3
(Thickness × Width× Span = 4×4×30, a_0=1.0 in)

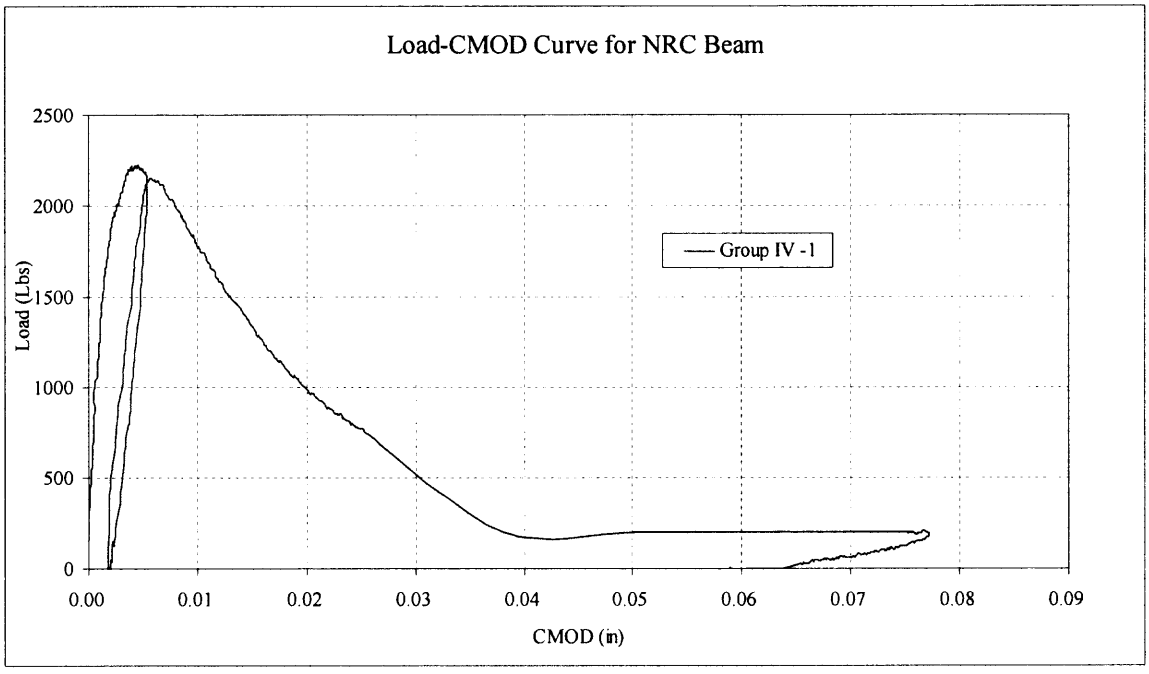

Figure B12a Load-CMOD Curve for NRC Beam S2GIV B1
(Thickness × Width× Span = 6×6×24, a_0=1.30 in)

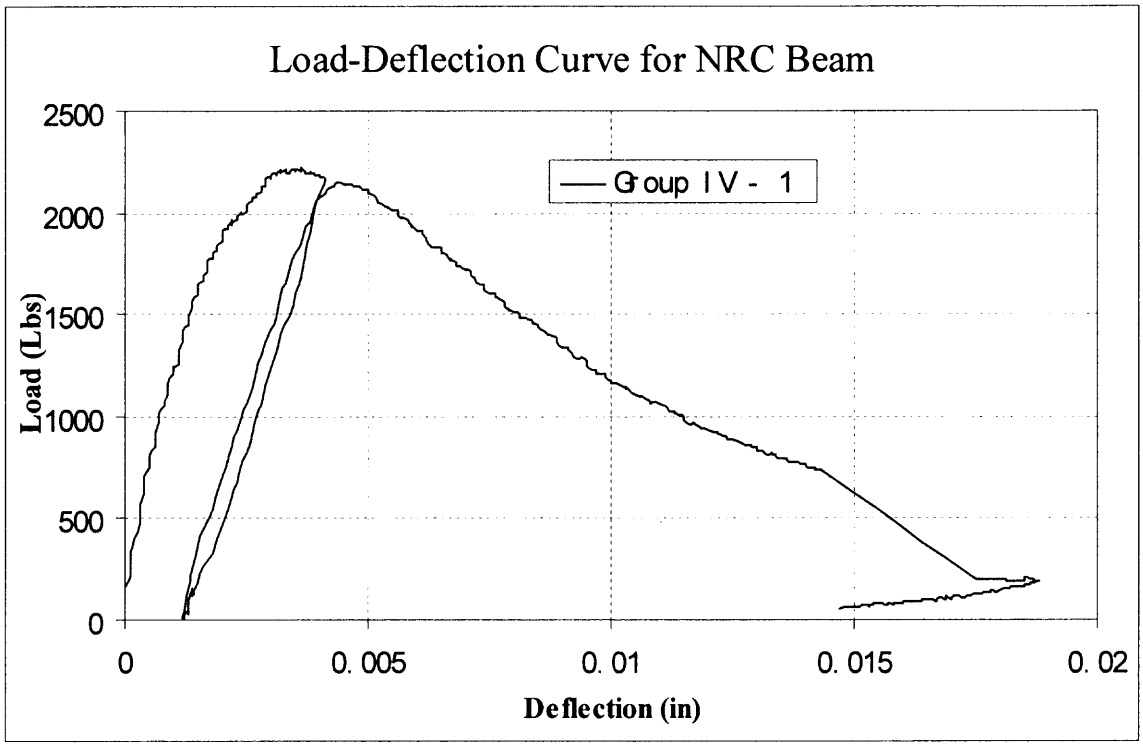

Figure B12b Load-Deflection Curve for NRC Beam S2GIV B1
(Thickness × Width× Span = 6×6×24, a_0=1.30 in)

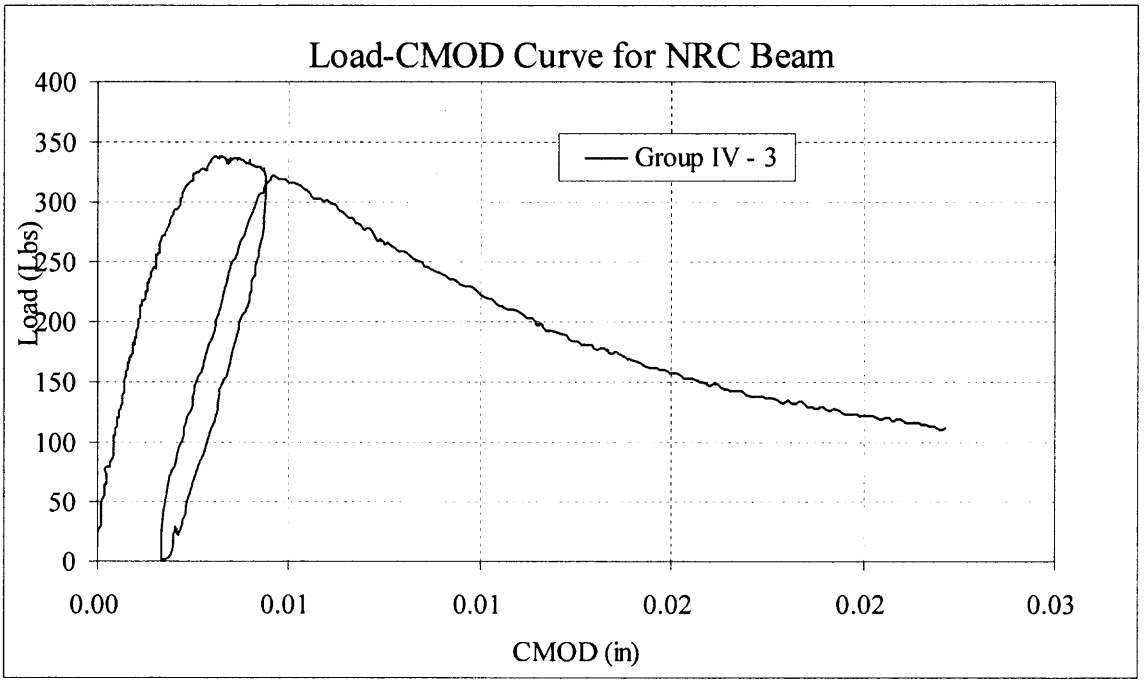

Figure B13a Load-CMOD Curve for NRC Beam S2GIV B2
(Thickness × Width× Span = 6×6×24, a_0=1.40 in)

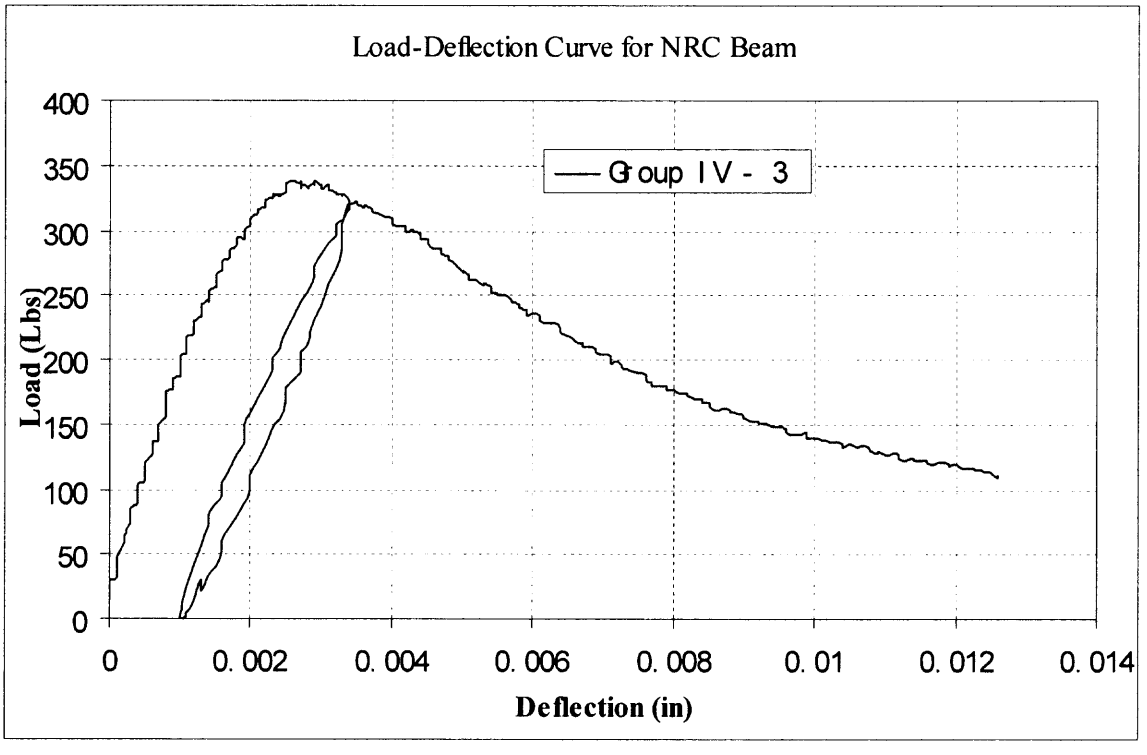

Figure B13b Load-Deflection Curve for NRC Beam S2GIV B3
(Thickness × Width× Span = 6×6×24, a_0=1.40 in)

APPENDIX C

RESULTS OF THE THIRD SERIES OF EXPERIMENTS

In this series test, total 16 beam specimens were tested on Concrete in January, 2004. The relationships between Load, Load line deflection, CMOD and Crack Growth were measured and recorded using MTS and Ultrasonic Device.

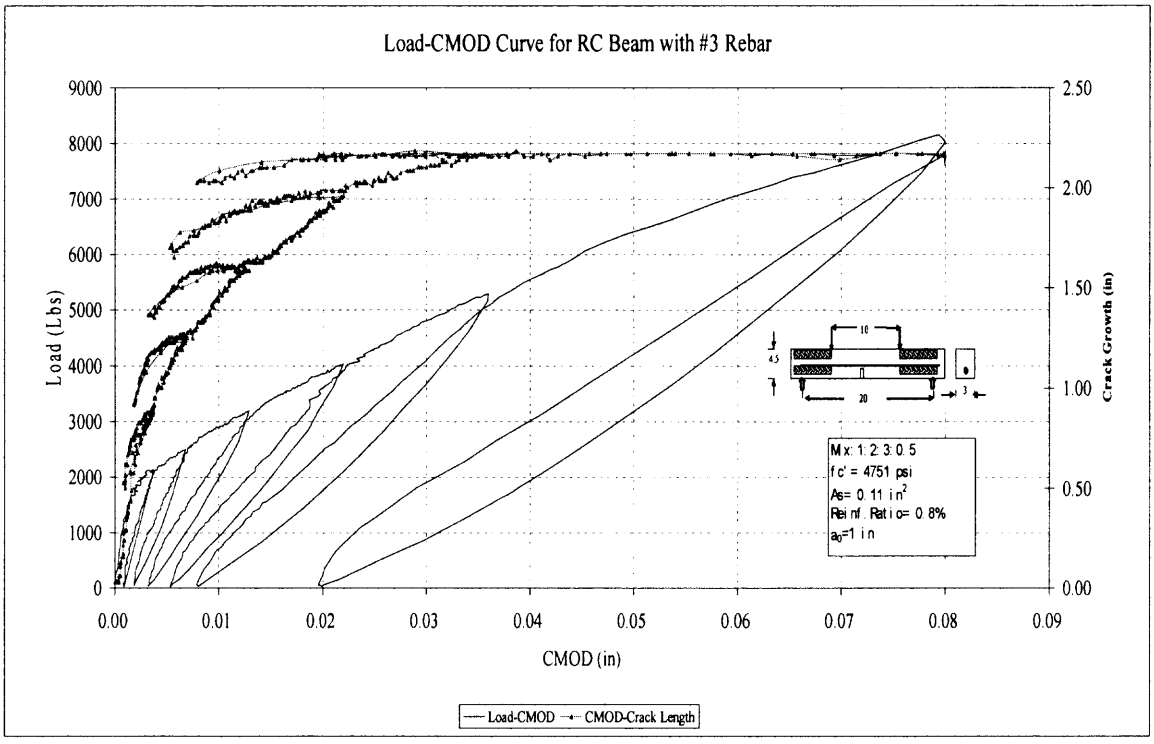

Figure C1a Load-CMOD with Crack Growth Curve for RC Beam S3GI B1

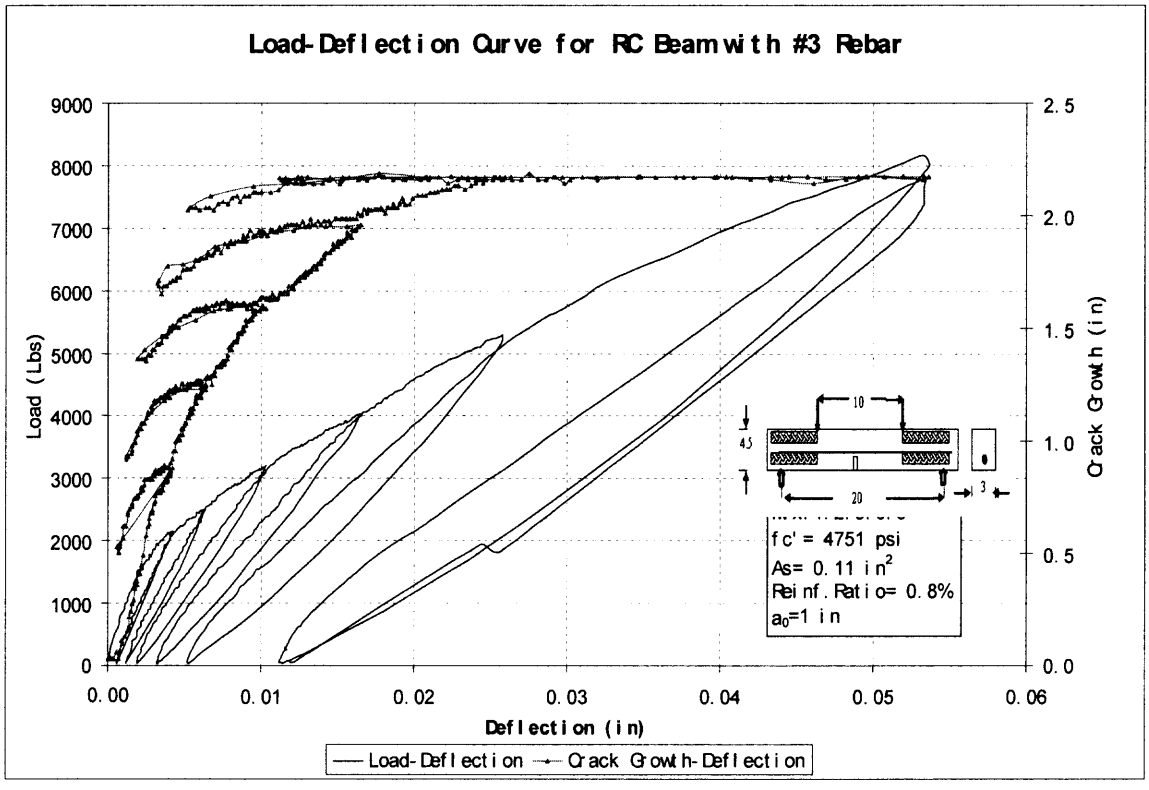

Figure C1a Load-Deflection with Crack Growth Curve for RC Beam S3GI B1

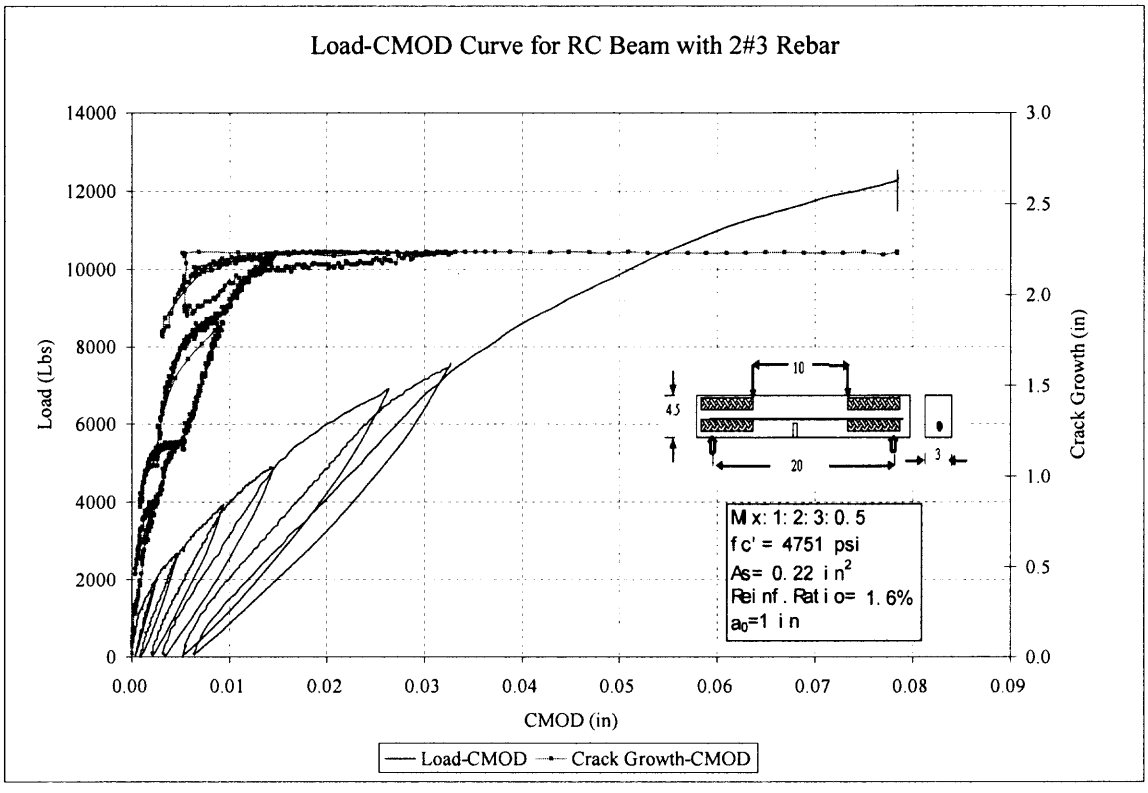

Figure C2a Load-CMOD with Crack Growth Curve for RC Beam S3GI B2

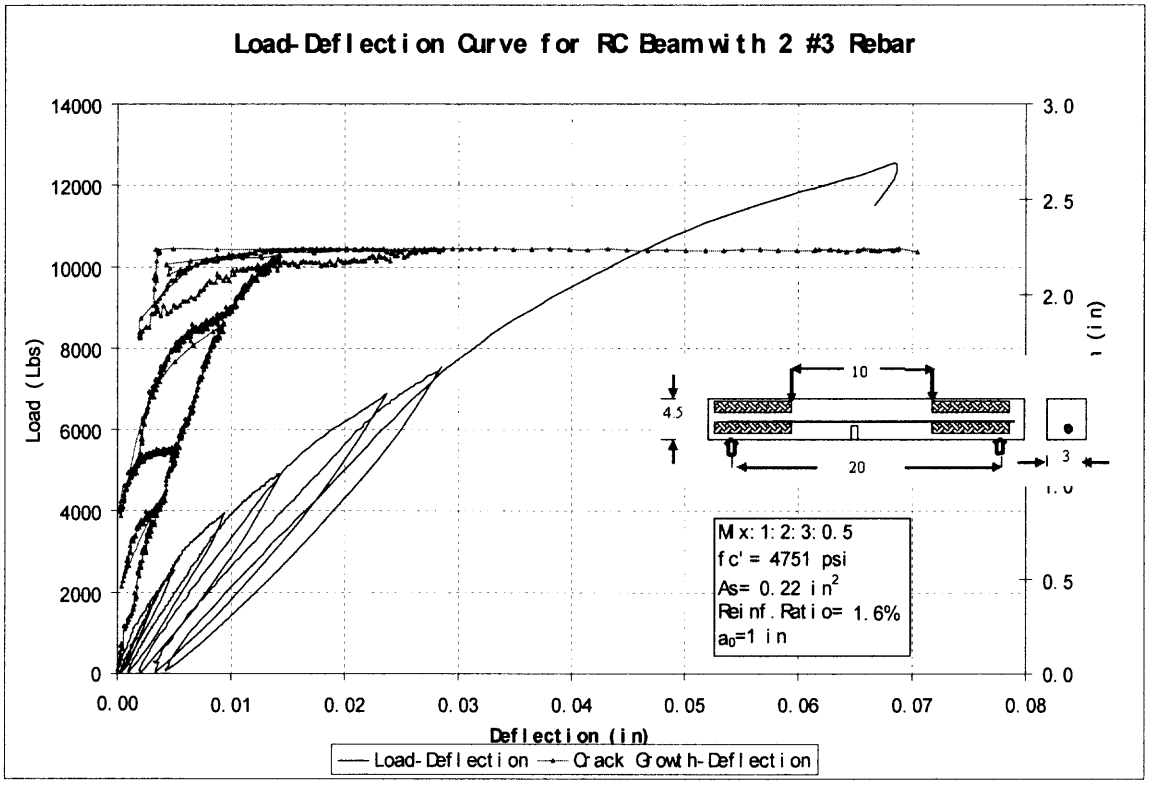

Figure C2b Load-Deflection with Crack Growth Curve for RC Beam S3GI B2

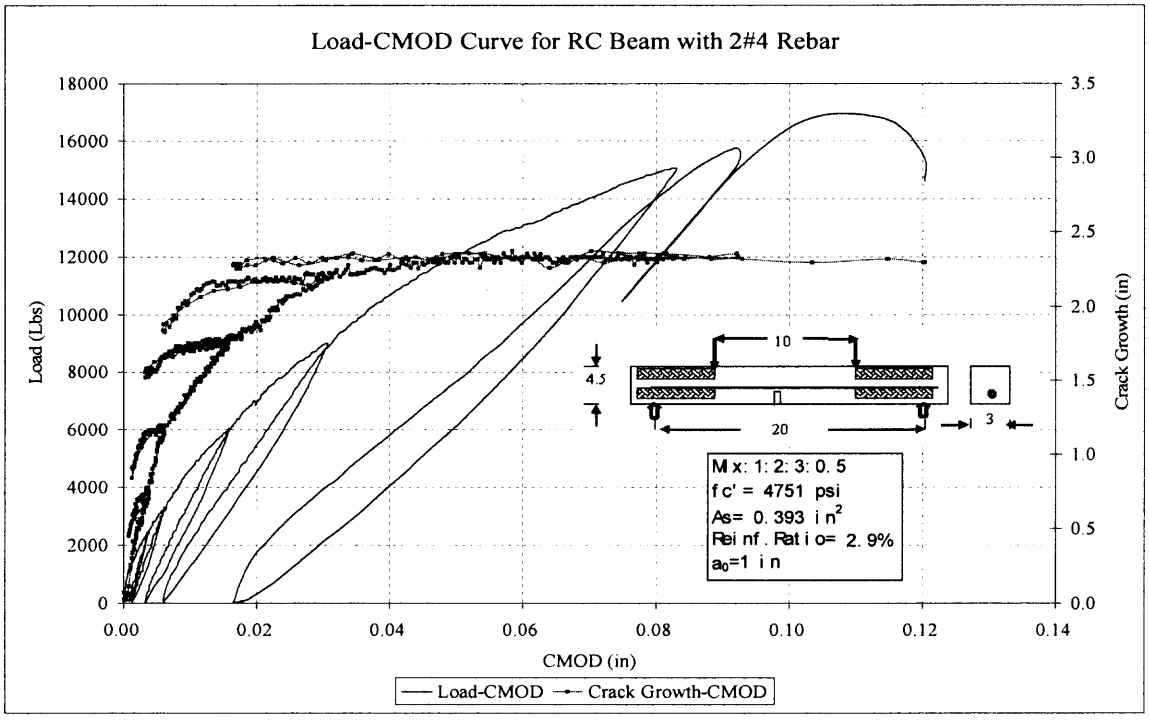

Figure C3a Load-CMOD with Crack Growth Curve for RC Beam S3GI B3

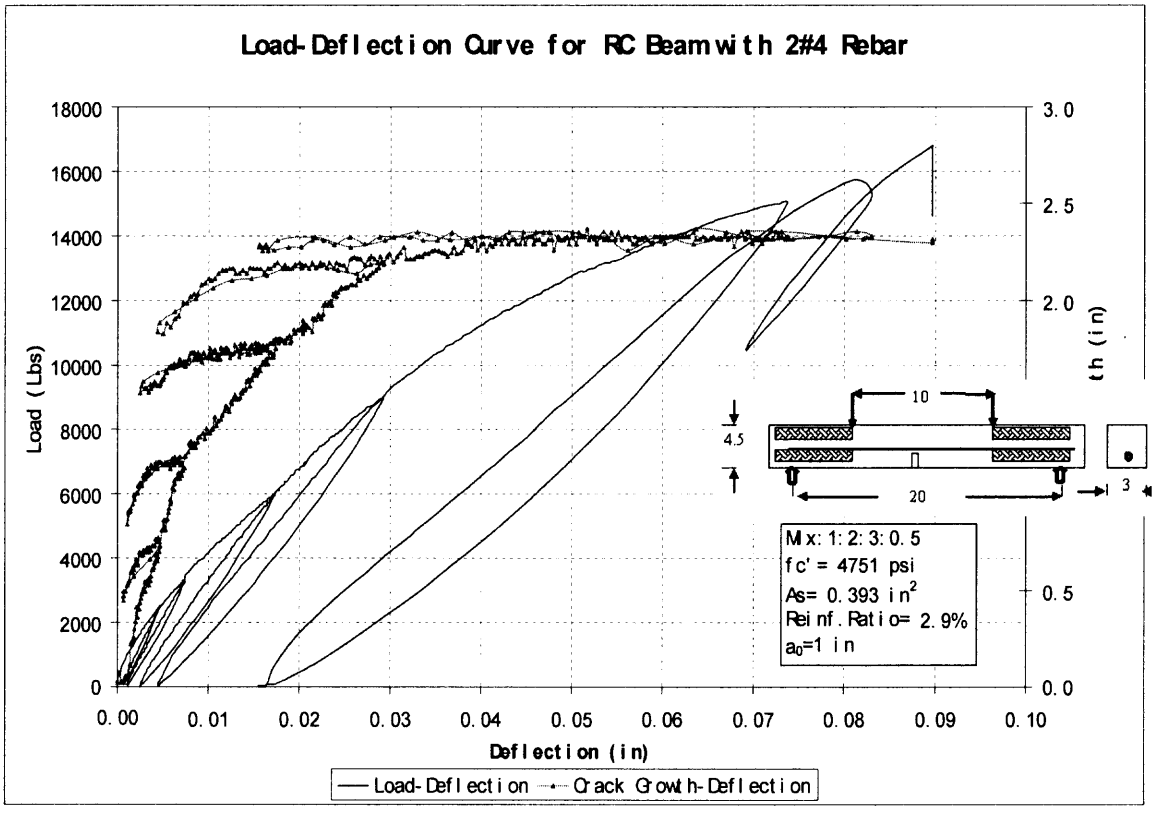

Figure C3b Load-Deflection with Crack Growth Curve for RC Beam S3GI B3

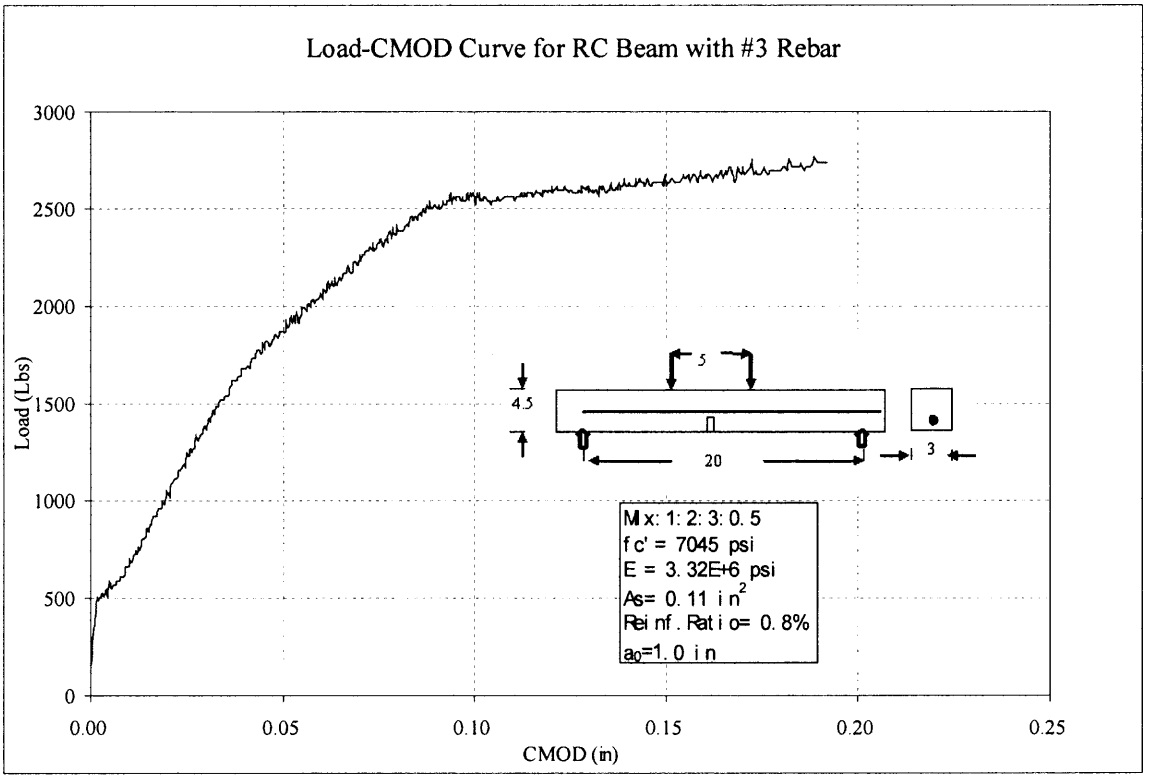

Figure C4a Load-CMOD Curve for RC Beam S3GII B1(0624-0930)

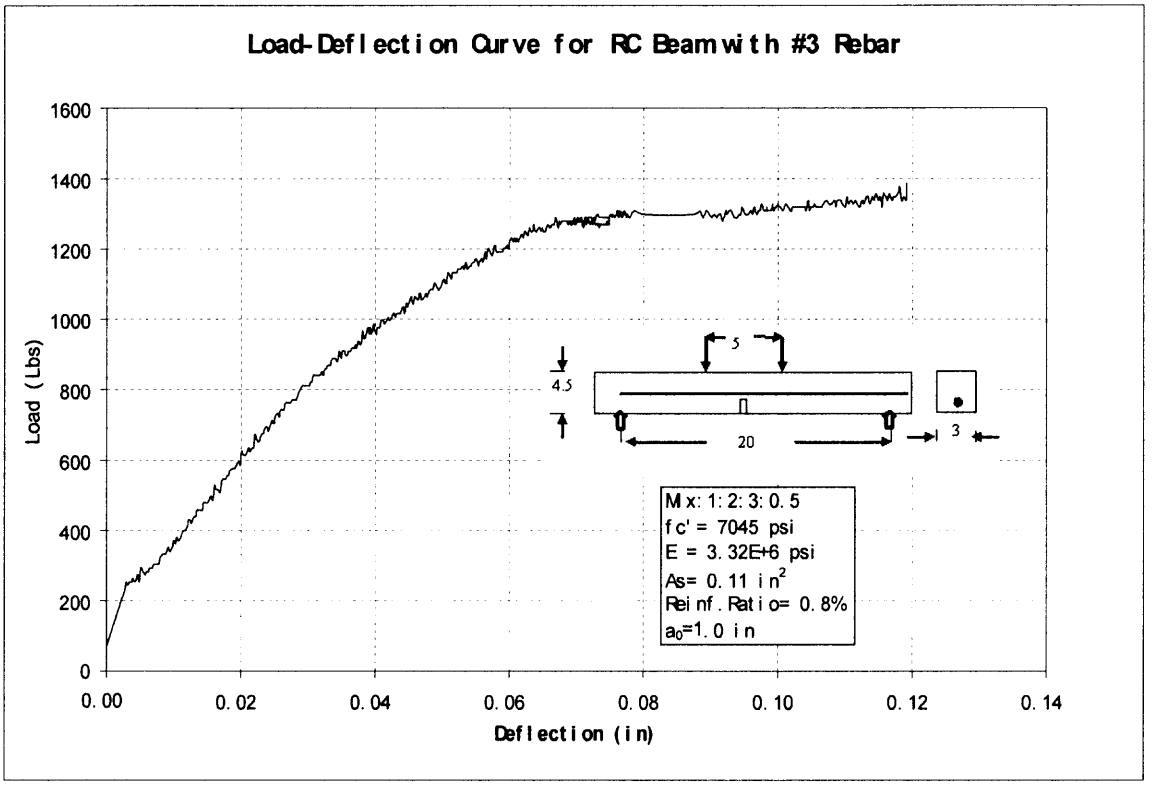

Figure C4b Load-Deflection Curve for RC Beam S3GII B1(0624-0930)

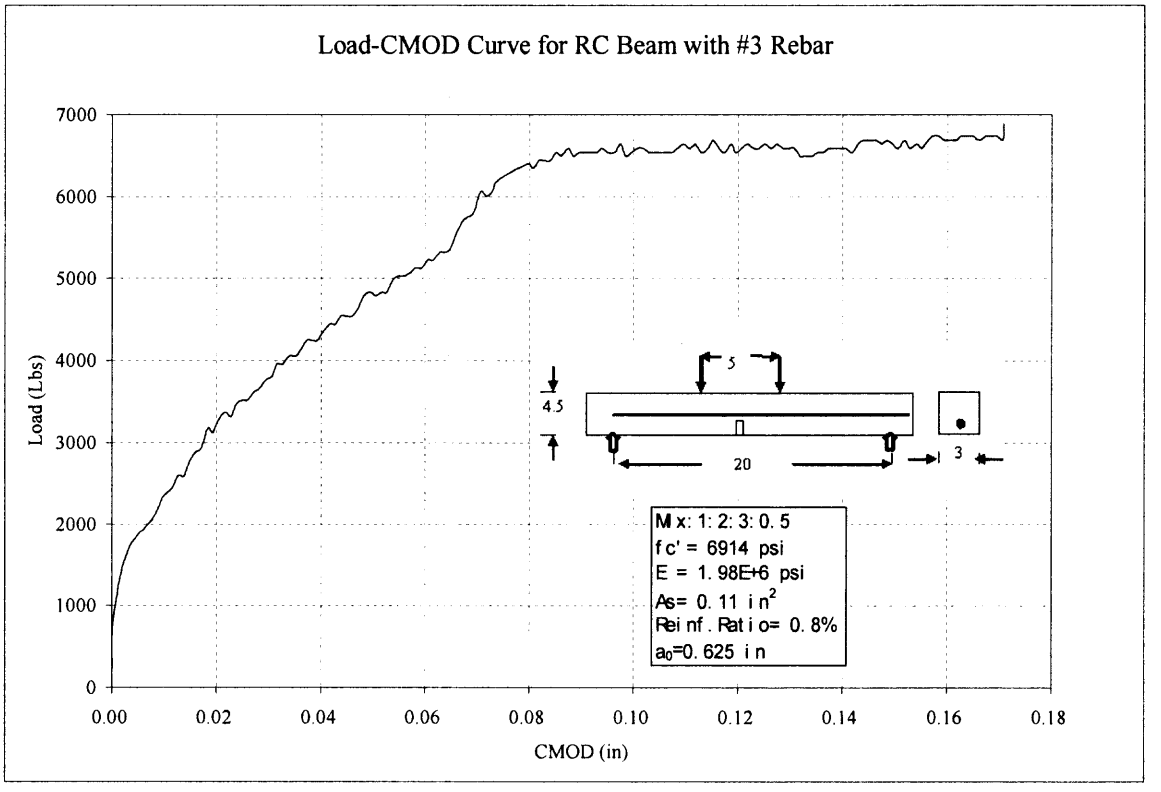

Figure C5a Load-CMOD Curve for RC Beam S3GII B2(0705-1003)

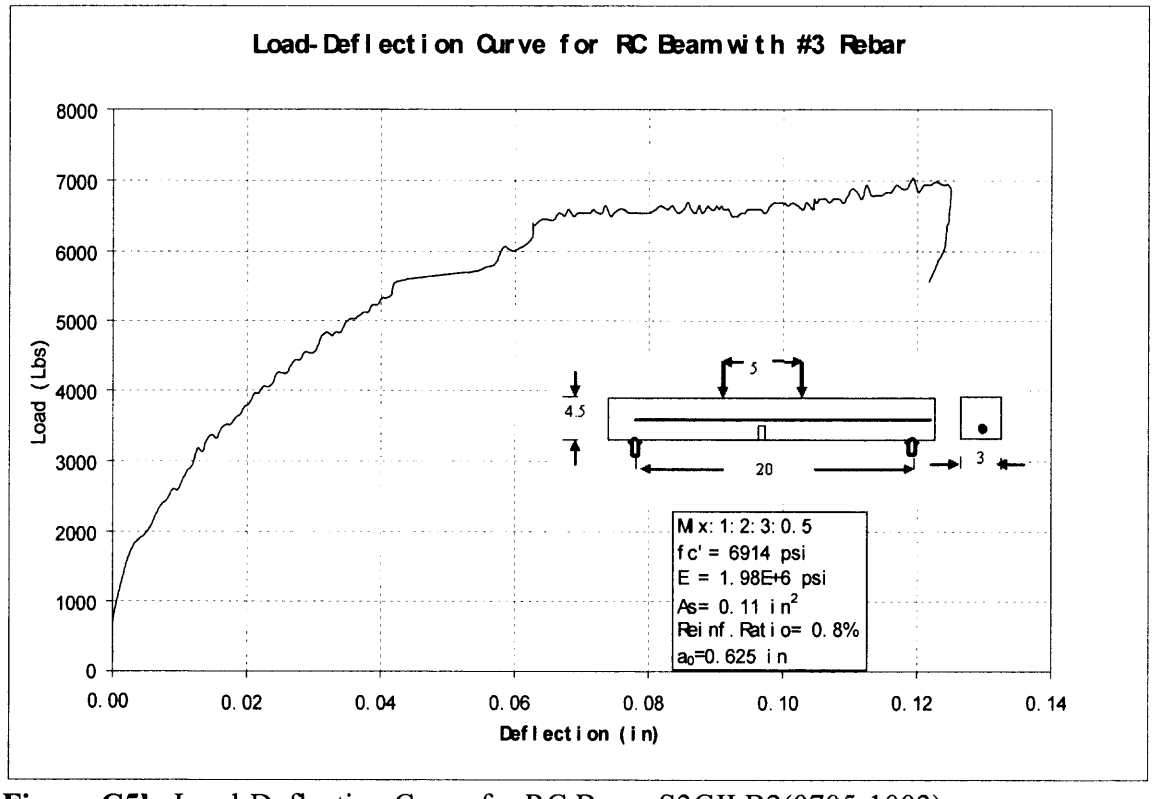

Figure C5b Load-Deflection Curve for RC Beam S3GII B2(0705-1003)

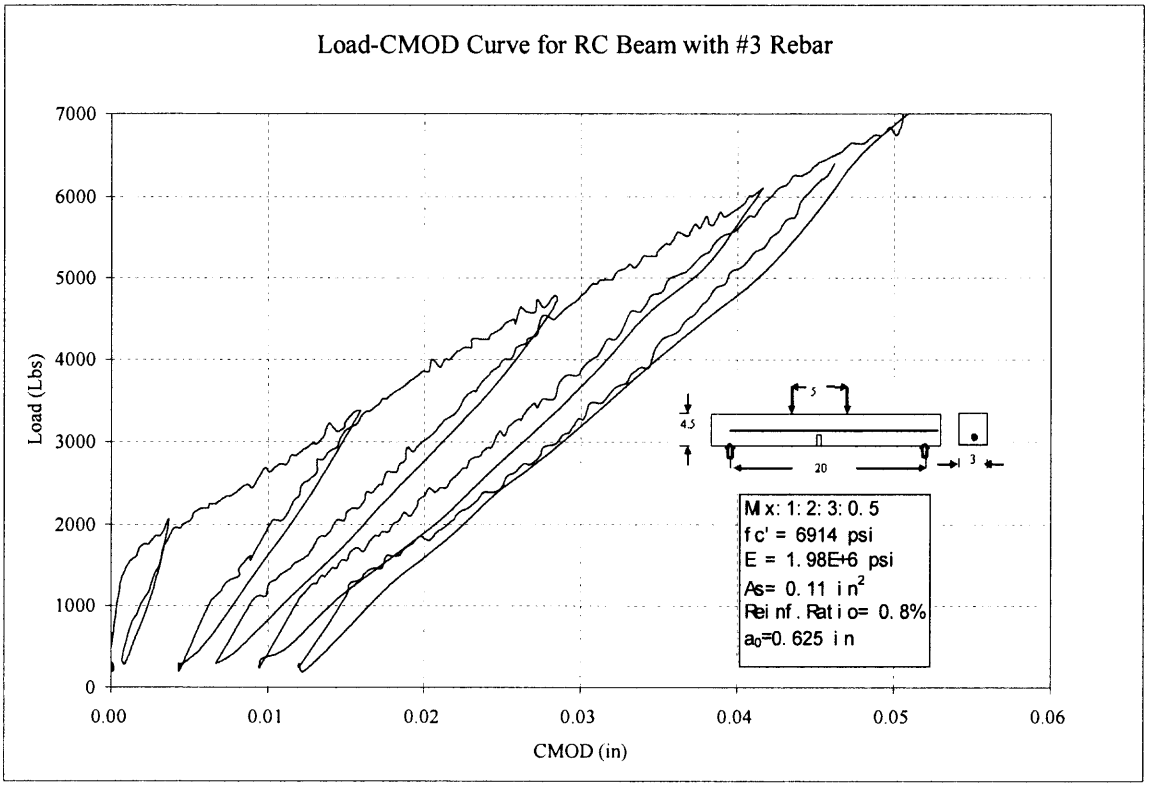

Figure C6a Load-CMOD Curve for RC Beam S3GII B3(0705-1003)

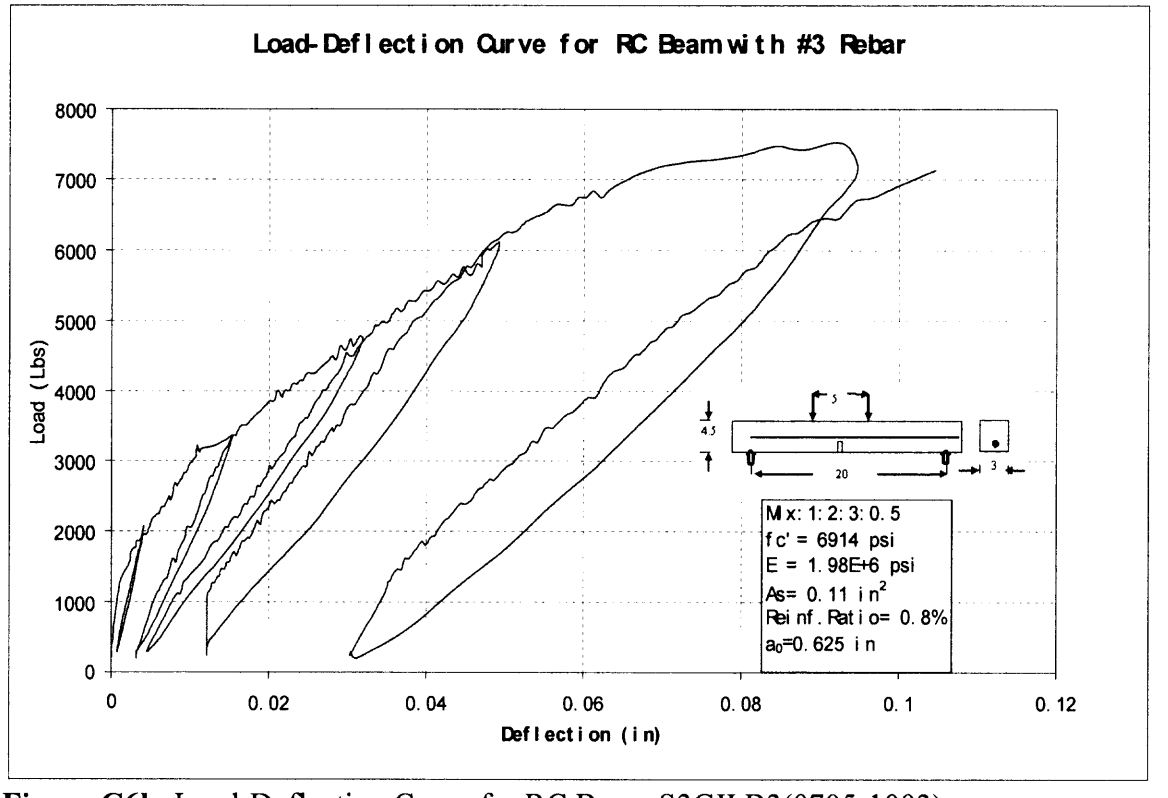

Figure C6b Load-Deflection Curve for RC Beam S3GII B3(0705-1003)

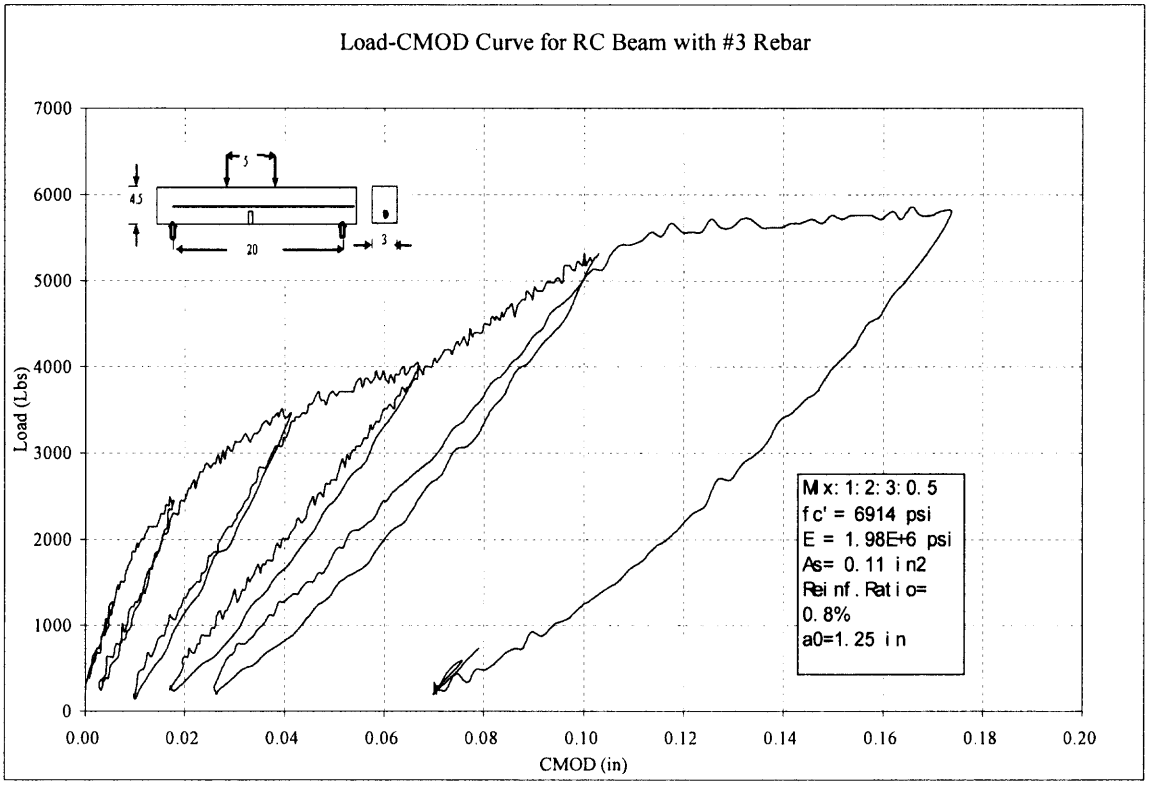

Figure C7a Load-CMOD Curve for RC Beam S3GII B4(0707-1003)

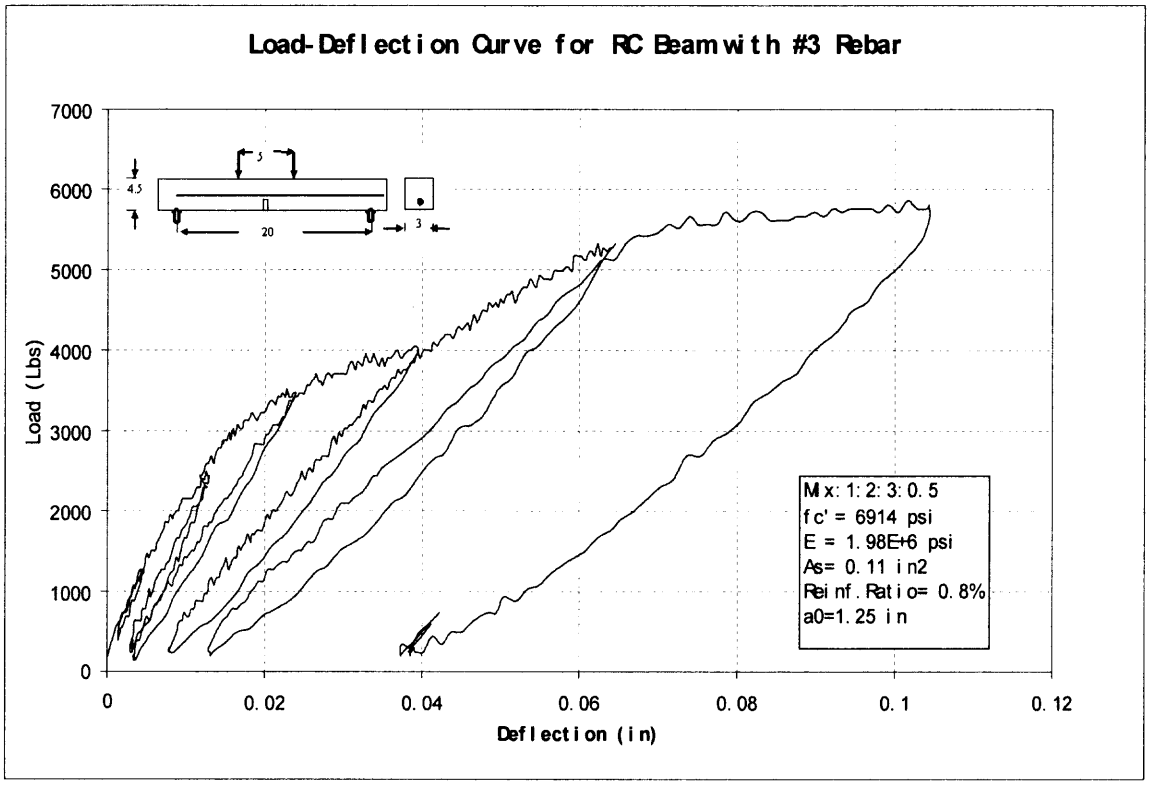

Figure C7b Load-Deflection Curve for RC Beam S3GII B4(0707-1003)

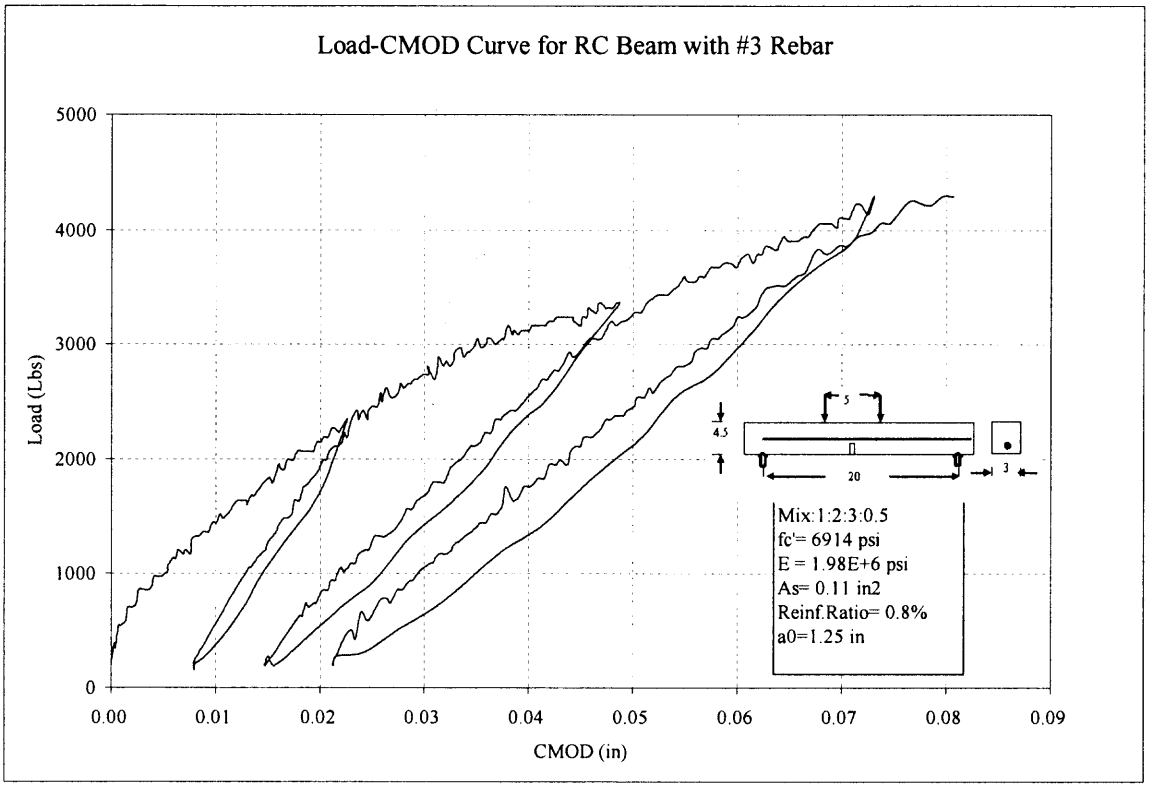

Figure C8a Load-CMOD Curve for RC Beam S3GII B5(0707-1003)

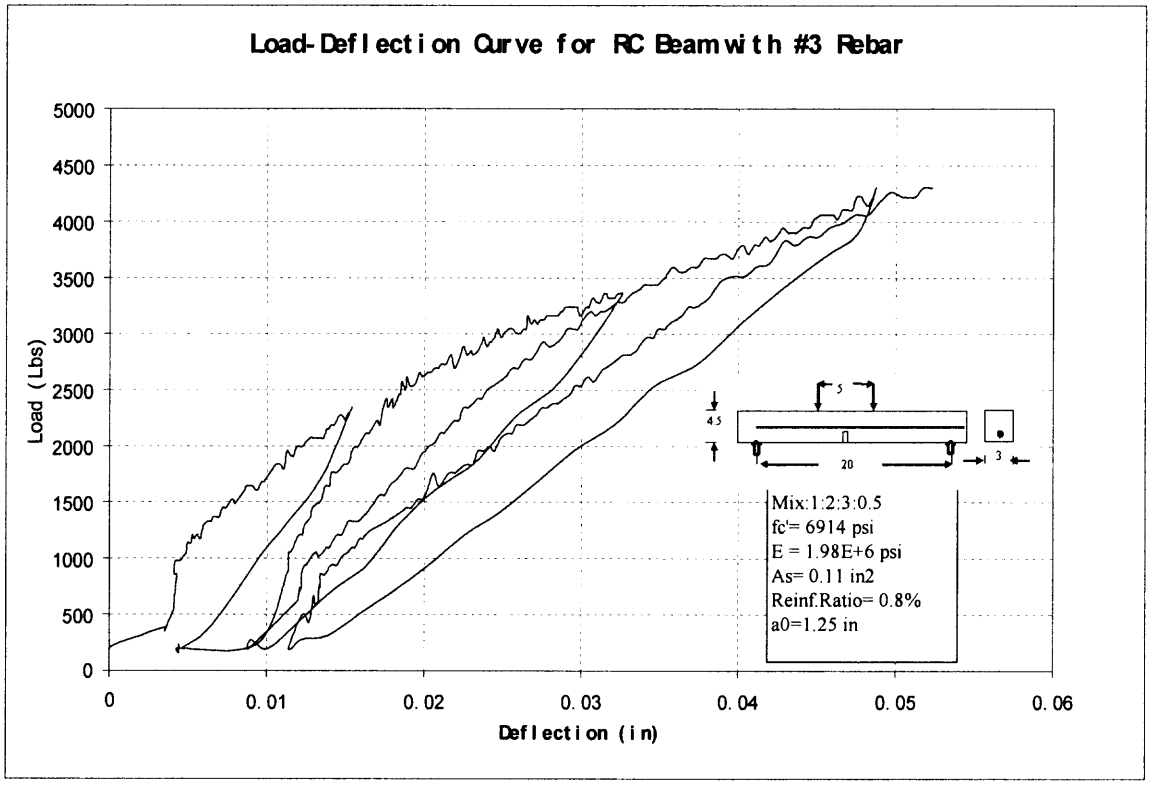

Figure C8b Load-Deflection Curve for RC Beam S3GII B5(0707-1003)

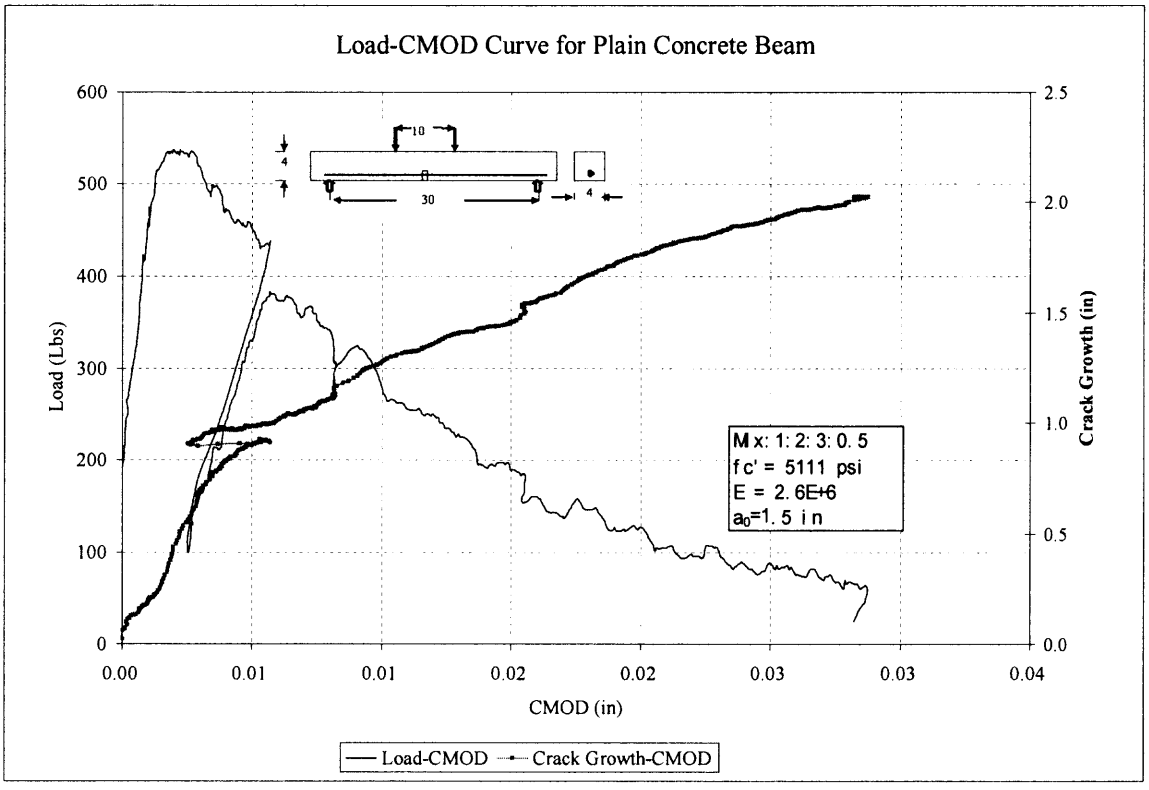

Figure C9a Load-CMOD & Crack Growth for NRC Beam S3GIII B1(0928-1010)

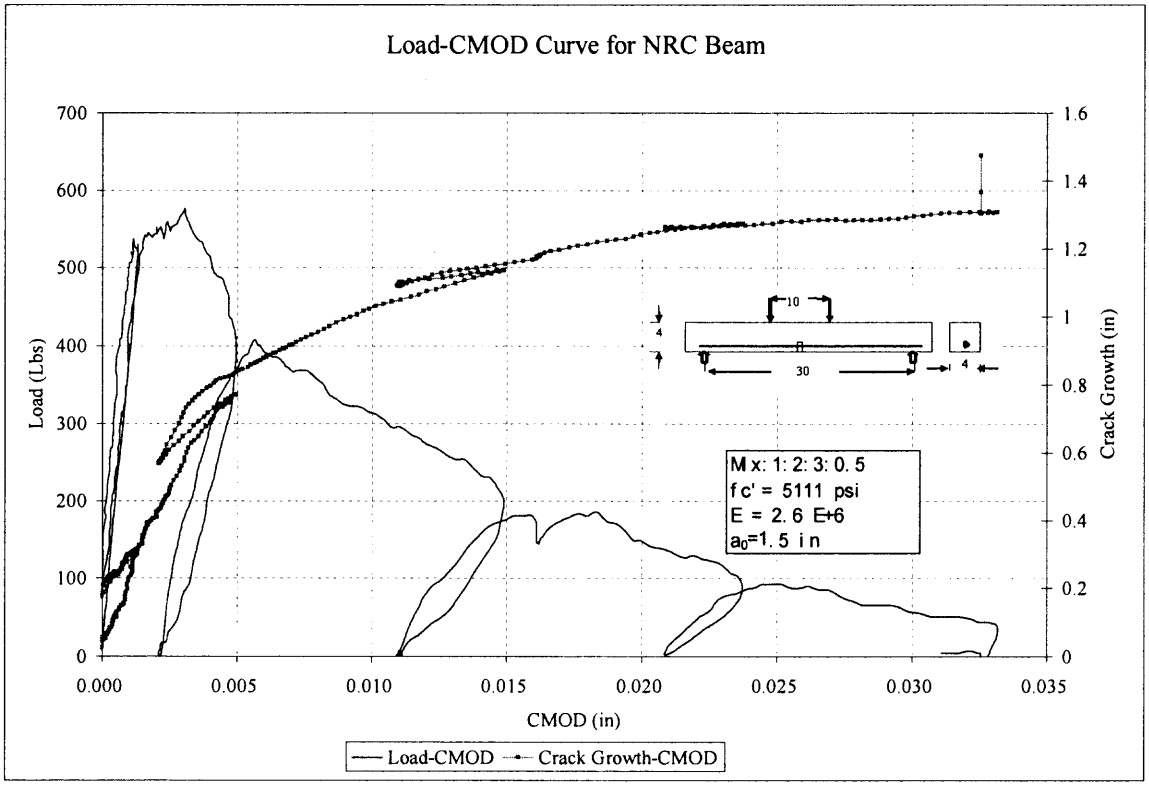

Figure C10a Load-CMOD &Crack Growth for NRC Beam S3GIII B2(0928-1018)

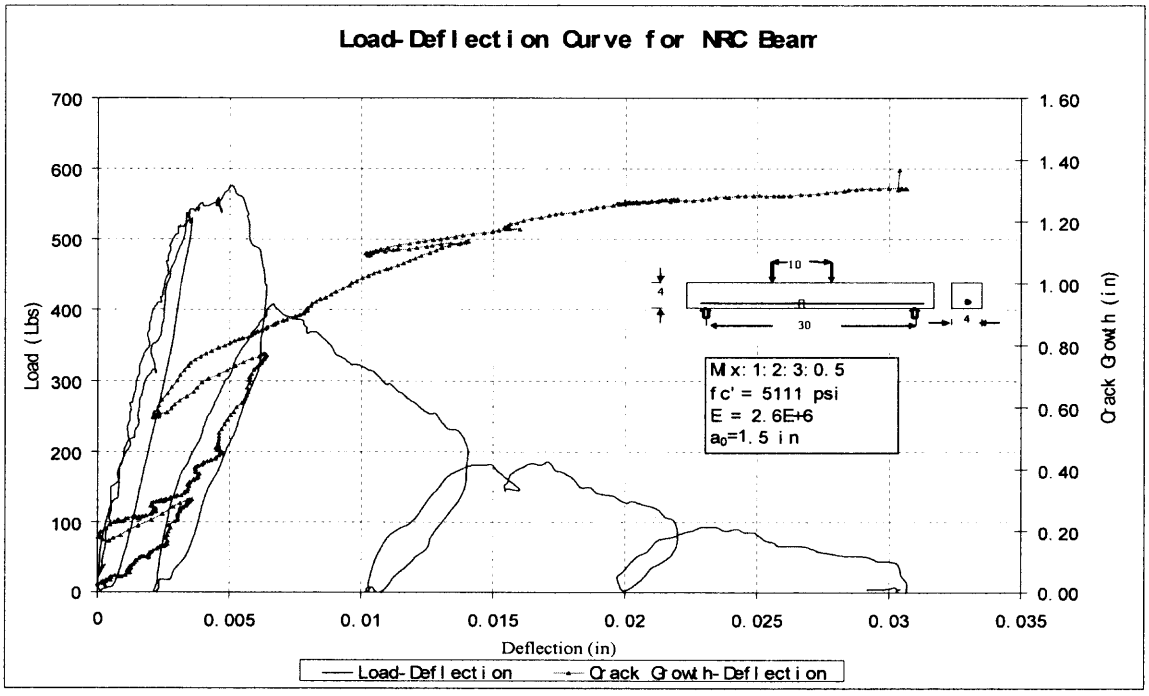

Figure C10a Load-Deflection &Crack Growth for NRC Beam S3GIII B2(0928-1018)

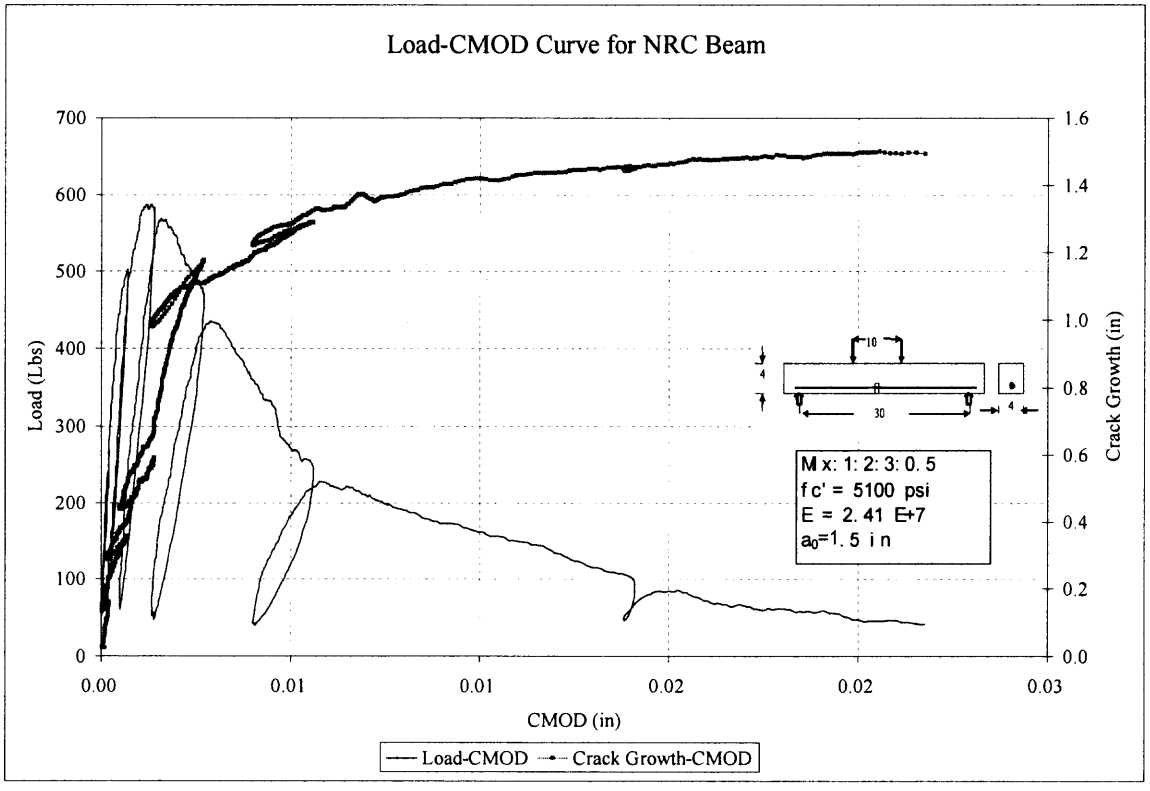

Figure C11a Load-CMOD &Crack Growth for NRC Beam S3GIII B3(0928-1025)

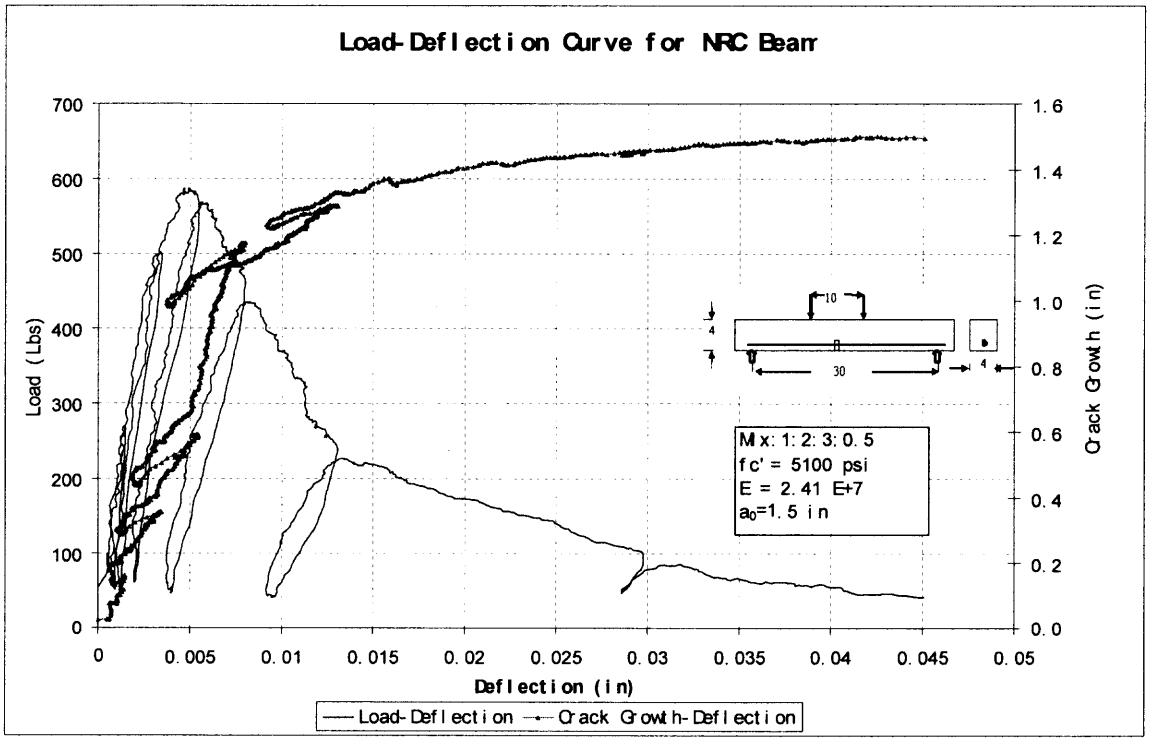

Figure C11b Load-Deflection & Crack Growth for NRC Beam S3GIII B3(0928-1025)

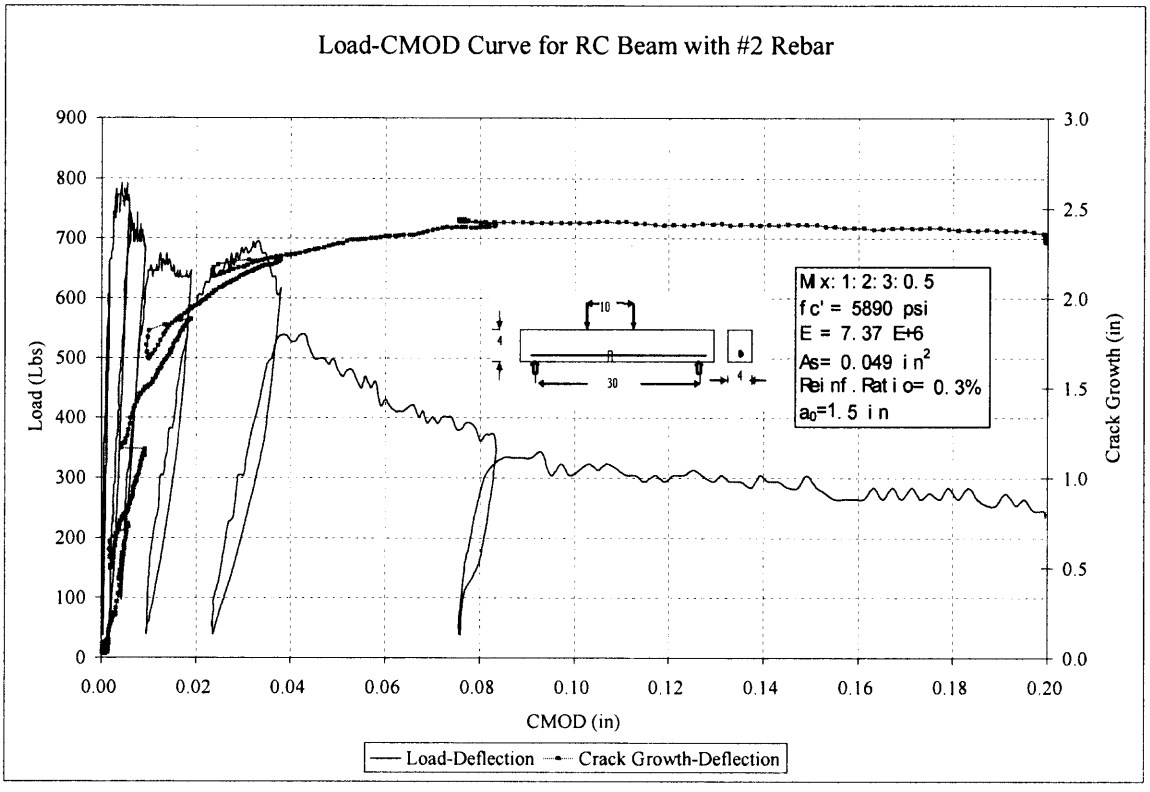

Figure C12a Load-CMOD &Crack Growth for NRC Beam S3GIII B4(0927-1025)

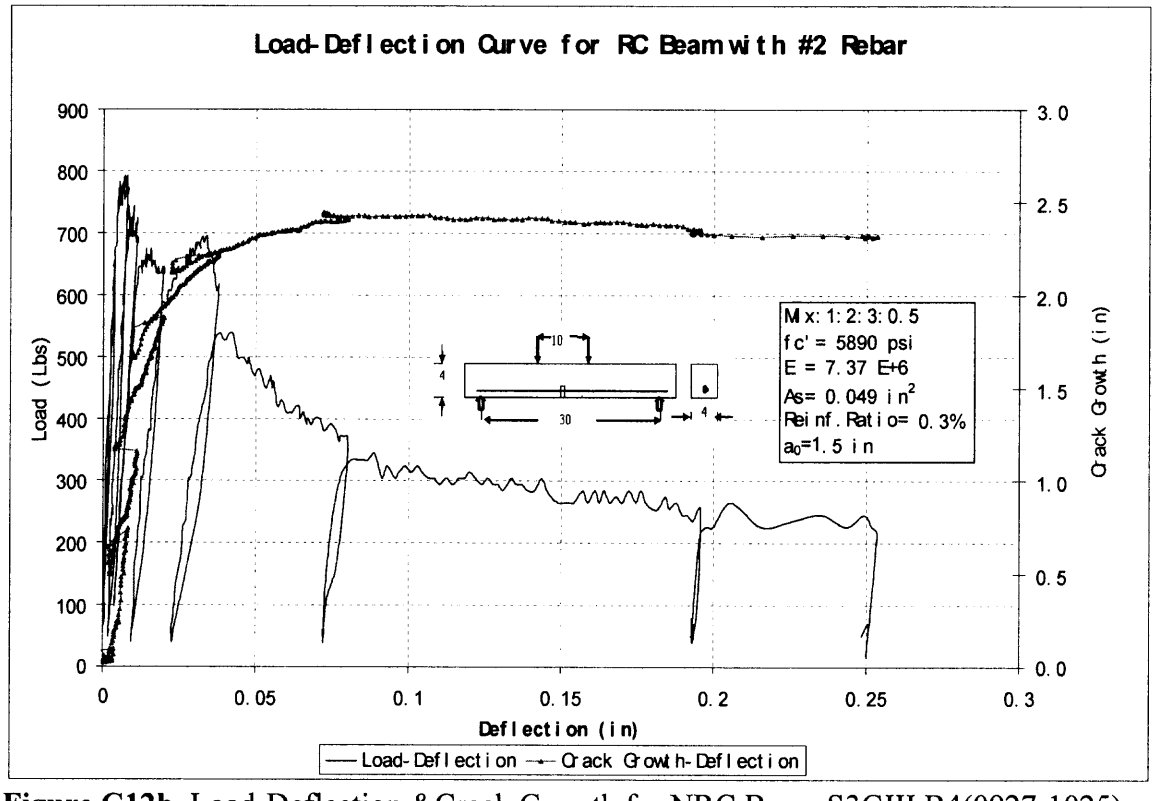

Figure C12b Load-Deflection &Crack Growth for NRC Beam S3GIII B4(0927-1025)

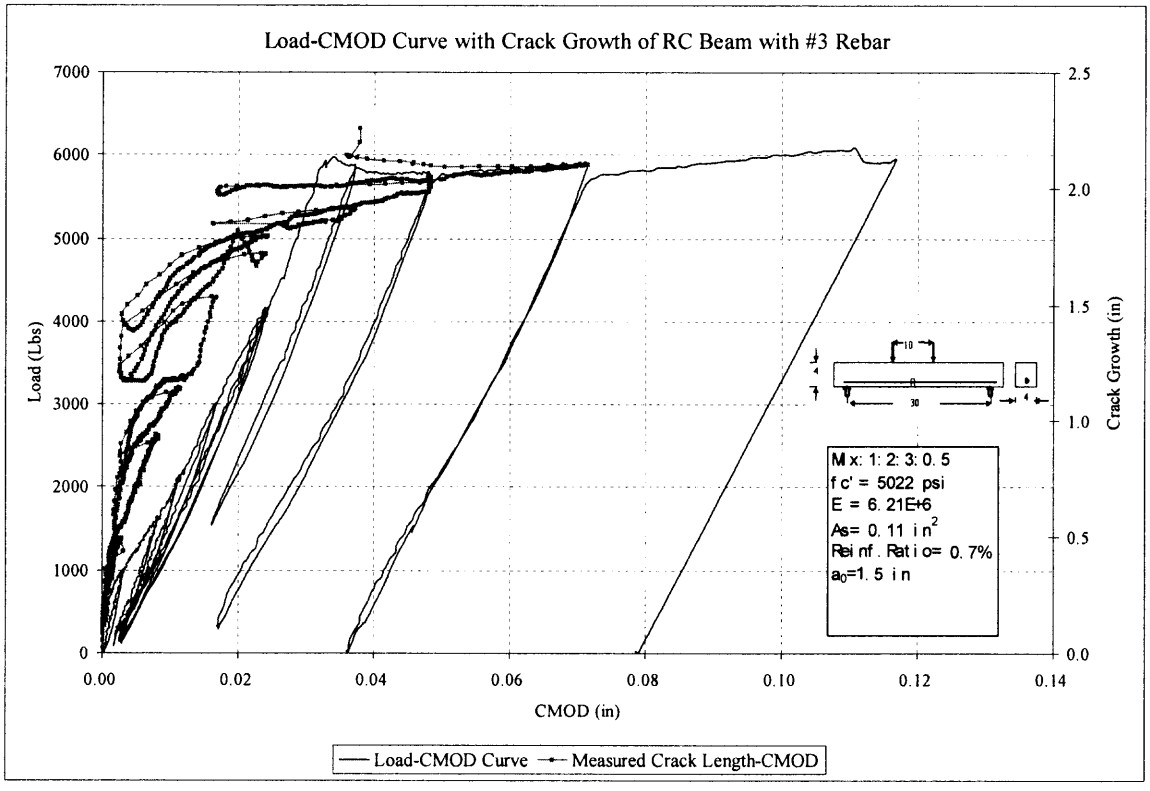

Figure C13a Load-CMOD &Crack Growth for RC Beam S3GIII B5(0920-1010)

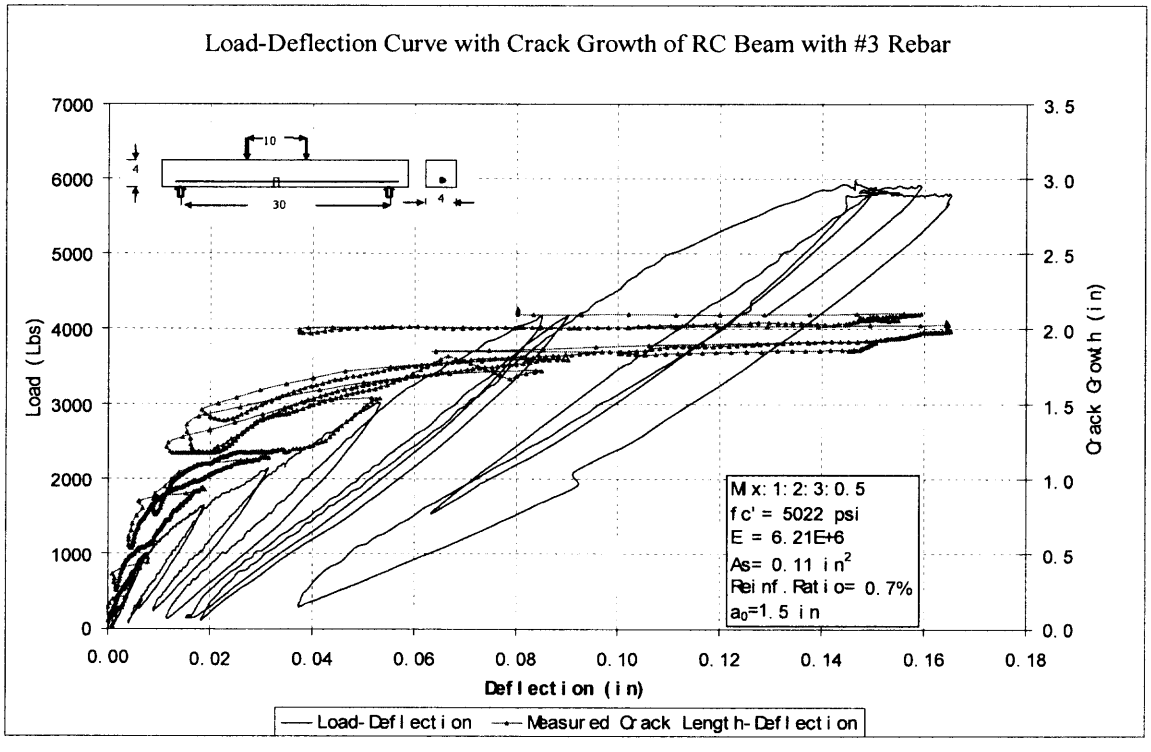

Figure C13b Load-Deflection&Crack Growth for RC Beam S3GIII B5(0920-1010)

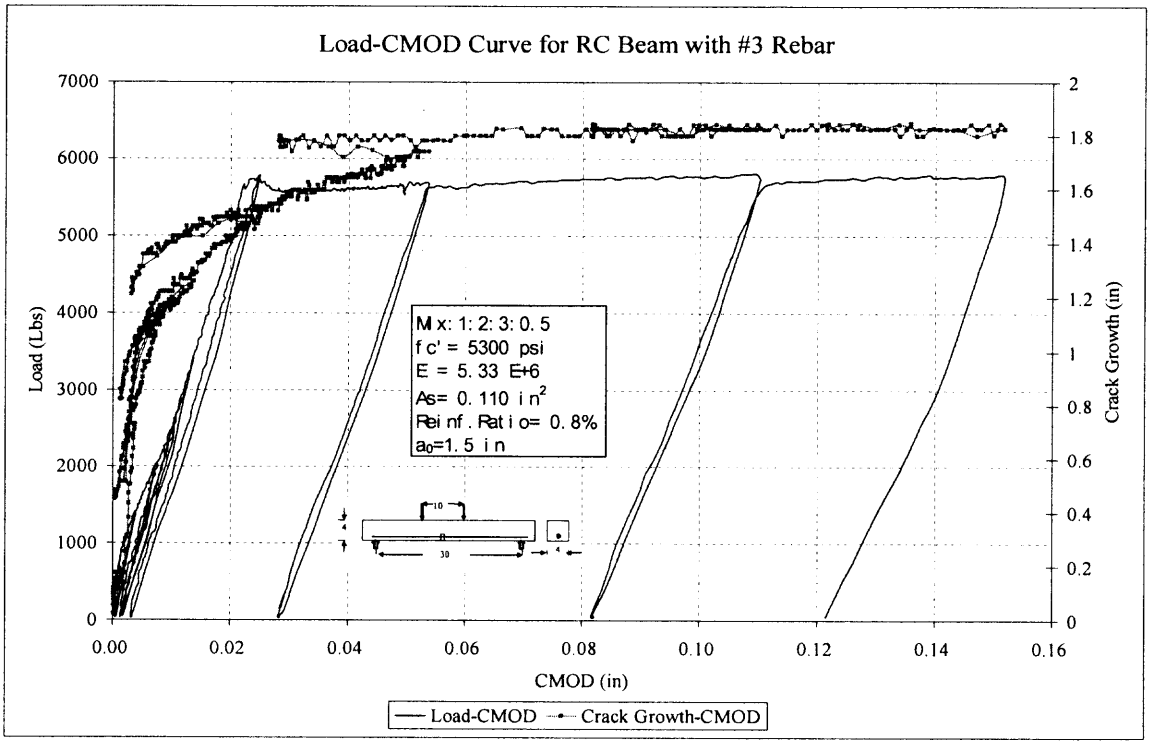

Figure C14a Load-CMOD &Crack Growth for NRC Beam S3GIII B6(0922-1025)

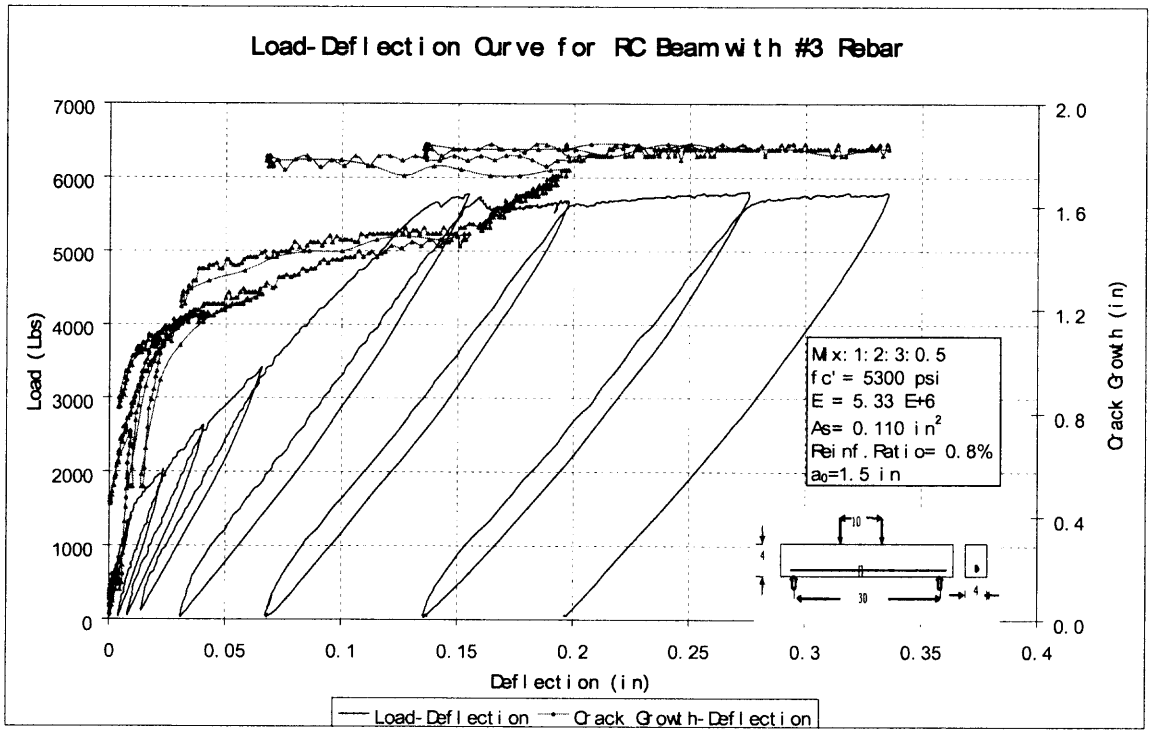

Figure C14b Load-Deflection &Crack Growth for NRC Beam S3GIII B6(0922-1025)

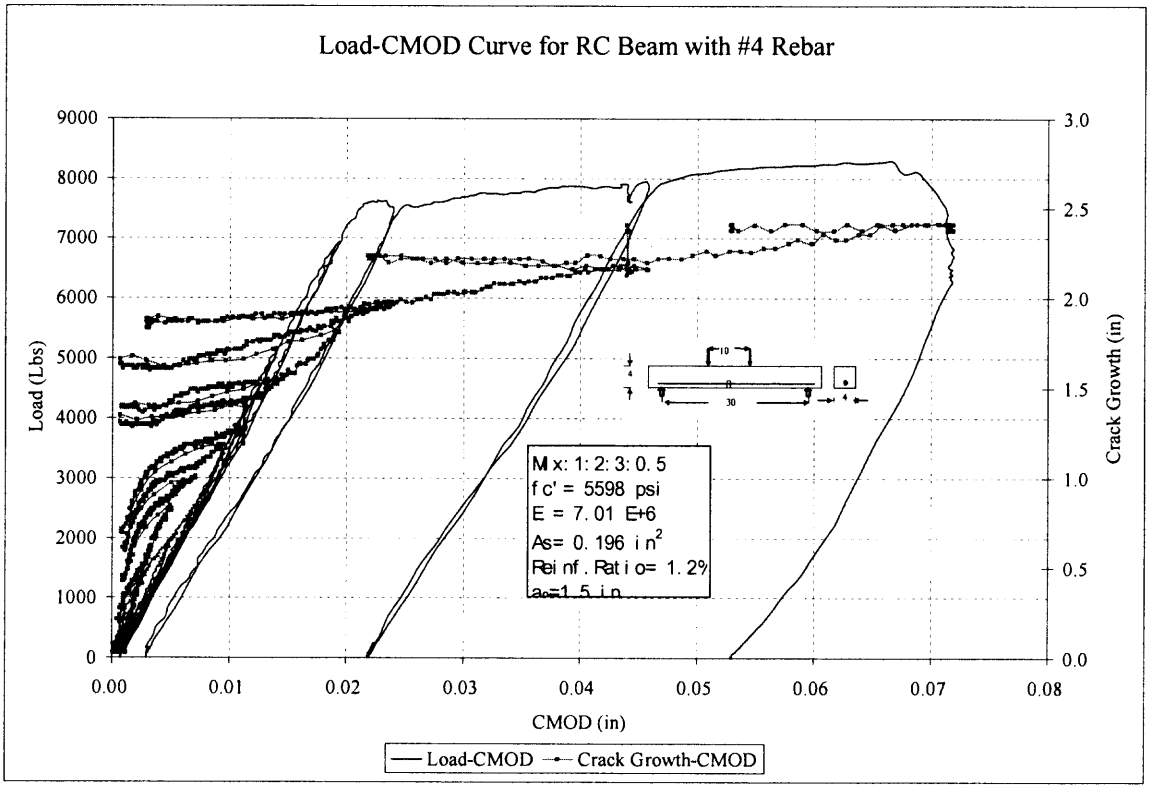

Figure C15a Load-CMOD &Crack Growth for RC Beam S3GIII B7(0920-1018)

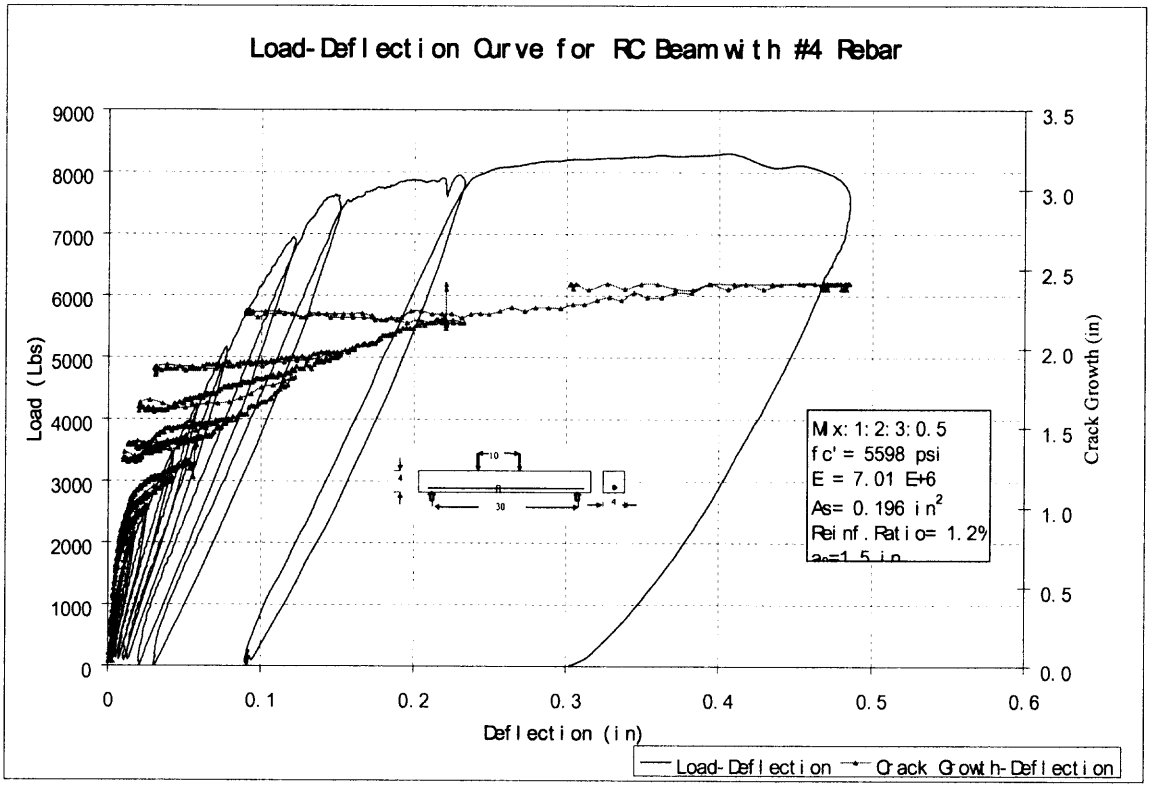

Figure C15b Load-Deflection &Crack Growth for RC Beam S3GIII B7(0920-1018)

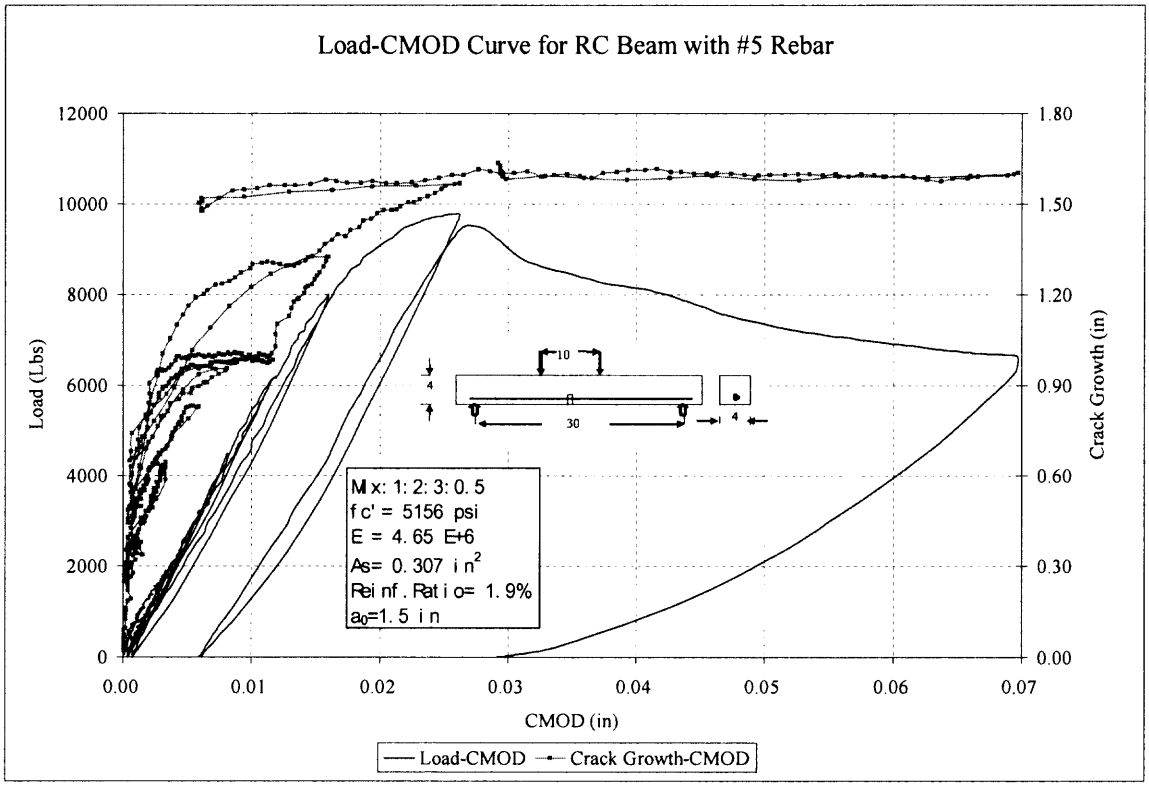

Figure C16a Load-CMOD &Crack Growth for RC Beam S3GIII B8(0922-1018)

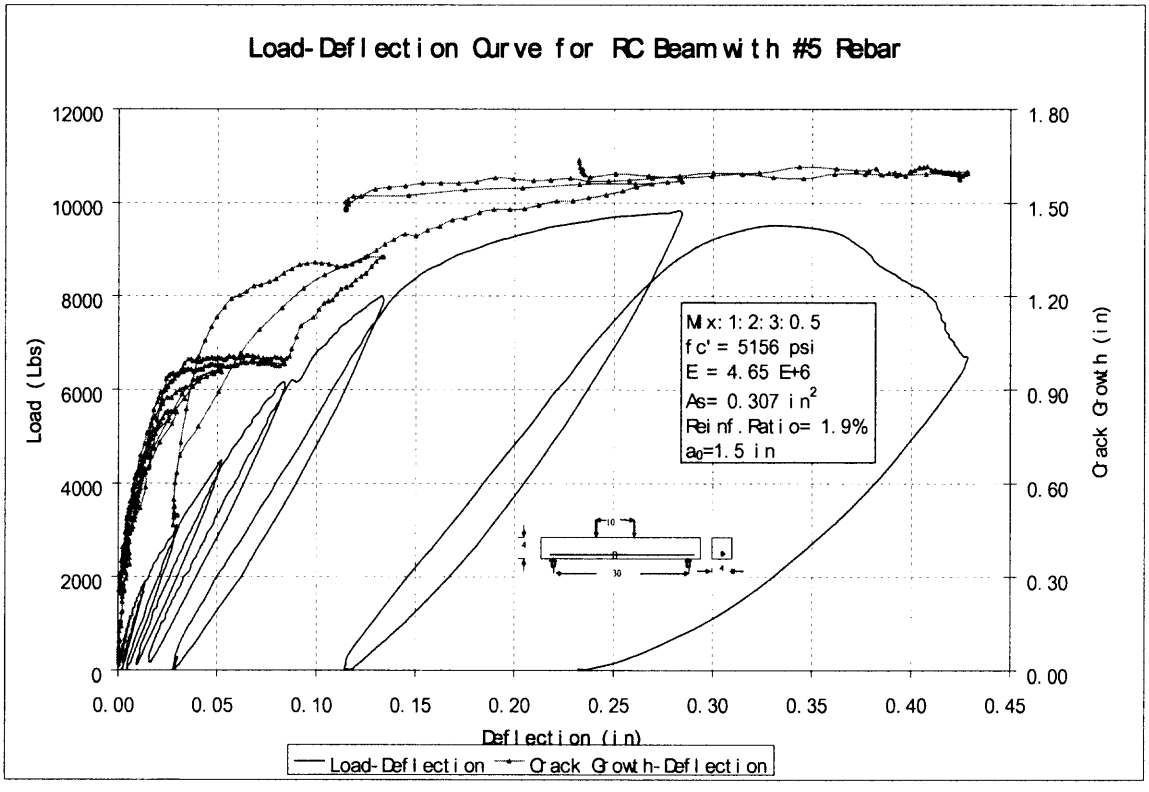

Figure C16b Load-Deflection &Crack Growth for RC Beam S3GIII B8(0922-1018)

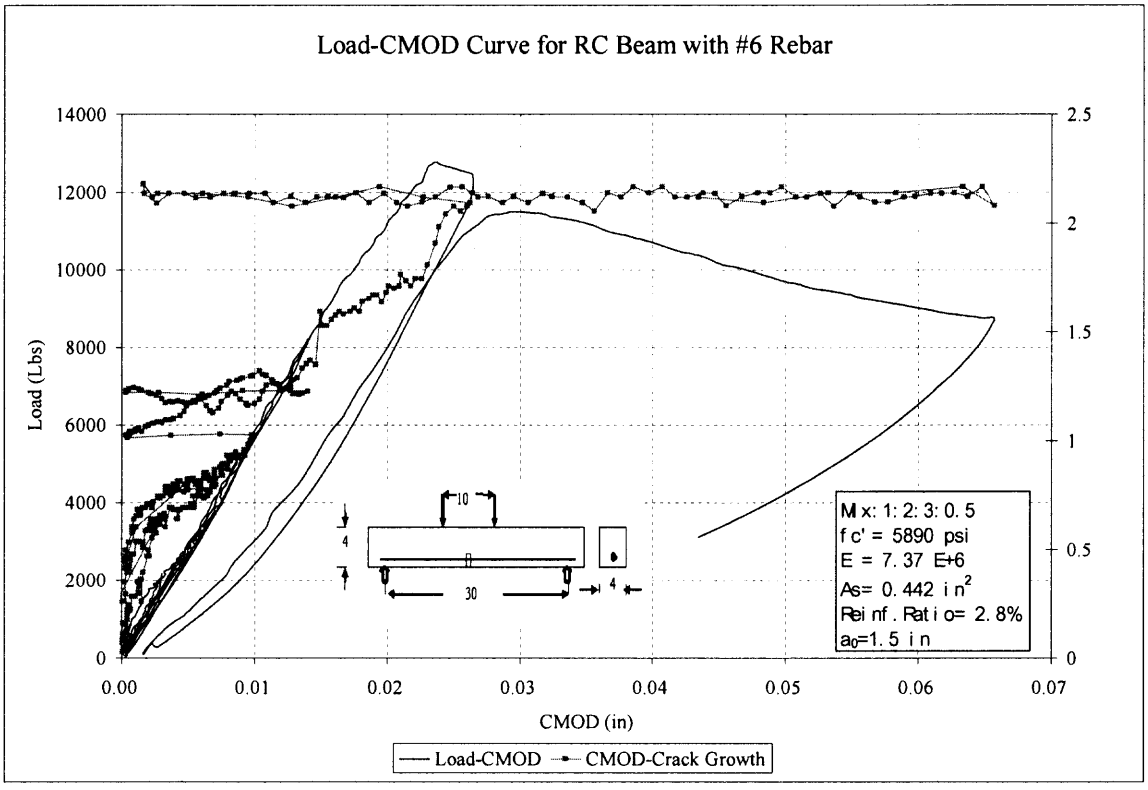

Figure C17a Load-CMOD &Crack Growth for RC Beam S3GIII B9(0927-1025)

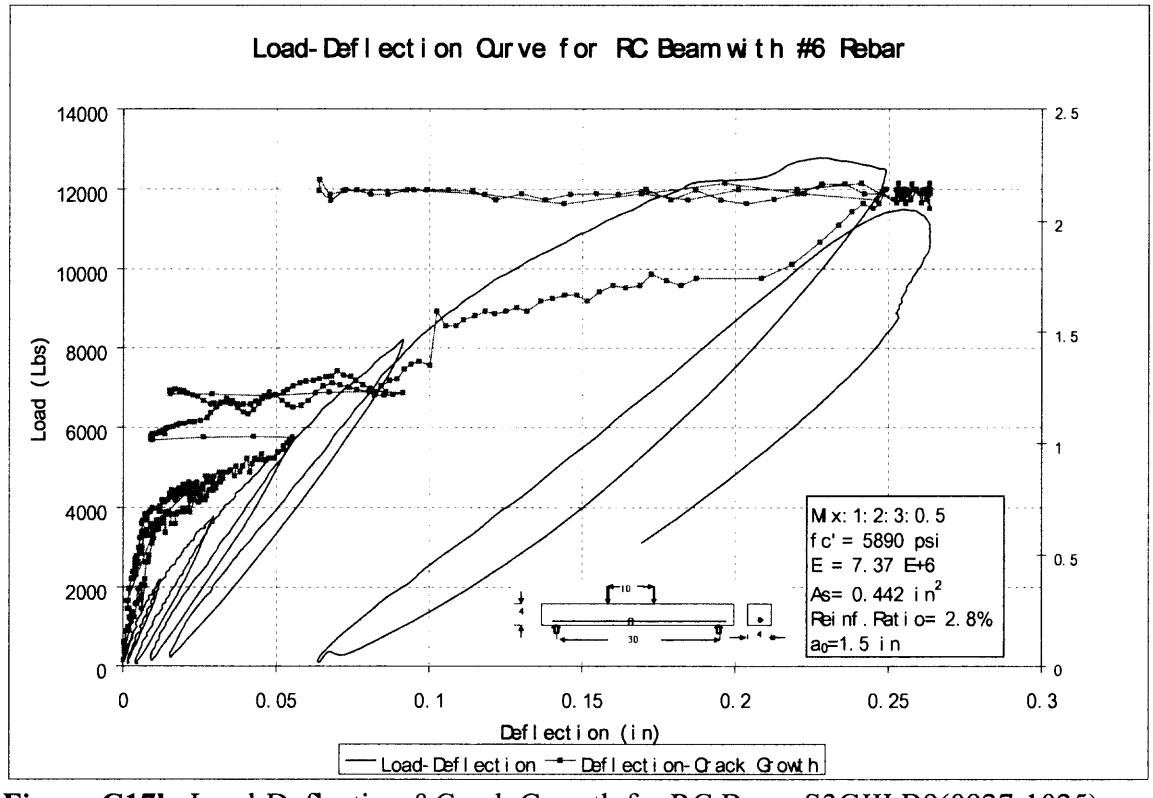

Figure C17b Load-Deflection &Crack Growth for RC Beam S3GIII B9(0927-1025)

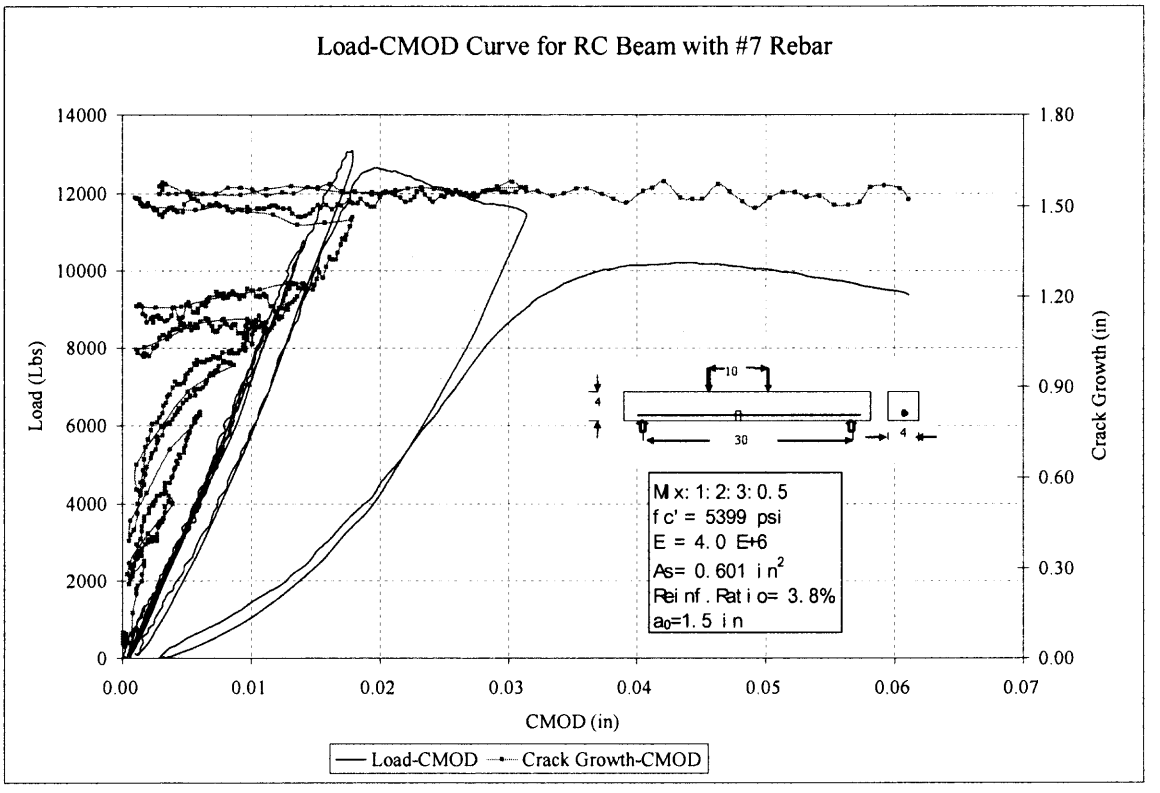

Figure C18a Load-CMOD &Crack Growth for RC Beam S3GIII B10(0920-1018)

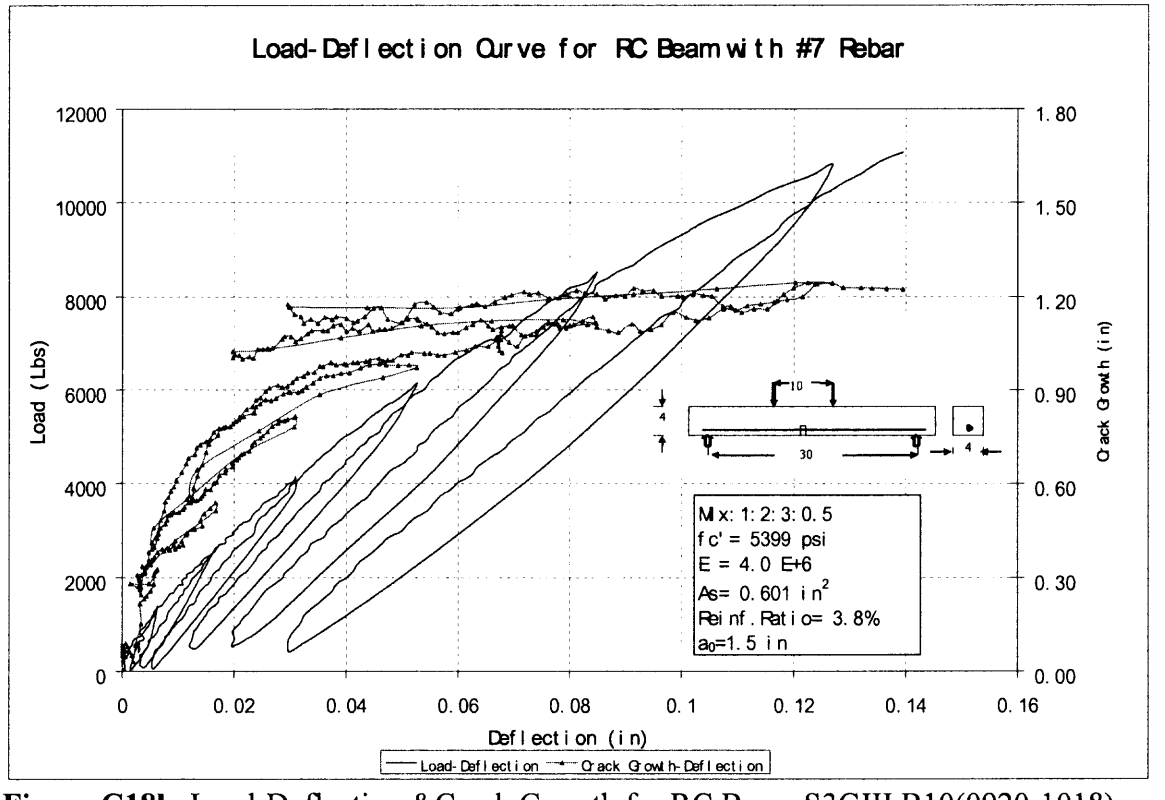

Figure C18b Load-Deflection &Crack Growth for RC Beam S3GIII B10(0920-1018)

REFERENCES

1. A. Carpinteri and Bernardina Chiaia (1995), Size-effects on nominal tensile strength of concrete structures: multifractality of material ligaments and dimensional transition from order to disorder, *Materials and Structures, vol.28*, 311-317.

2. A. Carpinteri and Bernardina Chiaia (1996), Size effects on concrete fracture energy: dimensional transition from order to disorder, *Materials and Structures, vol. 29* 259-266.

3. A. Carpinteri, Giuseppe Ferro (1994), Size effects on tensile fracture properties: a unified explanation based on disorder and factuality of concrete microstructure, *Materials and Structures, vol. 27*, 563-571.

4. A. Carpinteri, Giuseppe Ferro and Giulio Ventura (2003), Size Effect on Flexural Response of Reinforced Concrete Element with a Nonlinear Matrix, *Enegineering Fracture Mechanics 70*, 995-1013.

5. A.A Griffith (1925), The theory of rupture, *in Proceedings of the First International Conference for Applied Mechanics*, 55-63.

6. A.A. Griffith (1921), The phenomena of rupture and flow in solids, *Philosophical Transactions of the Royal Society of London*.

7. B.L.Karihaloo and P.Nallathambi (1989b), An improved effective crack model for the determination of fracture toughness of concrete, *Cement and Concrete Research vol.19*, 603-610.

8. B.L.Karihaloo and P.Nallathambi (1986), Determination of specimen-size independent fracture toughness of plain concrete, *Magazine of Concrete Research vol.38, No.135*, 67-76.

9. B.L.Karihaloo and P.Nallathambi (1995), *Fracture Mechanics and Structural Concrete*, Longman Scientific & Technical.

10. B.L.Karihaloo and P.Nallathambi (1989a), Fracture toughness of plain concrete from three-point bend specimens, *Materials and Structures, 22* 185-193.

11. B.L.Karihaloo and P.Nallathambi (1990), Size-effect prediction from effective crack for plain concrete, *Materials and Structures 23*, 178-185.

12. C.E. Inglis (1913), Stresses in a plate due to the presence of cracks and sharp corners, *Transactions of the Institution of Naval Architects 55*, 219-230.

13. C.R.CHEN, O.Kolednik, I.Scheider,T.Siegmund,A.Tatschl and F.D. Fiescher (2003), On the determination of the cohesive zone parameters for the modeling of micro-ductile crack growth in thick specimens, *International Journal of Fracture I20,*517-536.

14. Cheer-Germ Go, Stuart E. Swartz, and Kuo-kuang (1984), Stress intensity factors for single-edge notch beam, *Journal of Engineering Mechanics, ASCE, vol.110,No.4.* 629-633.

15. Chengshen Qiang, Tianxi Tang, S.P.Shah (1996), Relationship between fracture parameters from two parameter fracture model and from size effect model, Materials and Structures vol. 29, 79-86.

16. Crescentino Bosco and Alberto Carpinteri (1992), Fracture behavior of beam cracked across reinforcement, *Theoretical and Applied Fracture Mechanics 17,* 61-68.

17. D.S. Dugdale (1960), Yielding of steel sheets containing slits, *Journal of the Mechanics and Physics of Solids, vol. 8,* 100-104.

18. Daniel C,Jansen,W.Jason Weiss and Stefan H.F.Schleuchardt(2000), Modified testing procedure for the two parameter fracture model for concrete, *International Journal of Fracture* 105 107–125.

19. Dominique Francois (1984), Fracture and damage mechanics of concrete, *Application of Fracture Mechanics To Cementitious Composites, NATO-ARW*, S.P.Shah, editor, 141-156.

20. E.Orowan (1955), Energy criteria of fracture, *Welding Journal, Research Supplement, vol.34 (3)* ,157-160.

21. F.H.Wittmann & I.Metzener-Gheorghita (1985), Fracture toughness of concrete determined on large specimens, *Materials and Structures, Vol. 18*.

22. G.I. Barenblatt (1962), The mathematical theory of equilibrium cracks in brittle fracture, *Advances in Applied Mechanics, vol.7*, 55-129.

23. G.R.Irwin (1957), Analysis of stresses and strains near the end of a crack transversing a plate, *Journal of Applied Mechanics, vol. 24,* 361-364.

24. G.R.Irwin (1962), Crack extension force for a part-through crack in a plate, *Journal of Applied Mechanics, vol.29*, 651-654.

25. G.R.Irwin (1954), Critical energy rate analysis of fracture strength, *Welding Journal, Rresearch Supplement, vol.33(4),* 193-198.

26. G.R.Irwin (1948), Fracture dynamics. Fracture of Metals, *American Society for Metals, Cleveland,* 147-166.

27. G.V.GUINEA (1995), Modeling the fracture of concrete: the cohesive crack, *Materials and Structures,vol. 28*,187-194.

28. H.Horii,A.Hasegawa and F.Nishino(1987), Fracture process and bridging zone model and influencing factors in fracture of concrete. *Fracture of Concrete And Rock, Edited by S.P.Shah and Stuart E.Swartz* 205-219.

29. H.M. Westergaard (1939), Bearing pressures and cracks, *Journal of Applied Mechanics, vol 6* , 49-53.

30. Hiroyuki Okamura et. al. (1975), Deformation and strength of cracked member under bending moment and axial force, *Engineering Fracture Mechanics, Vol.7*, 531-539.

31. Hans W. Reinhardt, Shilang Xu (1999), Crack extension resistance based on the cohesive force in concrete, *Engineering Fracture Mechanics 64* ,563-587.

32. Hillerborg, A.(1985), The theoretical basis of method to determine the fracture energy G_f of concrete, *Materials and Structures, V.18, No. 106,* 291-296.

33. Hillerborg, A., Modeer, M., and P.E. Petersson (1976), Analysis of crack formation and crack growth in concrete by means of fracture mechanics and finite elements, *Cement and Concrete Research*, Vol. 6, 773-782.

34. Hillerborg, A., (1985), Results of three comparative test series for determining the fracture energy G_F of concrete, *RILEM Technical Committees 50, Materials and Structures, Vol.18 , No.106,* 407-413.

35. Hiroshi Tada, Paul C.Paris and George, R, Irwin (2000), *The Stress Analysis of Cracks Handbook, third edition, ASME Press.*

36. I.I.Luchko and V.F.Lazar and V.M.Chubrikov (2001), Strength of a cracked reinforced-concrete element from the viewpoint of fracture mechanics, *Materials Science, vol.37,No.1,* 25~37.

37. I.I.Luchko and V.F.Lazar (2002), Evaluation of stresses in reinforced-concrete beam elements, their strength, and crack resistance, *Materials Science, vol.38* ,136~150.

38. J.M.L. Reis and A.J.M.Ferreira (2003), The influence of notch depth on the fracture mechanics properties of polymer concrete, *International Journal of Fracture 124*,33-42.

39. J.Planas , M.Elices , G.V.Guinea (1992), Measurement of fracture energy using three-point bend test: Part2-influence of bulk energy dissipation, *Materials and Structures, V.25,* 305-312.

40. J.R.Rice (1974), Limitations to the small scale yielding approximation for crack tip plasticity, *Journal of the Mechanics and Physics of Solids,vol.22*,17-24.

41. Jenq, Y.S., and Shah, S.P.(1985a), A fracture toughness criterion for concrete, *Engineering and Fracture Mechanics, V.21, No.5* ,1055-1069.

42. Jenq, Y.S., and Shah, S.P.(1985b), Two parameter fracture model for concrete, *Journal of Engineering Mechanics, ASCE, V.111, No.10* ,1227-1241.

43. Jun zhang, Victor C.Li and Henrik Stang (2001), Size-effect on fatigue in bending of concrete. *Journal of Materials in Civil Engineering,* 446-453.

44. K.T.Sundara Raja Iyengar, et.al (2002), Analysis of crack propagation in strain-Softening Beams, *Engineering Fracture Mechanics 69*,761-778.

45. Lertwattanaruk, P.(2000), The influence of high performance matrices on fracture behavior of concrete , *Ph.D,Dissertation, Department of Civil and Environmental Engineering, New Jersey Institute of Technology, Newark, New Jersey.*

46. M. Elices, G.V.Guinea and J.Planas (1997), On the measurement of concrete fracture energy using three-point bend tests, *Materials and Structures vol. 30,* 375-376.

47. M.Stder, J.Pierrzyk, K.Peters, J.Botsis ans P. Giaccara (2002), Studies on bridging tractions- simultaneous bridging tractions and COD measurements, *International Journal of Fracture 114*,379-399.

48. Methi Wecharatana (1982), Fracture resistance in cementitious composites, Ph.D Disseration, University of Illinois at Chicago Circle, at Chicago.

49. Methi Wecharatama and S. P. Shah (1983), Predictions of nonlinear fracture process zone in concrete, *Journal of Engineering Mechanics Vol.109, No.5* ,1231-1246.

50. Methi Wecharatama and S.P.Shah (1982), Slow crack growth in cement composites, *ASCE, vol.108, No.ST6* ,1400-1413.

51. P.C. Taylor , R.B. Tait (1999), Effects of fly ash on fatigue and fracture properties of hardened cement mortar, *Cement & Concrete Composite.21* ,223-232.

52. P.E. Petersson (1980), Fracture energy of concrete: method of determination, *Cement and Concrete Research,* Vol. 10, 78-89.

53. Rajendra K. Navalurkar, Cheng-Tzu T. Hsu, et.al. (1999), True fracture energy of concrete, *ACI Material Journal, V.96,No.2,* 213-225.

54. Ralph J.Destefano, Jack Evans, Maher K.Tadros and Chuanbing Sun (2003), Flexural crack control in concrete bridge structures, ISHPC.

55. RILEM,TC 50-FMC (1985), Fracture mechanics of concrete, "Determination of the Fracture Energy of Mortar and Concrete by Means of the Three-Point Bend Test on Nothched Beams" RILEM Recommendation, *Material and Structure,V. 18* 285-296.

56. Robert J.Frosh (1999), Another look at cracking and crack control in reinforced concrete, *ACI Structural Journal, V96, No.3*, 437~442.

57. S.E. Swartz, S.T. Yap (1988), The influence of dead load on fracture energy measurements using the RILEM method, *Materials and Structures, vol.21*, 410-415.

58. S.Marfla &E.Sacco (2001), A fracture evolution procedure for cohesive materials, *International Journal of Fracture 110*, 241-261.

59. Sawamg Ratanalert & Methi Wecharatama (1989), Evaluation of the fictitious crack and two-parameter fracture, *Fracture Mechanics: Application to Concrete*, Eds.By Li V.C. and Z.P.Bazant, SP-118, American Concrete Institute, Detroit.

60. Shah, S.P. (1990a), Determination of fracture parameters (K_{IC} *and* $CTOD_C$) of plain concrete using three-point bend tests, *RILEM Technical Committee 89-FMT, Material and Structures, V.23* ,457-460.

61. Shah, S.P. (1990b), Size-effect method for determining fracture energy and process zone of concrete, *RILEM Technical Committee 89-FMT, Material and Structures, V.23*, 461-465.

62. Shilang Xu, Hans W. Reinhardt (2000), A simplified method for determining double-K fracture parameters for three-point bending tests, *International Journal of Fracture104*,181-209.

63. Shilang Xu, Hans W. Reinhardt(1998), Crack extension resistance and fracture properties of quasi-brittle softening materials like concrete based on the complete process of fracture, *International Journal of Fracture 92*,71-99.

64. Shilang Xu, Hans W. Reinhardt (1999a), Determination of double –K criterion for crack propagation in quasi-brittle fracture, part II : analytical evaluating and practical measuring methods for three-point bending notched beams. *International Journal of Fracture 98*, 151-177.

65. Shilang Xu, Hans W. Reinhardt (1999c), Determination of double-K criterion for crack propagation in quasi-brittle fracture , part III : compact tension specimens and wedge splitting specimens, *International Journal of Fracture 98*,179-193.

66. Shilang Xu, Hans W. Reinhardt,Zhumin Wu and Yanhua Zhao (2003), Comparison between the double-K model and the two parameter fracture model, *Otto-Graf-Journal Vol.14.*

67. Takashi Matsumoto, Victor C.Li (1999), Fatigue life analysis of fiber reinforced concrete with a fracture mechanics based model, *Cement &Concrete Composites 21*, 249-261.

68. Tianxi Tang and Z.P.Bazant (1996), Variable-notch one-size test method for fracture energy and process zone length, *Engineering Fracture Mechanics, vol.55,No.3*, 383-404.

69. V.E.Saouma, D.Natekar and E.Hansen (2003), Cohesive stresses and size effects in elastic-plastic and quasi-brittle materials, *International Journal of Fracture 119*,287-298.

70. Vidmantas Jokubaitis and Petras Pukelis (2005), Influence of longitudinal reinforcement on development of normal cracks, *Journal of Civil Engineering and Management, Vol.XI, No.1*, 33-37.

71. Wei Yang, W.R.Grace, S.P.Shah (2001), A geometry and size dependent fracture resistance curve, *International Journal of Fracture 109*, 23-28.

72. Yoshinori Kitsutaka (1997), Fracture parameters by polylinear tension-softening analysis, *Journal of Engineering Mechanics* ,444-450.

73. Z.P. Bazant and Mohammad T.Kazenu (1990), Size effect in fracture of ceramics and its use to determine fracture energy and effective process zone length, *J.Am.Ceram.Soc.73 [7]* ,1841-1853.

74. Z.P.Bazant (1996), Analysis of work-of-fracture method for measuring fracture energy of concrete. *Journal of Engineering Mechanics, ASCE 122* , 138-144.

75. Z.P.Bazant ,QianYu and Goangseupzi (2002), Choice of standard fracture test for concrete and its statistical evaluation, *International Journal of Fracture 118* ,303-337.

76. Z.P.Bazant and P.A. Pfeiffer (1987), Determination of fracture energy from size effect and brittleness number, *ACI material journal, Vol.84, No. 6* , 463-480.

77. Z.P.Bazant (1984), Size effect in blunt fracture: concrete, rock, metal, *Materials and Structure, v25*,518-535.

78. Z.P.Bazant (2002), Concrete fracture models: testing and practice, *Engineering Fracture Mechanics, vol 69*,165-205.

79. Z.P.Bazant (1999), Size effect on structural strength: a review, *Archive of Applied Mechanics 69* , 703-725.